Novel redox indicators for optical detection of NADH

Dissertation

zur Erlangung des Doktorgrades der Naturwissenschaften

(Dr. rer. nat.)

an der Fakultät Chemie und Pharmazie

der Universität Regensburg

vorgelegt von

Maksim Fomin

aus Tomilino (Russland)

November 2015

The experimental work was carried out between October 2011 and October 2015 at Roche Diagnostics GmbH under the supervision of Dr. Dieter Heindl and Prof. Dr. Burkhard König.

Submission of thesis: 12.11.2015

Date of colloquium: 14.01.2016

Board of Examiners:

Prof. Dr. Frank-Michael Matysik (Chairman)

Prof. Dr. Burkhard König (1st Referee)

Prof. Dr. Joachim Wegener (2nd Referee)

PD Dr. habil. Axel Dürkop (Examiner)

DECLARATION

This dissertation is the result of my own work and includes nothing, which is the outcome of work done in collaboration except where specifically indicated in the text. It has not been previously submitted, in part or whole, to any university of institution for any degree, diploma, or other qualification.

Regensburg, den 12.11.2015

Maksim Fomin

Page intentionally left blank.

In memory of Helga Kammerl

6. Mai 1948 — 6. Januar 2015

SUMMARY

The rapid, sensitive, and selective sensing of nicotinamide adenine dinucleotides NAD(P)H is of significant interest for applications in diagnostic assays, synthesis of chiral compounds and drug discovery. The redox couple $NAD(P)^+$/NAD(P)H plays a crucial role in energy metabolism and has been used as a biomarker to detect altered cancer-cell metabolism. Furthermore, NAD(P)H detection is desirable for *in vitro* analysis of NAD^+-dependent enzymes, which is important in the context of high-throughput screening and the development of these enzymes for industrial applications. Moreover, $NAD(P)^+$-dependent glucose dehydrogenase (GDH) has been widely utilized for glucose sensors in point-of-care (POC) testing.

Optical techniques proved to be a powerful tool for quantitation of analytes in biological fluids. Both NADH and NADPH absorb light at 340 nm and have intrinsic fluorescence. Direct NAD(P)H detection does not provide adequate sensitivity for most applications. In this regard, colorimetric and fluorescent indicators are particularly attractive, because they are able to change their absorption spectra to a longer wavelength upon reaction with a target analyte. The key considerations in a search for a tailor made NADH indicator include water-solubility, rate of reaction with NADH and sensitivity. Up to now, it still remains a challenge to develop an indicator meeting all these demands.

The aim of this thesis was to discover a small molecule indicator for NADH detection.

Chapter 1 introduces the concepts of test strip development for blood glucose monitoring and gives a brief overview of research activities in this area.

Chapter 2 describes, for the first time, that a colorimetric indicator — directly accepting electrons from an enzymatic reaction — can be utilized for glucose sensing on a dry chemistry test strip. The glucose assay reagent included a quinone-functionalised Ru (II) complex, the artificial cofactor $cNAD^+$ and mutated GDH. An absorbance response was observed at 840 nm in proportion to glucose concentration.

Chapter 3 presents a new optical NADH indicator to analyze intracellular metabolic pathways at the single-cell level. The design is based on an electron-deficient heterocycle (active acceptor) conjugated to a polymethine chain of the cyanine dye scaffold. Such compounds are nearly colourless and nonfluorescent. Upon hydride transfer from NADH to the active acceptor moiety, cyanine chromophore is unmasked leading to a sensitive absorbance and fluorescence response.

ZUSAMMENFASSUNG

Ein schneller, empfindlicher und selektiver Nachweis von Nicotinamidadenindinukleotid NAD(P)H ist für Anwendungen im Bereich diagnostischer Assays, der Synthese von chiralen Produkten und der Wirkstoffentwicklung von großem Interesse. Das Redoxpaar $NAD(P)^+$/NAD(P)H spielt eine entscheidende Rolle im Energiestoffwechsel und wurde als Biomarker für die Untersuchung des veränderten Stoffwechsels von Krebszellen verwendet. Darüber hinaus ist die Detektion von NAD(P)H für die *in vitro* Analyse NAD^+-abhängiger Enzyme bedeutend. Dies spielt eine Rolle im Zusammenhang mit Hochdurchsatz-Screening und der Entwicklung solcher Enzyme für industrielle Anwendungen. Außerdem wird die $NAD(P)^+$-abhängige Glukosedehydrogenase (GDH) in Glukosesensoren im Bereich der patientennahen Labordiagnostik intensiv genutzt.

Optische Methoden erwiesen sich als geeignete Werkzeuge für die Quantifizierung von Analyten in biologischen Fluiden. Sowohl NADH als auch NADPH absorbieren Licht bei 340 nm und zeigen intrinsische Fluoreszenz. Ein direkter NAD(P)H Nachweis weist allerdings keine ausreichende Sensitivität für die meisten Anwendungen auf. Deswegen sind kolorimetrische und fluoreszierende Indikatoren teilweise attraktiv, da sich ihr Absorptionsspektrum nach Reaktion mit einem gewünschten Analyten zu längeren Wellenlängen hin verschiebt. Die wichtigsten Überlegungen bei der Suche nach einem maßgeschneiderten NADH Indikator beinhalten dessen Wasserlöslichkeit, die Reaktionsgeschwindigkeit mit NADH und die Sensitivität. Bis zum jetzigen Zeitpunkt stellt die Entwicklung eines solch gewünschten Indikators eine Herausforderung dar.

Das Ziel dieser Arbeit war es einen niedermolekularen Indikator für die NADH-Detektion zu finden.

Kapitel 1 führt das Konzept der Teststreifenentwicklung für die Blutzuckermessung ein und gibt einen kurzen Überblick der Forschungsarbeiten auf diesem Gebiet wieder.

Kapitel 2 zeigt zum allerersten Mal, dass ein kolorimetrischer Indikator, der Elektronen direkt aus einer enzymatischen Reaktion aufnimmt, für die Glukosemessung auf einem trockenen Teststreifen verwendet werden kann. Dazu wurden ein Quinon-funktionalisierter Rutheniumkomplex, der künstliche Kofaktor $cNAD^+$ und eine GDH-Mutante verwendet. Dabei wurde das Absorptionssignal bei 840 nm in Abhängigkeit der Glukosekonzentration bestimmt.

Kapitel 3 zeigt einen neuen optischen NADH Indikator für die Analyse intrazellulärer Stoffwechselwege bei Einzelzelluntersuchungen. Dieser basiert auf einem elektronenarmen Heterozyklus (aktiver Akzeptor), der zu einer Polymethinkette des Cyaninfarbstoffgerüsts konjugiert vorliegt. Solche Verbindungen sind nahezu farblos und nicht fluoreszent. Nach einem Hydridtransfer von NADH auf den aktiven Akzeptorteil des Cyaninfarbstoffs erzielt man eine sensitive Absorption- und Fluoreszenzantwort.

CONTENTS

Page intentionally left blank.

1 INTRODUCTION TO BLOOD GLUCOSE TEST STRIP DEVELOPMENT AND PROJECT OBJECTIVES

1.1 Diabetes

A long time ago, Aretaeus of Cappadocia, one of the most celebrated physicians of the late Hellenistic period, gave the first clear and complete description of diabetes:[1] *"Diabetes is a remarkable affliction, not very frequent among men… The course is the common one, namely, the kidneys and the bladder; for the patients never stop making water, but the flow is incessant, as if from the opening of aqueducts… The nature of the disease, then, is chronic, and it takes a long period to form; but the patient is short-lived, if the constitution of the disease be completely established; for the melting is rapid, the death speedy. Moreover, life is disgusting and painful; thirst, unquenchable…"*, the term comes from the Greek verb *διαβαίνω* (diabaino), which means *"to go or run through"*. Communications of Aretaeus remained unknown in the West until 1552, when the first Latin edition was published in Venice, and so it was introduced into medical nomenclature. In 1675 Thomas Willis added the Greek word "*mellitus*".[2] He noted that diabetes — also known as "the pissing evil" — produced urine which was "wonderfully sweet, like sugar or honey".[2] The major turning point in the history of diabetes mellitus (commonly referred to as diabetes) happened centuries later. In the summer of 1921, Banting and Best discovered insulin — a treatment for diabetes and already in the winter of 1922, the life of a young boy was saved by the treatment. This can be considered to be one of the most spectacular events in medicine.[3-4]

There are two major types of diabetes, type 1 diabetes (T1D) and type 2 diabetes (T2D). Both of them are defined by high blood glucose levels (hyperglycaemia).[5] This requires continuous management of glucose levels and on-time treatment in order to prevent dangerous complications, which can provoke damage to the eyes, kidneys, feet and heart. In T1D, hyperglycaemia results from insulin deficiency caused by autoimmune destruction of pancreatic *β*-cells.[6] In T2D, the body does not use insulin properly.[7] This is known as the insulin resistance. At first, *β*-cells in pancreas produce extra insulin to compensate for it. Over time the pancreas is not able to produce enough insulin to keep glycaemia at normal levels. T1D is caused by genetics and environmental factors that trigger the disease; T2D results from combination of genetic, environmental and lifestyle factors.[8-9] No cure has yet been found for diabetes — lifelong treatment is needed for the patients.

Modern day medical practices rely on self-monitoring of blood glucose levels (SMBG).[10] Routine glucose measurements (often several times a day) are required to

monitor abnormal glucose levels, indicating illness, and to determine changes in diet and physical exercise, or in the medical treatment. A key challenge in diabetes care is supporting patients in their efforts to efficiently self-manage the disease, while maintaining a good quality of life.[10]

The World Health Organization (WHO) estimates 347 million people living with diabetes in 2013; and WHO projects that it will be the 7th leading cause of death in 2030. Three out of four people with diabetes now live in low- and middle-income countries. Over the next 20 years, Africa, Middle East and South-East Asia regions will be affected with diabetes most.[11],[12]

In 2013, globally, healthcare costs for diabetes reached $548 billion, equivalent to 11% of total health spending. Unsurprisingly, high-income countries spent vastly more on diabetes-related costs than lower-income countries: only 20% of global health spending on diabetes was made in low- and middle-income countries, where 80% of people with diabetes live.[12] In resource-poor countries, high-tech diagnostic aids are inaccessible to the bulk of population. The first Global Diabetes Plan 2011–2021 agreed actions on diabetes, setting as the highest priority the improvement of the health of people who already have diabetes.[13] Monitoring of blood glucose levels is currently the only recognized and widely used method for the diagnosis and management of diabetes.[14] Up to now, manufacturing of glucose measuring devices, meeting all the demands, still remain a significant challenge. Design and development of low-cost and technologically advanced glucose sensors would definitely have a beneficial impact on the global health situation.

1.2 Glucose monitoring

The history of glucose monitoring could be tracked back in 1500 BC. An ancient Hindu writing described "a disease of honeyed urine" — as it was observed, ants were attracted to urine of certain people. Probably it was the first method to test glucose in urine, as a sign of diabetes. During mediaeval times the technique was refined — physicians would taste urine to look for the sweet taste of sugar.[15] Luckily for the physicians, chemical analysis made the tasting unnecessary in the 20th century as Stanley Benedict devised a copper reagent for measurement of glucose in urine.[16] The first tests were performed by heating urine with Benedict's reagent: glucose present in urine was oxidised, and the blue cupric sulphate reduced, causing a colour change from blue to green to yellow to orange. Semiquantitative results were obtained by visually

comparing the colour formed with a colour chart provided. This became, with modifications, the mainstay of glucose monitoring in diabetes for over 50 years.[17]

Another big step for the physicians was launch of urine reagent strip, Clinistix, in 1957.[18] The strips utilized an enzyme, for more specific reaction, and a chromogenic reagent to provide a read-out. When glucose was present in urine, a deep blue colour was observed on the strip. There was no longer need to heat the urine. Despite these advances, urine testing had a number of significant limitations. The method only shows elevated glucose levels, while hypoglycaemia remains undetected, and urine glucose can only be retrospective to the current glucose status.[19]

In 1965, Ames research team under Ernie Adams went on to develop the first blood glucose test strip, Dextrostix.[20] The paper reagent strip utilized a glucose oxidase/peroxidase reaction, and it was designed for visual evaluation.[21] In late 1960s Anton Clemens at Ames developed an instrument to produce quantitative blood glucose results with Dextrosix. The key idea was using of reflected light from a surface of a solid strip, which was captured by a photoelectric cell to produce a signal, which was displayed by a moving pointer. The original Ames Reflectance Meter (ARM) weighed 1.2 kg, cost around $495 and was available mainly for a doctor's office.

The first generation of blood glucose meters allowed to access current level of glycaemia.[17, 22] The "revolution" for patients and physicians came, when the test strip based glucose meters were widely introduced in 1980s, and the SMBG practice became a commonplace in the 1990s. Patients were taught how to use blood glucose readings to guide their decisions on immediate treatment. Nowadays it is an essential component of intensive management of T1D.[23-24]

Since the 1980s, continuous development by many competing companies has led SMBG devices to an ease of use, high technical performance, and affordability. SMBG instruments have evolved into almost standard size and shape, and have become nice examples of consumer electronics (**Figure 1.1**). The strips have not changed their appearances for many years, but the active area of the strips (chemical matrix) has universally become smaller, enabling lower sample volume to be analyzed (typically around 1 μL). Improvements in technology have facilitated the test strips to do this difficult job in as little as five seconds.[23]

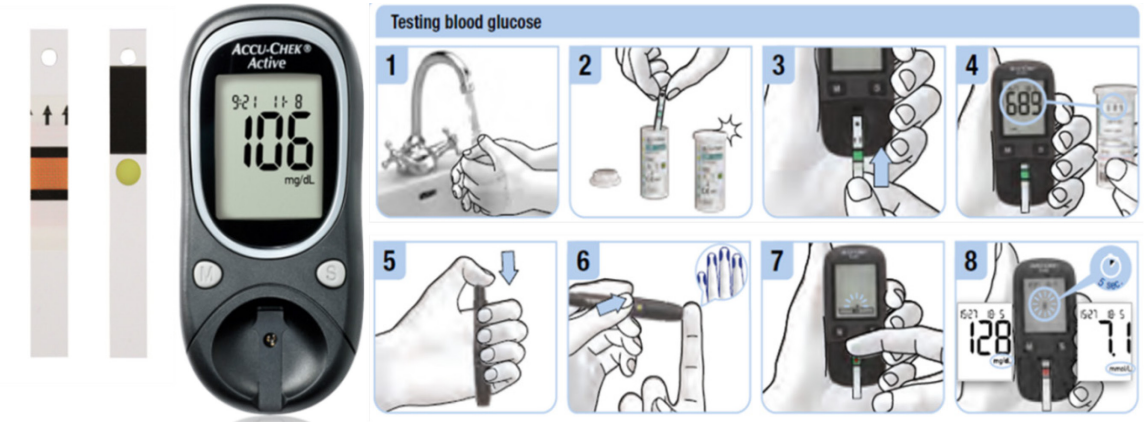

Figure 1.1 Example of a glucose meter (Accu-Chek Active) and SMBG routine.

There are now about forty glucose meters available on the market. By 2008, worldwide sales of these products climbed to an astonishing $8.8 billion, which accounted for approximately 22% of the entire *in vitro* diagnostics industry.[25] Due to constant technological improvements, SMBG became readily available for a vast number of patients. The recently published norm ISO 15197:2013 serves as a yardstick for glucose meter manufacturers.[26],[27] This specifies that 95% of results should be within ±0.83 mmol/L of the reference glucose method for concentrations <5.6 mmol/L, and within 15% for higher concentrations. The American Diabetes Association (ADA) has suggested that the systems should achieve an analytical performance <5% with blood glucose levels between 30 and 400 mg/dL.[28]

Enzymatic methods have been proven to be a powerful approach and have attracted much attention, on account of their simplicity and practicality. Even though good selectivity and high sensitivity are obtained with these enzymatic sensors,[29] inevitable drawbacks still limit their analytical applications such as chemical and thermal instabilities, interferences originating from complex nature of the blood.[30-31]

1.3 A photometric test strip

Photometric techniques are usually considered as the "gold standard" signal generation method in point-of-care (POC) devices.[32-35] In comparison to the other market leader, the electrochemical detection, optical methods may have a lower cost per test, especially in view of the increasing availability of cheap, high-quality optoelectronic components such as charge-coupled device (CCD) detectors and light emitting diodes (LEDs).[36-42]

The common components included in a photometric strip are: an enzyme, a mediator, an indicator and film forming components, all coated on a plastic support in dry form. An example of a photometric strip, Accu-Chek Active (Roche), is shown in **Figure 1.2**.

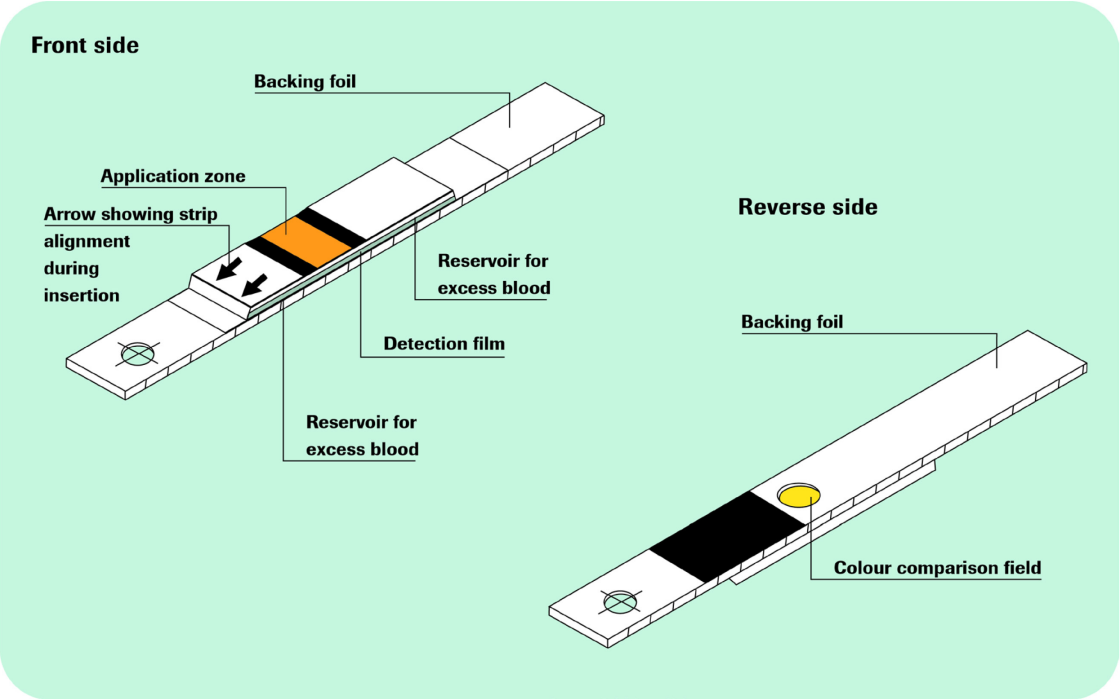

Figure 1.2 Glucose measurement principle. The test consists of multiple layers. Enzyme reaction takes place in the bottom layer and the colour change observed from below.[23]

Roche photometric glucose meters employ a measurement principle shown in **Figure 1.3**. A drop of blood is placed on top of a test strip, where it diffuses rapidly (in about 0.5 s) into a chemistry layer. The "mirror" layer also acts as a filter to prevent erythrocytes from entering the chemistry layer. A few seconds after the dye formation, a photometric signal is observed from the bottom side of the strip. The photometric measurement is done by illumination with LED light. A part of the diffuse reflection arrives at a photodetector and is converted to a current. Volumes down to a few nanoliters can be measured with state of the art layers.

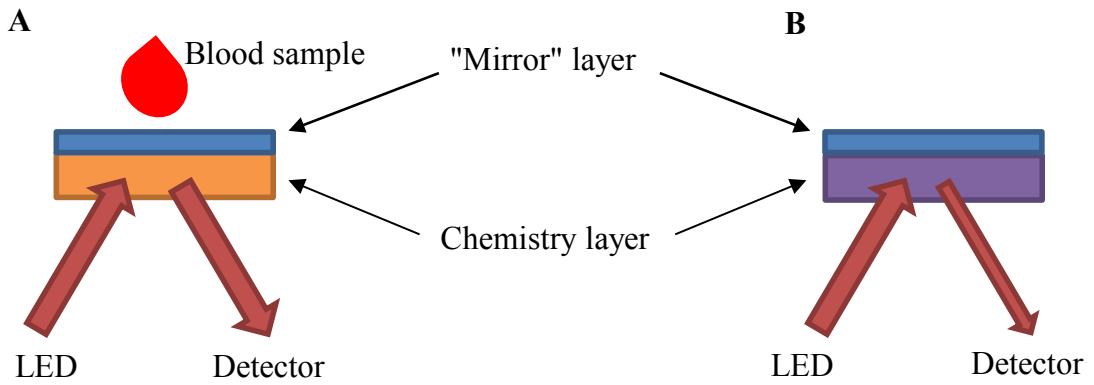

Figure 1.3 Illustration of the setup for the measurement of glucose levels in blood. **A** — Dry chemistry layer containing an enzyme, a coenzyme and an indicator, before addition of the blood sample; **B** — the chemistry layer after addition of the blood sample, showing a colour forming reaction which reduces the amount of reflected light.

1.4 Glucose biosensors: the challenge and opportunity

The first-generation glucose biosensors are based on oxidase enzymes, which employ oxygen as a co-substrate to generate hydrogen peroxide (**Scheme 1-1**). The electrons are then transferred to an acceptor, enabling colorimetric and/or amperometric detection. Today most commercially available glucose sensors are of the second generation.[43] In a colorimetric version of the detection method: an oxidoreductase enzyme oxidizes glucose to gluconolactone; electrons from glucose are then transferred to an oxidized form of a mediator molecule, thereby converting it to a reduced form; this mediator in turn delivers the electrons to a redox indicator molecule, which in turn forms colour.

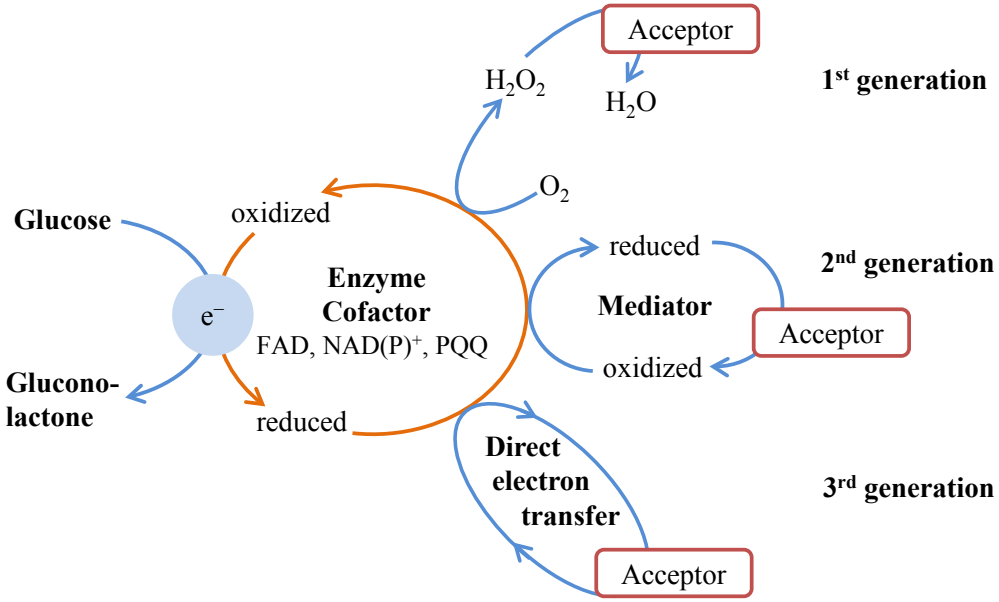

Scheme 1-1 Enzymatic detection of glucose. Electrons from the glucose oxidation reaction are first taken up by the enzyme's cofactor and then transferred to either oxygen (first generation), or the artificial mediator (second generation), or directly to the acceptor (third generation). The acceptor is ether an electrode or a redox indicator.

The redox indicators show a bathochromic shift (a change of spectral band position in the absorption spectrum to a longer wavelength) upon reduction. The indicators commonly used in the test strips are phosphomolybdic acids (PMO)[44] or tetrazolium salts (MTT, WST *etc*).[45-46] Both are not directly reduced by the enzyme, instead they require a mediator compound.

Artificial mediators were one of the key breakthroughs, which took glucose biosensors forward and allowed them for home testing of blood glucose. The mediator is usually a small organic molecule or an enzyme capable of existing in both an oxidized and a reduced form, and it reacts quickly to donate or receive electrons.[47] Examples of mediators commonly used in photometric glucose test strips are nitrosoanilines,[48] phenazines[49] or diaphorase.[50]

The main enzymes used in commercial glucose test strips are glucose oxidase (GOx) or glucose dehydrogenases (GDH). These enzymes are coupled to a cofactor (**Figure 1.4**), such as flavin adenine dinucleotide (FAD), nicotinamide adenine dinucleotide (NAD^+), or pyrrolo-quinoline quinine (PQQ).[29]

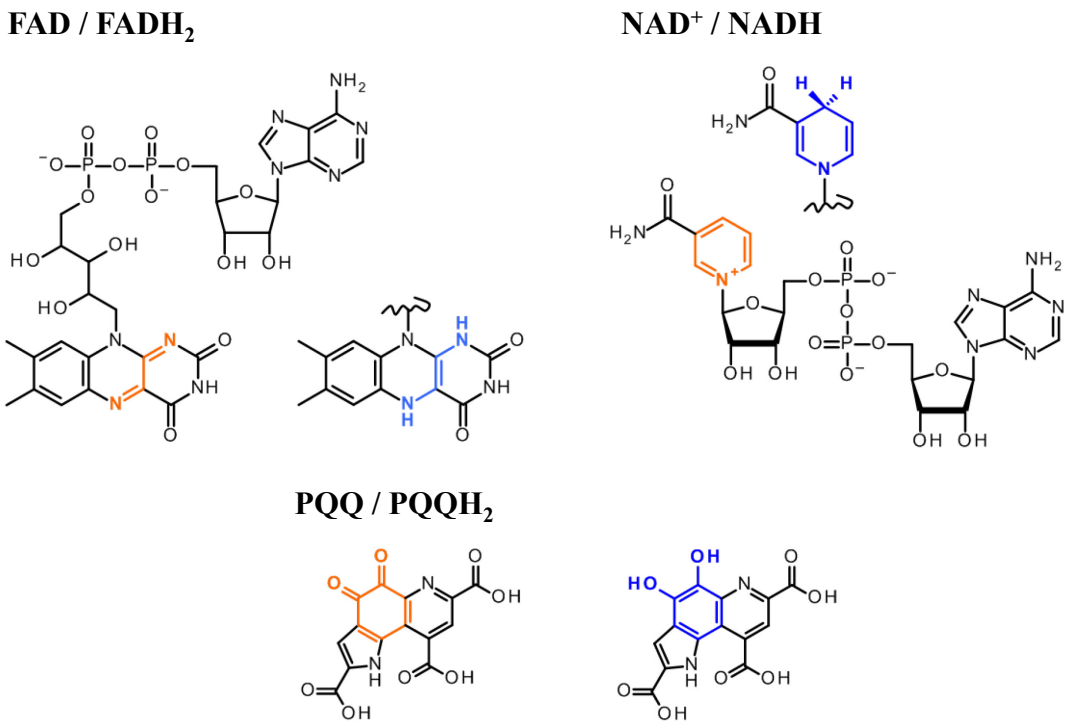

Figure 1.4 Cofactors used by GOx and GDHs. The structures of FAD, PQQ, and NAD are shown in their oxidized state. Regions that undergo reduction are in orange, with the reduced form drawn nearby, redox active sites are marked with blue colour.

Modern photometric test strips achieve the required sensitivity and selectivity. The test strip chemistry has good shelf-life stability under normal storage conditions. However, it is essential for the companies to further improve robustness of the strips.[51] In order to achieve longer shelf-life, their storage and distribution should include protection from moisture, freezing, excessive heat and from light. The test strips are usually packaged in containers with desiccant materials, incorporated into the cap of the container, to prevent undesired exposure to moisture from the environment. However, this method has not been effective for eliminating the risks of sensor degradation due to faulty storage by the patient. It often happens, that users forget to reseal the container between uses or leave test strips inside a parked car on a sunny day (light and high temperature) or in a bathroom (high humidity). Another known measure is the use of a deliquescent material in the chemical matrix to decrease the sorption of water in the material. Both methods increase production costs. It is disadvantageous for low-income countries. For example in tropical climate zones, the storage often has to be carried out under harsh conditions (high temperature and humidity).[52]

In the past years considerable effort has been done to develop enzymes with improved stability for diagnostic purposes.[29, 53-54] However, the mediators and/or redox indicators used in the test strips generally react sensitively to extreme storage conditions, and are degraded over time.[51] This circumstance certainly affects accuracy of the measurement. In the case of SMBG, inaccurate results can be easily overlooked and may even cause clinical risk to the patient.

The development of a new redox indicator, accepting electrons directly from an enzyme, will lead to a simpler colorimetric technique and therefore lower cost. This is the so called third-generation glucose biosensor (**Scheme 1-1**).[22] Until now only a few cases have been reported where enzymes transfer electrons directly to an indicator for photometric detection.[55-57] The elegance of the solution, in developing a novel system with a reagent combining both functions of the mediator and the chromogenic agent, would possibly allow storage and worldwide shipping at ambient temperature, securing analytical performance of the enzyme-linked assays.

1.5 In a search for an ideal glucose converting enzyme

When searching for an enzyme for diagnostic purposes, such as glucose measurements, one of the most important parameters is substrate specificity. Relying on an enzyme that recognizes also saccharides other than glucose (such as mannose, maltose, D-galactose, and D-xylose) would lead to an overestimation of glucose levels in blood and result in incorrect therapeutic decisions. In addition, stability of the enzyme is also an important factor, as its inactivation during storage would also result in inaccurate and inconsistent measurements. Luckily, a multitude of different enzymatic systems derived from bacterial and fungal microorganisms are now available on the market. Ferri *et al* gave a good overview of the present knowledge on redox enzymes currently utilized in commercially available glucose monitoring systems.[29]

Glucose oxidase

Glucose oxidase (FAD-GOx, EC 1.1.3.4) is the "gold standard" enzyme used in commercial glucose sensors. FAD molecule binds to the active sites of this enzyme, forming the adduct (FAD-GOx), which is reduced to $FADH_2$-GOx by glucose. The enzyme normally returns to its active oxidized state by transferring the electrons to molecular oxygen, resulting in the production of hydrogen peroxide.

$$glucose + FAD - GOx \rightarrow gluconolactone + FADH_2 - GOx$$

$$FADH_2 - GOx + O_2 \rightarrow FAD - GOx + H_2O_2$$

Stable FAD-GOx is commercially available at low cost and seems to be advantageous in terms of sugar specificity.[58] However, the natural second substrate of this enzyme is oxygen. Consequently, for the same patient, glucose measures of venous, capillary, and arterial blood, would give different values because of various oxygen content. To this account, natural or artificial mediators were proposed to re-oxidize $FADH_2$-GOx. Obviously, the redox indicators would also have to compete with oxygen for the electrons from $FADH_2$-GOx.[59] As an alternative to GOx, GDH family of enzymes brought our attention.

Pyrroloquinoline quinone glucose dehydrogenase

PQQ-dependent GDH (PQQ-GDH, EC 1.1.5.2) is a dimeric enzyme composed of two identical protein monomers with each monomer binding PQQ molecule and three calcium ions. One of the three calcium ions activates the PQQ cofactor. The oxidation mechanism of glucose by PQQ-GDH is similar to that of FAD-GOx with the exception that the reduced form ($PQQH_2$-GDH) is not oxidized by O_2.

$$glucose + PQQ - GDH \rightarrow gluconolactone + PQQH_2 - GDH$$

PQQ-GDH is a particularly efficient enzymatic system, with a rapid electron transfer rate. However, native PQQ-GDH oxidizes also a variety of saccharides such as mannose, maltose and lactose, *etc.* In August of 2009, the US FDA agency's public health notification stated that the PQQ-GDH based sensors can cause potentially fatal errors in the glucose measurements in patients on medications which contain nonglucose sugars. Therefore, FDA recommended the public and healthcare facilities to avoid PQQ-GDH based glucose test strips, which were used by many commercial glucose meters.[60]

Intensive work has been dedicated to improve the specificity of PQQ-GDH. From the patent literature,[61] it is known that mutations have been used to reduce interferences to below 2% of the native enzyme.

Flavin adenine dinucleotide dependent glucose dehydrogenases

The FAD-dependent GDHs (FAD-GDH, EC 1.1.99.10) have received much attention for their potential applications in sensor development. These enzymes combine the oxygen independence of PQQ-GDH with the high specificity of GOx toward glucose. Moreover FAD-GDHs utilize a variety of external electron acceptors.[62]

Bacterial FAD-GDH is a thermostable hetero-oligomeric enzyme complex made up of a catalytic subunit harboring FAD in its redox center, a multiheme cytochrome-complex

electron-transfer subunit, and a chaperone-like subunit required for proper folding and secretion of catalytic subunit. Although the catalytic subunit alone shows high catalytic activity, the electron-transfer subunit facilitates the transfer of electrons between the active-site cofactor and the artificial electron acceptors, giving this enzyme a catalytic activity similar to or even higher than that of PQQ-GDH. Bacterial FAD-GDH's unique direct electron transfer ability makes this enzyme an interesting candidate for the third generation glucose sensors.[63] Although sensors employing bacterial FAD-GDH are on the market, the enzyme is not commercially available.

Fungi derived FAD-GDH was successfully expressed in *E. coli* and, despite not having their native glycosylation, showed GDH activity and a high specificity for glucose. Diagnostic reagent-grade fungal FAD-GDH is commercially available.

FAD-GDH enzymes have only a single active center.[63] An ordered sequence of reactions is necessary to transfer the electrons from glucose to an external electron acceptor, before another molecule of glucose could be again oxidized to gluconolactone. The transfer of electrons from a reduced state ($FADH_2$-GDH) to the acceptor is the rate limiting step in the reaction. Also mediator inhibition phenomena have been reported for FAD-GDH.[23]

Nicotinamide adenine dinucleotide (phosphate) dependent glucose dehydrogenase

$NAD(P)^+$-dependent GDH ($NAD(P)^+$-GDH, EC 1.1.1.47) is different from the aforementioned dehydrogenases. The mechanism of catalysis also involves the binding of an oxidized cofactor and glucose. However, after an electron transfer from glucose, the ordered release of gluconolactone is followed by the cofactor — after reduction, NAD(P)H is not bound to the enzyme.[53]

$$glucose + NAD(P)^+ \rightarrow gluconolactone + NAD(P)H + GDH$$

$NAD(P)^+$ cofactors are abundant and inexpensive substrates, and they demonstrate very high activity up to 550 U/mg with GDH. In addition, the enzymatic oxidation of glucose is not reversible, due to the spontaneous hydrolysis of gluconolactone.[64]

NAD(P)H is produced first-hand depending on glucose concentration. The interaction with the artificial electron acceptors is a non-enzymatic one, and thus an inhibition of the enzymatic reaction is not expected. This makes $NAD(P)^+$-GDH a very attractive enzyme for potential application in glucose assays in combination with the proposed redox indicator.

1.6 Chemistry

We chose NAD(P)$^+$-dependent GDH to develop a simplified assay for optical determination of blood glucose on the test strip. The glucose detection mechanism is shown in **Scheme 1-2A**. This involves an ordered binding of cofactor NAD(P)$^+$ and glucose, followed by a release of glucono-*δ*-lactone and reduced NAD(P)H. The reduced cofactor then transfers electrons to the redox indicator. The reduction induces a shift of the absorbance band to a longer wavelength in the visible range (**Scheme 1-2B**). Hence, a remarkable change in the absorbance strength could be observed. This could be conveniently monitored by UV-Vis spectroscopy (**Scheme 1-2B**) and even observed by the naked eyes (**Scheme 1-2C**). The increase in absorbance corresponds to an increase of glucose concentration in a sample.

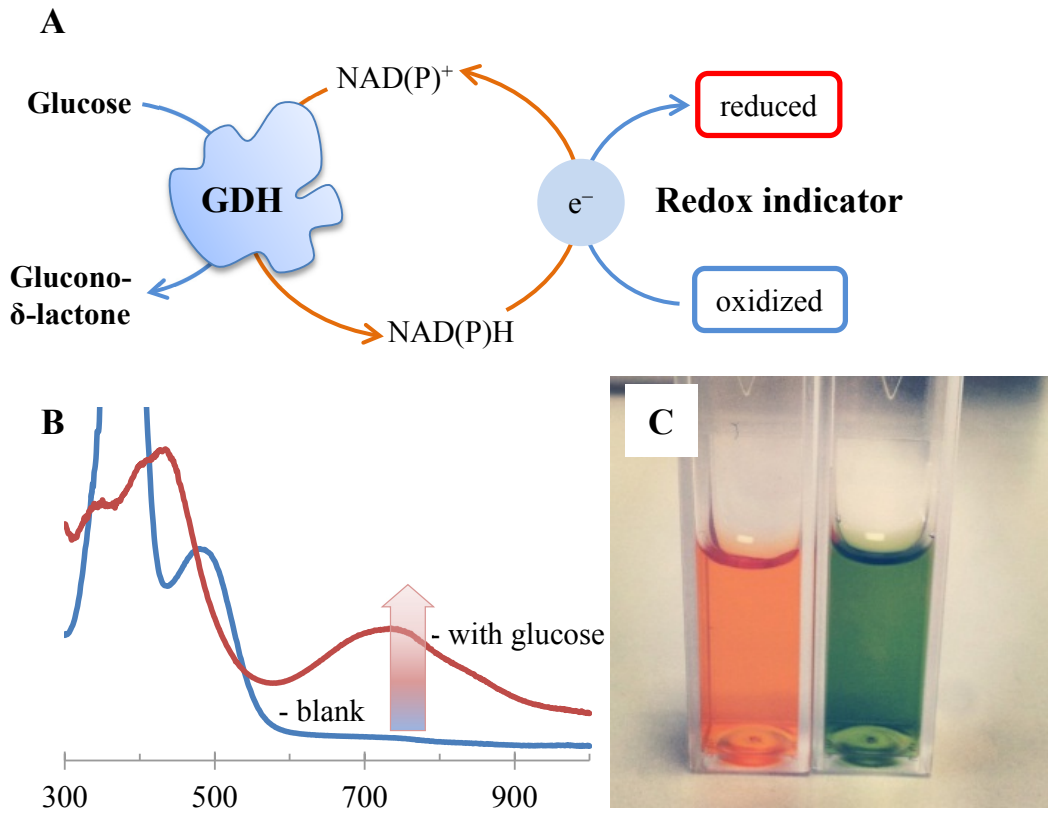

Scheme 1-2 Colour forming reaction of a redox indicator in the presence of glucose. **A** — The NAD(P)H can be generated from NAD(P)$^+$ by oxidation of a glucose catalyzed by GDH; **B** — UV-Vis spectra example of oxidized (blue) and reduced (red) forms of a redox indicator; **C** — Colour forming reaction can be observed by naked eyes: a solution of a redox indicator before (left) and after (right) glucose addition.

In principle, the amount of NAD(P)H formed according to **Scheme 1-2** can be directly followed at 340 nm. However, the sensitivity of NAD(P)H-coupled assays is not high, due to their low extinction coefficient.[65] A number of optical NAD(P)H sensors has been previously proposed, which include noble metal (*e.g.* Au and Ag)

nanoparticles(NPs),[55, 57, 66-68] quantum dots (QDs)[56-57] and genetically-encoded glucose sensing enzymes.[69-70] However, these sensors require from minutes to hours for analysis making them unsuitable for SMBG test strips. Moreover, their implementation in dry chemistry is difficult.

An elegant alternative would be the use of a small organic molecule, where electrons could be directly transferred from NAD(P)H, causing a colorimetric signal at longer wavelengths. Molecules able to oxidize NAD(P)H had been previously reported;[48, 71-77] but the majority of them do not show a bathochromic shift upon reduction. Examples of redox indicators showing the desired colorimetric response are nitrosoaniline[48] and quinone[77] derivatives. The drawback of these compounds is the low extinction coefficient of their reduced forms. A very well-known redox indicator is phosphomolybdic acid (PMO). This compound however has the disadvantage that the redox states are not well defined and the reduced form of PMO tends to have multiple broad absorption lines.[78] Moreover, PMO is only slowly reduced by NADH, therefore a mediator has to be used.[44] Tetrazolium salts[79] and resazurin[80-81] are used as redox indicators as well, but these compounds are not very stable and also require the use of a mediator like 5-methylphenazine methosulfate (PMS) or diaphorase to work in presence of dehydrogenases.

It is therefore still necessary to design an easy to obtain and efficient indicator for NAD(P)H. Several parameters have to be considered.

Dry chemistry

Typical coating formulations are described in patent literature.[82-85] Common components of the chemistry layer include reactive ingredients (*e.g.* enzymes, cofactors, indicators *etc*), dispersants, organic fillers, mineral fillers, pigments, surfactants, pH modifiers, buffer agents, viscosity modifiers, stabilizers, defoamers, flow modifiers *etc.*

Roche employs a blade coating technique to place a detection film on a plastic strip, which is followed by a drying process. Short intensive drying (50–85°*C*, 15 min) is advantageous to avoid denaturation of the enzyme and unwanted pre-reactions of the mediator and the indicator. The enzyme survives well in the drying process. The critical phase is the time when temperature rises towards the end of drying process, when a little water is present. This phase can be made as short as a few seconds. The product of this process is a dry detection layer, which is then processed into individual test strips.[23]

The reactive ingredients are also able to work in classical wet analytics. However, there are obviously differences compared to an analytical test running in a solution. Preparation of test strip compositions is a rather complex technological process; hence such experiments in laboratory are time-consuming, tedious, and costly. To demonstrate feasibility of our strategy, it would be more convenient to investigate new redox indicators for optical monitoring of glucose in a solution.

Enzyme

A mutant of NAD(P)$^+$-GDH suitable for applications in the test strips was identified by previous investigators at Roche.[85] Double mutant of GDH (E170K/Q252L = GlucDH2) from *Bacillus subtilis* is able to provide extraordinary catalytic performance: it has a high affinity to glucose under ambient conditions of pH and temperature,[86] as in solution and in the dry chemistry.[84] GlucDH2 from *Bacillus subtilis* has an isoelectric point of 4.7–4.8, relative molecular weight (MW) of 126 kDa and is comprised of four subunits of MW 31.5 kDa each.

Baik *et al* discovered the role of residues Q252L and E170K for GDH stabilization. Assisted by crystal structures from the wild-type and mutant GDHs from *Bacillus megaterium* IWG3,[87-88] Baik *et al* determined that a cooperative effect between Q252L and E170K stabilizes the tetramer structure by strengthening the hydrophobic interactions within the interface. Eduardo Vazquez-Figueroa *et al* demonstrated improvement in stability of GlucDH2 from *B. subtilis* in comparison to the wild-type GDH: from *ca.* 20 min at 25°*C* to *ca.* 3.5 days at 65°*C*, a 10^6-fold improvement. The enzyme shows a pH optimum at 8.0, and a broad activity range in pH 6.0–10.5. To assure its functionality an NAD(P)$^+$ cofactor needs to be present (**Figure 1.5**).[86]

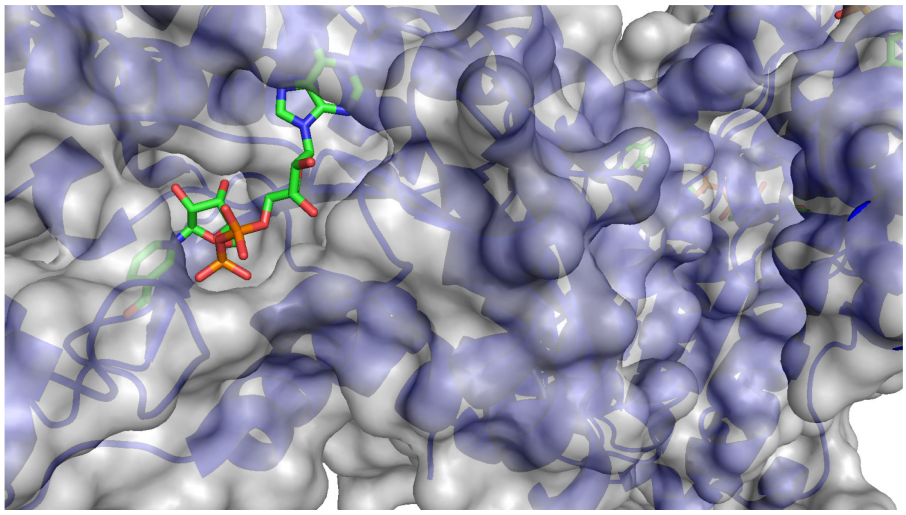

Figure 1.5 Crystal structure IWG3 of the GlucDH2 enzyme with a close-up of the region harbouring NAD$^+$.

Coenzyme

Out of two natural cofactors, only the NAD^+ cofactor has been commonly utilized in the test strip chemistry. The long-term stability of NAD^+ in dry test turned out to be restricted. Luckily, its stable analogue — carba nicotinamide adenine dinucleotide ($cNAD^+$) — has proven to be a conceivable alternative as the co-enzyme for enzymatic reactions with GDH on the test strips.[89-90] In $cNAD^+$, the 2,3-hydroxycyclopentane ring replaces the *β*-D-ribonucleotide ring (**Figure 1.6**).

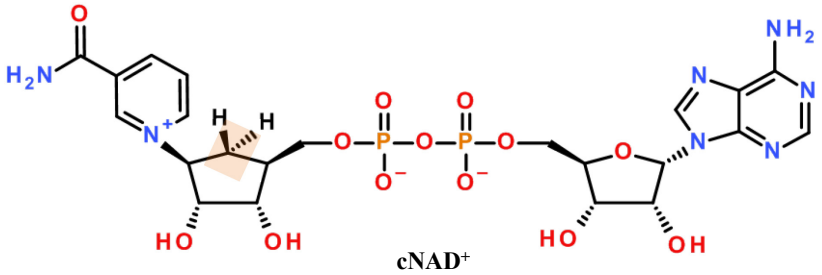

Figure 1.6 Structure of Carba-NAD.

As the result, $cNAD^+$ is more stable concerning hydrolytic cleavage than NAD^+. Furthermore, $cNAD^+$ in combination with GlucDH2 is a rapid, selective and robust system for quantitative determination of glucose.[84-85]

Effect of pH

Enzyme activity is always affected by several parameters, the pH of the solution being one of them. To our best knowledge, the full pH-activity profile of GlucDH2 was not reported previously. For other characterized GDH enzymes from *Bacillus subtilis*, an optimal pH in a neutral to slightly alkaline pH is described.[64, 91-92]

The oxidized cofactor (NAD^+) has long been known to be unstable toward basic conditions, as NAD^+ hydrolysis rate dramatically increases above pH 8.0.[93-94] Several publications describe the catalytic decomposition of the reduced cofactor (NADH) as a function of pH and temperature.[93, 95-96] Wu and co-workers reported that NADH is undergoing rapid hydration below pH 6.[95] In addition, a number of reports described that electron acceptors for NADH often have lower stability at alkaline pHs.[97-99] It is also known that the mechanism of NADH oxidation by electron accepting molecules could be affected by pH.[73]

Optimum pH for the assay is a combination of kinetic parameters for the enzymatic oxidation of glucose, and further electron transfer from NADH to an acceptor molecule. Moreover, the assay reagents should be stable both under storage conditions and within the test. We chose pH in the range of 6.0–8.0 for further studies.

Salt concentration

Most GDH variants are stabilized with increased NaCl concentration. In addition, the enzymes are well compatible with positively charged small organic electron acceptors (*e.g.* phenazines), also in high concentrations.[100]

Effect of temperature

The rate of enzymatic glucose detection can be increased by raising temperature, with a corresponding increase in sensitivity. However, blood glucose monitoring is usually carried out at ambient temperature.

Blood composition and interferences

The components of serum are very complex, which often interferes with blood glucose sensing.[30] Serum contains various amino acids, peptides, proteins, carbohydrates, vitamins *etc*. The selectivity of a glucose biosensor depends on two major factors: the enzyme–substrate reaction and the following reaction to generate a signal. The enzyme–substrate reaction is very specific due to the nature of enzyme functionality. GDH can only react with glucose without any substantial interference from other types of sugars. However, there are other possible interferences in enzymatic glucose determination, such as reducing species in blood (ascorbic acid and glutathione) and nucleophiles (*e.g.* cysteine and lysine). Such substances could provoke a non-enzymatic reduction of a redox indicator. The blood samples, especially those from patients under specialized treatment in hospitals, may contain up to 5 mM of ascorbic acid.[101] Plasma glutathione levels are typically in micromolar range.[102]

Wavelength consideration

Absorbance maxima for NADH and cNADH are found at 340 nm and 360 nm, respectively. The extinction coefficient of cNADH equals that of NADH and amounts to 6.22 $mM^{-1}cm^{-1}$. The direct monitoring is limited due to interferences by other chromogenic species in blood, because the sensitivity of NADH-coupled tools is low.[65]

One of the most important components of blood is haemoglobin. It can be found in two forms, deoxygenated (Hb) and oxygenated (HbO_2). The absorption spectrum is different in these two types: HbO_2 has two maxima at 541 nm and 577 nm within the visible range, while Hb has only one peak at 555 nm. Longwave sensing is highly desirable in view of the strong intrinsic absorbance and fluorescence of serum.[31, 103]

1.7 A tailor made redox indicator

Considerations in a search for a tailor made indicator include water-solubility, rate of reaction with NADH, stability in mixtures with enzymes, redox potential, interferences (mainly with ascorbic acid), availability and cost, and intellectual property rights. The rate of the reaction with NADH is the key parameter, because the fastest assays are now completed in five seconds. An oxidized form of the indicator should be nearly colourless, and a reduced form should have an absorption band at longer wavelengths (preferably more than 600 nm). It would help to minimize the interference from background absorbance of blood or serum samples. Otherwise, the chromophore should have an extinction value significantly higher than of the reduced coenzymes ($6.22\ mM^{-1}cm^{-1}$). This would allow the assay to achieve better sensitivity than the direct spectrophotometric measurement of NADH or cNADH, at 339 and 360 nm, respectively. For the application on the test strips, the desired indicator should be compatible with aqueous buffer solutions. In addition, the best electron acceptors for NADH, from a prior state of art, commonly utilize a positive charge at the redox centres. The above mentioned considerations provided a basis for the design of a new NADH indicator.

1.8 Aims of the study

The overall aim of the study was to design and synthesize new redox indicators and evaluate their possible application for glucose sensing on a dry chemistry test strip. The study was focused on the development of a small organic indicator for NADH detection *via* enzymatic redox reactions.

More specifically, the aims were:

I To design and synthesize new redox indicators compatible with aqueous buffer solutions, and to evaluate their spectral properties in an oxidized and reduced form.

II To investigate new compounds for optical NADH sensing *via* direct electron transfer.

III To explore the use of such indicators in a GlucDH2-coupled enzymatic assay of glucose.

IV To demonstrate application of this assay in blood glucose test strips.

1.9 References

[1] K. Laios, M. Karamanou, Z. Saridaki, G. Androutsos. Aretaeus of Cappadocia and the first description of diabetes. *Hormones* **2012**, *11*, 109-113.

[2] D. R. Owens. History and Vision: What is Important for Patients with Diabetes? *Diabetes Technol. Ther.* **2008**, *10*, S-5-S-9.

[3] L. Rosenfeld. Insulin: Discovery and Controversy. *Clin. Chem.* **2002**, *48*, 2270-2288.

[4] H. Dominiczak Marek. Linking Research and Innovative Clinical Practice: The Story of Diabetes Mellitus. *Clin. Chem. Lab. Med.* **2003**, *41*, 1104–1106.

[5] K. G. M. M. Alberti, P. f. Zimmet. Definition, diagnosis and classification of diabetes mellitus and its complications. Part 1: diagnosis and classification of diabetes mellitus. Provisional report of a WHO consultation. *Diabetic Med.* **1998**, *15*, 539-553.

[6] D. Daneman. Type 1 diabetes. *The Lancet*, *367*, 847-858.

[7] S. E. Inzucchi, R. M. Bergenstal, J. B. Buse, M. Diamant, E. Ferrannini, M. Nauck, A. L. Peters, A. Tsapas, R. Wender, D. R. Matthews. Management of Hyperglycemia in Type 2 Diabetes: A Patient-Centered Approach: Position Statement of the American Diabetes Association (ADA) and the European Association for the Study of Diabetes (EASD). *Diabetes Care* **2012**, *35*, 1364-1379.

[8] Frances M. Ashcroft, P. Rorsman. Diabetes Mellitus and the β Cell: The Last Ten Years. *Cell* **2012**, *148*, 1160-1171.

[9] J. P. Crandall, W. C. Knowler, S. E. Kahn, D. Marrero, J. C. Florez, G. A. Bray, S. M. Haffner, M. Hoskin, D. M. Nathan. The prevention of type 2 diabetes. *Nat. Clin. Pract. End. Met.* **2008**, *4*, 382-393.

[10] S. Garg, I. B. Hirsch. Self-monitoring of blood glucose. *Int. J. Clin. Pract.* **2010**, *64*, 1-10.

[11] International Diabetes Federation. IDF Diabetes Atlas update poster, 6th edn. Brussels, Belgium: International Diabetes Federation, 2014.

[12] T. Scully. Diabetes in numbers. *Nature* **2012**, *485*, S2-S3.

[13] International Diabetes Federation. Global Diabetes Plan 2011-2021. Brussels: IDF, **2011**. Available online: http://www.idf.org/sites/default/files/Global_Diabetes_Plan_Final.pdf (accessed on 26 October 2015).

[14] World Health Organization. Definition and diagnosis of diabetes mellitus and intermediate hyperglycaemia: report of a WHO/IDF consultation. Geneva (Switzerland): WHO, **2006**. Available online: http://www.who.int/diabetes/publications/Definition%20and%20diagnosis%20of%20diabetes_new.pdf (accessed on 26 October 2015).

[15] L. Ratheau, N. Jeandidier, F. Moreau, S. Sigrist, M. Pinget. How technology has changed diabetes management and what it has failed to achieve. *Diabetes Metab.* **2011**, *37 Suppl 4*, S57-64.

[16] H. Pollack. Stanley Rossiter Benedict: Creator of Laboratory Tests for Glycosuria. *Diabetes* **1953**, *2*, 420-421.

[17] S. F. Clarke, J. R. Foster. A history of blood glucose meters and their role in self-monitoring of diabetes mellitus. *Br J Biomed Sci* **2012**, *69*, 83-93.

[18] P. Voswinckel. A marvel of colors and ingredients. The story of urine test strip. *Kidney Int Suppl* **1994**, *47*, S3-7.

[19] S. Walford, E. A. M. Gale, S. P. Allison, R. B. Tattersall. Self-monitoring of blood-glucose. Improvement of diabetic control. *The Lancet* **1978**, *311*, 732-735.

[20] R. J. Jarrett, H. Keen, C. Hardwick. "Instant" Blood Sugar Measurement Using Dextrostix and a Reflectance Meter. *Diabetes* **1970**, *19*, 724-726.

[21] M. A. Genshaw, W. I. White. Glucose indicator and method. U.S. Patent 4,211,845 A, 24 November 1978.

[22] E.-H. Yoo, S.-Y. Lee. Glucose Biosensors: An Overview of Use in Clinical Practice. *Sensors* **2010**, *10*, 4558-4576.

[23] J. Hönes, P. Müller, N. Surridge. The technology behind glucose meters: test strips. *Diabetes Technol. Ther.* **2008**, *10*, S-10-S-26.

[24] V. Scognamiglio. Nanotechnology in glucose monitoring: Advances and challenges in the last 10 years. *Biosens. Bioelectron.* **2013**, *47*, 12-25.

[25] M. D. Hughes. The Business of Self-Monitoring of Blood Glucose: A Market Profile. *J. Diabetes Sci. Technol.* **2009**, *3*, 1219-1223.

[26] International Organization for Standardization . Geneva: International Organization for Standardization; 2013. ISO 15197:2013: In vitro diagnostic test systems -- requirements for blood-glucose monitoring systems for self-testing in managing diabetes mellitus.

[27] M. Link, C. Schmid, S. Pleus, A. Baumstark, D. Rittmeyer, C. Haug, G. Freckmann. System Accuracy Evaluation of Four Systems for Self-Monitoring of Blood Glucose Following ISO 15197 Using a Glucose Oxidase and a Hexokinase-Based Comparison Method. *J. Diabetes Sci. Technol.* **2015**.

[28] K. Tonyushkina, J. H. Nichols. Glucose Meters: A Review of Technical Challenges to Obtaining Accurate Results. *J. Diabetes Sci. Technol.* **2009**, *3*, 971-980.

[29] S. Ferri, K. Kojima, K. Sode. Review of Glucose Oxidases and Glucose Dehydrogenases: A Bird's Eye View of Glucose Sensing Enzymes. *J. Diabetes Sci. Technol.* **2011**, *5*, 1068-1076.

[30] H. A. Krebs. Chemical Composition of Blood Plasma and Serum. *Annu. Rev. Biochem.* **1950**, *19*, 409-430.

[31] O. S. Wolfbeis, M. Leiner. Mapping of the total fluorescence of human blood serum as a new method for its characterization. *Anal. Chim. Acta* **1985**, *167*, 203-215.

[32] A. K. Yetisen, in Holographic Sensors, Springer International Publishing, **2015**, pp. 1-25.

[33] S. A. Soper, K. Brown, A. Ellington, B. Frazier, G. Garcia-Manero, V. Gau, S. I. Gutman, D. F. Hayes, B. Korte, J. L. Landers, D. Larson, F. Ligler, A. Majumdar, M. Mascini, D. Nolte, Z. Rosenzweig, J. Wang, D. Wilson. Point-of-care biosensor systems for cancer diagnostics/prognostics. *Biosens. Bioelectron.* **2006**, *21*, 1932-1942.

[34] L. Gervais, N. de Rooij, E. Delamarche. Microfluidic Chips for Point-of-Care Immunodiagnostics. *Adv. Mater.* **2011**, *23*, H151-H176.

[35] F. B. Myers, L. P. Lee. Innovations in optical microfluidic technologies for point-of-care diagnostics. *Lab Chip* **2008**, *8*, 2015-2031.

[36] G. Comina, A. Suska, D. Filippini. Autonomous Chemical Sensing Interface for Universal Cell Phone Readout. *Angew. Chem. Int. Ed.* **2015**, n/a-n/a.

[37] V. Gubala, L. F. Harris, A. J. Ricco, M. X. Tan, D. E. Williams. Point of Care Diagnostics: Status and Future. *Anal. Chem.* **2012**, *84*, 487-515.

[38] A. W. Martinez, S. T. Phillips, M. J. Butte, G. M. Whitesides. Patterned Paper as a Platform for Inexpensive, Low-Volume, Portable Bioassays. *Angew. Chem. Int. Ed.* **2007**, *46*, 1318-1320.

[39] A. W. Martinez, S. T. Phillips, G. M. Whitesides. Three-dimensional microfluidic devices fabricated in layered paper and tape. *Proc. Natl. Acad. Sci.* **2008**, *105*, 19606-19611.

[40] Y. Xia, J. Ye, K. Tan, J. Wang, G. Yang. Colorimetric visualization of glucose at the submicromole level in serum by a homogenous silver nanoprism-glucose oxidase system. *Anal. Chem.* **2013**, *85*, 6241-6247.

[41] L. Shen, J. A. Hagen, I. Papautsky. Point-of-care colorimetric detection with a smartphone. *Lab Chip* **2012**, *12*, 4240-4243.

[42] A. W. Martinez, S. T. Phillips, E. Carrilho, S. W. Thomas, H. Sindi, G. M. Whitesides. Simple Telemedicine for Developing Regions: Camera Phones and Paper-Based Microfluidic Devices for Real-Time, Off-Site Diagnosis. *Anal. Chem.* **2008**, *80*, 3699-3707.

[43] R. Tirimacco, G. Koumantakis, R. Erasmus, A. Mosca, S. Sandberg, D. Watson Ian, B. Goldsmith, P. Gillery. Glucose meters – fit for clinical purpose. *Clin. Chem. Lab. Med.* **2013**, *51*, 943.

[44] J. Hoenes, H. Wielinger, V. Unkrig. Use of a sparingly soluble salt of a heteropoly acid for the determination of an analyte, a corresponding method of determination as a suitable agent therefor. U.S. Patent 5,240,860 A, 2 December 1989.

[45] M. Ishiyama, Y. Miyazono, K. Sasamoto, Y. Ohkura, K. Ueno. A highly water-soluble disulfonated tetrazolium salt as a chromogenic indicator for NADH as well as cell viability. *Talanta* **1997**, *44*, 1299-1305.

[46] A. Zhu, R. Romero, H. R. Petty. An enzymatic colorimetric assay for glucose-6-phosphate. *Anal. Biochem.* **2011**, *419*, 266-270.

[47] A. Heller, B. Feldman. Electrochemical Glucose Sensors and Their Applications in Diabetes Management. *Chem. Rev.* **2008**, *108*, 2482-2505.

[48] J. Hoenes, V. Unkrig. Colorimetric determination of an analyte using benzyl alcohol dehydrogenase and a chromogenic redox-indicator. U.S. Patent 5,445,943 A, 8 April 1993.

[49] C. D. Wilsey, M. Ghoshal, H. Wieder. Matrix composition with alkylphenazine quaternary salt and a nitrosoaniline. U.S. Patents 8,008,037 B2, 27 March 2008.

[50] X. Gao, X. Li, Q. Wan, Z. Li, H. Ma. Detection of glucose via enzyme-coupling reaction based on a DT-diaphorase fluorescence probe. *Talanta* **2014**, *120*, 456-461.

[51] S. Duvall, S. Kachel, G. C. Lica, W. Schabel, P. Scharfer. Improved matrix stability compositions and methods. WO2014/037372 A1, Sep. 6, 2012.

[52] M. Ducorps, L. Papoz, J. C. Cuisinier-Raynal, D. Simon. Reliability of glucose measurement by glucose test strips in tropical conditions. *Diabetes Res. Clin. Pract.* **1992**, *17*, 51-54.

[53] A. Basner, G. Antranikian. Isolation and Biochemical Characterization of a Glucose Dehydrogenase from a Hay Infusion Metagenome. *PLoS ONE* **2014**, *9*, e85844.

[54] H. Aiba, Y. Nishiya, M. Azuma, Y. Yokooji, H. Atomi, T. Imanaka. Characterization of a thermostable glucose dehydrogenase with strict substrate specificity from a hyperthermophilic archaeon Thermoproteus sp. GDH-1. *Biosci., Biotechnol., Biochem.* **2015**, 1-9.

[55] L. Zhang, Y. Li, D. W. Li, C. Jing, X. Chen, M. Lv, Q. Huang, Y. T. Long, I. Willner. Single gold nanoparticles as real-time optical probes for the detection of NADH-dependent intracellular metabolic enzymatic pathways. *Angew. Chem.* **2011**, *50*, 6789-6792.

[56] R. Freeman, R. Gill, I. Shweky, M. Kotler, U. Banin, I. Willner. Biosensing and Probing of Intracellular Metabolic Pathways by NADH-Sensitive Quantum Dots. *Angew. Chem.* **2009**, *121*, 315-319.

[57] L. Bahshi, R. Freeman, R. Gill, I. Willner. Optical Detection of Glucose by Means of Metal Nanoparticles or Semiconductor Quantum Dots. *Small* **2009**, *5*, 676-680.

[58] R. Wilson, A. P. F. Turner. Glucose oxidase: an ideal enzyme. *Biosens. Bioelectron.* **1992**, *7*, 165-185.

[59] T. Semashko, R. Mikhailova, A. Ramanaviciene, A. Ramanavicius. Specificity of Glucose Oxidase from Penicillium funiculosum 46.1 Towards Some Redox Mediators. *Appl. Biochem. Biotechnol.* **2013**, *171*, 1739-1749.

[60] U.S. Food and Drug Administration. FDA public health notification: potentially fatal errors with GDH-PQQ glucose monitoring technology. Available online: http://www.fda.gov/MedicalDevices/Safety/AlertsandNotices/PublicHealthNotifications/ucm176992.htm (accessed on 26 October 2015).

[61] M. Boenitz-Dulat, D. Beck, P. Kratzsch, R. Schmuck, H. von der Eltz. Mutants of pyrroloquinoline quinone dependent soluble glucose dehydrogenase. U.S. Patent 2009/0148874 A1, 13 April 2006.

[62] K. Mori, M. Nakajima, K. Kojima, K. Murakami, S. Ferri, K. Sode. Screening of Aspergillus-derived FAD-glucose dehydrogenases from fungal genome database. *Biotechnol. Lett* **2011**, *33*, 2255-2263.

[63] M. N. Zafar, X. Wang, C. Sygmund, R. Ludwig, D. Leech, L. Gorton. Electron-Transfer Studies with a New Flavin Adenine Dinucleotide Dependent Glucose Dehydrogenase and Osmium Polymers of Different Redox Potentials. *Anal. Chem.* **2012**, *84*, 334-341.

[64] A. Weckbecker, W. Hummel, in Microbial Enzymes and Biotransformations, *Vol. 17* (Ed.: J. Barredo), Humana Press, **2005**, pp. 225-238.

[65] A. von Ketteler, D.-P. Herten, W. Petrich. Fluorescence Properties of Carba Nicotinamide Adenine Dinucleotide for Glucose Sensing. *ChemPhysChem* **2012**, *13*, 1302-1306.

[66] L. Tang, X. Lei, G. Zeng, Y. Liu, Y. Peng, M. Wu, Y. Zhang, C. Liu, Z. Li, G. Shen. Optical detection of NADH based on biocatalytic growth of Au–Ag core–shell nanoparticles. *Spectrochim. Acta Mol. Biomol. Spectrosc.* **2012**, *99*, 390-393.

[67] S. Liu, Z. Du, P. Li, F. Li. Sensitive colorimetric visualization of dihydronicotinamide adenine dinucleotide based on anti-aggregation of gold nanoparticles via boronic acid-diol binding. *Biosens. Bioelectron.* **2012**, *35*, 443-446.

[68] B. Shlyahovsky, E. Katz, Y. Xiao, V. Pavlov, I. Willner. Optical and Electrochemical Detection of NADH and of NAD+-Dependent Biocatalyzed Processes by the Catalytic Deposition of Copper on Gold Nanoparticles. *Small* **2005**, *1*, 213-216.

[69] Y. Zhao, J. Jin, Q. Hu, H.-M. Zhou, J. Yi, Z. Yu, L. Xu, X. Wang, Y. Yang, J. Loscalzo. Genetically Encoded Fluorescent Sensors for Intracellular NADH Detection. *Cell Metab.* **2011**, *14*, 555-566.

[70] S. Siedler, G. Schendzielorz, S. Binder, L. Eggeling, S. Bringer, M. Bott. SoxR as a Single-Cell Biosensor for NADPH-Consuming Enzymes in Escherichia coli. *ACS Synth. Biol.* **2013**, *3*, 41-47.

[71] T. Yomo, I. Urabe, H. Okada. Electrostatic and redox potential effects on the rate of electron-transfer reaction of nicotinamide adenine dinucleotides with 1-substituted 5-ethylphenazines. *BBA - Bioenergetics* **1990**, *1017*, 139-142.

[72] C. J. F. Noorden, J. Tas. Advantages of 1-methoxyPMS as an electron carrier in dehydrogenase cytochemistry. *Histochem. J.* **1982**, *14*, 837-842.

[73] G. Hilt, T. Jarbawi, W. R. Heineman, E. Steckhan. An Analytical Study of the Redox Behavior of 1,10-Phenanthroline-5,6-dione, its Transition-Metal Complexes, and its N-Monomethylated Derivative with regard to their Efficiency as Mediators of NAD(P)+ Regeneration. *Chem. Eur. J.* **1997**, *3*, 79-88.

[74] B. Persson, L. Gorton. A comparative study of some 3,7-diaminophenoxazine derivatives and related compounds for electrocatalytic oxidation of NADH. *J. Electroanal. Chem. Interfacial Electrochem.* **1990**, *292*, 115-138.

[75] J. W. Bunting, A. W. C. Ng. Rates of Oxidation of 1-Benzyl-1,4-dihydronicotinamide by Pyrazinium, Quinoxalinium, and Phenazinium Cations. *Bioorg. Chem.* **1993**, *21*, 156-169.

[76] J. F. J. Engbersen, A. Koudijs, H. C. van der Plas. Reaction of NADH models with methylene blue. *Recl. Trav. Chim. Pays-Bas* **1985**, *104*, 131-138.

[77] D. Heindl, R. Herrmann, J. Hones, H.-P. Josel, M. Junius-Comer, H. Merdes, A. Schmidt, E. Selbertinger. Redox-active compounds and their use. U.S. Patent 6,057,120 A, Sep. 24, 1996.

[78] J. E. Going, S. J. Eisenreich. Spectrophotometric studies of reduced molybdoantimonylphosphoric acid. *Anal. Chim. Acta* **1974**, *70*, 95-106.

[79] J. P. Albarella, S. W. Felman, J. J. Landi, K. L. Marfurt. Water-soluble tetrazolium salts. U.S. Patent 7,767,822 B2, 14 January 2005.

[80] L. P. Candeias, D. P. S. MacFarlane, S. L. W. McWhinnie, N. L. Maidwell, C. A. Roeschlaub, P. G. Sammes, R. Whittlesey. The catalysed NADH reduction of resazurin to resorufin. *J. Chem. Soc., Perkin Trans. 2* **1998**, 2333-2334.

[81] A. Zhu, R. Romero, H. R. Petty. An enzymatic fluorimetric assay for glucose-6-phosphate: application in an in vitro Warburg-like effect. *Anal. Biochem.* **2009**, *388*, 97-101.

[82] W. R. Knappe, F. Wittmann, D. Mosoiu, C. Horn, J. Hoenes. Transparent support; quantitative analysis. U.S. Patent 2006/0003397 A1, Feb. 18, 2004.

[83] W. R. Knappe. Mediators for photometric tests and means and methods relating to use thereof. U.S. Patent 2008/0213808 A1, Sep. 4, 2008.

[84] W. Roedel, C. Horn, N. Steinke, N. Bucci, T. Meier, R. Schmuck, R. Nagel, D. Heindl. Stabilization of enzymes with stable coenzymes. U.S. Patent 2012/0276565 A1, Aug. 20, 2009.

[85] C. Horn, C. Gaessler-Dietsche, D. Heindl, J. Hoenes, T. Meier, R. Schmuck. Fast reaction kinetics of enzymes having low activity in dry chemistry layers. U.S. Patent 2014/0322737 A1, Feb. 19, 2009.

[86] E. Vázquez-Figueroa , J. Chaparro-Riggers , A. S. Bommarius. Development of a Thermostable Glucose Dehydrogenase by a Structure-Guided Consensus Concept. *ChemBioChem* **2007**, *8*, 2295-2301.

[87] S.-H. Baik, F. Michel, N. Aghajari, R. Haser, S. Harayama. Cooperative Effect of Two Surface Amino Acid Mutations (Q252L and E170K) in Glucose Dehydrogenase from Bacillus megaterium IWG3 on Stabilization of Its Oligomeric State. *Appl. Environ. Microbiol.* **2005**, *71*, 3285-3293.

[88] K. Yamamoto, G. Kurisu, M. Kusunoki, S. Tabata, I. Urabe, S. Osaki. Crystal Structure of Glucose Dehydrogenase from Bacillus megaterium IWG3 at 1.7 Å Resolution. *J. Biochem.* **2001**, *129*, 303-312.

[89] D. Heindl, J. Hoenes, C. Horn, C. Gaessler-Dietsche. Stable NAD/NADH derivatives U.S. Patent 8,809,013 B2, 28 July 2005.

[90] J. T. Slama, A. M. Simmons. Carbanicotinamide adenine dinucleotide: synthesis and enzymological properties of a carbocyclic analog of oxidized nicotinamide adenine dinucleotide. *Biochemistry* **1988**, *27*, 183-193.

[91] R. F. Ramaley, N. Vasantha. Glycerol protection and purification of Bacillus subtilis glucose dehydrogenase. *J. Biol. Chem.* **1983**, *258*, 12558-12565.

[92] W. Hilt, G. Pfleiderer, P. Fortnagel. Glucose dehydrogenase from Bacillus subtilis expressed in Escherichia coli I: purification, characterization and comparison with glucose dehydrogenase from Bacillus megaterium. *BBA - Protein Struct. M.* **1991**, *1076*, 298-304.

[93] O. H. Lowry, J. V. Passonneau, M. K. Rock. The Stability of Pyridine Nucleotides. *J. Biol. Chem.* **1961**, *236*, 2756-2759.

[94] N. Oppenheimer. NAD hydrolysis: Chemical and enzymatic mechanisms. *Mol. Cell. Biochem.* **1994**, *138*, 245-251.

[95] J. T. Wu, L. H. Wu, J. A. Knight. Stability of NADPH: effect of various factors on the kinetics of degradation. *Clin. Chem.* **1986**, *32*, 314-319.

[96] L. Rover Jr, J. C. B. Fernandes, G. d. O. Neto, L. T. Kubota, E. Katekawa, S. l. H. P. Serrano. Study of NADH Stability Using Ultraviolet–Visible Spectrophotometric Analysis and Factorial Design. *Anal. Biochem.* **1998**, *260*, 50-55.

[97] B. W. Carlson, L. L. Miller. Mechanism of the oxidation of NADH by quinones. Energetics of one-electron and hydride routes. *J. Am. Chem. Soc.* **1985**, *107*, 479-485.

[98] T. Yomo, H. Sawai, I. Urabe, Y. Yamada, H. Okada. Synthesis and characterization of 1-substituted 5-alkylphenazine derivatives carrying functional groups. *Eur. J. Biochem.* **1989**, *179*, 293-298.

[99] V. Simanek, V. Preininger. Pseudobase formation from quaternary pyridinium, quinolinium and isoquinolinium cations. *Heterocycles* **1977**, *6*, 475-497.

[100] H. Freitag, C. D. Wilsey. Reagents and assay methods including a phenazine-containing indicator. EP0606296 B1, 19 September 1991.

[101] S. Ohno, Y. Ohno, N. Suzuki, G.-I. Soma, M. Inoue. High-dose Vitamin C (Ascorbic Acid) Therapy in the Treatment of Patients with Advanced Cancer. *Anticancer Res.* **2009**, *29*, 809-815.

[102] P. S. Samiec, C. Drews-Botsch, E. W. Flagg, J. C. Kurtz, P. Sternberg Jr, R. L. Reed, D. P. Jones. Glutathione in Human Plasma: Decline in Association with Aging, Age-Related Macular Degeneration, and Diabetes. *Free Radical Biol. Med.* **1998**, *24*, 699-704.

[103] M.-S. Steiner, A. Duerkop, O. S. Wolfbeis. Optical methods for sensing glucose. *Chem. Soc. Rev.* **2011**, *40*, 4805-4839.

2 A "MEDIATORLESS" INDICATOR FOR COLORIMETRIC DETECTION OF GLUCOSE ON A DRY CHEMISTRY TEST STRIP

2.1 Introduction

The detection of glucose dehydrogenase (GDH)-catalyzed reactions is an active research area due to industrial applications. NAD^+-dependent GDH is widely used in glucose sensing dry chemistry test strips. In the strips, glucose is oxidized to gluconolactone by GDH while NAD^+ is reduced to NADH. Electrons from NADH are then transferred to a mediator, which in turn delivers the electrons to a redox indicator, thus providing a colorimetric read-out.[1] However, the mediators and/or redox indicators used in the test strips generally react sensitively to extreme storage conditions, and degrade over time.[2-3] In tropical climate zones test strips are stored often under harsh conditions of high temperature and humidity.[4] A reagent, combining both functions of the mediator and the chromogenic agent, may lead to a more stable system. Of particular interest in this regard are small molecule indicators, where electrons can be directly transferred from NADH, causing a colorimetric signal at longer wavelengths. Such compounds would provide a simpler colorimetric detection method. This would possibly allow storage and worldwide shipping of glucose test strips at ambient temperature, securing the analytical performance of the enzyme-linked assays.

Quinones are a good starting point in the search for a new redox indicator. The quinone/semiquinone/hydroquinone ($Q/SQ^{\bullet -}/H_2Q$) triad is a vital link in the movement of electrons through cells and tissues.[5] The presence of quinone derivatives in interstellar stardust has led experts to hypothesize a crucial role for pyrroloquinoline quinone (PQQ) in the evolution of life on Earth.[6] PQQ shows an extraordinary molecular stability and its analogues can act as NADH indicators. Hilt *et al* reported that transition-metal complexes of 1,10-phenanthroline-5,6-dione are efficient catalysts for NADH oxidation at physiological pHs.[7] Heindl and colleagues showed that quinone functionalized acceptors are useful for the colorimetric NADH detection.[8] Around the same time, Ambroise *et al* investigated spectral properties of a Ru(II) complex with the aqphen[9] ligand, where its reduction with dithionite resulted in a new absorption band in the visible range.[10]

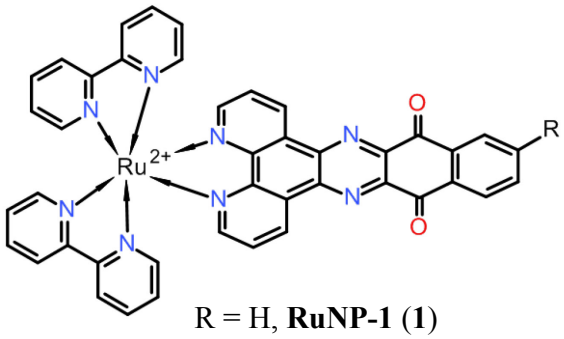

R = H, **RuNP-1** (**1**)
R = Cl, **RuNPCl-2** (**2**)

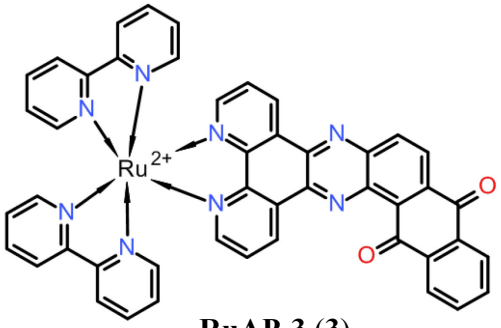

RuAP-3 (**3**)

Figure 2.1 Molecular structure of Ru (II) complexes studied in this report.

Despite extensive literature on the reduction of 1,10-phenanthroline-5,6-dione, its transition-metal complexes, and its *N*-monomethylated derivatives by NADH, we have been unable to locate any study on the reaction of larger quinone-functionalized polypyridinic ligands with NADH. This finding motivated us to investigate Ru(II) complexes with the ligands nqphen[11] **(1–2)** and aqphen **(3)** for quantitative NADH sensing in aqueous buffer solutions (**Figure 2.1**). It is known that both complexes, **RuNP-1** and **RuAP-3** have high electron acceptor character. In addition, we designed **RuNPCl-2** to explore the impact of the Cl group in the reduction kinetics. The Cl-connected aromatic ring may change the electronic density of the nqphen moiety through its electron-withdrawing effect. The new ligand can also be functionalized by displacement of the Cl group as a potential route to new derivatives. Looking at the published data, the electrochemical results indicate that aqphen is a stronger electron acceptor than the nqphen ligand.[12] There are two possible pathways to transfer the electrons from NADH to a quinone moiety.[13] Cyclic voltammetry studies of aqphen show a favoured one-electron reduction mechanism compared to the alternative mechanism *via* hydride transfer. We hypothesized that if the quinone moiety is reduced with NADH by a pathway similar described by Hilt *et al*,[7] a coloured semiquinone would be formed.[14-16]

Here we show that **RuAP-3** displays sensitive colorimetric response upon reduction with NADH, a rapid reaction time and good stability in phosphate buffer at neutral pH. This facilitated its application in an enzymatic glucose assay in solution as well as in dry chemistry. In this proof-of-principle study, we showed that **RuAP-3** could be utilized for quantitative determination of glucose on a test strip.

2.2 Results and Discussion

2.2.1 Synthesis of ruthenium complexes

The synthetic routes for **1–3** are outlined in **Scheme 2-1**. The **RuAP-3** was kindly provided by Roche Diagnostics GmbH as water soluble TFA salt. Complexes **RuNP-1** and **RuNPCl-2** were synthesized in two steps and isolated as hexafluorophosphate salts using adapted literature procedures.[10, 17] Each synthetic step presented here is straightforward and provides yields of 27 to 94% of the desired product in pure form.

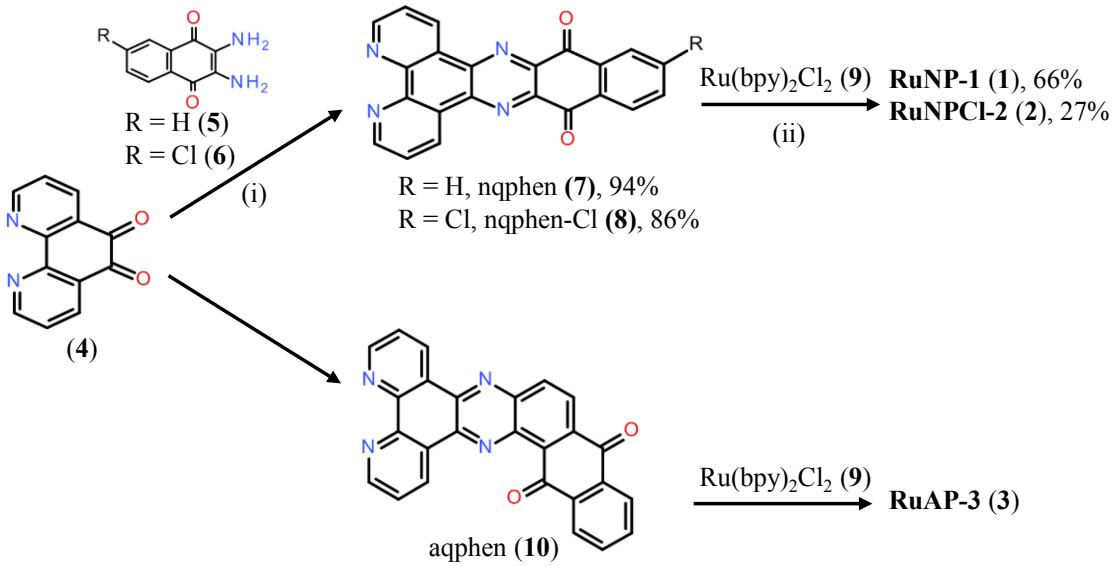

Scheme 2-1 Synthesis of the complexes **1**, **2** and **3**. *Reagents and conditions:* (i) AcOH, 75°*C*, 3 h; (ii) MEG, reflux, Ar, overnight.

The key building blocks **5** and **6** were synthesized according to the efficient two-step procedure previously reported by Chesneau *et al* (**Scheme 2-2**).[17] While 2,3-dichloronaphtoquinone (**11**) is commercially available material, 2,3,6-trichloronaphtoquinone (**12**) was synthesized in two steps (43%) as described previously (see experimental part for details).[18-19]

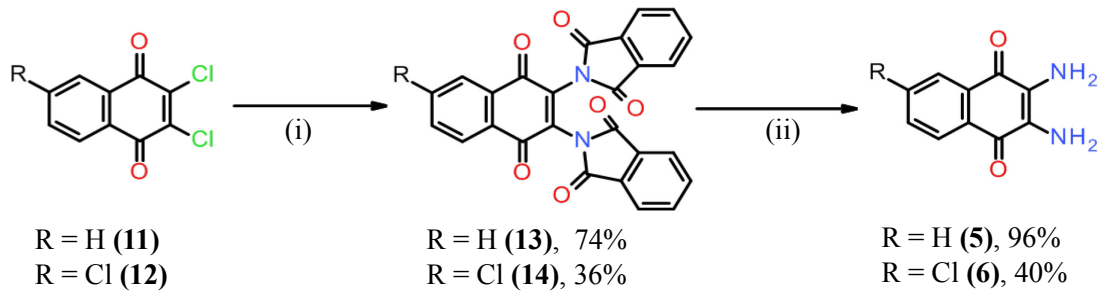

Scheme 2-2 Synthesis of the 2,3-diaminonaphtoquinones. *Reagents and conditions:* (i) potassium phthalidimide, anhydrous MeCN, reflux, 3 h; (ii) 64% aqueous hydrazine, 70°*C*, 3 h.

The nqphen ligands (**7–8**) were readily synthesized in excellent yields (~90%) *via* typical condensations of the appropriate diaminoquinone (**5-6**) with phendione **4** in glacial acetic acid. The known nqphen ligand **7**, which precipitated during the course of the reaction and appeared to be unsoluble in most solvents, was isolated by centrifugation. The new acceptor ligand **8** also showed low solubility in most common solvents. The better solubility of **8** in $CDCl_3$ allowed recording of a ^1H NMR spectrum, and HRMS (ESI) further confirmed its identity and purity. The bis-complex **9** was brought about in one step as described in literature.[20]

The key step of the synthesis corresponds to complexation of the electron accepting ligands (**7**–**8**) with $Ru(bpy)_2Cl_2$ (**9**) affording target complexes **RuNP-1** and **RuNPCl-2**. Chesneau *et al* previously prepared the complex **RuNP-1** by reaction of nqphen (**7**) with $Ru(bpy)_2Cl_2$ (**9**) in refluxing ethanol for six days in 54% yield.[17] In addition the method required purification by flash chromatography on deactivated alumina. Alternatively, we performed the synthesis of this complex in 76% yield in high purity without chromatographic purification. The modified synthesis was adapted from the original method of Ambroise *et al.*[10] Reaction of nqphen (**7**) with $Ru(bpy)_2Cl_2$ (**9**) in refluxing ethylene glycol for 14 h gave the desired complex **RuNP-1**. The previously unknown **RuNPCl-2** was synthesized by an analogous method.

2.2.2 Diquaternary derivatives

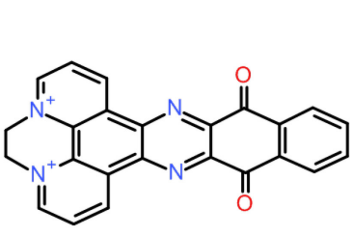

15

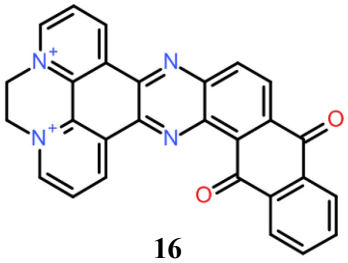

16

Figure 2.2 Molecular structure of diquaternary salts.

We also explored an alternative method to obtain water-soluble derivatives of the nqphen (**7**) and aqphen (**10**) ligands. Two new diquaternary salts (**15**–**16**) have been prepared *via* one-step alkylation procedure (see experimental part). Both of them react with NADH in aqueous solutions and display a colorimetric signal at longer wavelengths (see supplementary UV-Vis material). It was found that a broad absorbance band of **15** at 460 nm (pH = 7.0) overlaps with the one of its reduced form at 525 nm (**Figure 2.17S**). The NADH detection with **15** could be achieved at 600 nm, but the sensitivity is low (3.4 ± 0.1 $mM^{-1}cm^{-1}$). In case of compound **16**, a reliable NADH

determination was not achieved, as **16** is not stable in the neutral buffer: the solution displayed spectral changes after five minutes (pH = 7.0, data not shown) and longer incubation eventually led to precipitation. The observed properties limit the use of bis-alkylated derivatives (**15**–**16**) in the test strip development.

2.2.3 Characterization

Table 2-1 summarizes ^{1}H NMR data for the nqphen ligands (**7**–**8**) and the corresponding complexes (**1**–**2**). The characterization data for **RuNP-1** are in accordance of that reported by B. Chesneau *et al.*[17] Analysis of the ^{1}H NMR spectra of the new complex **RuNPCl-2** was facilitated by a comparison with **RuNP-1**. The nqphen pattern in the complexes (**1-2**) is similar to that of free ligands (**7**–**8**). Strong shielding of H_a and $H_{a'}$ could be explained as an effect of the backbonding of the metal, which shields these protons.[21] The extra chloride group in naphtoquinone moiety of **2** and **8** does not affect nqphen protons significantly.

Table 2-1 ^{1}H NMR chemical shifts in (ppm) for the complexes **1** and **2** (PF_6 salts) in MeCN-d_3 and for the ligands **7** and **8** in $CDCl_3$. Coupling constants (J) presented in Hz.

Complex	H_a / $H_{a'}$	H_b / $H_{b'}$	H_c / $H_{c'}$	H_g / $H_{g'}$	H_h / $H_{h'}$
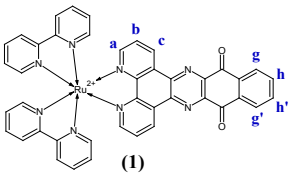 (1)	8.28 (dd) J_{ab} = 5.2 J_{ac} = 1.2	7.96 (dd) J_{bc} = 8.2 J_{ba} = 5.2	9.68 (dd) J_{cb} = 8.2 J_{ca} = 1.2	8.48 (dd) J_{gh} = 5.8 $J_{gh'}$ = 3.4	8.06 (dd) J_{hg} = 5.8 $J_{hg'}$ = 3.4
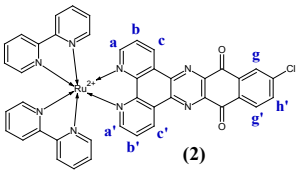 (2)	8.28 (dd) J_{ab} = 5.3 J_{ac} = 1.3	7.96 (dd) J_{bc} = 8.2 J_{ba} = 5.3	9.67 (dd) $J_{cb/c'b'}$ = 8.3 $J_{ca/c'a'}$ = 1.3 9.66 (dd) $J_{cb/c'b'}$ = 8.3 $J_{ca/c'a'}$ = 1.3	H_g: 8.44 (d): $J_{gh'}$ = 2.1 $H_{g'}$: 8.45 (d) $J_{g'h'}$ = 8.4	$H_{h'}$: 8.02 (dd) $J_{h'g'}$ = 8.2 $J_{h'g}$ = 1.4
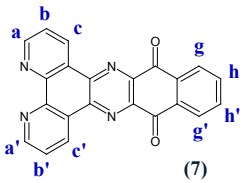 (7)	9.40 (dd) J_{ab} = 4.4 J_{ac} = 1.8	7.91 (dd) J_{bc} = 8.2 J_{ba} = 4.4	9.80 (dd) J_{cb} = 8.2 J_{ca} = 1.8	8.53–8.57 (m)	7.98 (dd) $J_{h'g'}$ = 5.8 $J_{h'g}$ = 3.4
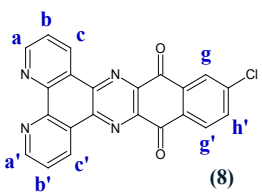 (8)	9.41 (dd) J_{ab} = 4.4 J_{ac} = 1.8	7.92 (dd) $J_{bc/b'c'}$ = 8.2 $J_{ba/b'a'}$ = 4.4 7.93 (dd) $J_{bc/b'c'}$ = 8.2 $J_{bc/b'c'}$ = 4.4	9.78 (dd) J_{cb} = 8.2 J_{ca} = 1.8	H_g: 8.49 (d) $J_{gh'}$ = 2.0 $H_{g'}$: 8.49 (d) $J_{g'h'}$ = 8.4	$H_{h'}$: 7.93 (dd) $J_{h'g'}$ = 8.4 $J_{h'g}$ = 2.0

For the complex **3**, assignments of proton and carbon signals in the aromatic region were determined by examining ^{1}H-^{1}H COSY and ^{1}H-^{13}C-hetero HSQC/HMBC experiments in MeOD-d_3. **Figure 2.3** shows the ^{1}H NMR spectrum of **3** and the assignments of ^{1}H NMR signals (see **Table 2-6S** in supplementary NMR spectra for the assignment of carbon resonances). The main effect observed due to coordination of aqphen to Ru(II) is the enhanced deshielding of the protons H_c and $H_{c'}$ of the phenanthroline (phen) fragment of the acceptor ligand, as the consequence of their coordination to the metal. Surprisingly, when compared to published data for aqphen-based complexes,[10, 22] protons H_g and $H_{g'}$ appear as two widely separate doublets (7.96 and 8.30 ppm) and these are consequently magnetically non equivalents. The same phenomenon was observed for protons H_h and $H_{h'}$ (7.78 and 7.93 ppm). With regard to the signals of the bipyridyl (bpy) ligands, the expected and characteristic pattern was observed. The ^{19}F spectrum of complex **3** exhibits a characteristic peak at −77.17 ppm for both TFA anions. HRMS (ESI^{+}) results are in agreement with the structure of complex **3** with a molecular ion peak at *m/z* 414.0771 presenting an isotopic distribution in agreement with the calculated pattern. The data obtained for **3** are consistent with those found in the literature for the analogous complex $[Ru(phen)_2(aqphen)]^{2+}$.[23]

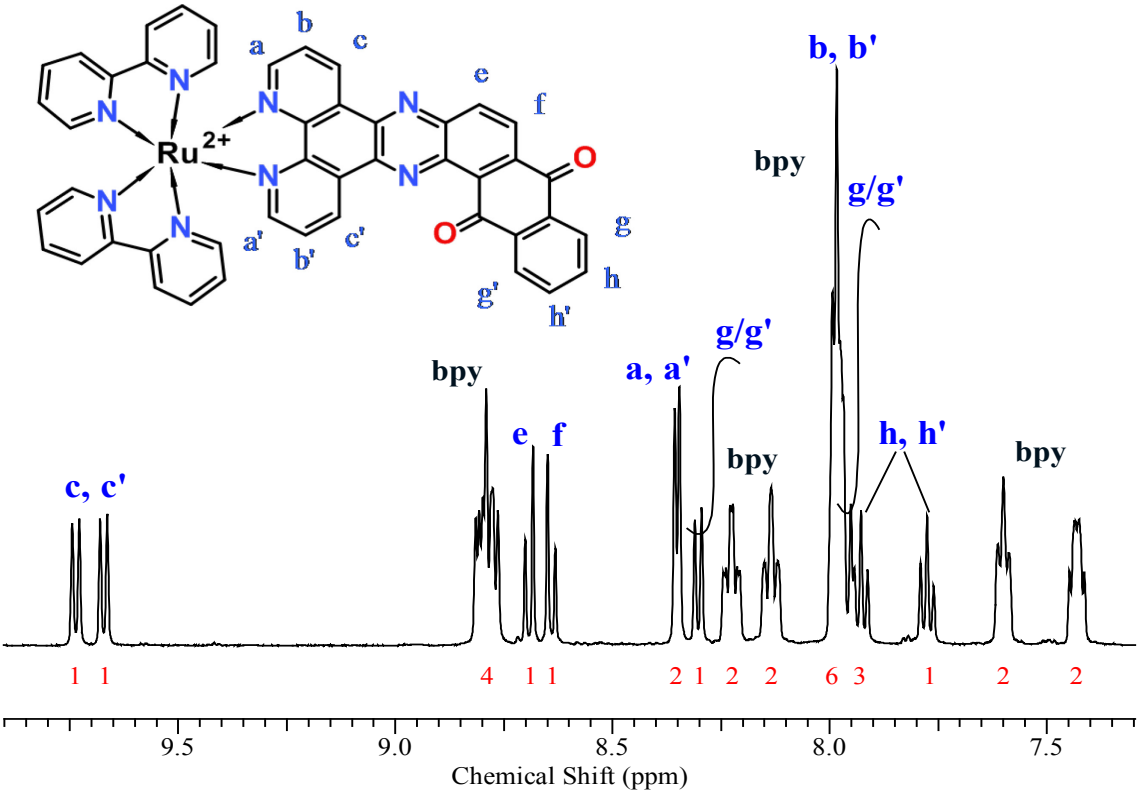

Figure 2.3 ^{1}H NMR spectra of 3 as TFA salts in MeOD-d_3 at 500 MHz.

2.2.4 UV-Vis properties of RuAP-3 and its response to NADH

Water-soluble chloride salts of **1** and **2** were obtained *via* anion exchange of their respective PF_6 salts using an Amberlyst A-26 resin (Cl-form), and the complex **3** was used as its water-soluble TFA salt. Their UV-Vis properties and reaction with NADH were investigated in phosphate aqueous solutions (50 mM) of pH 7.0 and 8.5 as a commonly used buffer system in the test strip development. While **1** and **2** did not show a colour forming reaction with NADH, it was found that complex **3** is suitable for NADH detection.

A characteristic absorption spectrum of **3** is shown in **Figure 2.4**. In the range 300–600 nm, the spectrum displays a broad band at 394 nm along with a shoulder at 434 nm. The band at 394 nm ($\varepsilon = 16.6$ $mM^{-1}cm^{-1}$) is characteristic of intra-ligand IL π-π^* transitions of the aqphen ligand, most probably localized on the quinone moiety. The broad structureless absorption band extending from 420 to 600 nm can be ascribed to the overlapping metal-to-ligand charge-transfer (MLCT) transitions to both bpy and aqphen ligands.[24]

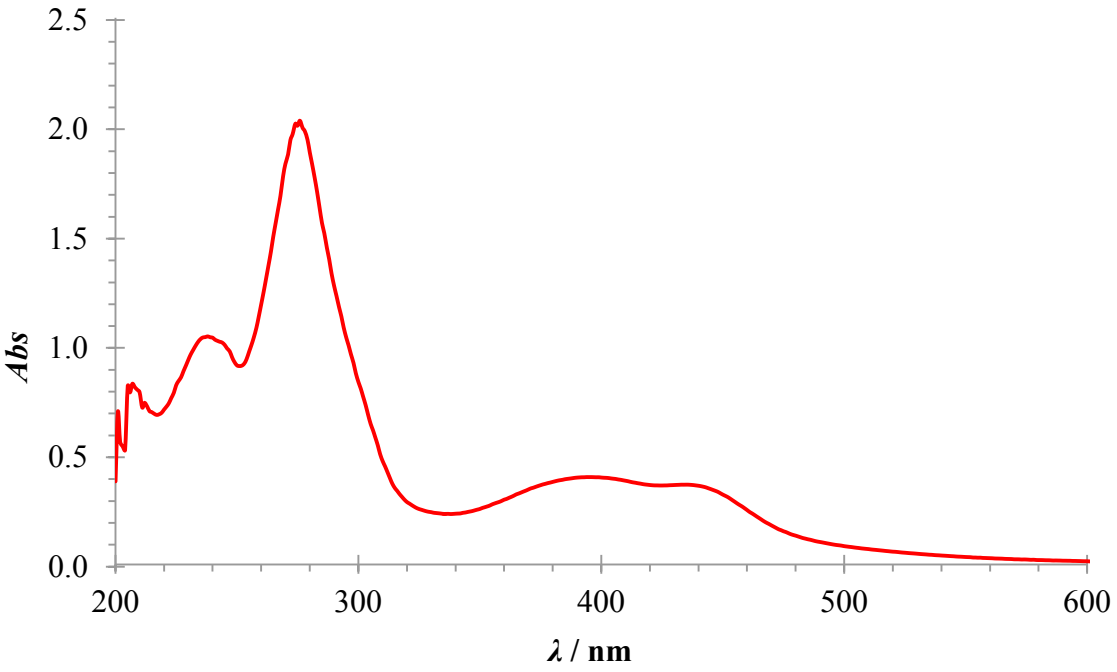

Figure 2.4 The UV-Vis absorption spectra of complex **3** (25 μM) in phosphate buffer (50 mM, pH 7.0).

Here our aim was to explore whether the ruthenium complex **3** can be used as an indicator in enzymatic glucose assays. In previous chapter we proposed the assay employing NAD^+-GDH, where the indicator would react with NADH non-enzymatically.[25] Hence, the colour forming reaction can be simply expressed as:

RuAP-3 + NADH ⇌ **RuAP-3^{red}** + NAD^+ **eq. (1)**

where $[\textbf{RuAP-3}]_0 > [NADH]$. The spectral properties of the indicator (**RuAP-3**) in the absence and presence of NADH were firstly examined at pH 7.0. As shown in **Figure 2.5A**, the indicator (**3**) itself is almost colourless above 800 nm; after ten minutes of incubation with NADH, a new absorption at about 840 nm appeared with a distinct colour change from orange to dark brown (**Figure 2.5B**). In the absence of NADH (control), the indicator (**3**) did not show any change in absorbance during the same period of time, suggesting that **RuAP-3** is rather stable and NADH is indeed involved in the colour-forming reaction. The analogous results were obtained in basic media (pH 8.5). Interestingly, the absorption spectra from the reduced system do not resemble the one reported for aqphen-hydroquinone reduced with dithionite,[10] suggesting a different reduction product. Moreover, during the experiments at pH 6.0 a new intensive band at 544 nm was generated (**Figure 2.19S**). These data indicate that under acidic and basic conditions two different species were formed. The reasons leading to such behaviour were pointed out in the paper by Hilt *et al* at an example of 1,10-phenanthroline-5,6-dione transition-metal complexes.[7]

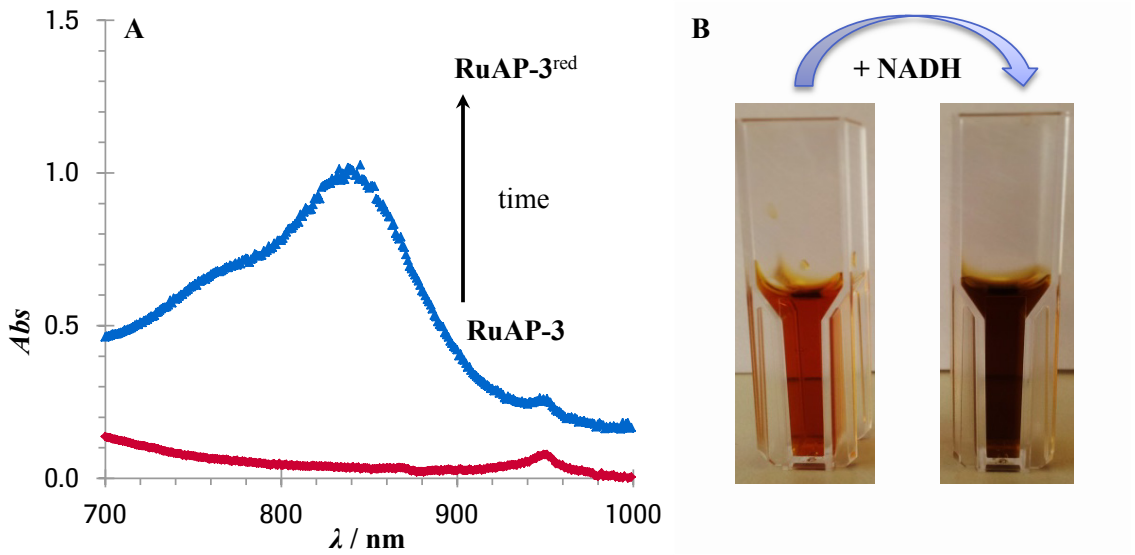

Figure 2.5 Representative UV-Vis spectra **(A)** and visible colour **(B)** changes upon treating the complex **3** (1.0 mM) with NADH (0.1 mM) in phosphate buffer (50 mM, pH 7.0), showing that the dye is formed with λ_{max} at 840 nm after adding NADH (incubation time 10 min).

Assay sensitivity is determined to be as follows:

$sensitivity = \Delta Abs^{840}/\Delta[NADH]_0$ **eq. (2)**

where ΔAbs^{840} is the increase of the absorbance due to **RuAP-3**^{red} formation. Accordingly, the sensitivity of complex **3** for NADH is given by the plot of the absorbance observed at 840 nm *vs* initial concentration of NADH. **Figure 2.6** depicts the calibration curves obtained upon treatment of the **RuAP-3** (100 µM) assay solutions with NADH (10–100 µM) at pH 7.0 and 8.5. The assay gave good linearities, with within-assay coefficients of variation of less than 5% (n = 6). The data clearly show that the yield of **RuAP-3**^{red} formation is pH-dependent and a remarkably better response for NADH was found at pH 7.0 (**Figure 2.6A**). The sensitivity was estimated to be 9.4 ± 0.3 OD/mM. Therefore, indicator **3** successfully fulfils both criteria for NADH sensing (pH 7.0): λ_{max} is above 600 nm and the sensitivity is higher than the intrinsic extinction coefficient of NADH (ε^{340} = 6.22 $mM^{-1}cm^{-1}$). On the other hand, the use of **RuAP-3** under basic conditions (pH 8.5) was found to be disadvantageous, because the sensitivity was twice lower than at neutral ones (**Figure 2.6B**).

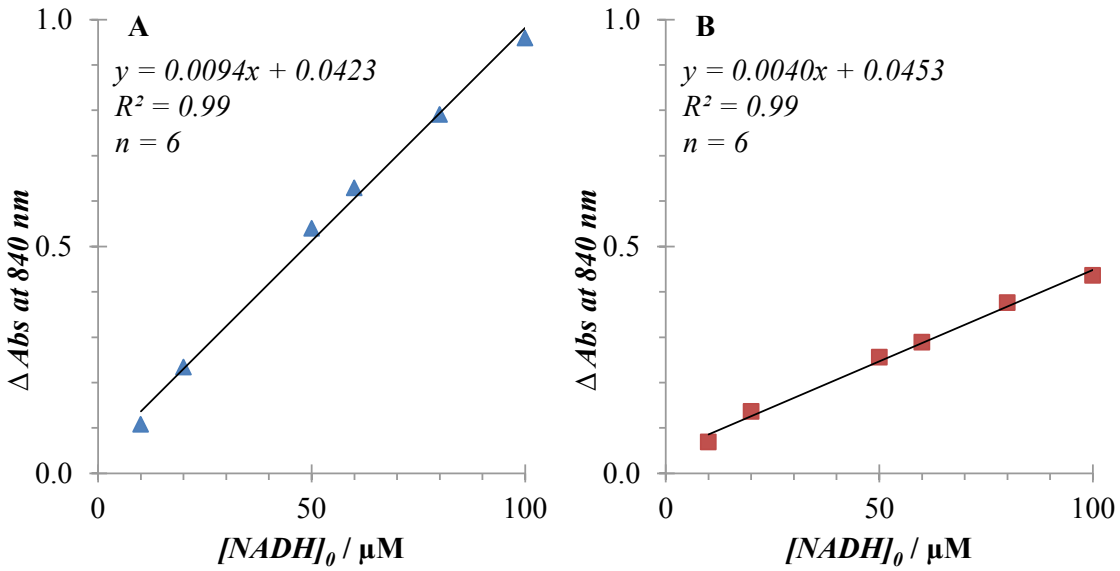

Figure 2.6 Calibration curves of absorbance changes at pH 7.0 (**A**) and 8.5 (**B**) of the complex **3** (100 µM) upon addition of NADH (10–100 µM). All experiments were performed in 50 mM phosphate buffer at pH 7.0 (**A**) and 8.5 (**B**) at 25°*C*, and each spectrum was obtained 3 min after NADH addition.

2.2.5 Time response and kinetic parameters

Our long term goal has been to design an indicator for application in the test strips, where the glucose concentration should be measured in a few seconds. We reasoned that time response could be evaluated under pseudo-first-order conditions. **Figure 2.7A** shows the time dependence of the spectra during the reaction of **RuAP-3** with NADH. The absorbance band increase was very fast within first thirty seconds ($t_{½}$ = 7 s) and levels off to a saturation value after about sixty seconds and then slowly decreases (**Figure 2.7A**). Additionally recorded UV-Vis spectra (30 min after NADH addition) further confirmed that the reduction product was slowly re-oxidized back to **RuAP-3** (data not shown). This UV-Vis behaviour is easy to understand: if the obtained product is a semiquinone, which results from one-electron reduction. Such species are well known to be unstable in solution under aerobic conditions. In nature, products of one-electron reduction serve as mediators in the transfer of a pair of electrons from NADH to molecular oxygen. In contrast, two-electron reduction of quinones leads to the formation of hydroquinones, which are in general less readily autooxidised by O_2 in comparison to the quinone radicals.

Additionally, the activity of electron transfer was evaluated using pseudo-first-order rate constant (k_{obs}). In order to obtain accurate results, it was determined at the initial stage of the above reaction, where a plot of $ln(Abs^{840})$ *vs* time gave a straight line. The experimental range was limited to the first seven seconds of the reaction. The Guggenheim plot according to **eq. (3)** is shown in **Figure 2.7B**.

$$ln(A_{t+dt} - A_t) = -kt + ln(A_\infty - A_0)\,(1 - e^{-kdt}) \qquad \textbf{eq. (3)}$$

Guggenheim plots of $ln(A_{t+dt} - A_t)$ *vs* time were found to be linear and to have correlation coefficients (R^2) greater than 0.95, indicating that the reaction was first order in the limiting reagent at the initial stage. The slope of the line defines a pseudo-first-order rate constant (k_{obs}). Hence, the activity is 0.075 ± 0.003 s^{-1} under experimental conditions, which is characteristic of a rapid response. In addition, values of k_{obs} were found to be proportional to the initial concentration of **3** in these solutions (data not shown).

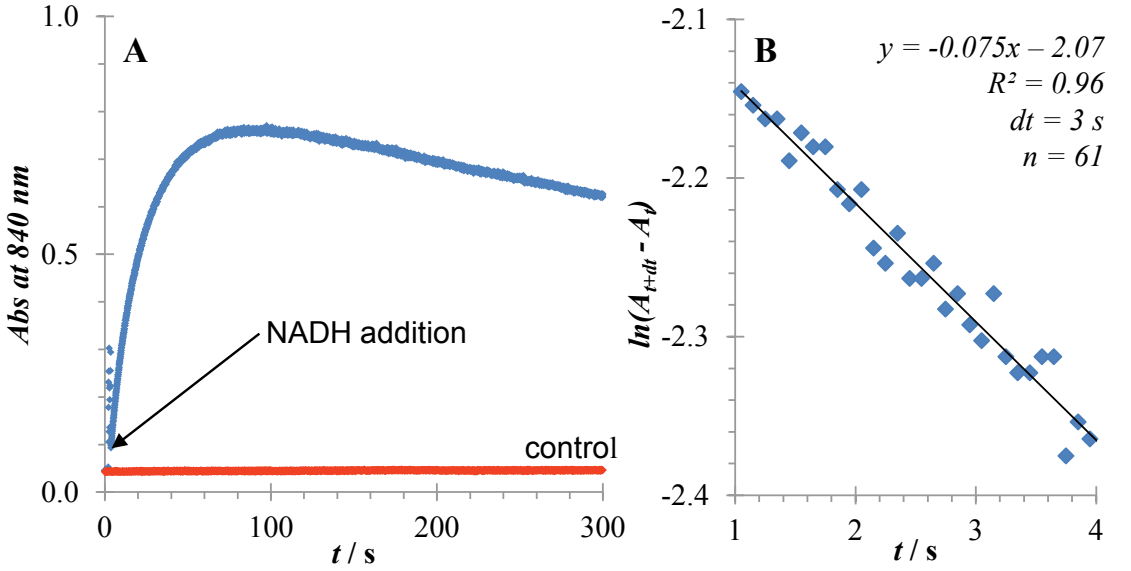

Figure 2.7 Pseudo first-order analysis of reaction of **RuAP-3** (1.0 mM) with NADH (50 µM) in phosphate buffer (50 mM, pH 7.0) at 25°*C*: **A** — time course of absorption intensity changes at 840 nm after addition of NADH the solution containing **RuAP-3**, at an interval of 0.1 s; **B** — Guggenheim plot of a pseudo-first-order region.

2.2.6 Stability

The chemical stability is one of the key parameters for application in the test strip. Following a common stress test, complex **3** (1.0 mM) was kept in the phosphate buffer (50 mM, pH 7.0) at 50°*C* for thirty minutes. Afterwards, the stability of **RuAP-3** was evaluated by measuring the UV-Vis spectra and electron-transfer activity at 25°*C*. The absorbance of **RuAP-3** remained unchanged, which implied that the compound was stable. Another test for **RuAP-3** consisted of measurements of k_{obs} by adding NADH (50 µM) to the **RuAP-3** (1.0 mM) assay solution. It was observed that **RuAP-3** kept more than 95% of the initial activity after the stress test (results not shown). In conclusion, both methods gave analogous results: **RuAP-3** remained unchanged after thirty minutes of incubation at 50°*C* in the phosphate buffer.

2.2.7 What are the differences between ascorbic acid and NADH as electron sources?

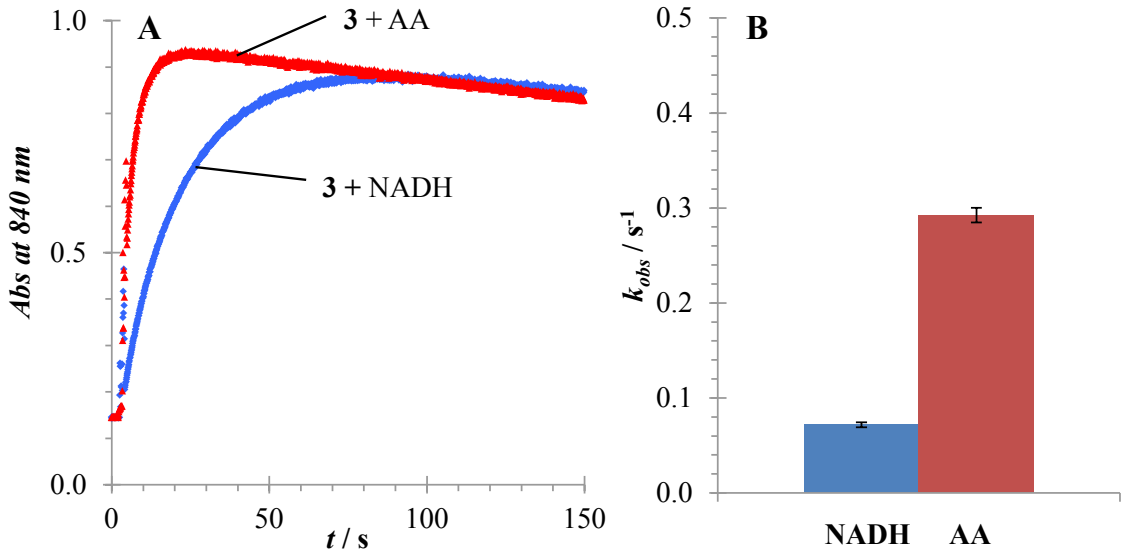

Figure 2.8 A — Representative UV-Vis spectra of the kinetics upon treating **RuAP-3** (1.0 mM) with NADH (50 µM) and AA (50 µM) in phosphate buffer (50 mM, pH 7.0), at an interval of 0.1 s; **B —** calculated k_{obs} from Guggenheim plots at the initial rates for reactions with NADH and AA.

To further study the versatility of **RuAP-3**, we investigated its selectivity toward another reductant existing in body fluids — ascorbic acid (AA). The indicator **RuAP-3** (1.0 mM) was treated with AA (50 µM) in phosphate buffer (pH 7.0, 50 mM). As shown in **Figure 2.8A**, AA gave the absorbance response comparable to that of the NADH sample, however indicating faster reduction kinetics. It was observed that AA had the activity (k_{obs}) of about four times over that of NADH (**Figure 2.8B**). This again supports the hypothesis that a semiquinone was formed under reduction, since AA is a stronger one-electron donor than NADH.[26] In addition, the detailed mechanism of the electron transfer reaction of AA with quinones was described by Sarlauskas *et al*, where one-electron reduction was also confirmed.[27] Despite the fact that AA would be a strong interfering substance for complex **RuAP-3** based glucose assays, it could be still studied for application in the test strips. The typical concentration of AA in blood is very low (<50 µM) compared to the normal concentration of glucose (about 5 mM). Only under special treatment in hospitals AA might reach values up to 5-mM.

2.2.8 Glucose dehydrogenase assay

The successful analysis of NADH encouraged us to investigate the colorimetric indicator **RuAP-3** in a glucose assay (**Scheme 2-3**). As a model system, **RuAP-3** was applied to analyze glucose in the presence of the double mutant of NAD^+-dependent glucose dehydrogenase (E170K/Q252L = GlucDH2).[28-29] In this system, GlucDH2 catalyzes the oxidation of glucose to gluconolactone with concomitant reduction of NAD^+ to NADH. The resulting reduced cofactor reduces **RuAP-3**, which leads to an increase in the absorbance. Accordingly, **Figure 2.9A** shows the time-dependent absorbance changes of **RuAP-3** upon its treatment with glucose (50 µM) in the presence of NAD^+/GlucDH2 in phosphate buffer (100 mM, pH 7.0). Control experiments — by excluding NAD^+ or GlucDH2 — revealed that all the components are essential to activate the colour change of the assay mixture to glucose (**Scheme 2-3**, **Figure 2.9**).

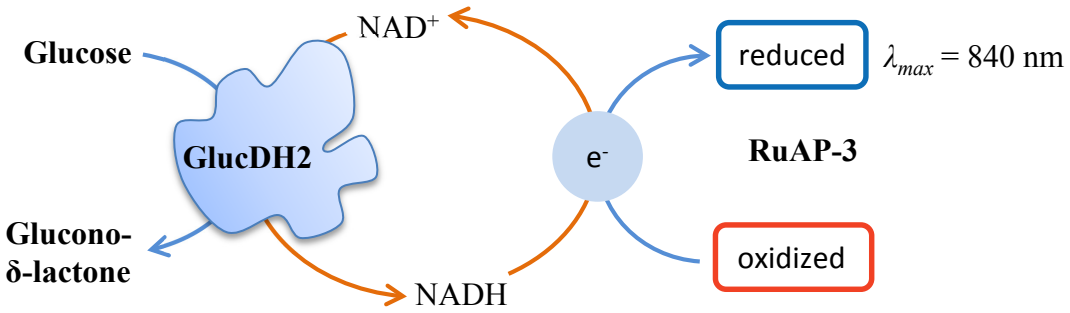

Scheme 2-3 Sensing mechanism of glucose in presence of glucose dehydrogenase (GlucDH2).

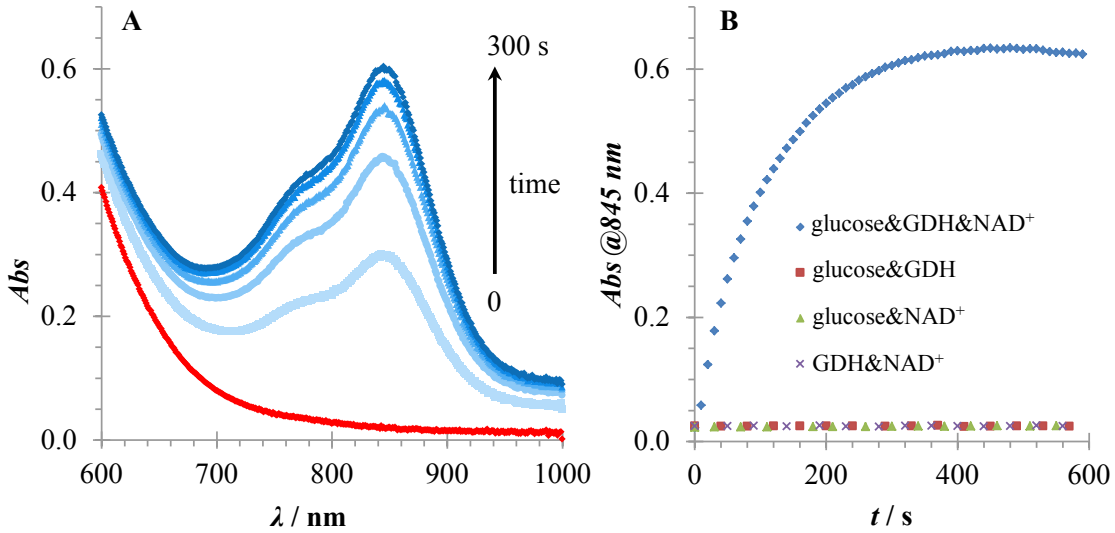

Figure 2.9 Real-time UV-Vis spectra **A** — of the mixture of **RuAP-3** (0.5 mM), NAD^+ (2.0 mM), glucose (50 µM) and GlucDH2 (245 U/mL, 6 µM) at different times: (0) prior to the addition of glucose, (300 s) after successive time intervals of 60 s; **B** — the plots of absorption intensity changes at 845 nm *vs* time for **RuAP-3** under different conditions in phosphate buffer (100 mM, pH 7.0), at an interval of 10 s.

This mutant glucose dehydrogenase is known to accept NAD^+, $NADP^+$, and $cNAD^+$ cofactors. The $cNAD^+$ is a carbocyclic NAD^+-analogue, which is resistant to hydrolysis. It is considered to be a promising alternative to NAD^+ in order to prolong shelf-life of the glucose test strips. Hence, we investigated the **RuAP-3**-coupled assay using besides the natural cofactor NAD^+, also its artificial analogue $cNAD^+$, in order to elucidate the differences in respect of time response and sensitivity (**Figure 2.10**).

Initial velocity of the dye formation from **RuAP-3** and the sensitivity were measured by adding different concentrations of glucose (0–120 µM) to the assay mixtures. **Figure 2.10** depicts the time response curves of the GlucDH2-catalyzed reactions as they were recorded at 845 nm for 600 seconds. The initial rates and absorbance increased with the higher concentration of glucose. The saturation end point was reached within 300 seconds for all glucose concentrations (20–120 µM). In contrast, the absorbance of **RuAP-3** in the absence of glucose remained unchanged during the same period of time, which implied that **RuAP-3** was stable in the detection system. The use of both cofactors led to absorbance response, and the properties of $cNAD^+$ in the assay closely resembled those of the parent coenzyme NAD^+.

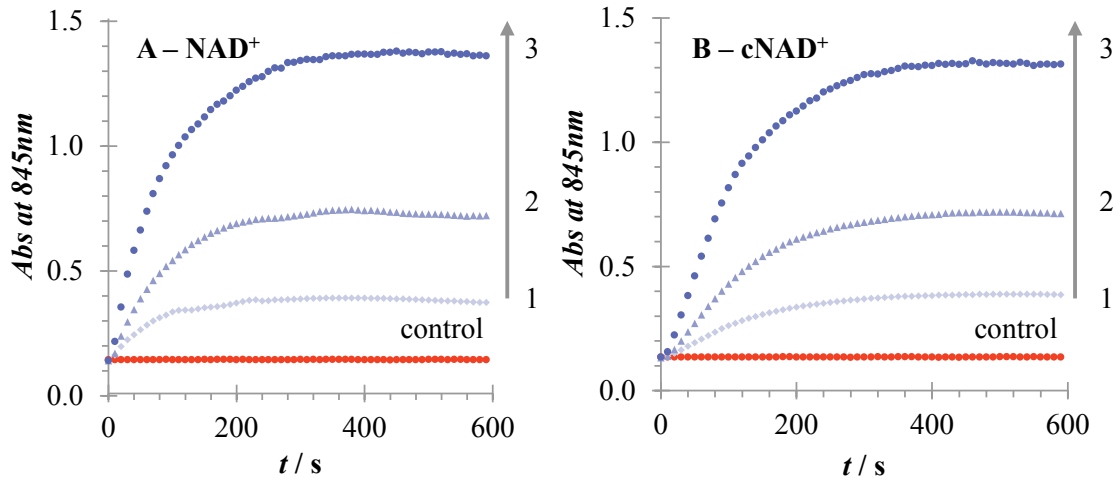

Figure 2.10 UV-Vis spectra of the kinetics at 845 nm upon treating an assay solution of **RuAP-3** (0.5 mM), coenzyme (2.0 mM) and GlucDH2 (245 U/mL, 6 µM) in phosphate buffer (100 mM, pH 7.0) with various glucose concentrations, 1–3: 20, 50, 120 µM, at an interval of 12 s. **A** — NAD^+; **B** — $cNAD^+$.

Under above conditions, kinetic parameters of the enzymatic reaction were estimated by fitting the data to the Michaelis–Menten equation (**Figure 2.20S**). The Michaelis constants (K_m) and the maxima of the initial velocity profile (V_{max}) are presented in **Table 2-2**. The K_m value was approximately 6-fold lower in the presence of NAD^+, indicating the higher affinity of the enzyme for glucose, where the natural cofactor was used. However, the maximum velocity (V_{max}) was higher in the presence of $cNAD^+$.

Kinetic parameters of the GlucDH2-coupled glucose assay are consistent with the data reported previously.[29] The dinucleotide analogue $cNAD^+$ was recognized as an efficient co-substrate in the oxidation of glucose to gluconolactone catalyzed by modified glucose dehydrogenases; and GlucDH2 also preferred the natural NAD^+ cofactor to the artificial one ($cNAD^+$).

Table 2-2*

Coenzyme	Sensitivity (± SD), OD/mM	K_m, mM	V_{max}, OD/s
NAD^+	9.0 ± 0.3	0.5	0.06
$cNAD^+$	9.2 ± 0.2	3.1	0.21

* — Kinetic measurements were conducted in phosphate buffer solution (100 mM, pH 7.0), GDH (245 U/mL, 6 µM), glucose (0–120 µM), 2.0 mM NAD^+ and accordingly 2.0 mM $cNAD^+$; the experimental range was limited to the first 30 s of the reaction. SD = standard deviation; OD = optical density.

As shown in **Figure 2.11**, a good linearity exists between the absorbance increase and the glucose concentration (20–120 µM range) in the presence of both, NAD^+ (**A**) and $cNAD^+$ (**B**) cofactors. The absorbance responses are linear with the correlation coefficients (R^2) of 0.99. The assays' sensitivity equals to 9.0 and 9.2 OD/mM, respectively. In summary, the NAD^+ based assay was faster, while the $cNAD^+$ based assay showed slightly better sensitivity. These preliminary results encouraged us to investigate the **RuAP-3** based assay for glucose measurement on a test strip.

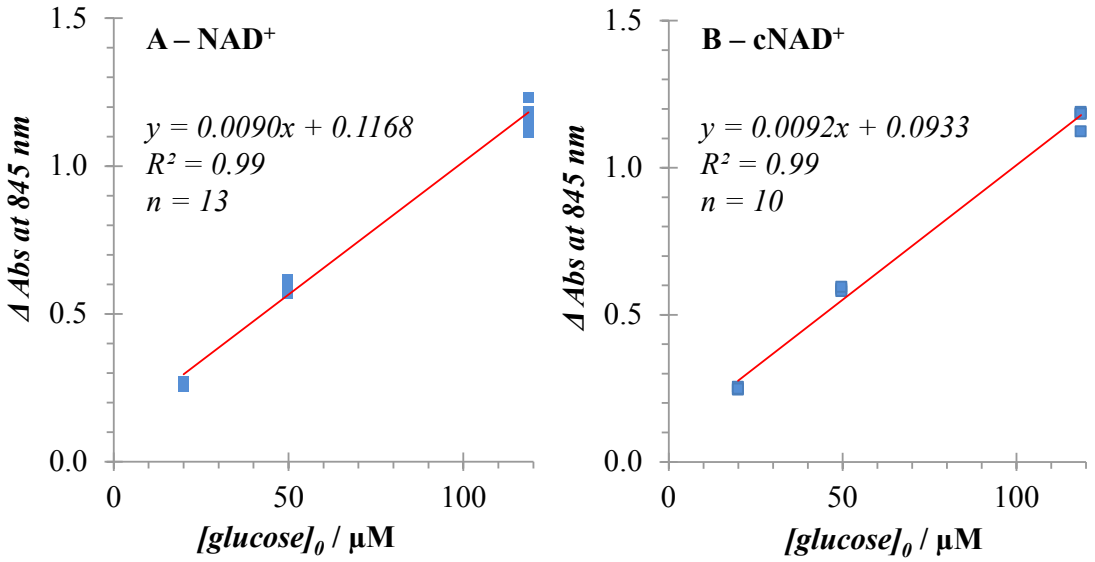

Figure 2.11 UV-Vis plot corresponding absorbance changes at 845 nm against the glucose concentration obtained with the assay solution at the reaction endpoint (slope < 2 OD%/s): **A** — NAD^+; **B** — $cNAD^+$.

2.2.9 Glucose assay with GDH/RuAP-3 on the test strips

Earlier coating experiments performed at Roche (data not disclosed) were used as guidelines in the selection of concentrations of the coating components. The coatings were processed into a test strip format using Accu-Chek Active platform. Glucose detection on the strip was based on the reduction of $cNAD^+$ to cNADH as a result of glucose reacting with the glucose dehydrogenase enzyme (GlucDH2).[2]

Figure 2.12 shows the detection setup and the structure of a glucose sensing test strip incorporating **RuAP-3**. The setup was based on the established configuration. Light from light-emitting diodes (LEDs) is shined on to the test strip opposite to the sampling position. The change in reflected absorbance is measured by charge-coupled device (CCD) detector. The signal from the test strip (remittance) was obtained as a relative signal. This was the percentage of the signal from a special reference strip set as the maximum remittance signal value.

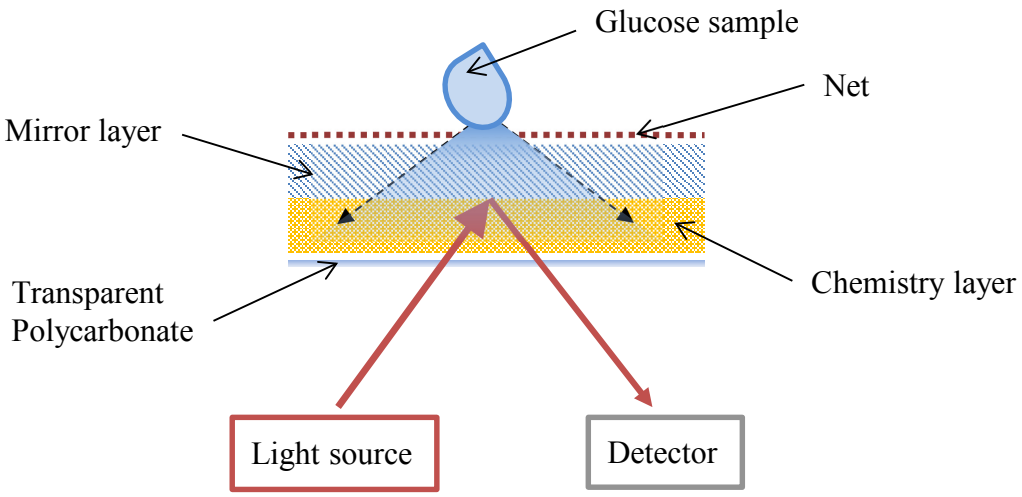

Figure 2.12 Schematic cross section through a test strip with a light source below the strip and glucose dissolved in PBS as a sample. The sample is placed on top of the mirror layer; the fine net distributes the drop evenly on the matrix surface. Glucose with the sample filtered through the separation layer by means of diffusion. The enzymatic reaction takes place in the chemistry layer. Colour formation from the reaction of glucose is observed by means of reflection photometry from the side opposite to the application of sample.

Formulation optimisation

Choice of a binder polymer played an important role to achieve homogeneity and consistency of the chemistry layer. We varied between two polymers to obtain the coatings: Gantrez S-97 and Mowiol 18-88. Firstly, we prepared a formulation using Gantrez S-97. However, after **RuAP-3** immersion into the formulation, we observed rapid formation of the large aggregates. Molecular structure of Gantrez S-97 shows that

it has negatively charged terminal groups in the polymer backbone at pH 7.5. Electrostatic attraction of Gantrez S-97 with oppositely charged **RuAP-3** may destabilize the particle suspension by the interpolymer complexation leading to the fast aggregation. To confirm this assumption, we mixed **RuAP-3** in a suspension of Gantrez S-97 in aqueous buffer at pH 7.5. Again, addition of **RuAP-3** initiated the coagulation of the polymer particles. This further indicated that changes in the system were brought about by electrostatic interactions between divalent cation **RuAP-3** and polyanionic Gantrez. In an alternative formulation, the neutral polymer Mowiol 18-88 was used. **RuAP-3** loaded suspensions showed no aggregation and allowed to establish a homogeneous dry layer.

The optimal composition was further selected by varying the concentration of **RuAP-3** in formulations. Coatings with 0.1, 0.2 and 2.0 g/m^2 of **RuAP-3** in the dry layer were prepared. By visual inspection, the produced layers were homogeneous. The flexibility of the coatings was tested by rolling the sheets into tight rolls; the films were able to bend without cracking. Glucose resolution performance of each coating was tested by adding PBS samples containing 0, 0.9, 1.9, 2.9, 6.1, 12.2 and 17.8 mM of glucose.

A spectrometric measurement of the coatings was performed ranging the wavelengths from 300 to 1000 nm. The spectrum was recorded initially from a dry strip and subsequently, after the addition of the 5-µL sample. The strips were monitored for 200 seconds.

In the formulations with lower concentrations of **RuAP-3** (0.1 and 0.2 g/m^2), the signal saturation was observed at glucose levels above 1mM, allowing only to obtain qualitative results (data not shown). In the lower range, the response differed strongly between the parallel measurements. Thus, the difference between glucose concentrations was indistinguishable. The coatings with **RuAP-3** at maximum possible concentration (2.0 g/m^2) produced enough response at 840 nm for the signal to be quantified (**Figure 2.13**, **Figure 2.14**). This concentration of **RuAP-3** was utilized to prepare test strips for the "proof-of-principle" study.

Characterisation of the coatings

As shown in **Figure 2.13A**, the sensing coating shows the maximum remittance at 840 nm upon exposure to glucose and the colour change could be visually observed (**Figure 2.13B**). The remittance profile matches with the Vis-spectra of the reduced **RuAP-3** in solution.

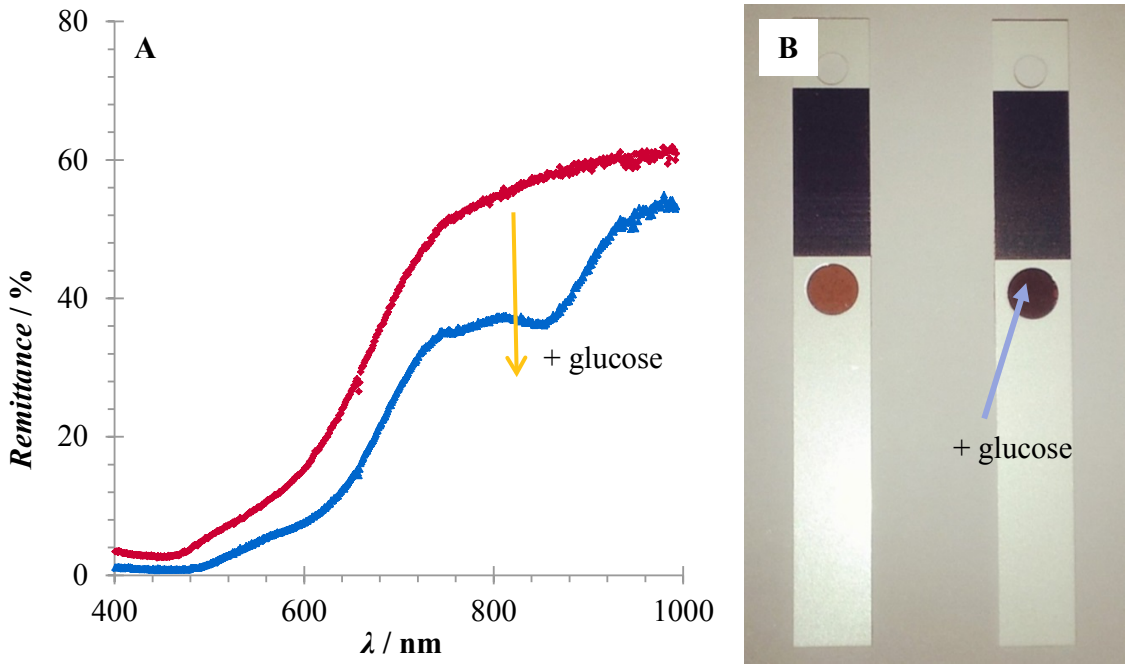

Figure 2.13 A — a change of remission spectra upon treating the test strip, containing **RuAP-3**, with glucose (6.1 mM), showing that the dye is formed with λ_{max} at 840 nm after 200 s of a glucose sample addition; **B** — test strips, containing **RuAP-3**: before glucose addition (left) and after (right).

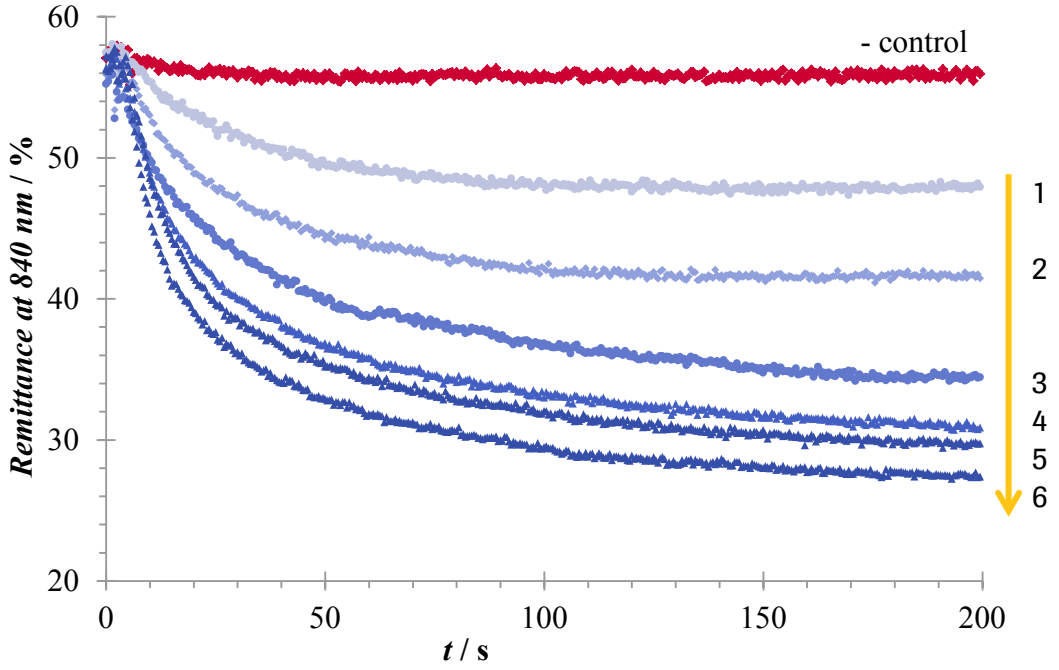

Figure 2.14 Remission spectra changes with various glucose concentrations, 1–6: 0.9, 1.9, 2.9, 6.1, 12.2, 17.8 mM.

Coating stability and homogeneity have been further estimated with a coefficient of variation (CV) between 5-10 parallel measurements of various glucose concentrations (**Figure 2.14**). The change in remittance intensity was normalized to the signal which was measured prior the glucose addition, at $t = 0$ seconds. **Figure 2.15** illustrates the relative remittance (RR) responses of the test strips to 6.1-mM glucose standards in PBS, over the initial 60 seconds. With increased time of the analysis, the standard deviations were significantly higher. We noticed that the signal was stable for about ten seconds of the reaction. By fitting the initial velocities *vs* glucose concentrations to the Michaelis–Menten equation (**Figure 2.21S**), we further confirmed that glucose and reaction products were homogeneously distributed in the dry layer at the initial stage.

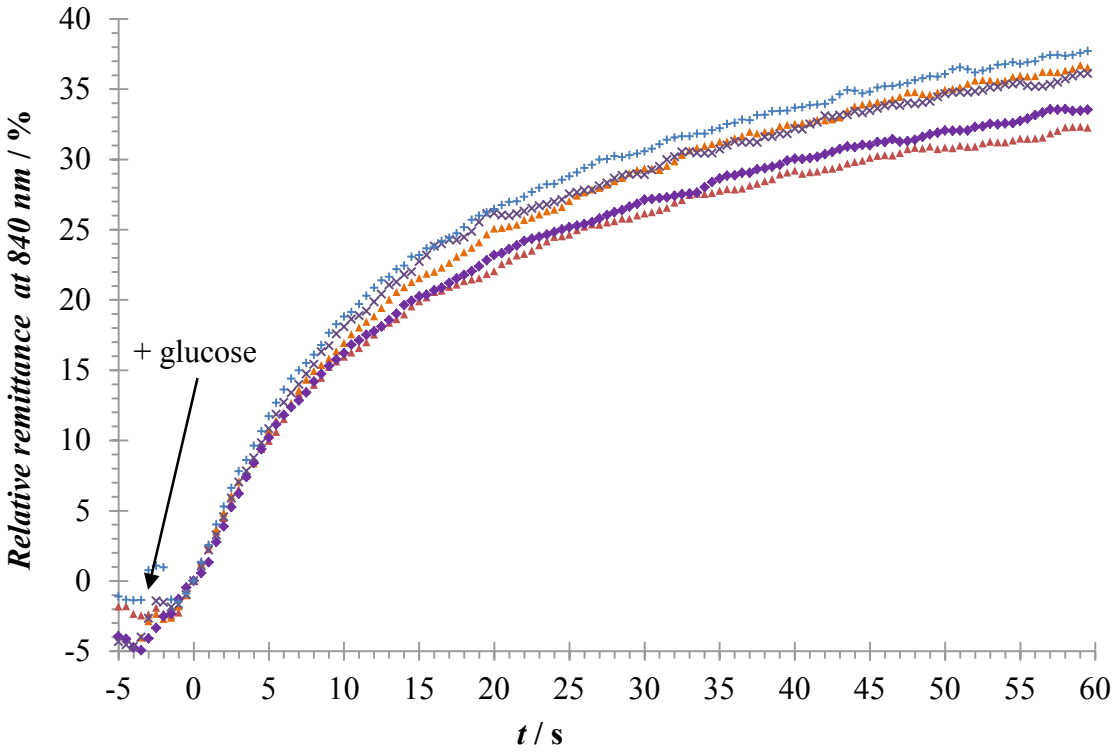

Figure 2.15 A plot showing the relative remittance of five parallel measurements at 6.1 mM of glucose on test strips.

As shown in **Figure 2.16**, the system linearity was held from 0.9 to 6.1 mM ($R^2 = 0.99$), the equation of linear regression was expressed as $RR = 2.11*[S] + 4.0$, where $[S]$ initial glucose concentration. The coefficient of variation in these remittance measurements varied between 6 and 15%. The detection limit was estimated to be 0.3 mM, which was quantified using 3.3 standard deviations of the blank. In the high concentration range (>6.1 mM), the reactive area of the coatings was exhausted, where most **RuAP-3** molecules were assumed to be reacted with cNADH.

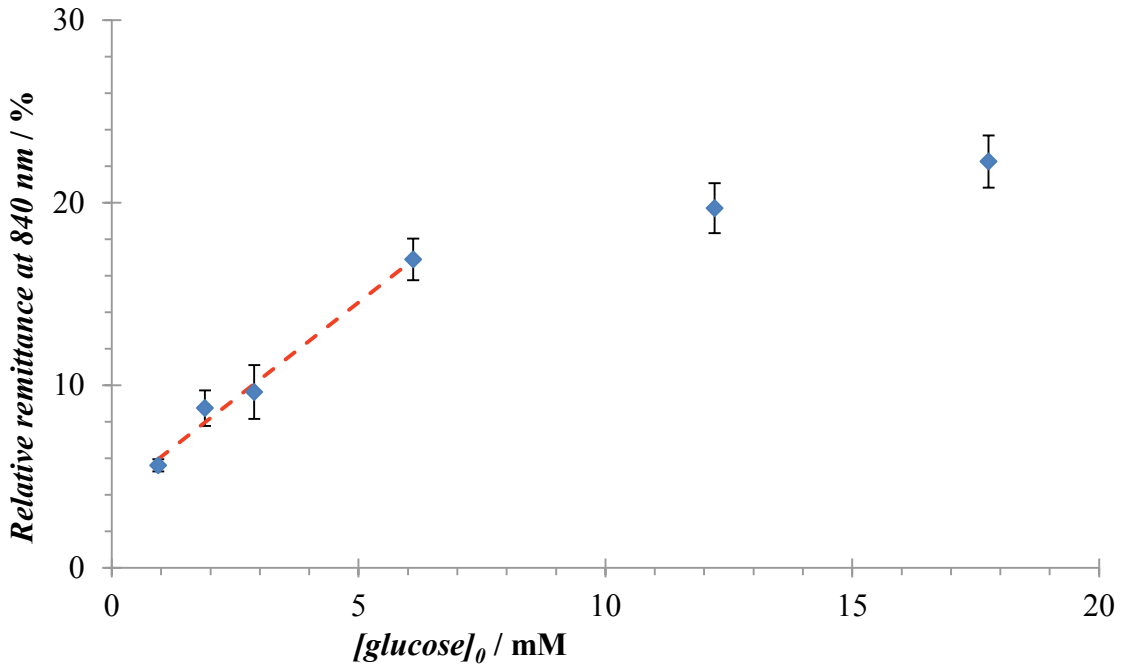

Figure 2.16 Calibration plot corresponding remission spectra changes of the determination of glucose on the test strip recorded after 10 s of reaction time. The dotted regression line (red) demonstrates a linear range — from 0.9 mM up to glucose concentration of 6.1 mM. The R^2 value of the fitting was >0.99. The error bars represent standard deviation.

Accuracy and precision are clearly dominated by quality of the coating in this case. The chemical system is open, *i.e.* the layer continuously admits water and glucose from the sample and allows out-diffusion of soluble ingredients like oxidized and reduced reagents, and possibly even enzyme. The key is a transfer rate control of the diffusion processes. After a few seconds, the optical signal from the layer was stable, but with time, the deviations between the dose-response curves were increasing (**Figure 2.15**). Our interpretation is that coatings of sub-optimal composition suffer from an inhomogeneous structure; which is leading to inhomogeneous distribution of the assay components through the depth of the layer. This needs to be studied further in order to develop more precise and reliable glucose assays in a dry chemistry format. However, the data are encouraging as the issue is well known in the coating development and it could be optimized in order to achieve a more precise and reliable assay.

2.3 Conclusions

For the first time, we demonstrated that a colorimetric indicator — directly accepting electrons from an enzymatic reaction — can be utilized for glucose sensing on a dry chemistry test strip. The design is based on the assembly of a quinone-functionalized Ru(II) complex, the artificial cofactor $cNAD^+$ and mutated GDH to trigger the optical response. **RuAP-3** is readily reduced by cNADH to give absorption at 840 nm in proportion to the glucose concentration — in a region free of intrinsic absorption of blood and that of therapeutics. The simpler reaction scheme and lack of the need for mediators add useful features to the present system. The ten-second detection time fulfils industrial standards of point-of-care glucose monitoring and might be acceptable for low-cost strips.

Based on these findings, it is concluded that the proposed "mediatorless" chemistry is technically viable. With future work, it can be realized as a new platform for blood glucose monitoring and possibly as low-cost diagnostic means for diabetes patients. Accordingly, the compositions of dry chemistries have to be optimized for this novel system in order to obtain strips with maximum stability, dynamic range and precision. Finally, potential obstacles are ascorbic acid and oxygen inferences that may limit wide application of the **RuAP-3** indicator. Thus detailed mechanism of electron transfer still needs to be studied.

In summary, we anticipate that these discoveries would open a new avenue for the development of small molecule indicators for glucose sensing enzymes.

2.4 Experimental part

2.4.1 Materials and methods

Synthesis

Reagents and solvents were purchased at the highest commercial quality from Acros Organics, Alpha-Aesar, Fluka, Sigma-Aldrich or VWR and used without further purification, unless otherwise stated. Solvents were used in p.a. quality and dried according to common procedures, if necessary.[30]

2,3-Dichloro-l,4-naphthoquinone 98% (**15**) was purchased from Sigma-Aldrich (Germany); phendione (**4**) was produced in the company (Roche); **RuAP-3** TFA salt was obtained by I. Barke and Dr. H.P. Josel (Roche).

1,2-Bis(triflyloxy)ethane was synthesized by following the reported procedure.[31]

Yields refer to chromatographically and spectroscopically (^{1}H NMR) homogeneous material, unless otherwise stated.

Bioassays

The phosphate buffer solutions were prepared by titration of 0.1 M KH_2PO_4 with 0.1 M K_2HPO_4 solutions and pH was adjusted to values 6.0, 7.0, 8.0 and 8.5 at 25°*C*.

Piperazine-N,N'-bis(2-ethanesulfonic acid) (PIPES; Sigma-Aldrich) and sodium chloride (Sigma-Aldrich) were used to prepare PIPES buffer solutions (25 mM PIPES; 101 mM NaCl, pH 6.1 and 7.0) at rt.

4-(2-Hydroxyethyl)piperazine-1-ethanesulfonic acid (HEPES; Sigma-Aldrich) and sodium chloride (Sigma-Aldrich) were used to prepare HEPES buffer solutions (25 mM HEPES; 101 mM NaCl, pH 8.0) at rt.

β-Nicotinamide adenine dinucleotide, reduced disodium salt hydrate (NADH, Grade I), β-nicotinamide adenine dinucleotide hydrate (NAD^+ free acid, Grade I), carba-nicotinamide adenine dinucleotide ($cNAD^+$) and modified glucose dehydrogenase lyophilisate (GlucDH2 361 U/mg) were from Roche Diagnostics GmbH.

Glucose used in the assays was β-D-glucose in PBS or water (anhydrous β-D-glucose, Merck KGaA, Darmstadt, Germany) in concentrations ranging from 0 to 20 mM.

All solutions were made up with ultra-pure Milli-Q (MQ) water (Millipore).

Coatings

The following components were used for the dry chemistry test strips: Sipernat FK 320DS (Evonik Industries AG, Hanau, Germany), poly(acrylic acid, sodium salt) PAS-Na (average molecular weight ~15 000 g/mol, Sigma-Aldrich, Steinheim, Germany), poly(4-vinylphenol) PVP25000 (average molecular weight ~25 000 g/mol, Sigma-Aldrich, Steinheim, Germany), Mowiol 18-88 (average molecular weight ~130 000 g/mol, Sigma-Aldrich, Steinheim, Germany), Gantrez S-97 BF (Ashland, Marl, Germany), Propiofan 70D (BASF, Ludwigshafen, Germany), Geropon T77 (Rhodia, Milan, Italy) and ZrO_2 TZ-3YS (Tosoh Corporation, Kaisei-cho, Japan). The supporting plastic film was Bayfol CR210 (125 μm thick, Bayer MaterialScience AG, Leverkusen, Germany).

pH

Values of pH were determined using a WTW pH 3310 meter with a SenTix81 electrode system. The glass electrode was calibrated by using standard buffers pH 4.0–9.0.

TLC

Reactions were monitored by thin layer chromatography (TLC) carried out on Merck silica plates 60 F254 and 60 RP-18 F254s, using shortwave UV light as the visualizing agent and a solution of $KMnO_4$ and heat as developing agent.

Flash LC

Column chromatography was performed using Merck silica gel (60, particle size 0.043–0.063 mm) by a method described by Still and co-workers.[32] Purity of fractions was controlled either by TLC or LC-MS.

UV-Vis

UV-vis spectra were recorded with a Cary 50 UV-Vis spectrometer (Varian, Palo Alto. California, U. S. A.) in air-equilibrated solutions at 25 ± 0.1 °*C*. A total assay volume of 1000 μL was used for each measurement. UV-Vis disposable cuvettes, BRAND semi-micro (1.5 mL), were used for all absorption measurements.

IR

IR-spectra experiments were recorded at the analytical department of Roche Diagnostics AG in Basel.

NMR

NMR spectra were recorded on a Bruker AVIII-600, DRX-500 and an Agilent 400-MR instruments and were calibrated using residual nondeuterated solvent as an internal reference.[33] The following abbreviations were used to explain NMR peak multiplicities: s = singlet, d = doublet, t = triplet, q = quartet, m = multiplet, br = broad.

HRMS and GC-MS

HRMS and GC-MS experiments were recorded at the analytical department of Roche Diagnostics AG in Basel.

2.4.2 General procedures

Anion exchange

Protocol 1. The resulting chloride salts of the complexes (**1–2**) were formed by stirring solutions of the respective PF_6 salts in MeCN (ca. 10 mM) with Amberlyst A-26 (Cl-form) anion exchange resin (chloride form) for 1 h. The resulting solutions were filtered and reduced in volume before being precipitated from solutions by slow addition of diethyl ether.

Protocol 2. A solution of a diquaternary salt (ca. 0.2-0.6 mmol) in 10–30 mL of the selected solvent was passed slowly through a column packed with ~3 cm^3 of Amberlyst A-26 (TFA form),[34] and then washed with 25 mL of solvent. The combined eluates were evaporated, and the residue obtained was dried under high vacuum. After Amberlyst A-26 (TFA form) had been stored in 1% TFA MeCN-H_2O (9:1).

UV–Vis spectroscopy: solubility measurement

The solubility of **RuAP-3** in water was determined by a method adapted from Guoxiu Wang *et al* using UV-Vis spectroscopy.[35]

*Reaction of NADH with **RuAP-3***

The following were mixed in a cuvette: 100 µL of 10.0 mM solution of the **RuAP-3** in MQ water, 900 µL of phosphate buffer (50 mM, pH 7.0) and 10 µL of 10.0 mM NADH solution in distilled water. UV-Vis spectra (300–1000 nm) was recorded every 1 min for 10 min after addition of NADH (resolution 1 nm).

*Kinetics studies of **RuAP-3** with NADH and AA*

The following were mixed in a cuvette: 100 µL of 10.0 mM stock solution of the **RuAP-3** in MQ water, 900 µL of phosphate buffer (50 mM, pH 7.0) and 5 µL of 10.0 mM reductant solution in MQ water. Kinetic data were obtained by following the

increase in absorbance at 840 nm as the reduced **RuAP-3** was formed. The absorbance data were recorded every 0.1 s for 300 s after addition of NADH. A pseudo-first-order rate constant (k_{obs}) was calculated from the initial linear parts by the Guggenheim method, from slope of the plots of $ln(A_{t+dt} - A_t)$ *vs* time using MS Excel software. Assays were performed at least in triplicate with a reproducibility of less than 5% error.

*Reaction of **RuAP-3** with glucose/GlucDH2*

Glucose solution (1.1 M): 2 g of β-D-glucose was dissolved in 10 mL MQ water. The solution was ready-to-use after a standing time of 2 hours at rt and adjustment of the mutarotation equilibrium. NAD^+ buffer solution (30.1 mM): 20.0 mg NAD^+ free acid was dissolved in 1.0 mL buffer solution. CarbaNAD^+ solution (29.2 mM): 20.0 mg $cNAD^+$ Na-salt was dissolved in 1.0 mL buffer solution. In order to prepare for the measurement, 10.0 mg of the GlucDH2 (361 U/mg) was dissolved in 1.0 mL of either NAD^+ or $cNAD^+$ buffer solution and kept for 60 min at rt, in order to allow a reconstitution. Subsequently it was diluted with buffer to 491 U/mL.

The following were mixed in a cuvette: 500 µL of 1.0 mM solution of **RuAP-3** in 100 mM phosphate buffer pH 7.0, 500 µL of GlucDH2 solution (in 100 mM phosphate buffer pH 7.0 containing either 4.0 mM NAD^+ or 4.0 mM $cNAD^+$) at a concentration of 491 U/mL, 0-12 µL of 10.0 mM solution of glucose in MQ water. The assay was initiated by the addition of glucose and incubated for 20 min. A UV-Vis spectrum was recorded as mentioned in descriptions under the figures. The linear portion of absorbance increase was used to determine the initial rate of reduction. The initial reaction rates were plotted according to the method of Lineweaver and Burk. The final presented values for K_m and V_{max} were determined by fitting initial rates to a hyperbolic v *vs* *[S]* plot with a MS Excel software by a method adapted from the procedure described by Gerdi Kemmer & Sandro Keller (**Figure 2.20S**).[36]

Test strips: measurements and analysis

Evaluation of the function and stability of the test strips involved both visual examinations of the coatings as well as measurements with a spectrometer. The coating quality and homogeneity were observed visually through the coating process. Mechanical stability of the coatings was evaluated by a simple scratching test. The flexibility of the coatings was tested by rolling the product sheets into tight rolls; the film has to be able to bend around the collector reel of the coating machine without cracking.

The remittance signal of the strips was measured with a spectrophotometer (TIDAS S 700, J&M Analytik AG, Germany). A calibration measurement was performed in the beginning of the measurement using a special reference strip (black&white references) to set the maximum remittance signal value. To control the initial spectrometric properties of the strips in a broadband spectrum, remittance of the dry strips was measured at wavelengths from 300 nm to 1000 nm.

The glucose resolution capacity of the coatings was evaluated by measuring the strip remittance with PBS samples at rt. The remittance was measured for 200 s, covering wavelengths from 300–1000 nm with an integration time of 550 ms in five parallel measurements. The spectrum was recorded initially from a dry strip without any sample to obtain the reference signal and subsequently, after the addition of the 5 µL sample of glucose in PBS, with three second intervals. The remittance values at 840 nm (*i.e.* the absorption maximum of **RuAP-3**) of each experiment have been extracted using Panorama software (LabCognition, Analytical Software GmbH).

2.4.3 Preparation of the complexes **1-3**

*Synthesis of **RuNP-1***

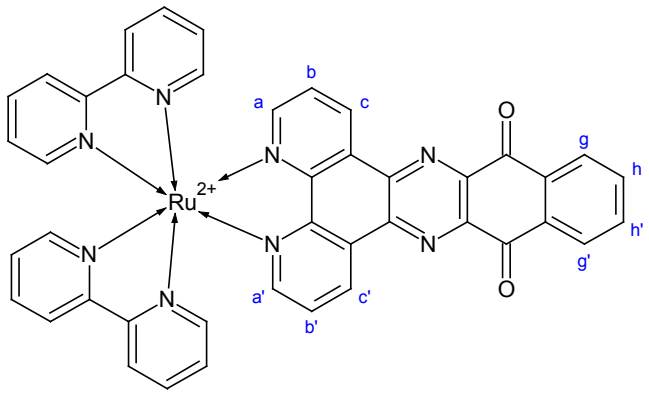

$Ru(bpy)_2Cl_2$ **9** (100 mg, 0.21 mmol) and nqphen **7** (76 mg, 0.21 mmol) were refluxed in ethylene glycol (10 mL) for 14 h. The resulting solution was cooled to the rt, after which water (4 mL) was added and the solution was filtered. Addition of solid NH_4PF_6 (90 mg, 0.55 mmol) to the filtrate precipitated the crude product (**1**). The latter was dissolved in a minimum amount of MeCN, and then ether (50 mL) was added rapidly with stirring. The resulting precipitates were collected by filtration and dried *in vacuo* to obtain **RuNP-1** (145 mg, 0.14 mmol) as PF_6 salt.

FW: 1065.71. **MF:** $C_{42}H_{26}F_{12}N_8O_2P_2Ru$. **Yield:** 66%. **Physical State:** red powder.

The characterization data for **1** are in accordance of that reported by Chesneau *et al.*[17]

UV-Vis (MeCN, PF_6 salt) λ_{max} (ε $mM^{-1}cm^{-1}$) 444 (17.0), 283 (92.8), 239 (44.6) nm.

^{1}H NMR (MeCN-d_3, 500MHz, COSY, HSQC; PF_6 salt): δ = 9.68 (dd, J = 8.2, 1.2 Hz, 2 H, H_c and $H_{c'}$), 8.51–8.58 (m, 4 H, bpy-H), 8.48 (dd, J = 5.8, 3.4 Hz, 2 H, H_g and $H_{g'}$), 8.28 (dd, J = 5.2, 1.2 Hz, 2 H, H_a and $H_{a'}$), 8.13 (td, J = 8.0, 1.4 Hz, 2 H, bpy-H), 8.06 (dd, J = 5.8, 3.4 Hz, 2 H, H_h and $H_{h'}$), 8.03 (td, J = 7.9, 1.5 Hz, 2 H, bpy-H), 7.96 (dd, J = 8.2, 5.2 Hz, 2 H, H_b and $H_{b'}$), 7.84–7.87 (m, 2 H, bpy-H), 7.68–7.72 (m, 2 H, bpy-H), 7.48 (ddd, J = 7.7, 5.6, 1.4 Hz, 2 H, bpy-H), 7.26 (ddd, J = 7.5, 6.0, 1.2 Hz, 2 H, bpy-H) ppm.

^{13}C NMR (MeCN-d_3, 126MHz, HSQC; PF_6 salt): δ = 181.8 (2C, C=O), 158.4 (2C, C_q), 158.1 (2C, C_q), 156.1 (2C, C_a and $C_{a'}$), 153.4 (2C, bpy-CH), 153.2 (2C, bpy-CH), 151.9 (2C, C_q), 146.5 (2C, C_q), 143.5 (2C, C_q), 139.2 (2C, bpy-CH), 139.1 (2C, bpy-CH), 136.7 (2C, C_h and $C_{h'}$), 135.4 (2C, C_c and $C_{c'}$), 135.0 (2C, C_q), 131.0 (2C, C_q), 128.9 (2C, C_g and $C_{g'}$), 128.8 (4C, C_b and $C_{b'}$, and bpy-CH), 128.6 (2C, bpy-CH), 125.5 (4C, bpy-CH) ppm.

Synthesis of ***RuNPCl-2***

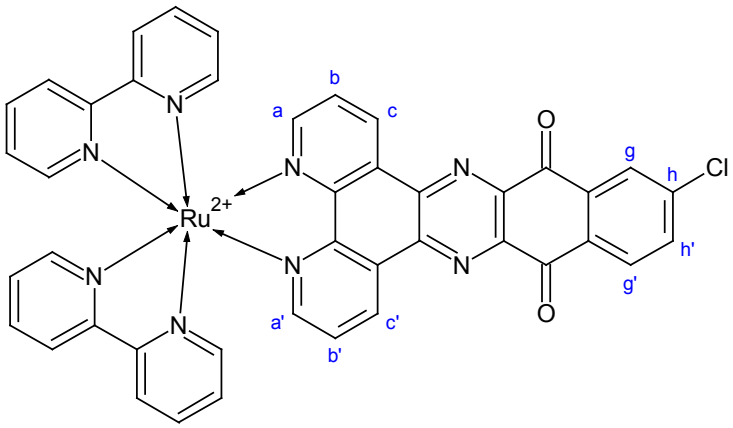

$Ru(bpy)_2Cl_2$ **9** (57 mg, 0.11 mmol) and nqphen-Cl **8** (50 mg, 0.13 mmol) were refluxed in ethylene glycol (5 mL) for 14 h under N_2. The resulting solution was cooled to rt, after which 2 mL of water was added and the solution was filtered. Addition of solid NH_4PF_6 (75 mg, 0.45 mmol) to the filtrate precipitated crude product (**2**). The latter was dissolved in a minimum amount of MeCN, and purified by column chromatography on silica (10 g) using MeCN-water-saturated KNO_3 (aq.) (90:10:0.2 v/v/v) as the eluent. NH_4PF_6 (excess) was used to precipitate the product. To eliminate NH_4PF_6 contamination, the filtrate was washed thoroughly with water. The material was dried *in vacuo* to obtain **RuNPCl-2** (30 mg, 0.03 mmol) as PF_6 salt.

MF: $C_{42}H_{25}ClF_{12}N_8O_2P_2Ru$. **FW:** 1100.15. **Yield:** 27%. **Physical State:** dark red solid.

IR (KBr, cm^{-1}) 1689 (C=O).

^{1}H NMR (MeCN-d_3, 600MHz, HSQC; PF_6 salt): δ = 9.67 (dd, J = 8.3, 1.3 Hz, 1 H, H_c or $H_{c'}$), 9.66 (dd, J = 8.3, 1.3 Hz, 1 H, H_c or $H_{c'}$), 8.56 (dd, J = 8.3, 0.7 Hz, 2 H, bpy-H), 8.45 (d, J = 8.4 Hz, 1 H, $H_{g'}$), 8.44 (d, J = 2.1 Hz, 1 H, H_g), 8.28 (dd, J = 5.3, 1.3 Hz, 1 H, H_a and $H_{a'}$), 8.13 (td, J = 8.0, 1.5 Hz, 2 H, bpy-H), 8.02–8.05 (m, 2 H, bpy-H), 8.02 (dd, J = 8.2, 1.4 Hz, 1 H, $H_{h'}$), 7.96 (dd, J = 8.2, 5.3 Hz, 2 H, H_b and $H_{b'}$), 7.84–7.87 (m, 2 H, bpy-H), 7.68–7.72 (m, 2 H, bpy-H), 7.47 (ddd, J = 7.7, 5.6, 1.3 Hz, 2 H, bpy-H), 7.25 (ddd, J = 7.3, 6.0, 1.1 Hz, 2 H, bpy-H) ppm.

^{13}C NMR (MeCN-d_3, 151MHz; PF_6 salt): δ = 180.9 (C_q, C=O), 180.8 (C_q, C=O), 158.2, 158.0, 156.2, 153.3, 153.1, 151.9, 151.9, 146.2, 146.1, 143.6, 143.5, 142.8, 139.2, 139.1, 136.5, 136.1, 135.3, 133.4, 130.9, 130.7, 128.8, 128.7, 128.5, 128.4, 125.4, 125.4 ppm.

HRMS (pos. ESI): *m/z* 405.0410 ($[M - 2PF_6]^{2+}$) calculated for C42H25ClN8O2Ru++: 405.0416 (Δ −1.5 ppm).

*Characterization of **RuAP-3***

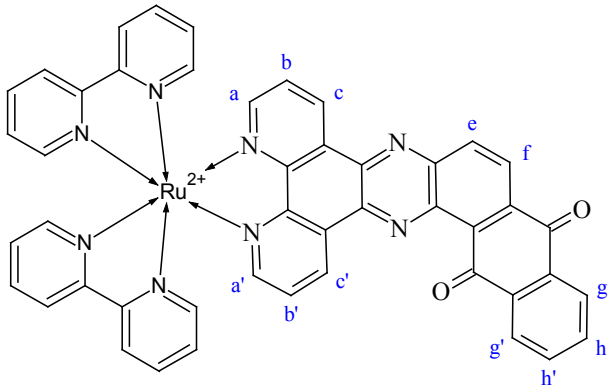

RuAP-3 TFA salt was a gift of I. Barke and Dr. H.P. Josel (Roche Penzberg).

MF: $C_{50}H_{28}F_6N_8O_6Ru$. **FW:** 1051.87. **Physical State:** brown powder.

UV-Vis (50 mM PB pH 7.0) λ_{max} (ε $mM^{-1}cm^{-1}$) 434sh (15.0), 394 (16.6), 275 (84.7), 237 (43.0) nm.

^{1}H NMR (MeOD-d_3, 500MHz, COSY, HMBC, HSQC; TFA salt): δ = 9.74 (d, J = 8.2 Hz, 1 H, H_c or $H_{c'}$), 9.67 (d, J = 8.2 Hz, 1 H, H_c or $H_{c'}$), 8.75–8.83 (m, 4 H, bpy-H), 8.69 (d, J = 8.8 Hz, 1 H, H_e), 8.64 (d, J = 8.8 Hz, 1 H, H_f), 8.35 (d, J = 5.4 Hz, 2 H, H_a and $H_{a'}$), 8.30 (d, J = 7.9 Hz, 1 H, H_g or $H_{g'}$), 8.20–8.25 (m, 2 H, bpy-H), 8.09–8.18 (m, 2 H, bpy-H), 7.97–8.00 (m, 6 H, bpy-H), 7.96 (d, J = 7.9 Hz, 1 H, H_g or $H_{g'}$), 7.93 (t, J = 7.6 Hz, 1 H, H_h or $H_{h'}$), 7.78 (t, J = 7.6 Hz, 1 H, H_h or $H_{h'}$), 7.60 (t, J = 6.1 Hz, 2 H, bpy-H), 7.37–7.49 (m, 2 H, bpy-H) ppm.

^{13}C NMR (MeOD-d_3, 126MHz): δ = 184.2 (C_q, C=O), 183.9 (C_q, C=O), 161.9 (q, J = 36.7, TFA), 158.9 (C_q, 2C), 158.7 (2C, C_q), 155.5 (C_a or $C_{a'}$), 155.3 (C_a or $C_{a'}$), 153.4 (2C, bpy-CH), 153.1 (2C, bpy-CH), 152.8 (C_q), 152.6 (C_q), 145.7 (C_q), 143.7 (C_q), 142.1 (C_q), 141.7 (C_q), 139.7 (2C, bpy-CH), 139.6 (2C, bpy-CH), 138.2 (C_q), 137.1 (H_e), 136.3(1) (H_h or $H_{h'}$), 136.3 (C_q), 136.0 (H_c or $H_{c'}$), 135.5 (H_c or $H_{c'}$), 135.2 (H_h or $H_{h'}$), 133.3 (C_q), 132.5 (C_q), 132.0 (C_q), 130.5 (C_q), 129.3 (C_f), 129.2 (2C, bpy-CH), 129.0 (2C, bpy-CH), 128.2 (H_g or $H_{g'}$), 127.6 (H_g or $H_{g'}$), 125.9 (4C, bpy-CH), 117.8 (q, J = 290.5, TFA) ppm.

^{19}F NMR (MeOD-d_3, 470MHz): δ = −77.17 (TFA) ppm.

HRMS (pos. ESI): *m/z* 414.0771 ($[M - 2TFA]^{2+}$) calculated for C46H28N8O2Ru++: 414.0774 (Δ −0.7 ppm).

Solubility in water: ≥ 60 mM.

2.4.4 Preparation of the ligands (**7**-**8**)

Synthesis of nqphen (7) as reported previously.[17]

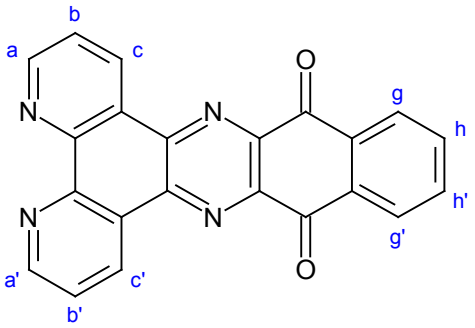

Step 1. To a solution of dichloride **11** (4.63 g; 20.4 mmol) in anhydrous acetonitrile (100 mL), potassium phthalimide (15.54 g, 83.9 mmol) was added. The reaction mixture was refluxed for 3 h, and then the hot solution was filtered. The precipitate was washed successively with acetonitrile (200 mL), water (200 mL) and methanol (200 mL). Diphtalimide **13** was dried *in vacuo* at 50°*C* and isolated as a pale yellow powder (6.60 g, 14.7 mmol) in 74% yield.

Step 2. To a suspension of diphtalimide **13** (4.48 g; 10.0 mmol) in water (300 mL) was added a 64% solution in water of hydrazine (40 mL). The solution was stirred for 15 min at rt then heated at 65-70°*C* for 3 h. The reaction mixture was allowed to stand at rt. The precipitate was filtered, and then washed with a large volume of water. Diamine **5** was dried overnight *in vacuo* at 100°*C* and isolated as a purple powder (1.80 g, 9.6 mmol) in 96% yield.

Step 3. A solution of diamine **5** (800 mg; 4.25 mmol) and phendione **4** (863 mg; 4.25 mmol) in glacial acetic acid (60 mL) was heated at 75°*C* for 3 h under N_2 atmosphere and the reaction was monitored by TLC (DCM/MeOH-drop). The reaction mixture was allowed to stand at rt. The precipitate was filtered, then washed with EtOH, DCM and ether to give nqphen **7** (1.44 g, 3.98 mmol) in 94% yield.

MF: $C_{22}H_{10}N_4O_2$. **FW:** 362.34. **Yield:** 68% (3 steps). **Physical State:** green powder.

The characterization data for **7** is in accordance of that reported by Diaz *et al.*[37]

^{1}H NMR ($CDCl_3$, 500MHz, HSQC): δ = 9.80 (dd, J = 8.2, 1.8 Hz, 2 H, H_c and $H_{c'}$), 9.40 (dd, J = 4.4, 1.8 Hz, 2 H, H_a and $H_{a'}$), 8.53–8.57 (m, 2 H, H_g and $H_{g'}$), 7.98 (dd, J = 5.8, 3.4 Hz, 2 H, H_h and $H_{h'}$), 7.91 (dd, J = 8.2, 4.4 Hz, 2 H, H_b and $H_{b'}$) ppm.

^{13}C NMR the analytical department provided us only with ^{1}H-HSQC overlay spectra report (see supplementary NMR spectra section).

*Synthesis of nqphen-Cl (**8**)*

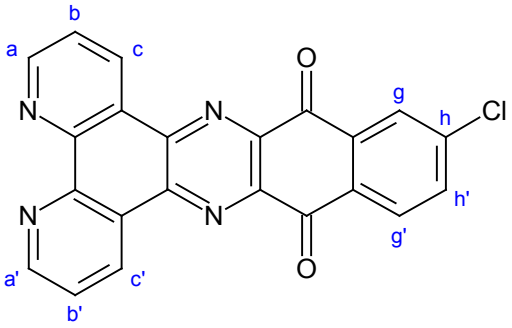

A mixture of diamine **6** (80 mg; 0.36 mmol) and phendione **4** (76 mg; 0.36 mmol) in glacial acetic acid (10 mL) was refluxed for 3 h under N_2. The reaction mixture was allowed to stand at rt. The precipitate was formed, which was collected, washed with EtOH, DCM and ether to yield **8** (123mg, 0.31 mmol).

MF: $C_{22}H_9ClN_4O_2$. **FW:** 396.78. **Yield:** 86%. **Physical State:** pale green powder.

^{1}H NMR ($CDCl_3$, 600MHz, HSQC): δ = 9.78 (dd, J = 8.2, 1.8 Hz, 2 H, H_c and $H_{c'}$), 9.41 (dd, J = 4.4, 1.8 Hz, 2 H, H_a and $H_{a'}$), 8.49 (d, J = 8.4 Hz, 1 H, $H_{g'}$), 8.49 (d, J = 2.0 Hz, 1 H, H_g), 7.93 (dd, J = 8.4, 2.0 Hz, 1 H, $H_{h'}$), 7.92 (dd, J = 8.2, 4.4 Hz, 1 H, H_b or $H_{b'}$), 7.92 (dd, J = 8.2, 4.4 Hz, 1 H, H_b or $H_{b'}$) ppm.

^{13}C NMR the Roche analytical department provided us only with ^{1}H-HSQC overlay spectra report (see supplementary NMR spectra section).

HRMS (pos. ESI): *m/z* 397.0484 ($[M + H]^+$) calculated for C22H10ClN4O2+: 397.0492 (Δ −2.0 ppm).

2.4.5 Preparation of the 2,3-diamino-6-chloro-1,4-naphtoquinone **(6)**

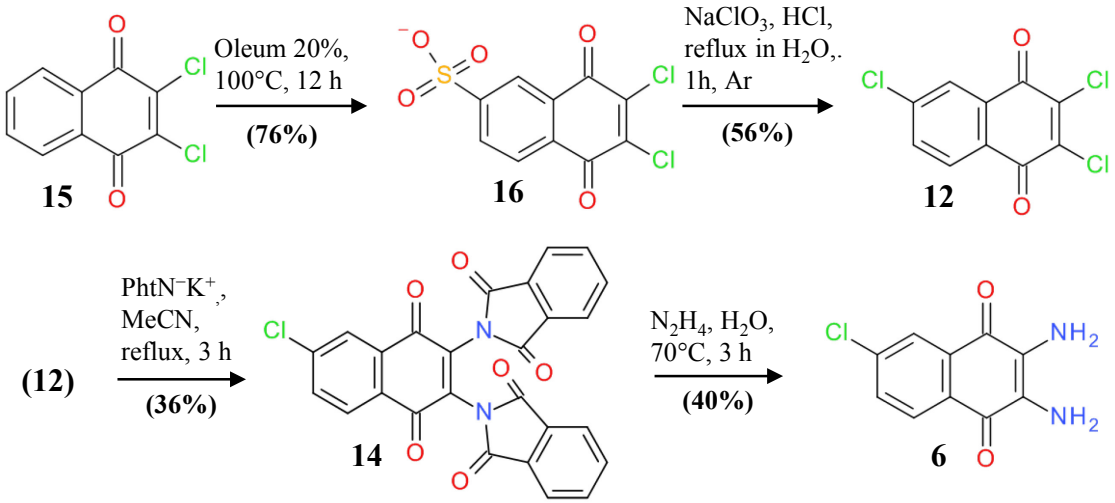

Synthesis of 2,3-dichloro-l,4-naphthoquinone-6-sulfonic acid sodium salt ***(16)***

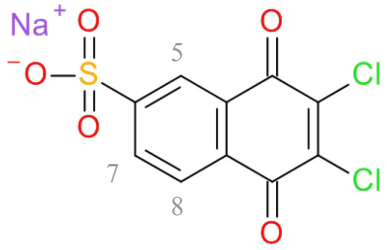

Compound **16** was synthesized as reported previously by Shishkina *et al*.[18]

Oleum 20% (36.0 mL) was added gradually with stirring to 2,3-dichloro-l,4-naphthoquinone **15** (10.0 g, 0.044 mol). The mixture was heated to 100°*C* and stirred under nitrogen atmosphere for 12 h (when a test sample of the reaction mixture did not give a clear solution in water). The red-brown mass was poured directly onto ice (250 g), filtered and washed well with water. Then NaC1 (about 25 g) was added to the filtrate: grey solid was obtained, washed with NaCl (saturated), ethanol, and dried at 100–120°*C* to give compound **16** (10.9 g, 0.033 mmol).

MF: $C_{10}H_3Cl_2O_5S$-Na. **FW:** 329.09. **Yield:** 76%. **Physical State:** grey solid.

HPLC UV-Vis (H_2O-MeCN 1:1) λ_{max} 209, 251, 257, 284, 355–342 sh. nm.

^{1}H NMR (DMSO-d_6, 500MHz): δ = 8.26 (dd, J = 1.2, 0.9 Hz, 1 H, C^7H), 8.06–8.08 (m, 2 H, C^5H and C^8H) ppm.

^{13}C NMR (DMSO-d_6, 126MHz): δ = 175.6 (C_q, C=O), 175.4 (C_q, C=O), 153.5 (C_q), 142.5 (2C, C_q), 131.1 (CH), 130.8 (C_q), 130.7 (C_q), 127.2 (CH), 123.9 (CH) ppm.

Synthesis of 2,3,6-trichloro-1,4-naphtoquinone ***(12)***

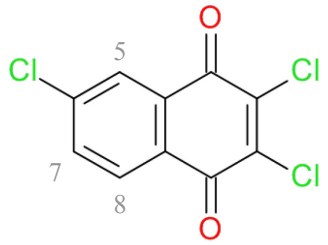

Following the modified procedure[18] described by Shishkina *et al*: a solution of $NaClO_3$ (1.94 g, 18.23 mmol) in water (25 mL) was added dropwise with stirring to a solution of **16** (2.00 g, 6.07 mmol) in water (100 mL) and HCI (conc., 4.5 mL) during 1 h under reflux in Ar. A yellowish white solid was gradually precipitated. The mixture was

further refluxed for 1 h, cooled to rt and left overnight at 4°*C*. The precipitate was filtered off, washed with cold water and dried to give **12** (0.89 g, 3.40 mmol).

MF: $C_{10}H_3Cl_3O_2$. **FW:** 261.49. **Yield:** 56%. **Physical State:** light-yellow solid.

The characterization data for compound **16** are in accordance of that reported by Shishkina *et al*.[18]

^{1}H NMR (acetone-d_6, 500MHz): δ = 8.05 (d, J = 8.2 Hz, 1 H, C^{8}H), 7.97 (d, J = 2.1 Hz, 1 H, C^{5}H), 7.83 (dd, J = 8.2, 2.1 Hz, 1 H, C^{7}H) ppm.

Synthesis of 2,3-diamino-6-chloro-1,4-naphtoquinone ***(6)***

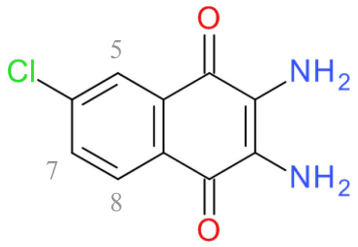

Step 1. To a solution of 2,3,6-trichloro-1,4-naphthoquinone **12** (0.89 g; 3.40 mmol) in anhydrous acetonitrile (25 mL), potassium phthalidimide (2.52 g, 13.61 mmol) was added. The reaction mixture was refluxed for 3 h, after the hot solution was filtered. The precipitate was washed successively with acetonitrile (100 mL), water (100 mL) and methanol (100 mL). 6-chloro-2,3-diphthalimido-1,4-naphthoquinone **14** was dried *in vacuo* at 50°*C* and isolated as a pale yellow powder (0.59 g, 1.22 mmol).

Step 2. To a suspension of **14** (0.59 g; 1.22 mmol) in water (40 mL) was added a 64% solution of hydrazine (1.2 mL). The solution was stirred for 15 min at rt, then heated at 65–70°*C* for 3 h. The reaction mixture was allowed to stand at rt. The precipitate was filtered, and then washed with a large volume of water. This material was dried overnight *in vacuo* at 100°*C* to give target compound **6** (110 mg, 0.49 mmol).

MF: $C_{10}H_7ClN_2O_2$. **FW:** 222.63. **Yield:** 14% (2 steps). **Physical State:** purple powder.

The characterization data for compound **6** are in accordance of that reported by Kul'bitskii *et al*.[19]

^{1}H NMR ($CDCl_3$, 600MHz): δ = 7.94 (d, J = 2.1 Hz, 1 H, C^{5}H), 7.92 (d, J = 8.3 Hz, 1 H, C^{8}H), 7.55 (dd, J = 8.2, 2.1 Hz, 1 H, C^{7}H), 4.13 (br. s., 4 H, NH_2) ppm.

GC-MS (EI-MS) *m/z* 222 (M^+).

2.4.6 Preparation of the diquaternary salts (**15–16**)

*Synthesis of compound **15***

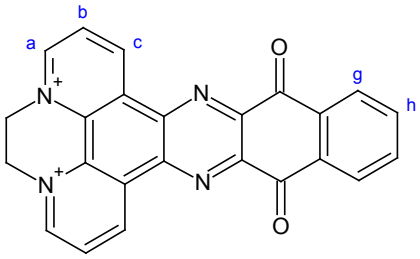

Nqphen **7** (0.78 g, 2.76 mmol) was suspended in 40 mL of 1,2-dibromoethane. The suspension was then brought to reflux for 7 d under Ar. A red precipitate was collected and taken up in water, filtered, concentrated and addition of NH_4PF_6 afforded a red precipitate. This was collected and washed with water (50 mL) and then dried *in vacuo* to give compound **15** (170 mg).

FW: 680.32. **MF:** $C_{24}H_{14}F_{12}N_4O_2P_2$. **Yield:** 9%. **Physical State:** red solid.

UV-Vis λ_{max} (ε $mM^{-1}cm^{-1}$) for **15** TFA salt (anion exchange, **protocol 2**):

(water) 356 (11.2), 314 (20.), 276 (38.8), 215 (24.5) nm;

(25 mM PIPES pH 6.1) 459 (2.9), 275 (35.2), 220 (21.2) nm;

(25 mM PIPES pH 7.0) 460 (8.8), 299 (33.1), 272 (30.3), 224 (22.9) nm;

(25 mM phosphate buffer pH 8.0) 461 (9.6), 300 (25.3), 268 (18.7), 226 (15.1) nm.

^{1}H NMR (MeCN-d_3, 600MHz, COSY, HMBC, HSQC; PF_6 salt): δ = 10.51 (d, J = 8.5 Hz, 2 H, H_c), 9.53 (d, J = 5.7 Hz, 2 H, H_a), 8.83 (dd, J = 8.5, 5.7 Hz, 2 H, H_b), 8.51 (dd, J = 5.7, 3.3 Hz, 2 H, H_g), 8.10 (dd, J = 5.7, 3.3 Hz, 2 H, H_h), 5.57 (s, 4 H, *N*-alk) ppm.

^{13}C NMR (MeCN-d_3, 126MHz, HMBC, HSQC; PF_6 salt): δ = 181.3 (C=O), 152.1 (C_a), 148.3 (C_q), 146.4 (Cc), 141.3 (C_q), 137.3 (Ch), 135.2 (C_q), 133.5 (C_q), 132.6 (C_q), 131.5 (Cb), 129.3 (Cg), 54.0 (N-CH_2) ppm.

^{31}P NMR (MeCN-d_3, 600 MHz; PF_6 salt) δ = 144.81 ppm.

^{19}F NMR (MeCN-d_3, 470MHz, PF_6 salt): δ = -72.23, -73.74 ppm.

HRMS (pos. ESI) *m/z* 195.0559 ($[M - 2PF_6]^{2+}$) calculated for C24H14N4O2++: 195.0553 (Δ 3.1 ppm).

Solubility in water: ≥10 mM.

Synthesis of compound ***16***

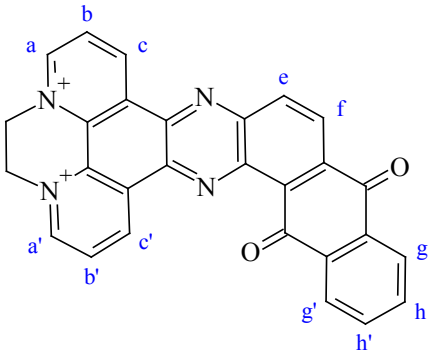

A solution of aqphen **10** (100 mg, 0.24 mmol) and 1,2-bis(triflyloxy)ethane (860 mg, 2.63 mmol) in dry DCM (20 mL) was stirred at rt for 16 h under Ar. A red precipitate was filtered, washed with DCM and dried *in vacuo* to give **16** (143 mg, 0.19 mmol).

MF: $C_{30}H_{16}F_6N_4O_8S_2$. **FW:** 738.59. **Yield:** 79%. **Physical State:** red solid.

UV-Vis λ_{max} (ε $mM^{-1}cm^{-1}$) for **16** TfO salt:

(25 mM PIPES pH 6.1) 385 (14.8), 291 (63.7), 241 (37.7) nm;

(25 mM PIPES pH 7.0) 486 (3.4), 382 (12.7), 292 (54.3), 241 (35.7) nm;

(25 mM HEPES pH 8.0) 486 (4.5), 381 (9.8), 293 (37.3), 243(33.3) nm.

^{1}H NMR (DMSO-d_6, 600MHz, COSY, HMBC, HSQC; TfO salt): δ = 10.46 (d, J = 7.9 Hz, 1 H, H_c or $H_{c'}$), 10.44 (d, J = 8.3 Hz, 1 H, H_c or $H_{c'}$), 9.91 (d, J = 5.4 Hz, 1 H, H_a or $H_{a'}$), 9.88 (d, J = 5.5 Hz, 1 H, H_a or $H_{a'}$), 9.05 (dd, J = 8.0, 5.9 Hz, 1 H, H_b or $H_{b'}$), 8.90–9.00 (m, 3 H, H_b or H_b, H_e and H_f), 8.31 (d, J = 7.6 Hz, 1 H, H_g or $H_{g'}$), 8.26 (d, J = 7.5 Hz, 1 H, H_g or $H_{g'}$), 8.04–8.07 (m, 1 H, H_h or $H_{h'}$), 7.95–8.00 (m, 1 H, H_h or $H_{h'}$), 5.70 (s, 4 H, *N*-alk) ppm.

^{13}C NMR (DMSO-d_6, 126MHz, HMBC, HSQC; TfO salt): δ = 182.8 (C=O), 182.3 (C=O), 150.3 (2C, C_a and $C_{a'}$), 144.4 (C_q), 143.4 (C_c or $C_{c'}$), 143.2 (C_c or $C_{c'}$), 141.0 (C_q), 139.5 (C_q), 138.1 (C_q), 137.6 (C_q), 135.8 (Ce), 135.3 (C_h or $C_{h'}$), 134.6 (C_q), 134.4 (C_h or $C_{h'}$), 133.0 (C_q), 132.8 (C_q), 131.8 (C_q), 131.1 (C_q), 130.6 (C_q), 130.0 (C_b or $C_{b'}$), 129.7 (2C, C_b or $C_{b'}$, C_f), 128.9 (C_q), 126.7 (C_g or $C_{g'}$), 126.5 (C_g or $C_{g'}$), 120.7 (CF_3, J = 323 Hz), 52.6 (aqphen-CH_2), 52.5 (aqphen-CH_2) ppm.

^{19}F NMR (DMSO-d_6, 470MHz, TfO salt): δ = −77.77 ppm.

HRMS (pos. ESI) *m/z* 442.1438 ($[M + 2H – 2TfO]^+$) calculated for C28H18N4O2+: 442.1430 (Δ 1.8 ppm).

Solubility in water: ≥2 mM.

2.4.7 Preparation of the dry chemistry layers

The general structure of the test strips is presented previously.[1] The dry chemistry layer on the test strips was composed of two layers, a bottom one with the sensing elements (enzyme and the indicator) — chemistry layer, and a top one with the reflecting pigment zirconium dioxide (TZ-3YS-E) — mirror layer. Of each variant at minimum 5 g of formulation (incl. solvent) was prepared. The filler and pigment compounds, binders and additives were dissolved in MQ water and incubated in ultra-sonication bath for 10 min to break down particle aggregates. Enzyme and coenzyme were dissolved in phosphate buffer (PB, 0.5 M, pH 7.5) and added to the formulation after sonication. Coating formulations were mixed for 1 h to ensure homogeneity. The pH value of the mixed formulations was adjusted to 7.5. After the pH adjustment the masses were centrifuged (50 rcf, 10 min, rt) to remove air bubbles and filtered through a mesh cloth (ø 32 µm) to remove remaining solid clots.

The composition of the mirror layer was the same in every experiment and was selected according to results of earlier coating experiments at Roche Diagnostics GmbH (data not disclosed). The composition of the mirror layer was from 19.97 g zirconium powder TZ-3YS, 20.57 g MQ water, 1.23 g of 35% poly(acrylic acid sodium salt) solution, 22.47 g of 7% Gantrez S-97 (pH 7.5), 7.92 g of 33% polyvinylpropionate dispersion (Propiofan70VAR), 0.98 g of 5% surfactant (Geropon T-77) with pH adjusted to 7.5.

The compositions of the chemistry layer based on Gantrez S-97: from 0.30 g of silica gel (Sipernat FK 320DS), 1.70 g of MQ water, 0.03 g of polyvinylpyrrolidone (PVP25000), 0.44 g of phosphate buffer solution (pH = 7.5, 0.5 M), 0.66 g of 7% Gantrez S-97 (pH 7.5), 0.36 g of 33% polyvinylpropionate dispersion (Propiofan70VAR), 0.002 g of Geropon T-77, 0.19 g of $cNAD^+$, 0.10 g of GlucDH2 and 1.21 g of 1.1% **RuAP-3**.

The compositions of the chemistry layer based on Mowiol 18-88 are listed in **Table 2-3**. The coating masses were then spread on the plastic film using a manual blade coating. The first layer, containing the enzyme and the indicator, was coated with a blade (see blade height in **Table 2-3**) and dried in a drying oven at +50°*C* for 15 min. After this, the mirror layer was applied on top of this with a blade height of 91 µm from the film and dried the same way.

Table 2-3 Coating formulations.

Component	Concentration (in wt.%)	Content in the coating solution (in wt.%)		
RuAP-3 conc., g/m^2		0.1	0.2	2.0
Sipernat FK 320DS	100	6.9	6.0	4.8
MQ water	100	38.4	33.8	63.0
PVP 25000	100	0.7	0.7	0.5
Mowiol 18-88	10	14.8	13.0	10.3
Propiofan70VAR	33.3	8.2	7.3	5.7
Geropon T-77	5.0	0.5	0.5	0.4
0.5 M PB, pH 7.5	100	9.9	8.7	6.9
cNAD$^+$	100	4.4	3.9	3.1
GlucDH2	100	2.2	1.9	1.5
RuAP-3	2	13.7	24.2	—
RuAP-3	100	—	—	3.8
Blade height, µm		70	80	101

2.5 References

[1] W. R. Knappe, F. Wittmann, D. Mosoiu, C. Horn, J. Hoenes. Test element with a one layer reaction film. U.S. Patent 7,629,175 B2, Feb. 18, 2004.

[2] W. Roedel, C. Horn, N. Steinke, N. Bucci, T. Meier, R. Schmuck, R. Nagel, D. Heindl. Stabilization of enzymes with stable coenzymes. U.S. Patent 2012/0276565 A1, Aug. 20, 2009.

[3] S. Duvall, S. Kachel, G. C. Lica, W. Schabel, P. Scharfer. Improved matrix stability compositions and methods. WO2014/037372 A1, Sep. 6, 2012.

[4] M. Ducorps, L. Papoz, J. C. Cuisinier-Raynal, D. Simon. Reliability of glucose measurement by glucose test strips in tropical conditions. *Diabetes Res. Clin. Pract.* **1992**, *17*, 51-54.

[5] J. P. Klinman, D. Mu. Quinoenzymes in Biology. *Annu. Rev. Biochem.* **1994**, *63*, 299-344.

[6] F. R. Krueger, W. Werther, J. Kissel, E. R. Schmid. Assignment of quinone derivatives as the main compound class composing 'interstellar' grains based on both polarity ions detected by the 'Cometary and Interstellar Dust Analyser' (CIDA) onboard the spacecraft STARDUST. *Rapid Commun. Mass Spectrom.* **2004**, *18*, 103-111.

[7] G. Hilt, T. Jarbawi, W. R. Heineman, E. Steckhan. An Analytical Study of the Redox Behavior of 1,10-Phenanthroline-5,6-dione, its Transition-Metal Complexes, and its N-Monomethylated Derivative with regard to their Efficiency as Mediators of NAD(P)+ Regeneration. *Chem. Eur. J.* **1997**, *3*, 79-88.

[8] D. Heindl, R. Herrmann, J. Hones, H.-P. Josel, M. Junius-Comer, H. Merdes, A. Schmidt, E. Selbertinger. Redox-active compounds and their use. U.S. Patent 6,057,120 A, Sep. 24, 1996.

[9] Ligand aqphen = 10,11-[1,4-naphtalendione]-dipyrido[3,2-a;2',3'-c]-phenazine

[10] A. Ambroise, B. G. Maiya. Ruthenium(II) Complexes of Redox-Related, Modified Dipyridophenazine Ligands: Synthesis, Characterization, and DNA Interaction. *Inorg. Chem.* **2000**, *39*, 4256-4263.

[11] Ligand nqphen = dipyrido[3,2-a:2′,3′-c]-benzo[3,4]-phenazine-11,16-quinone.

[12] E. Norambuena, C. Olea-Azar, Á. Delgadillo, M. Barrera, B. Loeb. Comparative evaluation of the acceptor properties of quinone derivatized polypyridinic ligands. *Chem. Phys.* **2009**, *359*, 92-100.

[13] B. W. Carlson, L. L. Miller. Mechanism of the oxidation of NADH by quinones. Energetics of one-electron and hydride routes. *J. Am. Chem. Soc.* **1985**, *107*, 479-485.

[14] T. Suzuki, S. Miyanari, Y. Tsubata, T. Fukushima, T. Miyashi, Y. Yamashita, K. Imaeda, T. Ishida, T. Nogami. Single-Component Organic Semiconductors Based on Novel Radicals that Exhibit Electrochemical Amphotericity: Preparation, Crystal Structures, and Solid-State Properties of N,N'-Dicyanopyrazinonaphthoquinodiiminides Substituted with an N-Alkylpyridinium Unit. *J. Org. Chem.* **2000**, *66*, 216-224.

[15] T. Suzuki, S. Miyanari, H. Kawai, K. Fujiwara, T. Fukushima, T. Miyashi, Y. Yamashita. Pyrazino-tetracyanonaphthoquinodimethanes: sterically deformed

electron acceptors affording zwitterionic radicals. *Tetrahedron* **2004**, *60*, 1997-2003.

[16] C. Yi, C. Blum, S.-X. Liu, T. D. Keene, G. Frei, A. Neels, S. Decurtins. Isolable Zwitterionic Pyridinio-semiquinone π-Radicals. Mild and Efficient Single-Step Access to Stable Radicals. *Org. Lett.* **2009**, *11*, 2261-2264.

[17] B. Chesneau, M. Hardouin-Lerouge, P. t. Hudhomme. A Fused Donor−Acceptor System Based on an Extended Tetrathiafulvalene and a Ruthenium Complex of Dipyridoquinoxaline. *Org. Lett.* **2010**, *12*, 4868-4871.

[18] R. P. Shishkina, V. I. Mamatyuk, E. P. Fokin. Sulfonation and sulfochlorination of 2,3-dichloro-1,4-naphthoquinones. *Izv. Akad. Nauk SSSR. Ser. Khim.* **1985**, 855-857.

[19] G. N. Kul'bitskii, L. S. Efros. Heterocyclic derivatives based on substituted 1,4-naphthoquinones. III. Sulfonation of naphth[2,3-d]imidazole-4,9-dione. *Zh. Org. Khim.* **1966**, *2*, 1305-1309.

[20] B. P. Sullivan, D. J. Salmon, T. J. Meyer. Mixed phosphine 2,2'-bipyridine complexes of ruthenium. *Inorg. Chem.* **1978**, *17*, 3334-3341.

[21] R. Díaz, A. Francois, M. Barrera, B. Loeb. Synthesis, characterization and theoretical studies of ruthenium(II) complexes with the quinone functionalized polypyridine ligand, Nqphen. *Polyhedron* **2012**, *39*, 59-65.

[22] C. Zúñiga, I. Crivelli, B. Loeb. Synthesis, characterization, spectroscopic and electrochemical studies of donor–acceptor ruthenium(II) polypyridine ligand derivatives with potential NLO applications. *Polyhedron* **2015**, *85*, 511-518.

[23] S. Arounaguiri, B. G. Maiya. "Electro-Photo Switch" and "Molecular Light Switch" Devices Based on Ruthenium(II) Complexes of Modified Dipyridophenazine Ligands: Modulation of the Photochemical Function through Ligand Design. *Inorg. Chem.* **1999**, *38*, 842-843.

[24] B. Abraham, C. V. Sastri, B. G. Maiya, S. Umapathy. Resonance Raman spectroscopic studies of [Ru(phen)2qdppz]2+ and its interactions with calf thymus DNA. *J. Raman Spectrosc.* **2004**, *35*, 13-18.

[25] J. Hönes, P. Müller, N. Surridge. The technology behind glucose meters: test strips. *Diabetes Technol. Ther.* **2008**, *10*, S-10-S-26.

[26] X.-Q. Zhu, Y.-Y. Mu, X.-T. Li. What Are the Differences between Ascorbic Acid and NADH as Hydride and Electron Sources in Vivo on Thermodynamics, Kinetics, and Mechanism? *J. Phys. Chem. B* **2011**, *115*, 14794-14811.

[27] Ž. Anusevičius, A. Ramanavičius, J. Šarlauskas. Some Aspects of Electron-Transfer Reaction of Ascorbate with Quinones. *Chem. Pap. - Chem. Zvesti* **1998**, *52*, 643-649.

[28] S.-H. Baik, F. Michel, N. Aghajari, R. Haser, S. Harayama. Cooperative Effect of Two Surface Amino Acid Mutations (Q252L and E170K) in Glucose Dehydrogenase from Bacillus megaterium IWG3 on Stabilization of Its Oligomeric State. *Appl. Environ. Microbiol.* **2005**, *71*, 3285-3293.

[29] C. Horn, C. Gaessler-Dietsche, D. Heindl, J. Hoenes, T. Meier, R. Schmuck. Fast reaction kinetics of enzymes having low activity in dry chemistry layers. U.S. Patent 2014/0322737 A1, Feb. 19, 2009.

[30] W. L. Armarego, C. L. L. Chai. Purification of laboratory chemicals, Butterworth-Heinemann, **2013**.

[31] M. J. Corr, M. D. Roydhouse, K. F. Gibson, S.-z. Zhou, A. R. Kennedy, J. A. Murphy. Amidine Dications as Superelectrophiles. *J. Am. Chem. Soc.* **2009**, *131*, 17980-17985.

[32] W. C. Still, M. Kahn, A. Mitra. Rapid chromatographic technique for preparative separations with moderate resolution. *J. Org. Chem.* **1978**, *43*, 2923-2925.

[33] H. E. Gottlieb, V. Kotlyar, A. Nudelman. NMR Chemical Shifts of Common Laboratory Solvents as Trace Impurities. *J. Org. Chem.* **1997**, *62*, 7512-7515.

[34] E. Alcalde, I. Dinarès, A. Ibáñez, N. Mesquida. A Simple Halide-to-Anion Exchange Method for Heteroaromatic Salts and Ionic Liquids. *Molecules* **2012**, *17*, 4007-4027.

[35] G. Wang, B. Wang, J. Park, J. Yang, X. Shen, J. Yao. Synthesis of enhanced hydrophilic and hydrophobic graphene oxide nanosheets by a solvothermal method. *Carbon* **2009**, *47*, 68-72.

[36] G. Kemmer, S. Keller. Nonlinear least-squares data fitting in Excel spreadsheets. *Nat. Protocols* **2010**, *5*, 267-281.

[37] R. Díaz, O. Reyes, A. Francois, A. Leiva, B. Loeb. Synthesis of a new polypyridinic highly conjugated ligand with electron-acceptor properties. *Tetrahedron Lett.* **2001**, *42*, 6463-6467.

2.6 Supplementary UV-Vis material

Table 2-4S UV-Vis absorption spectra of **15** and its reduction by NADH.*

	pH 6.1	pH 7.0	pH 8.0	Conditions
Oxidized form (rightmost abs.)				
λ_{max}, nm	459	460	461	see experimental part for details
ε, $mM^{-1}cm^{-1}$	2.9±0.3	8.8±0.5	9.6±0.3	
Reduced form				
λ_{max}, nm	526±1	525	526	$[\mathbf{15}]_0$ = 10–50 μM
ε, $mM^{-1}cm^{-1}$	6.8±0.1	6.9±0.1	6.50±0.03	$[NADH]_0$ = 1000 μM
NADH detection				
$\lambda_{max\ detection}$, nm	600	600	600	$[\mathbf{15}]_0$ = 200 μM;
Sensitivity, $OD*mM^{-1}$	3.6±0.1	3.4±0.1	1.9±0.1	$[NADH]_0$ = 5–100 μM

* — **15** + NADH reactions were monitored by UV-Vis in 400–1000 nm range every 1 min for 30 min. Sensitivity and extinction coefficient were calculated from the values recorded at equilibrium.

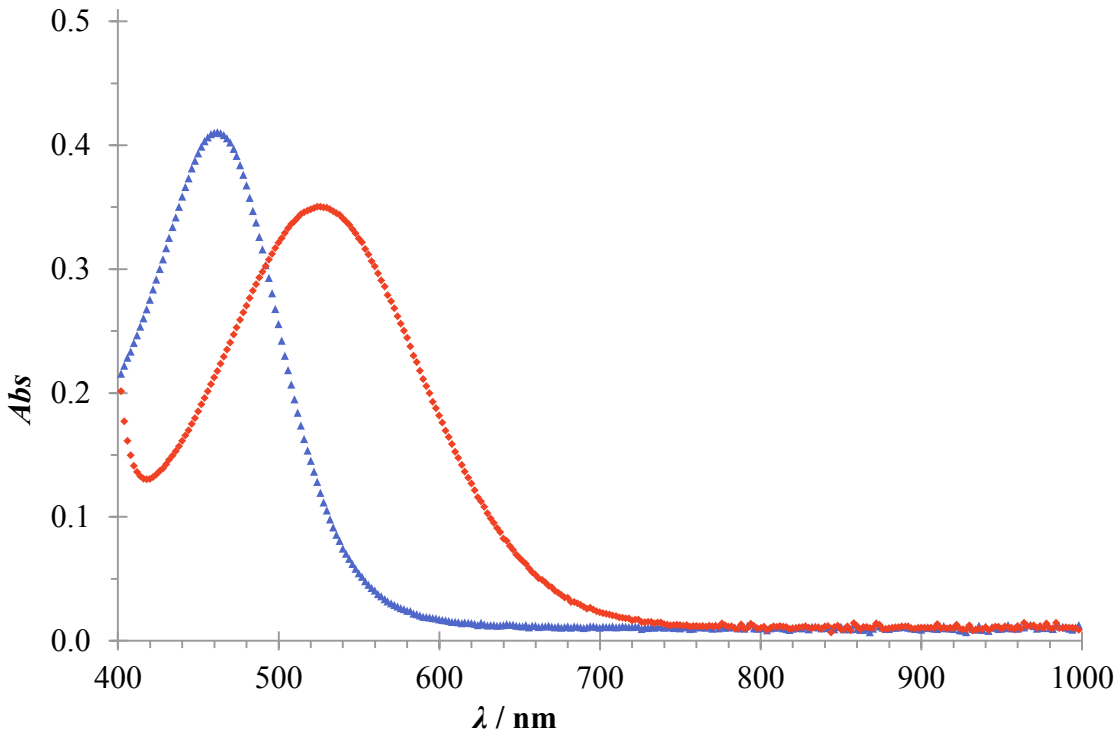

Figure 2.17S UV-Vis spectra changes upon treating **15** (50 μM) with NADH (1000 μM) in buffer (25 mM PIPES, 101 mM NaCl, pH 7.0): before addition of NADH (blue); after incubation time of 10 min (red).

Table 2-5S UV-Vis absorption spectra of **16** and its reduction by NADH.*

	pH 6.1	pH 7.0	pH 8.0	Conditions
Oxidized form (rightmost abs.)				
λ_{max}, nm	385	486	486	see experimental part for details
ε, $mM^{-1}cm^{-1}$	14.8	3.4	4.5	
Reduced form				
λ_{max}, nm	582	582	582	$[\mathbf{16}]_0$ = 20–100 μM; $[NADH]_0$ = 1000 μM;
ε, $mM^{-1}cm^{-1}$	10.1±0.2	4.7±0.3	3.9±0.1	
NADH detection				
$\lambda_{max\ detection}$, nm	800	n.d.	n.d.	$[\mathbf{16}]_0$ = 200 μM; $[NADH]_0$ = 20–100 μM;
Sensitivity, $OD*mM^{-1}$	3.4±0.3	n.d.	n.d.	

* — **16** + NADH reactions were monitored by UV-Vis in 400–1000 nm range every 1 min for 30 min. Sensitivity and extinction coefficient were calculated from the values recorded at equilibrium.

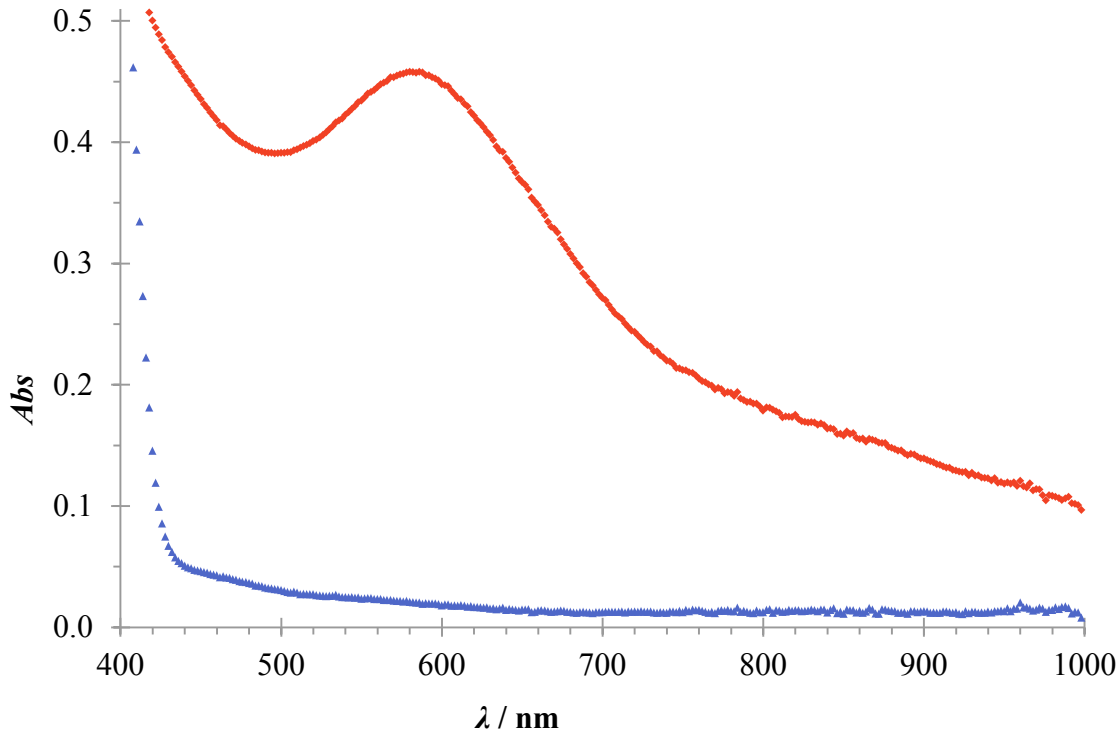

Figure 2.18S UV-Vis spectra changes upon treating **16** (50 μM) with NADH (1000 μM) in buffer (25 mM PIPES, 101 mM NaCl, pH 6.1): before addition of NADH (blue); after incubation time of 20 min (red).

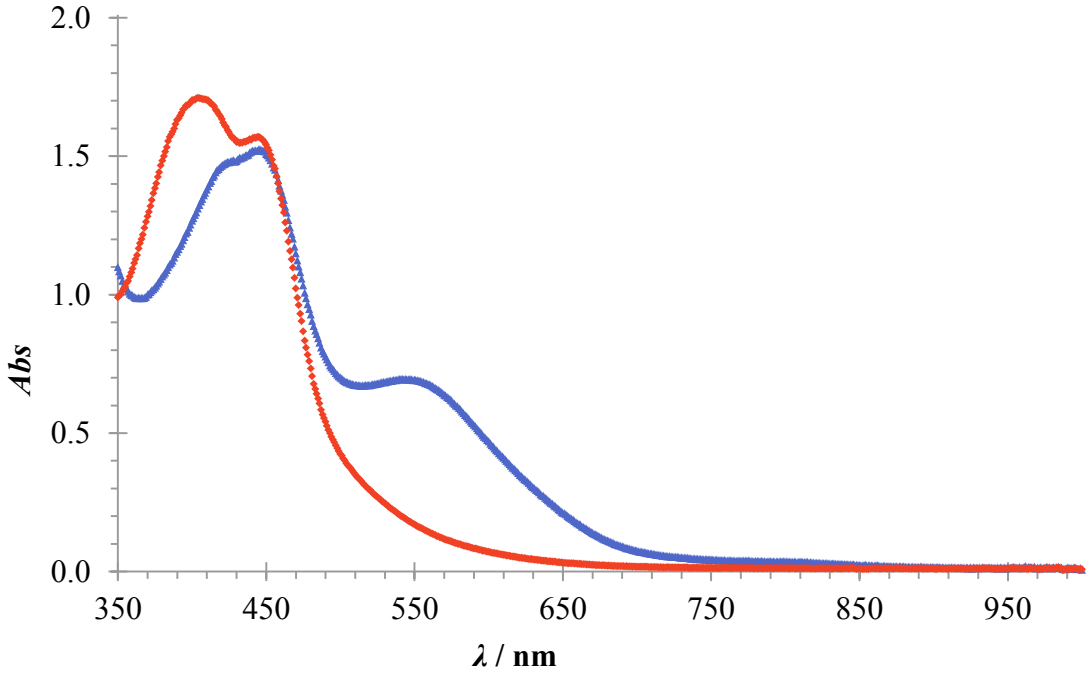

Figure 2.19S UV-Vis spectra changes upon treating the complex **RuAP-3** (100 μM) with NADH (50 μM) in phosphate buffer (50 mM, pH 6.0): before addition of NADH (red); after incubation time of 10 min (blue).

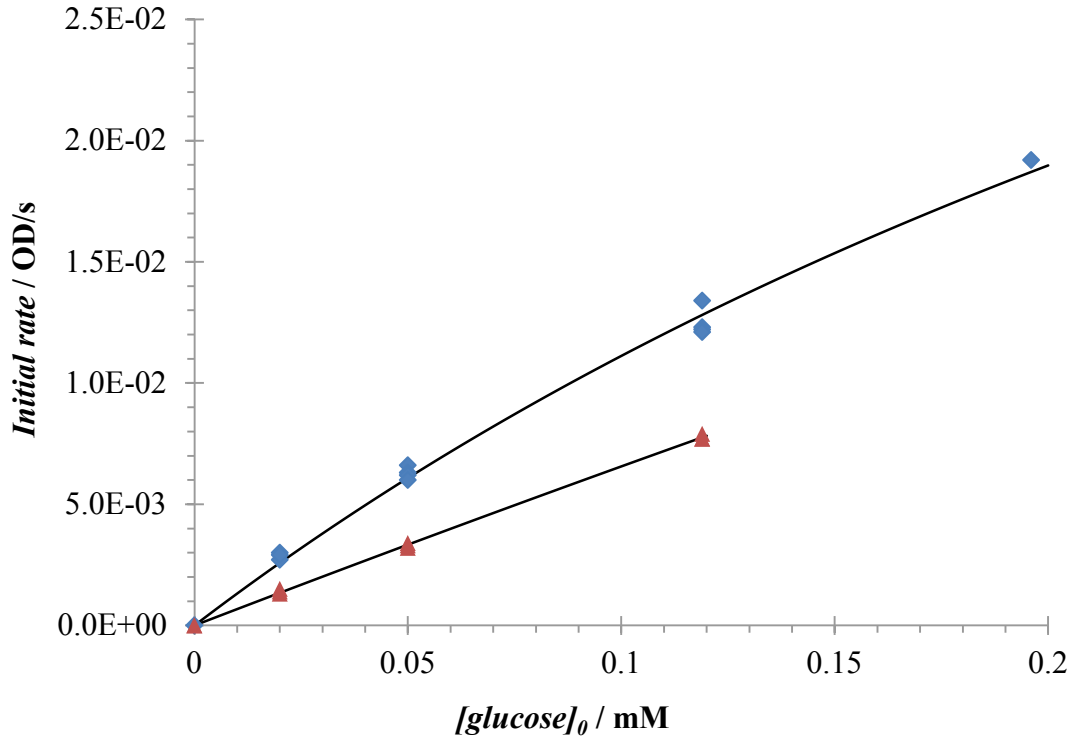

Figure 2.20S Michaelis–Menten equation fitting with a MS Excel software by a method adapted from the procedure described by Gerdi Kemmer & Sandro Keller.[36] **A** — NAD^+ (blue diamonds); **B** — $cNAD^+$ (red triangles).

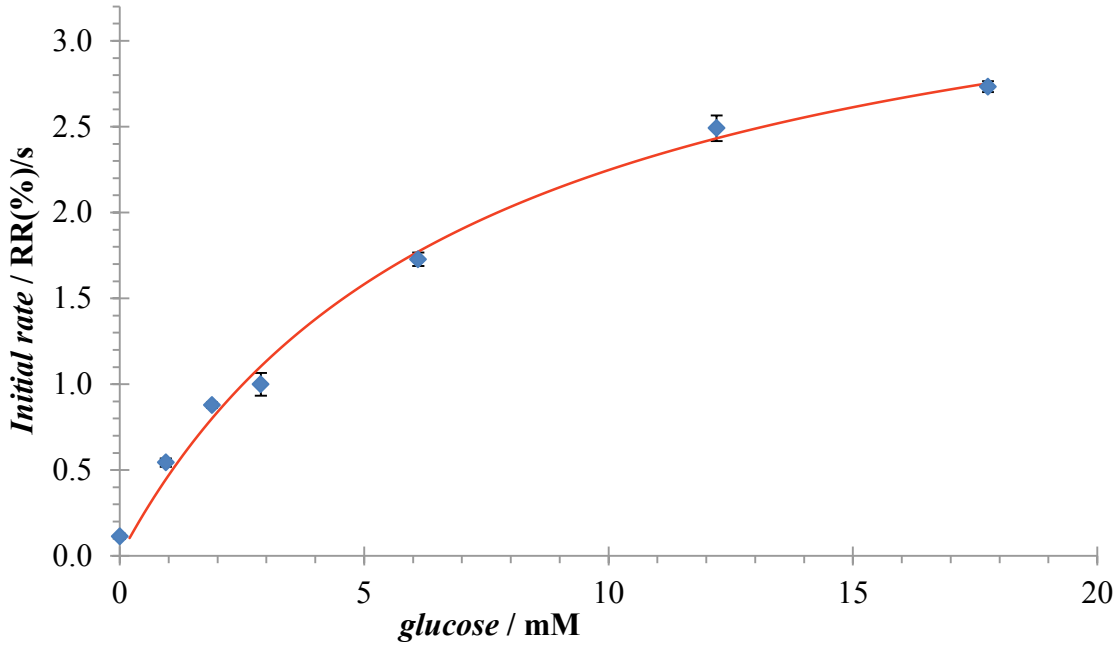

Figure 2.21S Michaelis–Menten plot for the enzyme-catalyzed reaction on test strips. The Michaelis-Menten equation was described as: $V = V_{max}[S]/(K_m + [S])$, where V is the reaction rate, $[S]$ is the glucose concentration (substrate), and K_m is the Michaelis constant. Reaction at each probe concentration was repeated five times, and the error bars represent standard deviations. Points were fitted using a model described by Gerdi Kemmer & Sandro Keller.[36] RR = relative remittance.

2.7 Supplementary NMR spectra

^{1}H NMR for **RuNP-1** PF_6 salt in MeCN-d_3

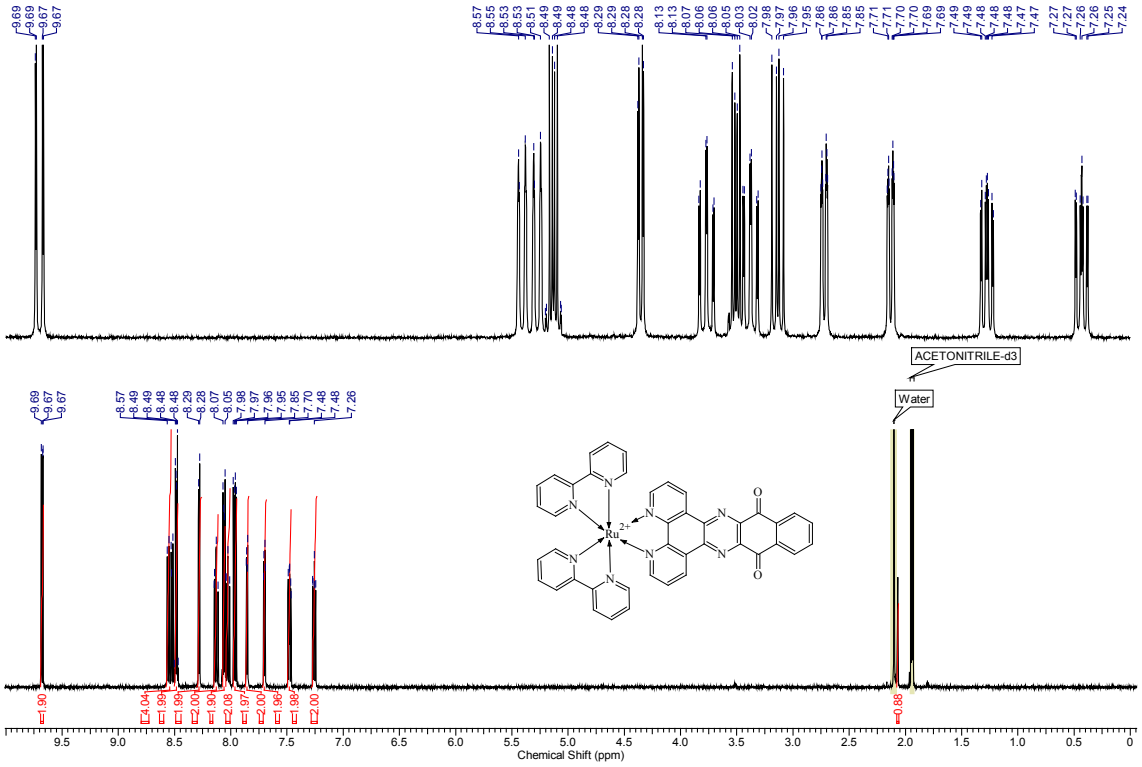

^{13}C NMR for **RuNP-1** PF_6 salt in MeCN-d_3

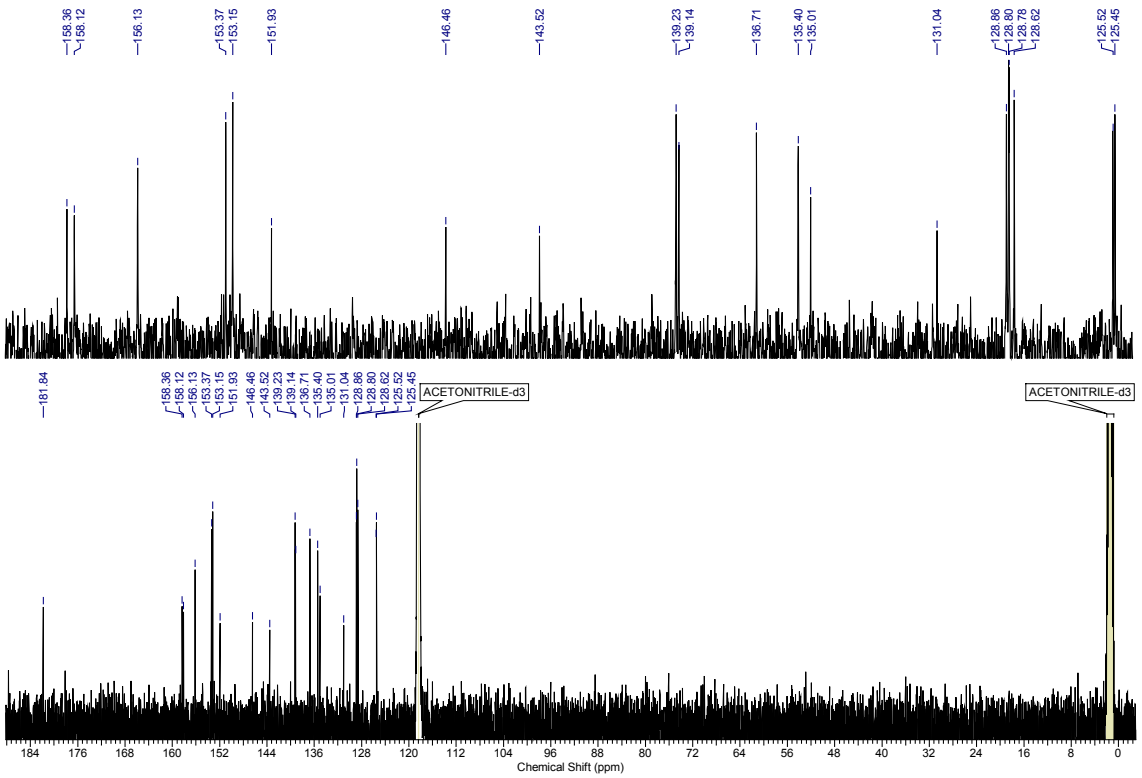

^{1}H NMR for **RuNPCl-2** PF_6 salt in MeCN-d_3

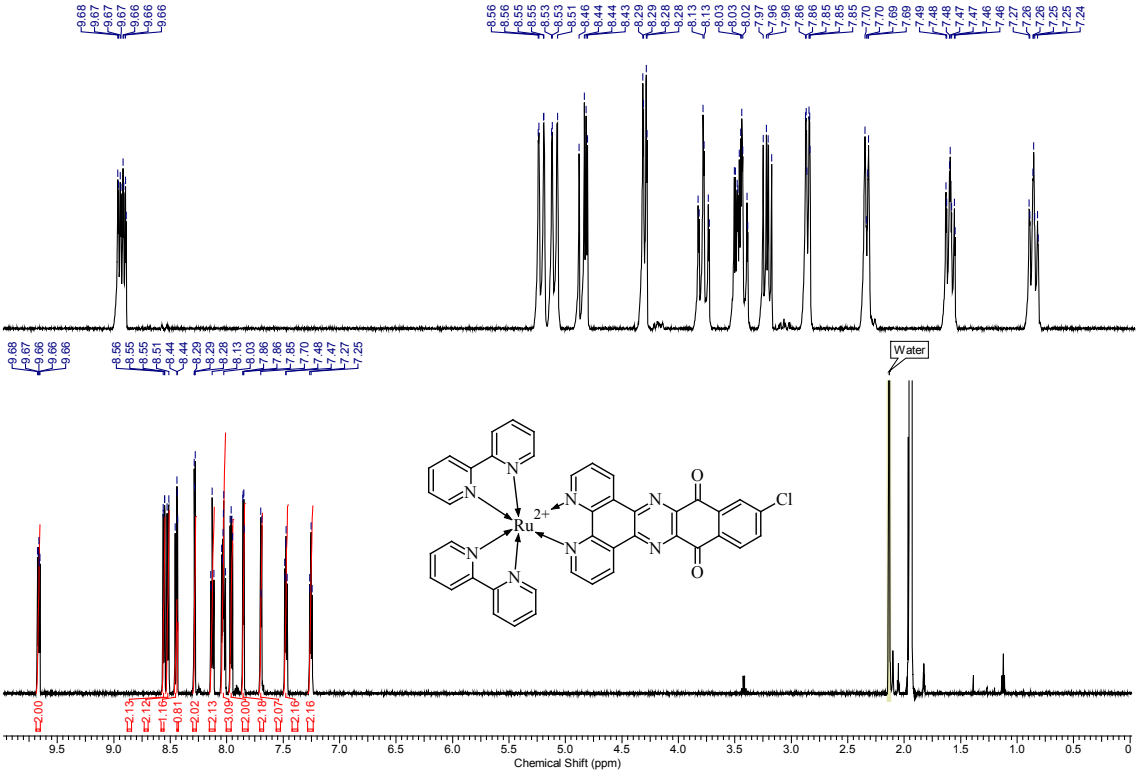

^{13}C NMR for **RuNPCl-2** PF_6 salt in MeCN-d_3

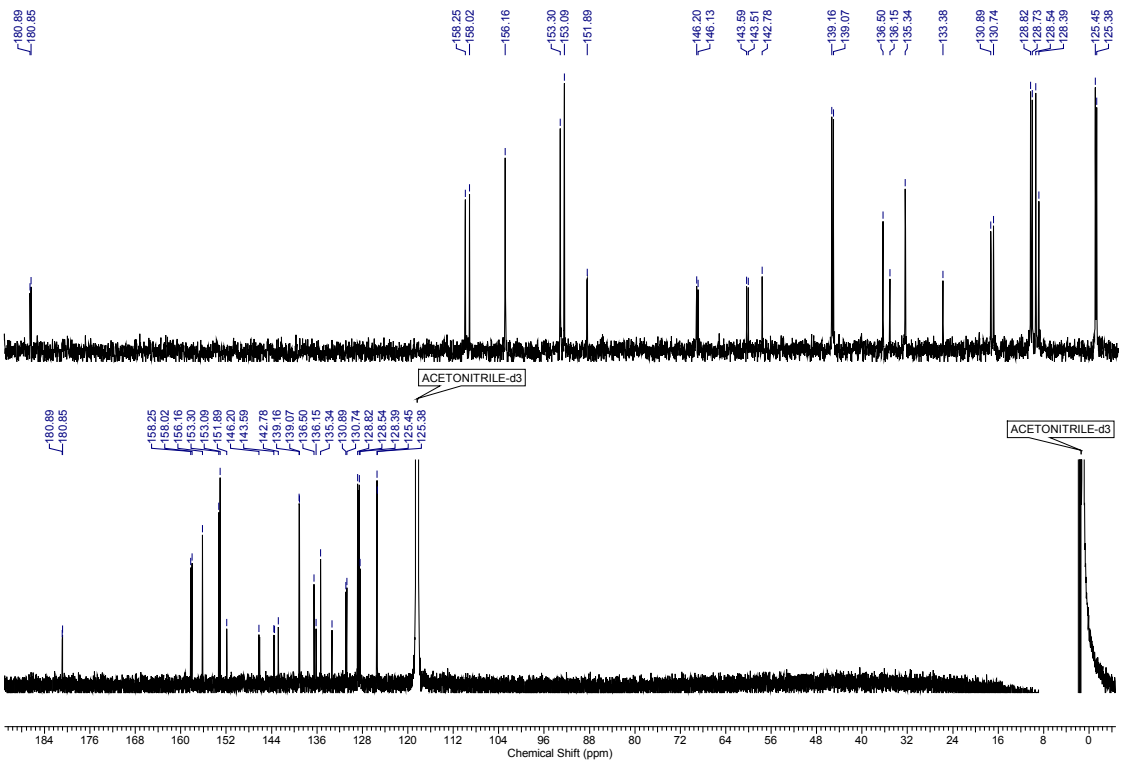

^{1}H NMR for **RuAP-3** TFA salt in MeOD-d_3

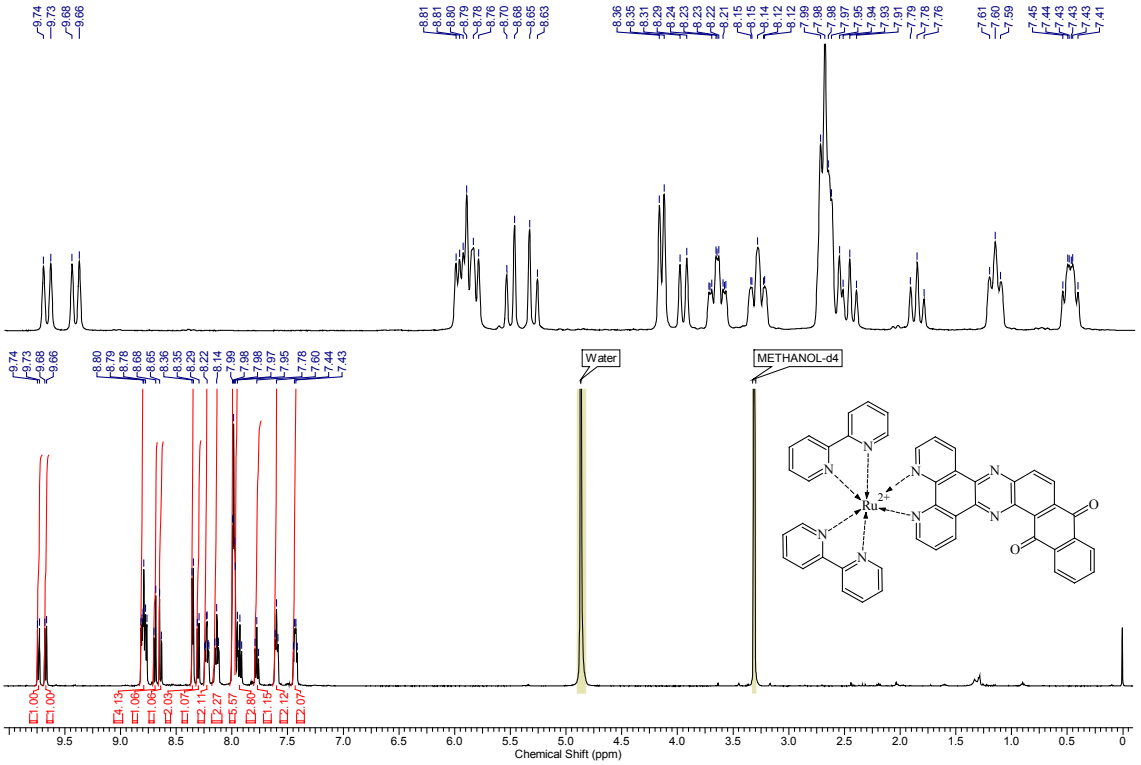

^{13}C NMR for **RuAP-3** TFA salt in MeOD-d_3

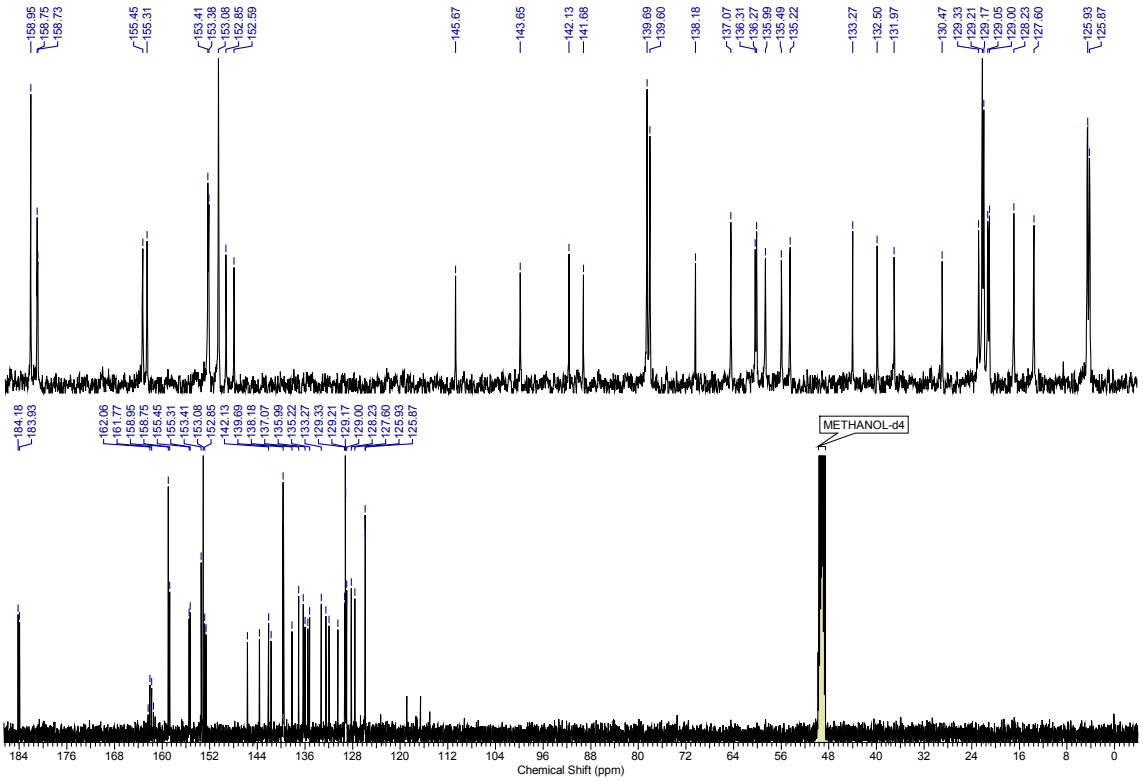

Table 2-6S NMR data for the complex **3** (below) as TFA salt in MeOD-d_3, assigned using COSY, HMBC, HMQC.

H_a / $H_{a'}$	H_b / $H_{b'}$	H_c / $H_{c'}$	H_e	H_f	H_g / $H_{g'}$	H_h / $H_{h'}$
^{1}H NMR chemical shifts (ppm) of **3** in MeOD-d_3 (500 MHz)						
8.35 (d)	7.98 (m)	9.74 (d)	8.69 (d)	8.64 (d)	8.30 (d)	7.93 (t)
$J_{ab/a'b'}$ = 5.4		$J_{cb/c'b'}$ = 8.2	J_{ef} = 8.80	J_{fe} = 8.80	$J_{gh/g'h'}$ = 7.9	$J_{hg/h'g'}$ = 7.6
		9.67 (d)			7.96 (d)	7.78 (t)
		$J_{cb/c'b'}$ = 8.2			$J_{gh/g'h'}$ = 7.9	$J_{hg/h'g'}$ = 7.6
C_a, $C_{a'}$	C_b, $C_{b'}$	C_c, $C_{c'}$	C_e	C_f	C_g, $C_{g'}$	C_h, $C_{h'}$
^{13}C NMR chemical shifts (ppm) of **3** in MeOD-d_3 (150 MHz)						
155.5	129.1	136.0	137.1	129.3	128.2	136.3
155.3	129.0	135.5			127.6	135.2

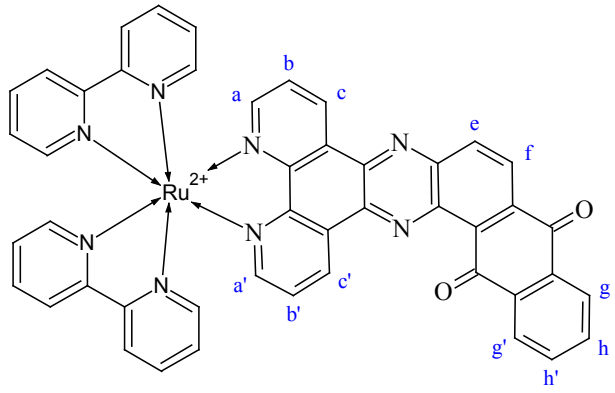

^{1}H NMR for nqphen (**7**) in $CDCl_3$

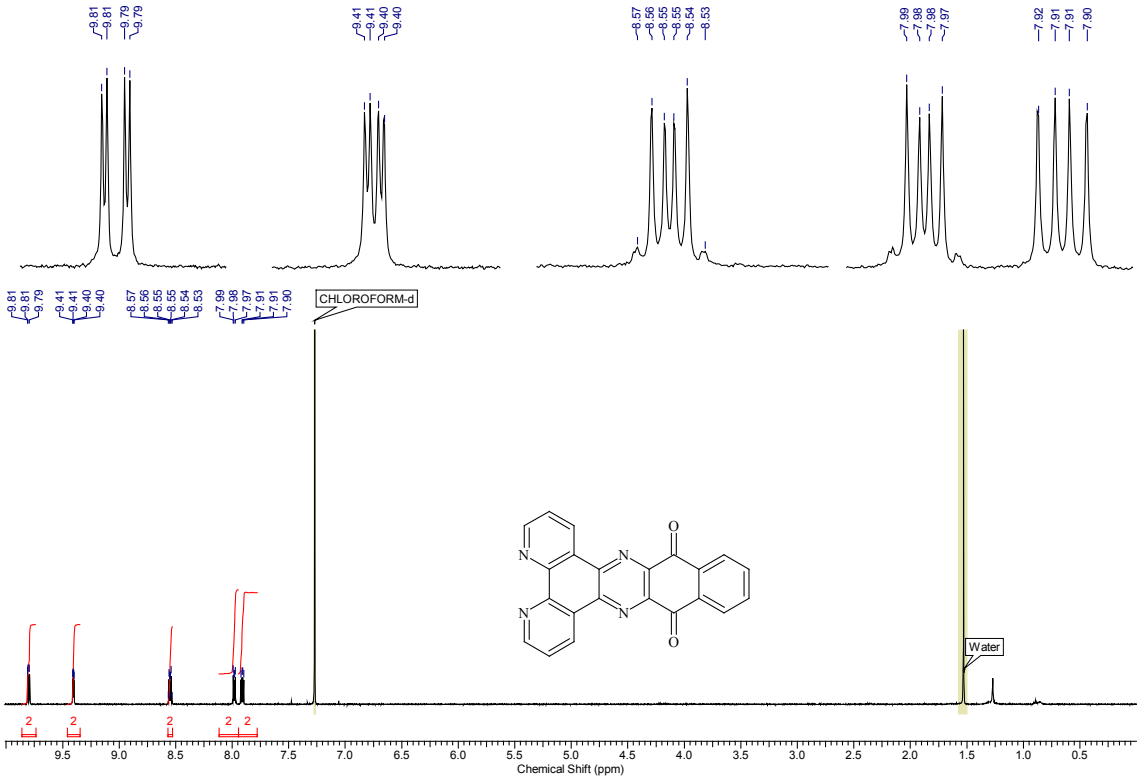

^{1}H-HSQC overlay spectra report for nqphen (**7**) in $CDCl_3$

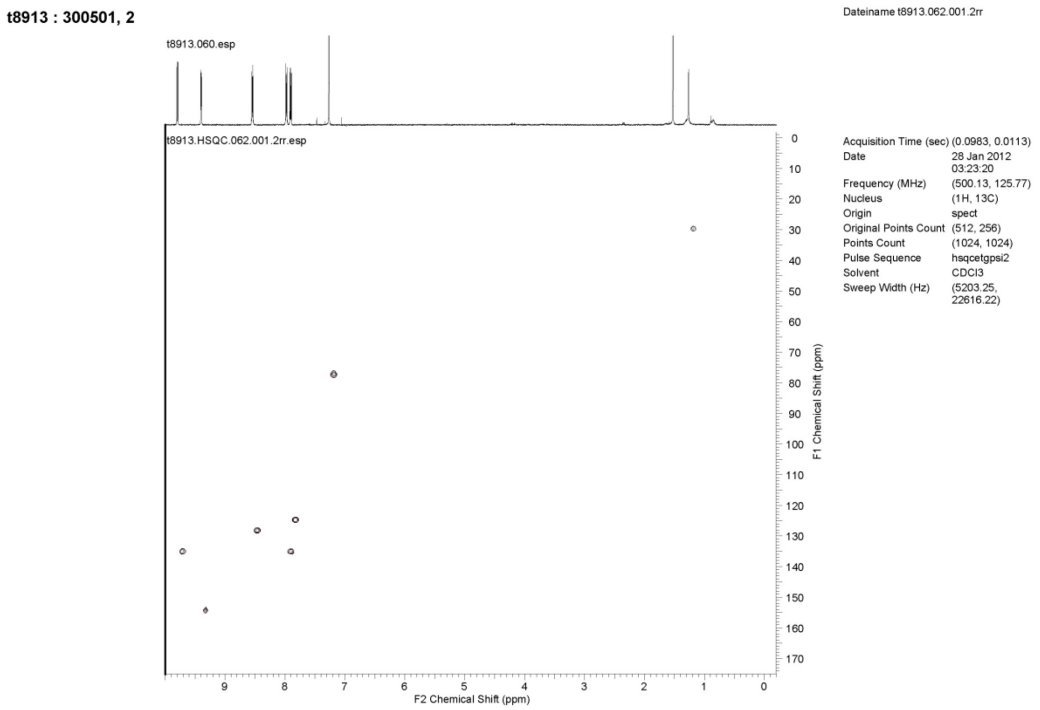

^{1}H NMR for nqphen-Cl (**8**) in $CDCl_3$

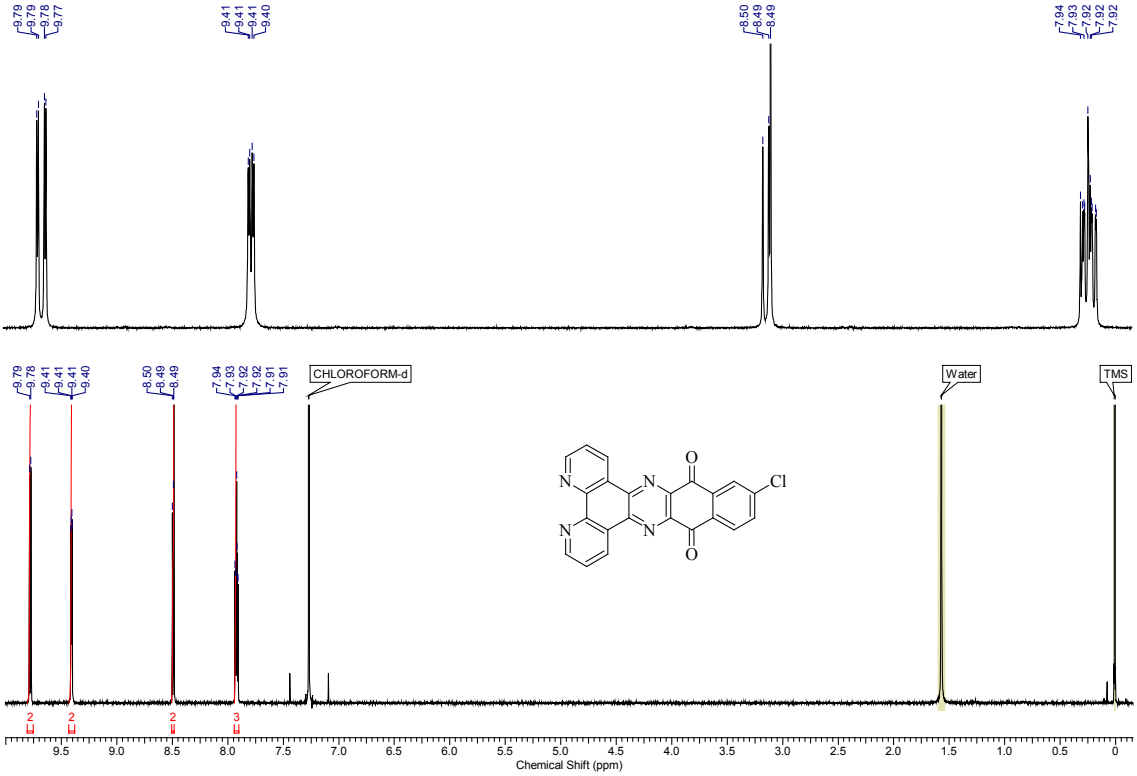

^{1}H-HSQC overlay spectra report for nqphen-Cl (**8**) in $CDCl_3$

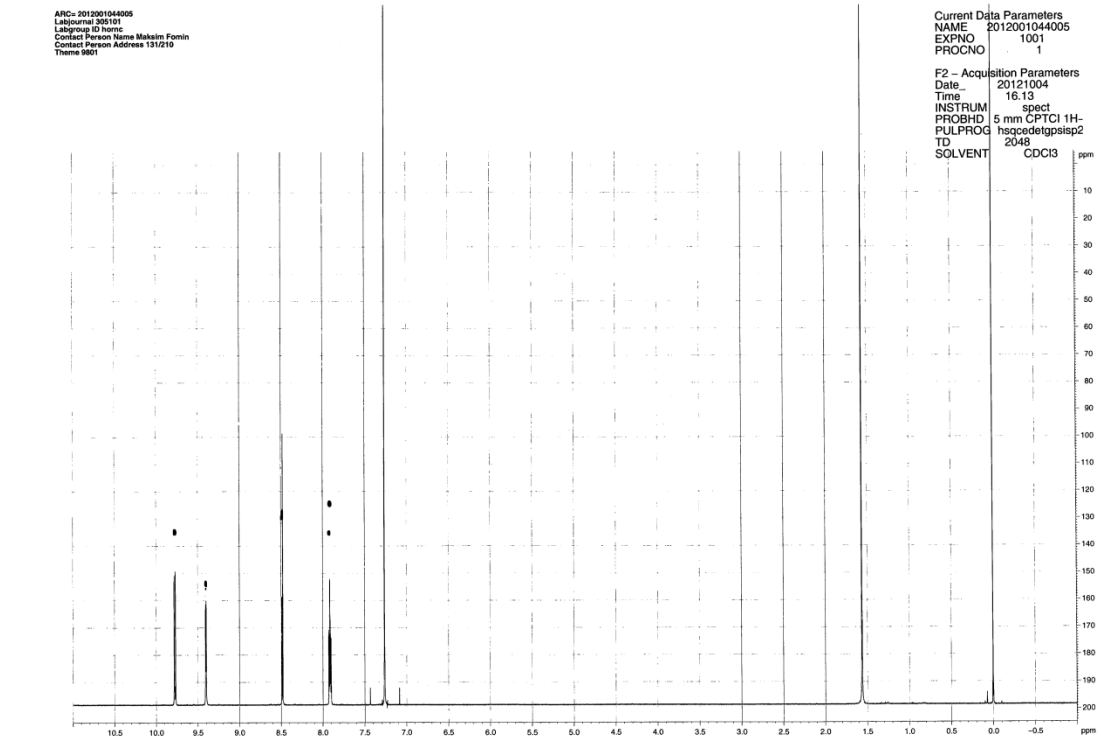

^{1}H NMR for **16** in DMSO-d$_6$

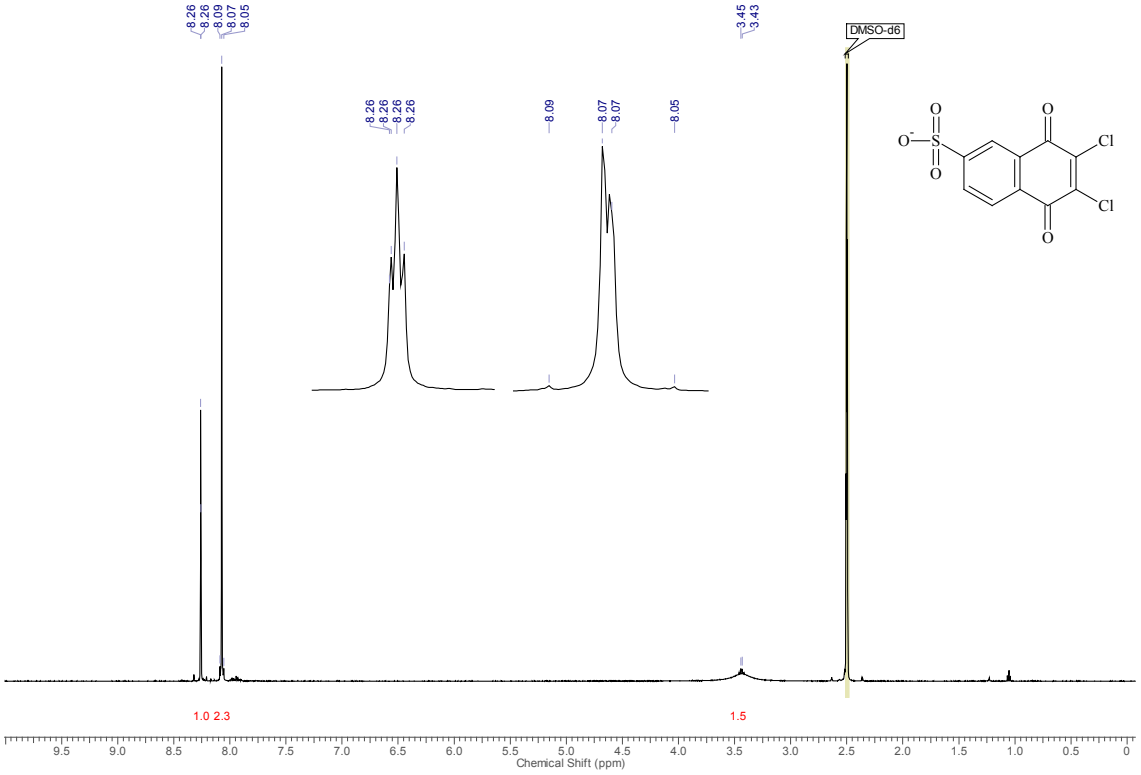

^{13}C NMR for **16** in DMSO-d$_6$

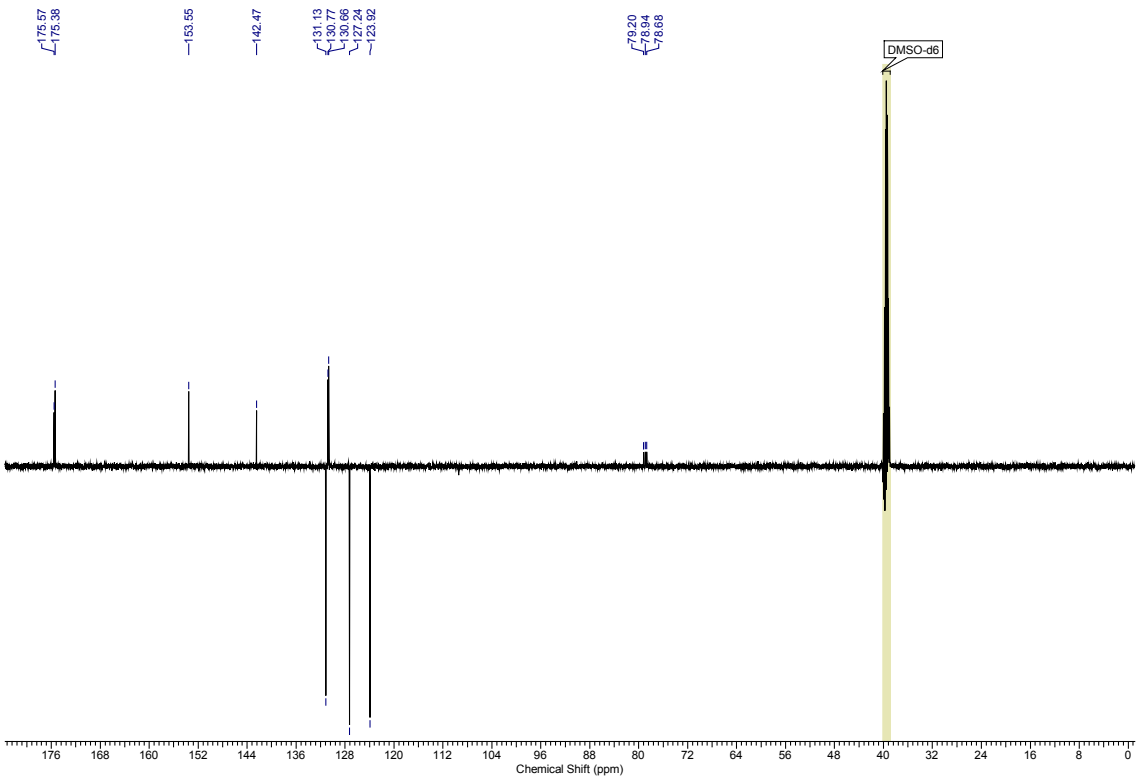

^{1}H NMR for **15** PF_6 salt in MeCN-d_3

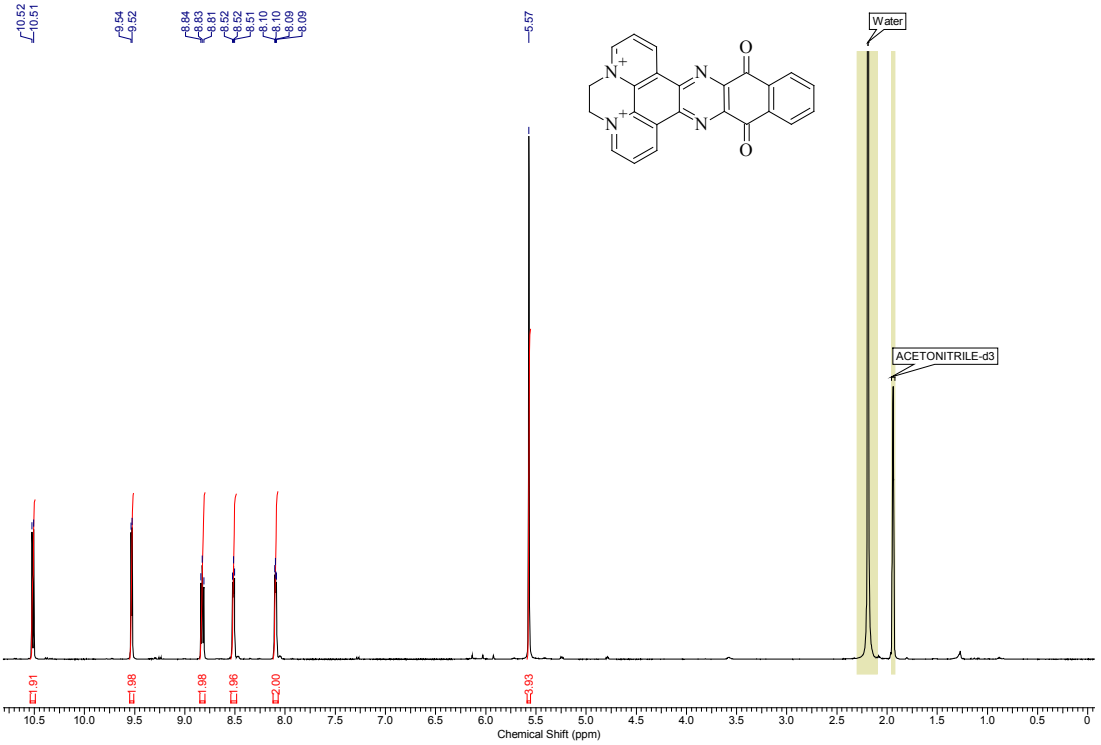

^{13}C NMR for **15** PF_6 salt in MeCN-d_3

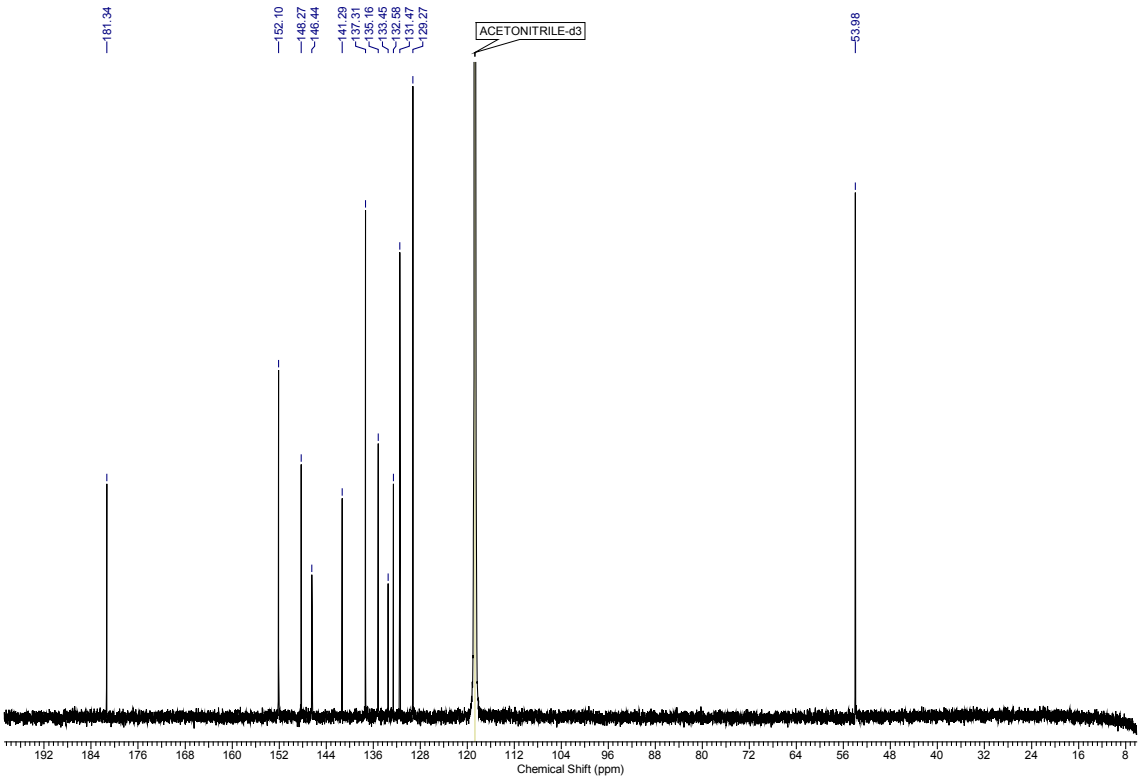

^{1}H NMR for **16** TfO salt in DMSO-d_6

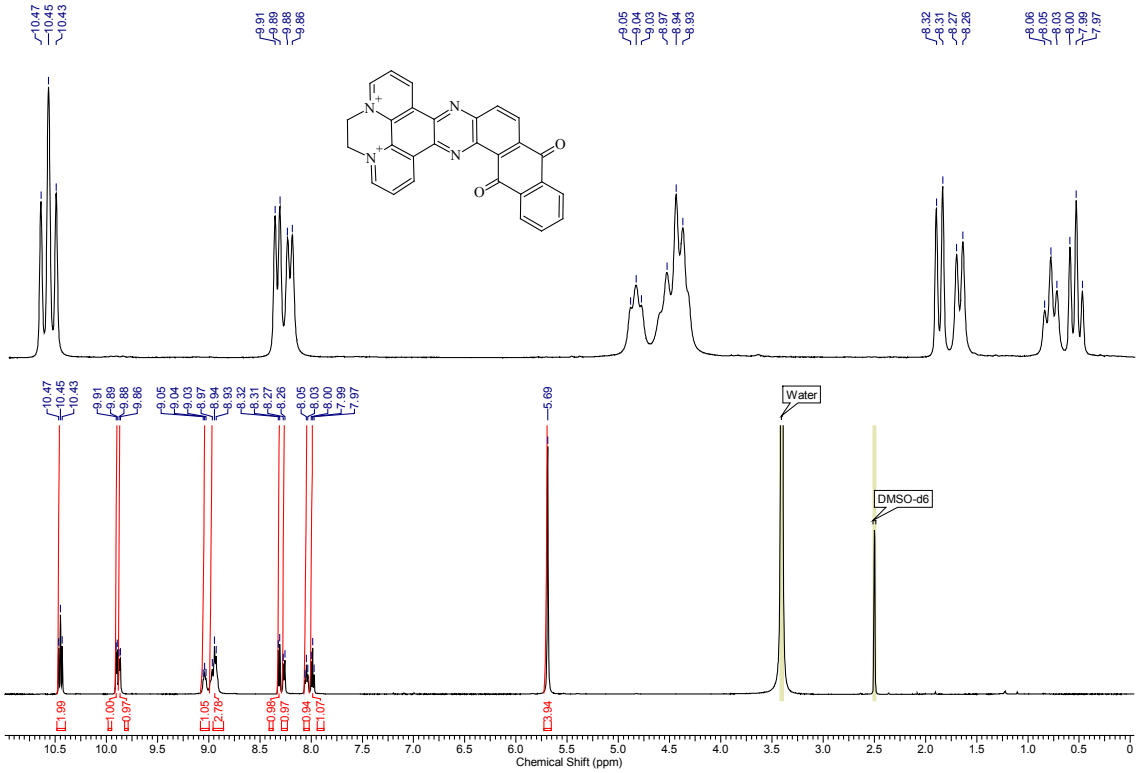

^{13}C NMR for **16** TfO salt in DMSO-d_6

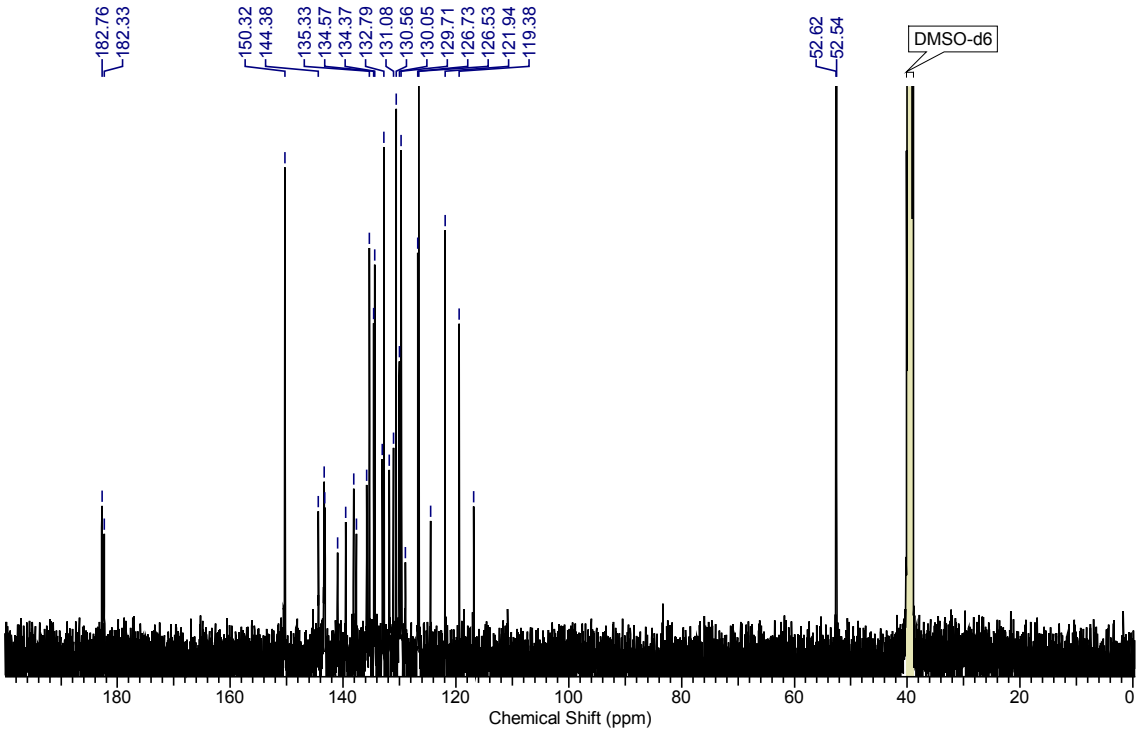

3 A RAPID RESPONSE "TURN-ON" FLUORESCENT AND COLORIMETRIC INDICATOR FOR NADH DETECTION AND ITS APPLICATION IN TUMOUR CELL IMAGING

Part of this chapter has been filed as a patent:

M. Fomin, P. Gebauer, C. Horn, D. Heindl // EP patent application nr. EP14181964.9 (filed on Aug. 22, 2014; not published yet).

Author contributions:

MF synthesized all the indicators, and measured their UV-Vis and fluorescence responses to NADH and glucose dehydrogenase enzyme. MF wrote the manuscript.

3.1 Introduction

The rapid, sensitive, and selective sensing of NAD(P)H is of significant interest for applications in diagnostic assays,[1-2] synthesis of chiral compounds[3-5] and drug discovery.[6-9] The redox couple NAD^+/NADH plays a crucial role in energy metabolism, being affected by glycolysis, tricarboxylic cycle and mitochondrial respiration. Since the pioneering work of Britton Chance metabolic imaging of NADH levels has extensively been used to monitor cellular viability and activity.[10] Recently, the increased intracellular NADH levels were reported to be linked to the abnormal formation of reactive oxygen species (ROS) and oxidative DNA damage.[11] All this renders NAD(P)H an attractive biomarker to assess metabolic states of cells associated with carcinogenesis and cell differentiation.[9] Furthermore, NAD(P)H detection is desirable for *in vitro* analysis of $NAD(P)^+$-dependent enzymes which release NAD(P)H upon reaction with a substrate. This is important in the context of high-throughput screening (HTS) and the development of these enzymes for industrial applications.[5]

An ideal NAD(P)H sensor for use in HTS on a single-cell level would comprise high sensitivity, lack of toxicity to living cells, stability, rapid response and ease of use. Both NADH and NADPH absorb light at 340 nm and have intrinsic fluorescence. This approach cannot be used to monitor NAD(P)H in a monolayer of cells — signal is too weak. Intracellular NAD(P)H concentration can be monitored by direct measurement using fluorescence lifetime imaging (FLIM).[12-14] However, the instrumental equipment necessary for FLIM is not widely available. Colorimetric and fluorescent indicators, which change their absorption spectra upon reaction with a target analyte, are unique tools to visualize biological events in living cells and organisms. To detect intracellular NAD(P)H levels, researchers have recently developed optical sensors based on gold nanoparticles (AuNPs),[7, 15] quantum dot (QD) conjugates[8] and genetically encoded fluorescent sensors.[6, 16-17] Small molecule indicators could be a simple and convenient alternative to such complex sensors, and are particularly attractive for quantitative HTS.

Despite the large interest, there are only few molecules available, which show a bathochromic shift upon reaction with NAD(P)H. Tetrazolium salts are extensively used in cell proliferation, cytotoxicity assays and enzymatic assays. In the presence of intermediate electron acceptors, such as phenazine methosulfate (PMS), tetrazolium salts are reduced by NAD(P)H to form formazan dyes.[18-19] However, formazans are generally nonfluorescent, and therefore may not be the dye of choice for all fluorescence microscopy applications. In another assay, NAD(P)H reduces the weakly

fluorescent molecule resaruzin to the highly fluorescent dye resorufin in the presence of diaphorase.[1, 20-21] In order to simplify a two-component detection system, Sammes *et al* employed an alternative strategy using a single substrate, that releases the masked fluorophore umbelliferone after reduction with NAD(P)H.[22] This system, however, is also plagued by several disadvantages. Firstly, at concentrations in the desired micromolar range, the reduction takes several hours to complete. Secondly, umbelliferone absorbs and emits in the violet–blue region of the spectrum,[23] while indicators with excitation and emission in the green range are optimal for biological imaging applications due to low autofluorescence. Up to now, it has remained a challenge to develop a small molecule indicator for NADH imaging in living cells.

Recently, we developed a new design for chromogenic NADH reagents where an electron-deficient heterocycle (active acceptor) is conjugated to a polymethine chain of the cyanine dye scaffold (latent acceptor).[24] The target molecules were conveniently prepared in two steps, so that every product was isolated pure by simple filtration. Their aqueous solutions are nearly colourless and nonfluorescent due to the two-acceptor (**2A**) molecular structure. While these reagents were initially developed for blood glucose monitoring in point-of-care devices, we discovered an additional feature of a 3-quinolinium derivative (**2ACy-2**) in reacting rapidly with NADH under physiological conditions. Upon hydride transfer from NADH to the active acceptor moiety of **2ACy-2**, the cyanine chromophore is unmasked. This leads to a sensitive absorbance (λ_{max} 537 nm) and fluorescence response (emission 561 nm).

As a model system, **2ACy-2** was used *in vitro* to analyze glucose in the presence of the NAD^+-dependent glucose dehydrogenase (GDH), where GDH catalyzes the oxidation of glucose to gluconolactone with simultaneous reduction of NAD^+ to NADH. The successful analysis of GDH-catalyzed reactions encouraged us to use **2ACy-2** for imaging intracellular NADH levels. To this end, we stained living human embryonic kidney cells (HEK-293) with our indicator. Confocal fluorescence microscope images revealed the cellular uptake of **2ACy-2**. We further confirmed the ability of **2ACy-2** indicator to reflect increased NADH levels by staining human colon cancer cell line HCT116, which lacks synthesis of cytochrome c oxidase 2 (SCO2 −/−). These cells show consistently higher levels of NADH compared to HCT116 wild type (WT) cells.[11, 25] Herein, we describe a new optical indicator to analyze intracellular metabolic pathways at the single-cell level.

3.2 Results and discussion

3.2.1 Design and synthesis of a redox indicator for NADH

Previously, we learned that the NAD(P)$^+$/NAD(P)H couple is an important marker of the redox status in biological systems, which also shows interesting spectral properties (**Figure 3.1**). The absorbance maximum of NAD$^+$ lies at 260 nm at neutral pH and is the result of a superposition of two separate chromophores: adenine and nicotinamide.[14] When NAD$^+$ is reduced to NADH, the nicotinamide moiety is transformed to a dihydronicotinamide one. Hence, the absorption band at 260 nm decreases and a new maximum occurs at 360 nm. Such bathochromic shift is due to the formation of a π-conjugated donor-acceptor system, wherein the nitrogen atom of the dihydropyridine entity provides electron density and the amide group acts as an acceptor. We envisioned that the chemical basis of such colour change could be incorporated in the design of new redox indicators for biological applications.

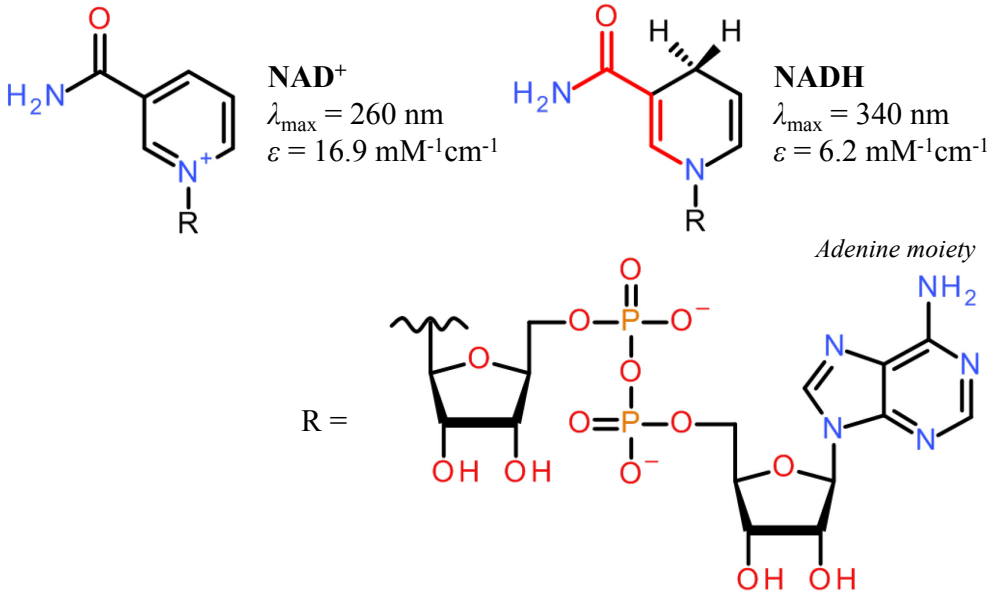

Figure 3.1 Molecular structures and UV-Vis spectral properties of NAD$^+$/NADH.[14]

Potentially, the new redox indicator framework could be composed of two acceptors (**2A**-design): an active electron-deficient heterocycle connected *via* the vinyl bridge to the indolium moiety which functioning as a latent acceptor (**Figure 3.2**). Electron-deficient heterocycles were selected from pyridinium (**Py**), quinolinium (**Q**), isoquinolinium (**IQ**) and phenazinium (**Pz**) cations, which are known to undergo two-electron reduction reactions with NADH.[26-27] The hydride transfer from NADH to the acceptor moiety of **2A** may lead to a new π-conjugated donor-acceptor system of the cyanine type (**Cy**). Moreover, the presence of charged quaternary nitrogens should enhance water-solubility of the aromatic ring structure.

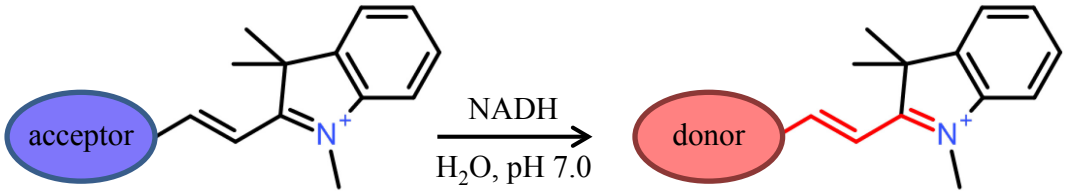

Two-acceptor π-system (**2A**) Cyanine dye (**Cy**)

Selected electron-deficient heterocycles:

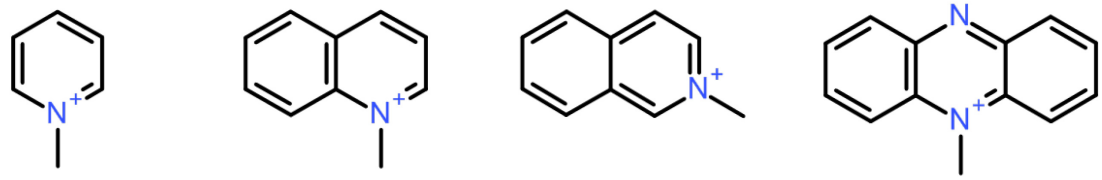

Pyridinium (**Py**) Quinolinium (**Q**) Isoquinolinium (**IQ**) Phenazinium (**Pz**)

Figure 3.2 The design concept of a redox indicator for NADH.

We designed and synthesized a series of six diquaternary salts (**Figure 3.3**). For compound **2ACy-3**, the nitrogen is located in the meta-position relative to the conjugated indolium group, which is why a bathochromic shift would not be expected, as the π-conjugated donor-acceptor system is absent.

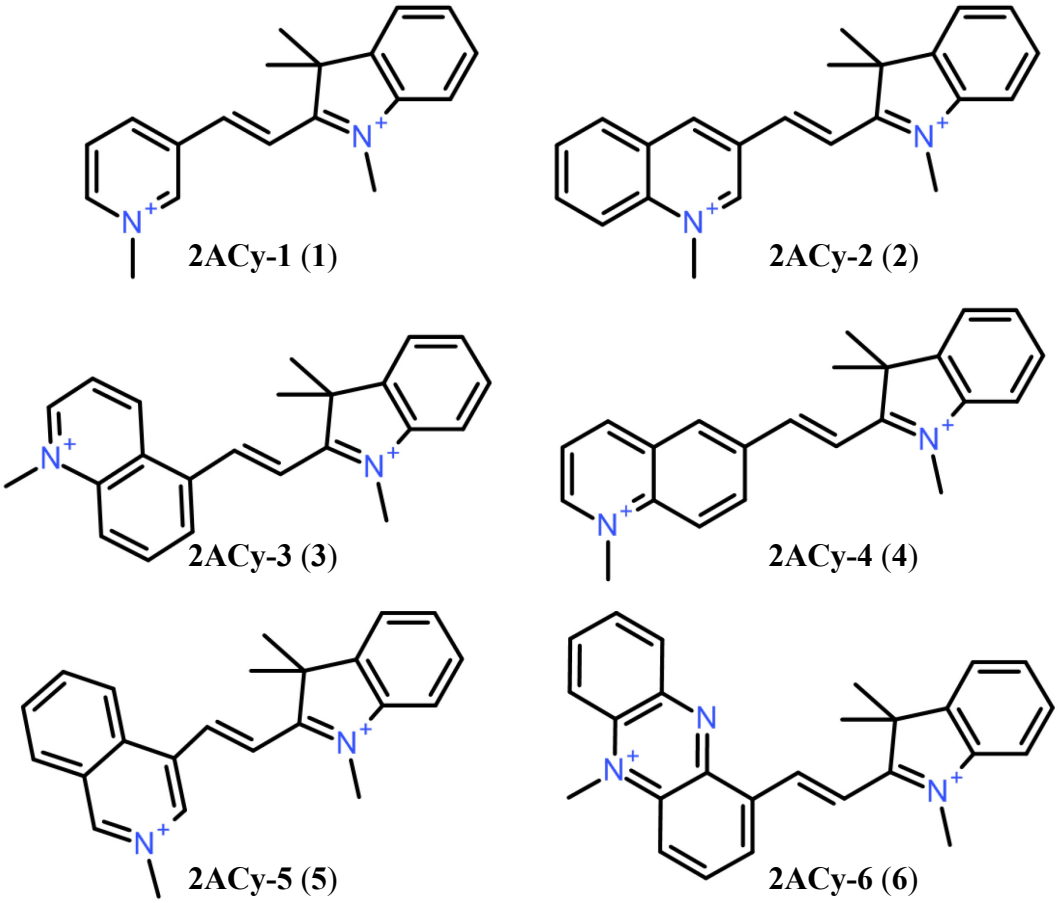

Figure 3.3 Molecular structures of the potential redox indicators. Anions are omitted for clarity.

Diquaternary salts **1–6** were prepared following the two-step route outlined in **Scheme 3-1**. Each step is convenient and pure products were obtained without the need for chromatography (for the yields, see **Table 3-1**). Purity and structures of isolated compounds were confirmed by HPLC-MS, NMR and HRMS experiments.

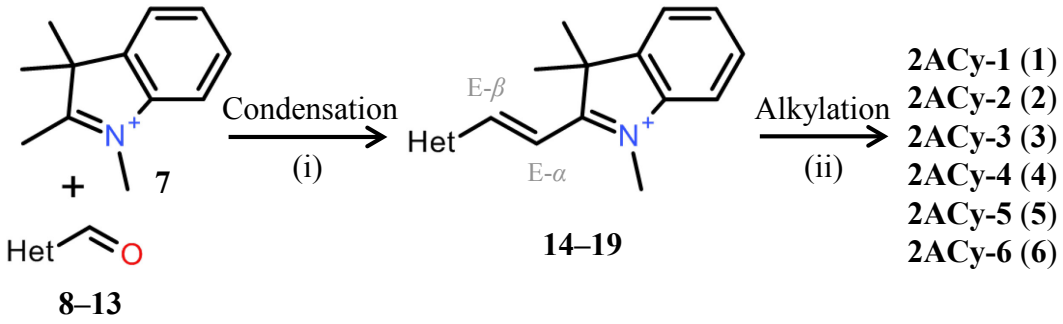

Het: 3-pyridyl, 3-quinolyl, 5-quinolyl, 6-quinolyl, 3-isoquinolyl, 1-phenazyl

Scheme 3-1 Synthesis of the diquaternary salts. *Reagents and conditions:* (i) piperidine (cat.), EtOH, reflux, 2–16 h; (ii) TfOMe (4–10 equiv.), DCM, rt, 16 h. For the yields and numbering, see **Table 3-1** below.

Table 3-1 Yields of the preparation of diquaternary salts (**1–6**).

Condensation step		**Alkylation step**		**Product**	
Heterocycles (number)	Yields (%)	Heterocycles (number)	Yields (%)	Name	Overall yields (%)
3-pyridyl (**8**)	77	3-pyridyl (**14**)	96	**2ACy-1**	74
3-quinolyl (**9**)	72	3-quinolyl (**15**)	91	**2ACy-2**	66
5-quinolyl (**10**)	80	5-quinolyl (**16**)	89	**2ACy-3**	71
6-quinolyl (**11**)	80	6-quinolyl (**17**)	99	**2ACy-4**	79
3-isoquinolyl (**12**)	79	3-isoquinolyl (**18**)	70	**2ACy-5**	55
1-phenazyl (**13**)	86	1-phenazyl (**19**)	20	**2ACy-6**	17

The synthesis procedure started with the condensation of aldehyde of choice (**8–13**) with indolium iodide (**7**) in the presence of a catalytic amount of piperidine. Aldehydes (**8–13**) and indolium salt **7** are inexpensive and commercially available material. The ^{1}H NMR spectra of resulting indolium salts **14–19** showed two characteristic doublets attributed to the *α,β*-unsaturated system of the vinyl bridge with a coupling constant between 16.4 and 16.7 Hz for their *trans* isomers. For compounds (**14–18**), the chemical shifts of protons at E-*α* and E-*β* positions were observed around 7.80–7.90 and 8.40–8.90 ppm, respectively. Substance **19** exhibits more deshielded protons at the E-*α* and E-*β*, with signals, 8.50 and 9.46 ppm, respectively. This can be attributed to a more powerful electron accepting ability of the phenazine moiety.

Alkylation of indolium salts (**14–19**), using an excess of TfOMe, conveniently led to the target diquaternary salts. In this series, only alkylation of **19** turned out to be difficult. According the general procedure (see experimental part), we obtained compound **2ACy-6** with the yield of 20%. This is caused by low nucleophilicity of nitrogen atoms of the phenazine moiety.

The structure of **2ACy-6** was assigned on the basis of 1D and 2D NMR analysis. TOCSY and NOESY NMR experiments revealed that the methyl group is located on 5-position of the phenazine ring (**Figure 3.4**). The especially strong NOE correlations were detected between the protons of the N^5-methyl group and the protons H-4, H-6. We assume that the steric hindrance, caused by the substituent at 1-position, defines the selectivity of the alkylation toward 5-position.

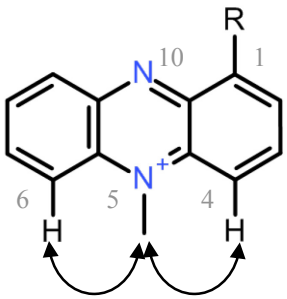

2ACy-6
R = vinyl–indolium moiety

Figure 3.4 Key NOE correlations observed for **2ACy-6**.

3.2.2 Preparation of 1,9-substituted 5-alkylphenazine derivatives

Although **2ACy-6** displayed the desired UV-Vis properties (see experimental part), we found this compound unstable in aqueous buffer solutions (pH 7.0) at room temperature. The decomposition was monitored by UV-Vis (data not shown) and was accompanied by the formation of precipitates after one hour of incubation of a 1-mM solution in phosphate buffer (50 mM, pH 7.0). The instability of **2ACy-6** may be attributed to the literature known elimination of the N^5-methyl group in the phenazinium ring.[28] Since 5-alkylphenazine derivatives were found to be useful as an electron carrier in many commercial applications, considerable efforts have been dedicated to develop their stable analogues.[29] Thus, 5-ethylphenazines proved more stable than 5-methylphenazines in aqueous solutions (pH 6–9),[28] as the N^5-ethyl group is not eliminated under these conditions.

Hence, we were motivated to prepare the 5-ethyl derivative of **19**. However, attempts to directly ethylate **19** were unsuccessful (**Scheme 3-2**), which led us to an alternative synthetic strategy. We assumed that the incorporation of an electron-donating ethoxy group in 9-position of the phenazine moiety may increase the nucleophilicity of the nitrogen atom in 5-position, which would enable access to the desired *N*-ethyl derivatives.

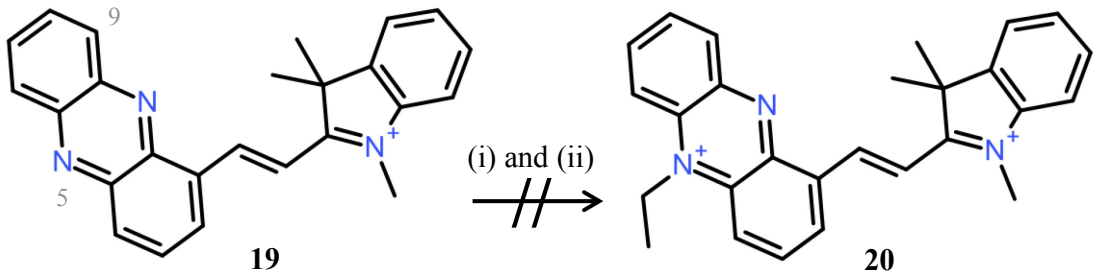

19 **20**

Scheme 3-2 An attempt to prepare the N-ethyl derivative of **2ACy-6**. *Reagents and conditions:* (i) TfOMe, DCM, rt, Ar; (ii) TfOMe, DCE, 80°*C*, Ar.

The successful synthetic strategy for the preparation of 9-ethoxy aldehyde **25** in 5 steps is shown in **Scheme 3-3**. It employs an Ullmann-type condensation as the key step which allowed for the formation of **23** in 31% yield in two steps. Alcohol **24** was prepared by activating the acid **23** with 1,1'-carbonyldiimidazole (CDI). The resulting *N*-imidazolide had to be isolated in order to obtain pure products. It was then immediately reacted with sodium borohydride in water to give **24** in excellent 84% yield. Oxidation of alcohol **24** with activated manganese (IV) oxide furnished aldehyde **25** in 71% yield.

As shown in **Scheme 3-4**, coupling of aldehyde **25** with indolium salt **7** in the presence of piperidine afforded compound **26** in 68% yield. Surprisingly, it was much harder to alkylate 9-ethoxy derivative **26** using TfOMe, than its predecessor **19**. Thus, more harsh conditions were employed for the methylation of **26**: a thirty-minute heating under sealed vessel conditions in 1,2-dichloroethane (DCE) at 100°*C* (**Scheme 3-4**). Also yields did not improve when the heating was prolonged up to several days.

The *N*-ethyl derivative **28** could not be obtained in this study. Evaluated conditions included varying temperatures up to 100°*C*, reaction times from minutes to five days, and using stronger alkylating agents (Meerwein's salt).[30]

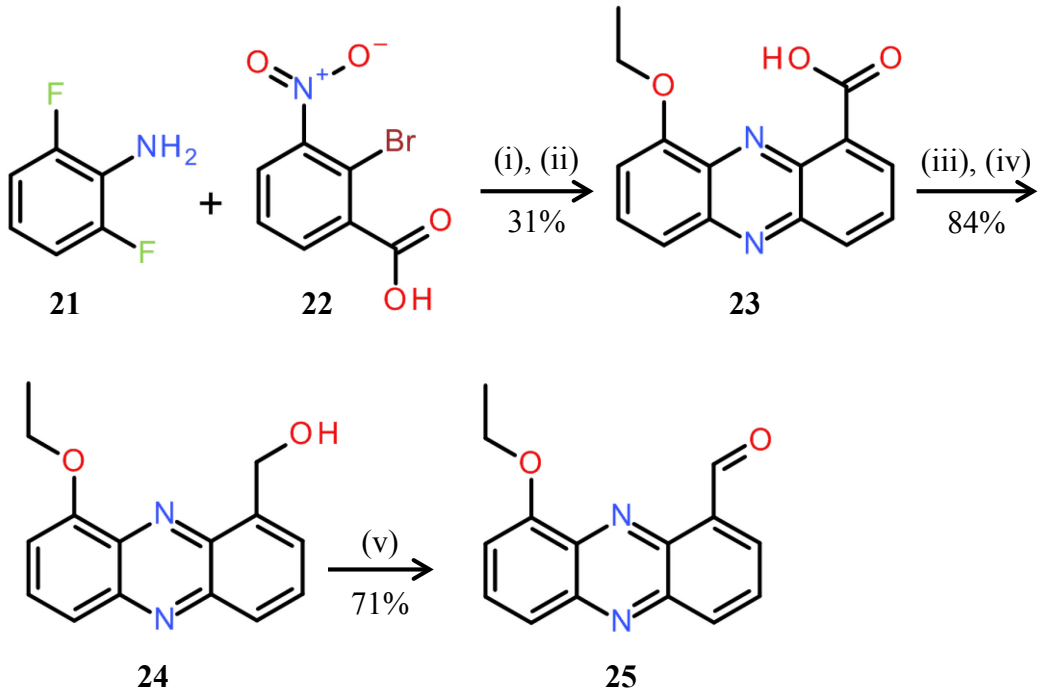

Scheme 3-3 Synthesis of the 9-ethoxyphenazine-1-carbaldehyde. *Reagents and conditions:* (i) CuCl, Cu, 4-ethylmorpholine, 2,3-butanediol, 80°*C*, 8 h; (ii) $NaBH_4$, EtOH, reflux, 3 d; (iii) CDI, DMF, 50°*C*, 1 h; (iv) $NaBH_4$, H_2O, rt, 1 h; (v) MnO_2, DCM, rt, 3 h.

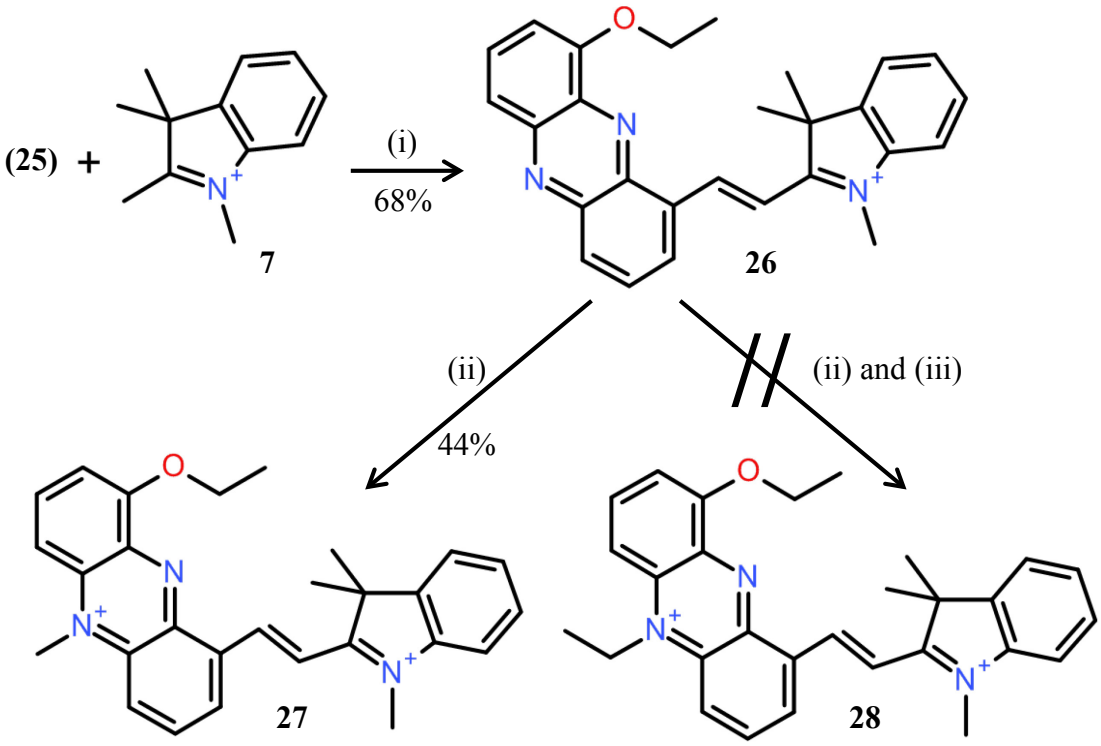

Scheme 3-4 Synthesis of the diquaternary salts. *Reagents and conditions:* (i) piperidine, EtOH, reflux, 3 h, Ar; (ii) TfOMe, DCE, 100°*C*, Ar, 30 min; (iii) Et_3OBF_4, DCE, 100°*C*, Ar.

3.2.3 Spectral properties of the indicators and their response to NADH

The spectral properties of **1–6** were evaluated to test the proposed reactivity toward NADH. Positively charged diquaternary salts **1–6** are soluble in water (>5 mM), which allowed to record UV-Vis spectra in aqueous solution (50 mM phosphate buffer, pH 7.0). The results are summarized in **Table 3-2**. The compounds contain a characteristic absorption band at ca. 360–380 nm. The high energy of this transition is caused by the presence of two electron-acceptor moieties. **2ACy-5** and **2ACy-6** display a high absorption in the visible range, whereas **2ACy-2** showed a definite, but small absorption band. The remaining compounds showed no visible absorption (400–700 nm) in the oxidized state.

Table 3-2 UV-Vis absorption spectra of the diquaternary salts (**2A**) and products of their reduction by NADH* recorded in phosphate buffer (50 mM, pH 7.0).

Name	λ_{max} (ε $mM^{-1}cm^{-1}$), nm	
	Two-acceptor π-system (**2A**)	**2A** + NADH
2ACy-1	363 (11.7), 291 (9.2), 251 (10.7)	546, 534sh.
2ACy-2	512 (0.8), 384 (19.5), 312 (13.5)	537, 515sh.
2ACy-3	383 (22.8), 340 (14.1)	—
2ACy-4	379 (23.2), 318 (15.9)	517
2ACy-5	514sh. (1.9), 487 (3.7), 372 (12.6), 345 (12.3)	524sh., 499
2ACy-6	481 (6.0), 394 (16.2), 377sh. (15.6), 261 (26.4)	740

* — **2A** + NADH reactions were monitored by UV-Vis in 400–1000 nm.

We further investigated molecules **1–6** (1.0–2.0 mM) with various NADH concentrations (0.02–0.5 mM). Of the six compounds, only **2ACy-3** showed no shift in the wavelength upon reduction, as no donor-acceptor π-conjugation in the reduced form of **2ACy-3** was established. Of the five compounds, **2ACy-2** and **2ACy-5** showed a shift of 25 and 12 nm, respectively; and the remaining three (**2ACy-1**, **2ACy-4** and **2ACy-6**) showed a larger shift. Remarkably, the maximum of **2ACy-6** was shifted to near-infrared region (NIR). The reduced compounds remained perfectly soluble in buffer (no turbidity and precipitation was noted) for several hours at room temperature. The fastest rates of reaction were observed for **2ACy-2** and **2ACy-6** (for details see **Table 3-4S** in supplementary material). However, free **2ACy-6** is not stable in buffer and its reduction product is rapidly oxidized under aerobic conditions (data not shown). Therefore, we chose **2ACy-2** as a lead structure for NADH sensing applications.

Optical properties of 2ACy-2

The spectroscopic evaluation of **2ACy-2** and its response to NADH were carried out under physiological conditions at 25°*C* in buffer solution (25 mM PIPES, 101 mM NaCl, pH 7.0). As shown in **Figure 3.5**, free indicator **2ACy-2** (5 μM) is of light-yellow colour and exhibits a very broad band in its absorption spectra with maxima at 312 and 384 nm. Furthermore, a band of low intensity is seen in the visible range (ε_{515} = 0.4 ± 0.1 $mM^{-1}cm^{-1}$). This band was not detected, when the spectra of **2ACy-2** were recorded in MQ water (actual pH <7).[31] This observation can be attributed to the known susceptibility of *N*-methyl heteroaromatic cations to pseudobase formation at pH ≥7.[32-35] We also prepared *N*-ethyl and *N*-octyl derivatives of **2ACy-2** in attempts to destabilize the [**2**-OH] adduct by steric effects; however, no profound decrease of the 515-nm band was observed (data not shown).

After adding NADH (excess) to the buffer solution (pH = 7) containing **2ACy-2** (5 μM), a new absorbance band at 537 nm appeared within five minutes, and remained stable for hours. During this process, the colour changed from light-yellow to pink. The increase in absorbance is so intense, that the red-shift is easily distinguished by the observer's eyes. The extinction coefficient of the resulting chromophore was also estimated by varying concentrations between 0.5–5.0 μM of indicator **2ACy-2** (ε_{537} = 81.9 ± 2.1 $mM^{-1}cm^{-1}$, **Figure 3.25S**). This value is significantly higher than those reported for tetrazolium salts (ε_{433} = 37.0 $mM^{-1}cm^{-1}$ for WST-1 being the most eminent), which are common NADH indicators used in cell-viability testing.[36-37]

Next, we examined the changes in the fluorescence emission spectra of **2ACy-2** in the absence or presence of NADH in the buffer solution (**Figure 3.6**). Free **2ACy-2** is essentially nonfluorescent; in contrast, the treatment with NADH (excess) caused a new emission band to appear at 561 nm, under identical conditions. An enhancement in the fluorescent intensity of up to 30-fold was observed. The strongly enhanced emission in the visible region allows bio-imaging applications.

Moreover, optical response of **2ACy-2** to NADH resembles spectra of trimethine cyanine dyes. This observation supports the hypothesis that NADH triggered the formation of a cyanine dye.

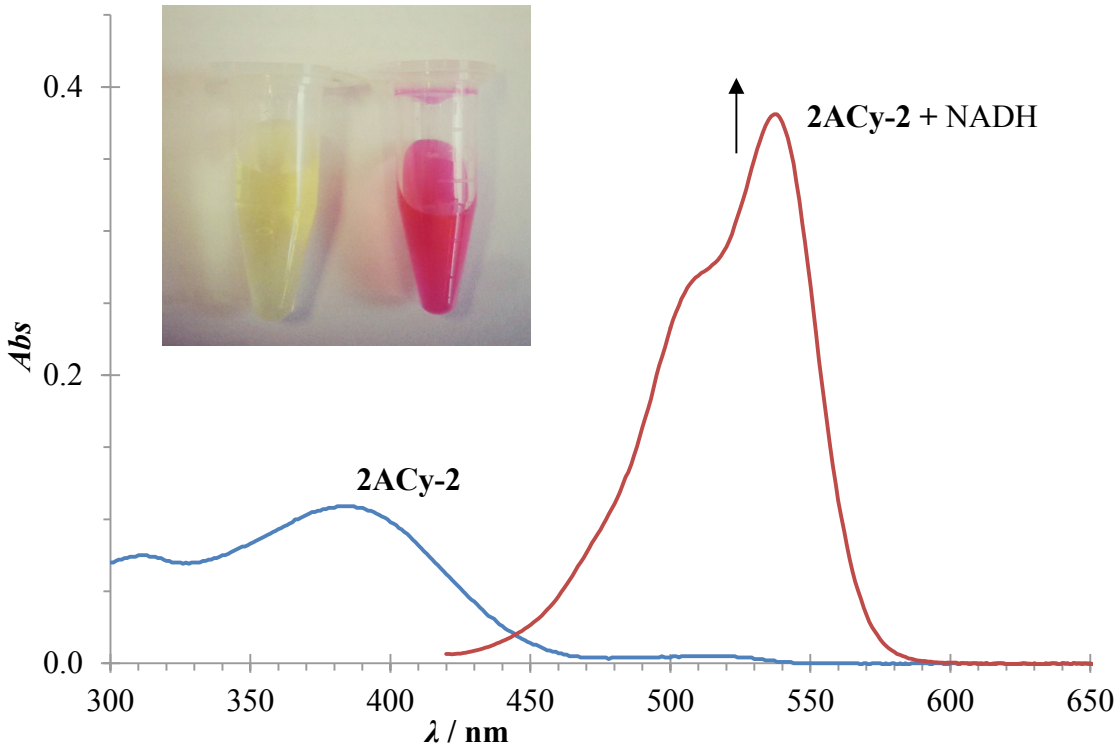

Figure 3.5 UV-Vis absorption spectra of **2ACy-2** (5 µM) in aqueous buffer solution (25 mM PIPES, 101 mM NaCl, pH 7.0) before (blue) and after (red) reaction with NADH (500 µM). The spectra were taken after incubation for 5 min at 25°*C*. Inset: the photograph depicts the colour change of the **2ACy-2** solution (20 µM) before (left) and after (right) the addition of excess NADH.

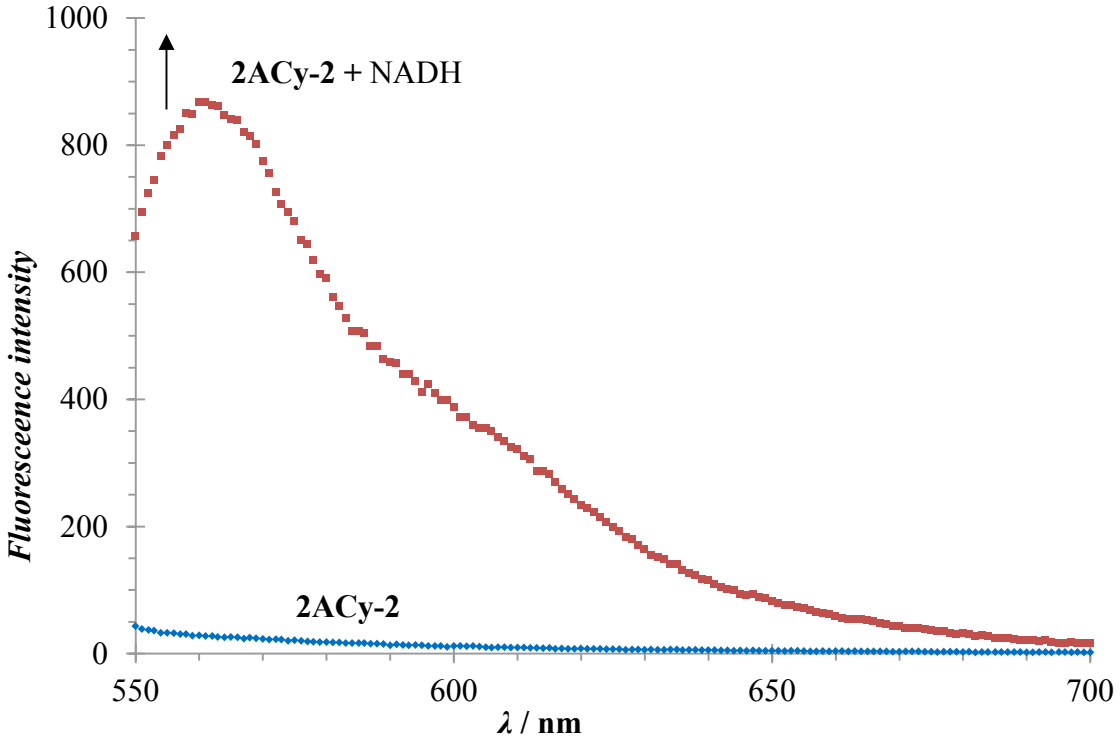

Figure 3.6 Fluorescence spectra of **2ACy-2** (5 µM) in aqueous buffer (25 mM PIPES, 101 mM NaCl, pH 7.0) solution before (blue diamonds) and after (red squares) reaction with NADH (500 µM). The spectra were taken after incubation for 5 min at 25°*C*. $\lambda_{ex}/_{em\ max}$ = 537 nm, slit widths: 5/5 nm.

Reaction mechanism

For better understanding of the detection process, we decided to identify the structure of the resulting chromophore (**Scheme 3-5**). We anticipated the transformation of the quinolinium moiety to a dihydro-derivative. Such behaviour was predicted according to literature on the reactions of 3-substituted quinolinium salts with NADH analogues.[26-27, 38-41] Roberts *et al* reported extensive ^{1}H NMR spectral characterization of their reduction products.[40] Bunting *et al* completed the picture by studying regioselectivity of the hydride transfer to quinolinium salts.[41] The results appear to be general for compounds with electron-withdrawing substituents in the 3-position. They are more susceptible to attack at the 4-position rather than at the 2-position of quinolinium moiety. However, a mixture of 1,2- and 1,4-dihydro isomers is also possible.

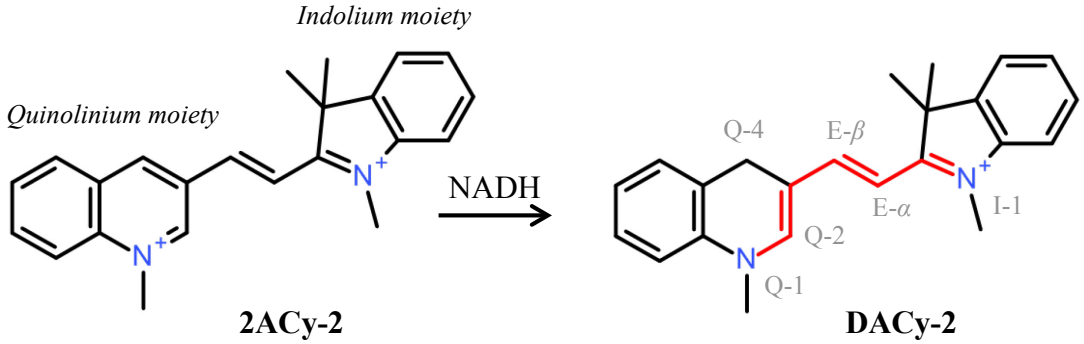

Scheme 3-5 NADH-sensing mechanism of **2ACy-2** in aqueous buffer solution (pH 7.0).

After reaction of **2ACy-2** with NADH in aqueous solution, the organic material was isolated by extraction with DCM. The HPLC-MS analysis confirmed the formation of a single product. The ESI-MS spectrum displayed a major peak with the molecular ion at *m*/*z* 329, indicating the hydride addition. The product was sufficiently air-stable to allow for NMR and UV-Vis spectral characterization. Visible spectra of this compound (data not shown) matched those observed in the presence of NADH (see **Figure 3.5** above). The structure was further elucidated by ^{1}H and ^{13}C NMR. Proton and carbon resonances were assigned using two-dimensional techniques (COSY, HSQC and HMBC; see **Table 3-3** below), which also allowed us to establish the proton-carbon network of **DACy-2** (see NMR supplementary material).

The comparison of ^{1}H NMR spectra of **2ACy-2** (**A**) and the product of its reaction with NADH (**B**) is shown in **Figure 3.7**. The results of these experiments evidence the hydride attack at the quinolinium moiety. As seen in **Figure 3.7**, aromatic protons Q-2 and Q-4 appeared as the new signals (the aromatic and methylene protons at δ 7.70 and 3.96 ppm, respectively). The reduction of the quinolinium moiety unmasked the electron-donating nitrogen atom (**Scheme 3-5** above). Hence, the signals of aromatic protons shifted up-field confirming the expected increase in electron density.

The protons of the vinyl group located at 7.98 ppm (J = 14.4 Hz) and 5.92 ppm (J = 14.4 Hz) corresponding to the positions E-α and E-β, respectively (**Figure 3.7B**). The coupling constants reveal that the vinyl bridge preserved the *trans* conformation upon hydride transfer. Remarkably, the proton at E-β showed long-range COSY correlation with the methylene protons at 3.96 ppm with a coupling constant of J = 1.5 Hz. Finally, a strong ^{1}H-^{13}C correlation (HMBC) was observed between the one-proton singlet at 7.70 ppm and the low-field signal of the methyl carbon at the position Q-1 (data not shown). These correlations would unlikely be observed if the methylene group was on the position Q-2. Hence, the above spectral data provided direct evidence for the exclusively 1,4-dihydro isomer (**DACy-2**).

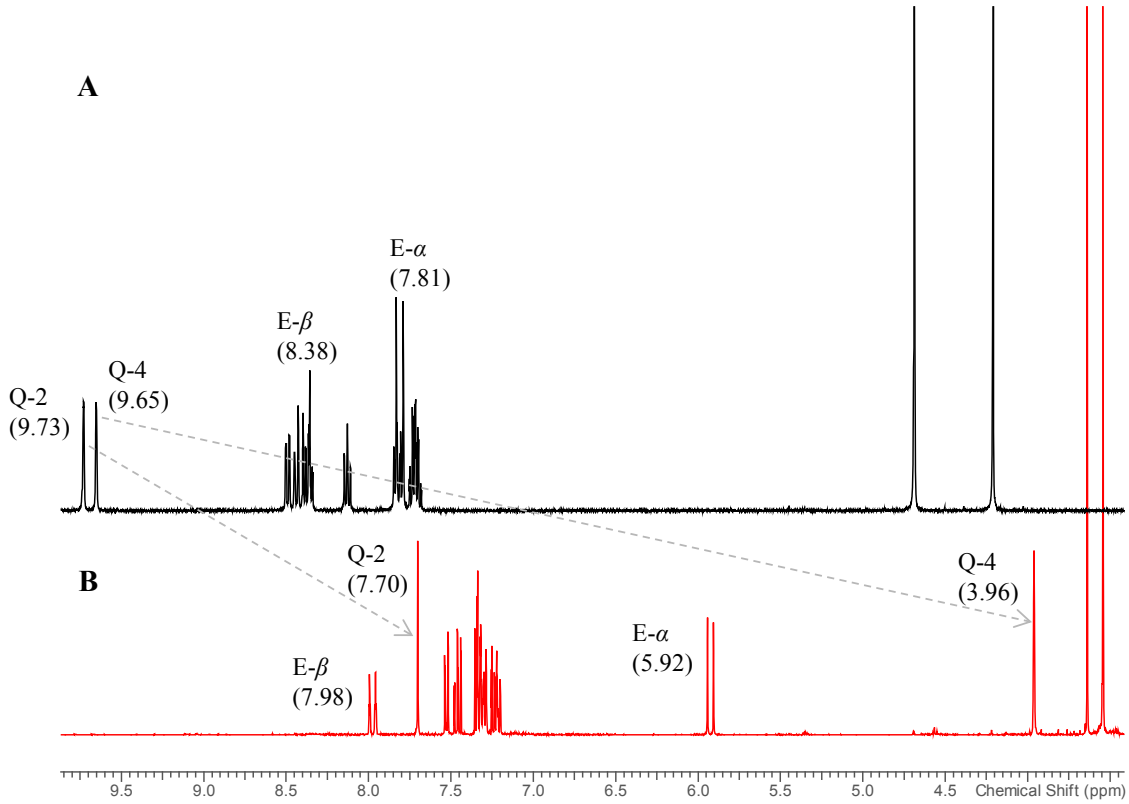

Figure 3.7 Stacked partial ^{1}H NMR (400 MHz) spectra of **2ACy-2** (**A**) and its reduction product **DACy-2** (**B**) in MeCN-d_3 at 25°*C*.

Table 3-3 ^{1}H and ^{13}C NMR signal assignment for **2ACy-2** and **DACy-2** in MeCN-d_3.*

Position	**2ACy-2**		**DACy-2**	
	δ ^{1}H (ppm); J (Hz)	^{13}C (ppm)	δ ^{1}H (ppm); J (Hz)	^{13}C (ppm)
Quinolinium moiety				
Q-N^{1}Me	4.69; s	47.5	3.54; s	40.5
Q-2	9.73; d, 1.2	151.4	7.70; s	154.5
Q-3	—	129.6	—	113.1
Q-4	9.65; d, 1.2	148.4	3.96; d, 1.5	25.6
Q-4a	—	130.8	—	124.6
Q-5	8.44; dd, 9.0, 0.6	133.1	7.27–7.35; m	130.0
Q-6	8.36; ddd, 9.0, 7.0, 1.5	139.1	7.19–7.23; m	115.9
Q-7	8.13; ddd, 8.2, 7.0, 0.6	132.7	7.27–7.35; m	127.8
Q-8	8.49; dd, 8.2, 1.5	120.5	7.23–7.26; m	126.5
Q-8a	—	140.5	—	136.4
Vinyl bridge				
E-α	7.81; d, 16.5	119.1	5.92; d, 14.4	98.9
E-β	8.38; d, 16.5	145.9	7.98; dt, 14.4, 1.5	153.1
Indolium moiety				
I-N^{1}Me	4.21; s	36.7	3.64; s	31.5
I-2	—	183.5	—	176.6
I-3	—	54.7	—	49.8
I-$C^{3}Me_2$	1.85; s	25.7	1.69; s	26.5
I-3a	—	145.4	—	141.4
I-4	7.82–7.86; m	117.2	7.50–7.55; m	122.3
I-5	7.73; ddd, 7.4, 7.3, 1.4	132.4	7.34; ddd, 7.9, 7.6, 1.0	125.9
I-6	7.70; ddd, 7.6, 7.3, 1.6	131.0	7.43–7.49; m	128.6
I-7	7.78–7.82; m	124.4	7.27–7.35; m	111.6
I-7a	—	143.2	—	142.7

* – For the numbering of **2ACy-2** and **DACy-2**, see below.

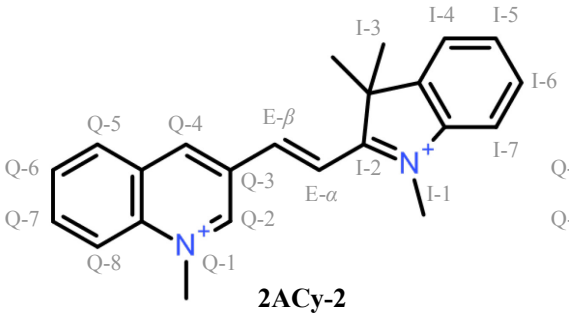

2ACy-2

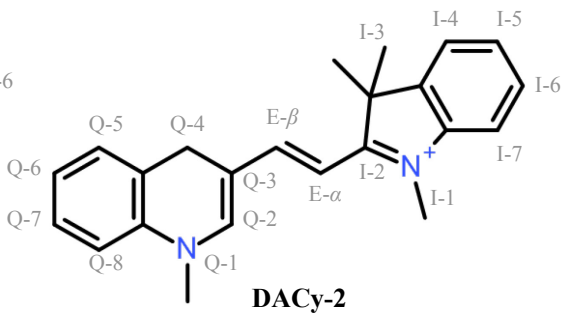

DACy-2

Time response and stability

These preliminary data indicated that **2ACy-2** could be used for real-time monitoring of NADH in biological assays. In this light, we studied the kinetic response of **2ACy-2** (50–250 μM) in presence of low NADH concentrations (see the example in **Figure 3.8**). A control solution of **2ACy-2** (100 μM) exhibited no noticeable changes at 536 nm. At the same time, upon introduction of NADH (5 μM), the absorbance intensity reached a plateau in five minutes. Additional analysis of the kinetic data gave the second-order rate constant (k_2) of 190.5 ± 9.3 $M^{-1}s^{-1}$ (**Figure 3.27S**), characteristic of a fast response for NADH. What is more important, the assay solutions are stable for hours at room temperature, as no obvious change in the absorption spectrum was detected. The rapid kinetic profile, stability and low background signal encouraged us to further investigate **2ACy-2** for NADH sensing. In this work, an assay time of five minutes was selected in the evaluation of its selectivity and sensitivity parameters.

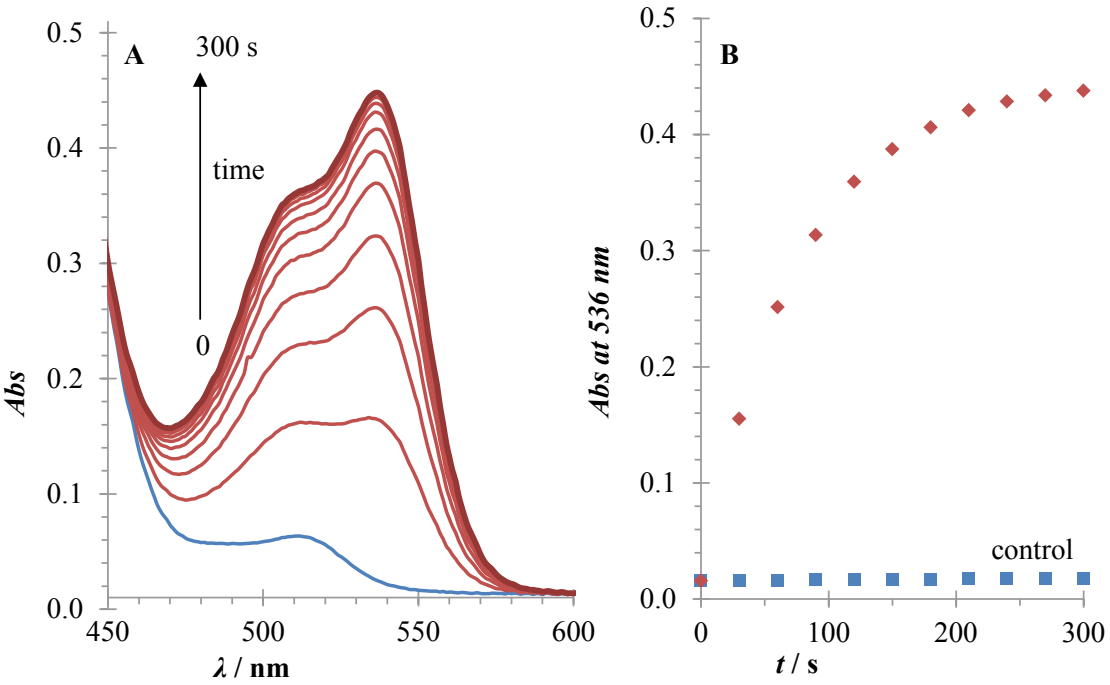

Figure 3.8 Kinetic response of **2ACy-2** to NADH under pseudo-first-order conditions (*[**2ACy-2**]$_0$* = 100 μM, *[NADH]$_0$* = 5 μM).

Limit of detection

To investigate its sensitivity, indicator **2ACy-2** (100 µM) was treated with various NADH concentrations (0.3–30.0 µM) in buffer solution (25 mM PIPES, 101 mM NaCl, pH 7.0), and the assay solution was monitored by UV-Vis spectroscopy. As shown in **Figure 3.9A**, a progressively enhanced absorbance intensity was observed with the increasing amount of NADH. A good linear response was obtained in the range between 0.3 and 20.0 µM (n = 29; R^2 = 0.996), as shown in **Figure 3.9B**. Obviously, at NADH concentrations higher than 20 µM, the spectrophotometer becomes a limiting factor (maximum reliable absorbance unit of 2). From the calibration plot, the detection limit of NADH was determined to be as low as 0.1 µM at 3σ/m, where σ is the standard deviation of the blank measurements of **2ACy-2** (100 µM) and m is the slope obtained from the linear plot of **2ACy-2** absorbance at 536 nm against NADH. The slope of 76.1 ± 0.9 OD/mM proves **2ACy-2** to be one of the most sensitive colorimetric indicators for NADH. This is particularly beneficial for application in cell assays as intracellular NADH concentrations are typically at micromolar levels.[42]

Emission experiments of **2ACy-2** with various NADH concentrations were carried out as well. The data are shown in UV-Vis supplementary material (**Figure 3.26S**).

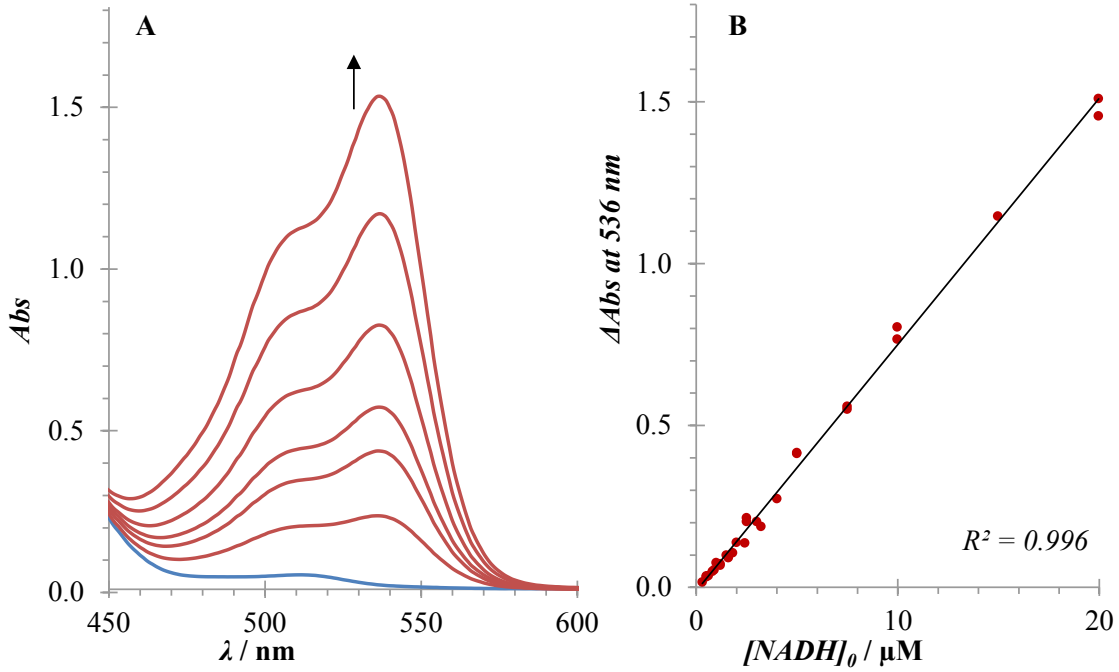

Figure 3.9 A — Absorbance responses of **2ACy-2** (100 µM, blue) to increasing concentrations of NADH: 2.5, 5.0, 7.5, 10.0, 15.0, 20.0 µM of NADH (red), respectively. **B** — relationship between the concentration of NADH and the absorbance of the reaction mixture. The spectra were taken after incubation for 5 min in 25 mM PIPES, 101 mM NaCl, pH 7.0 at 25°C.

Selectivity studies

Selectivity over competitive biological reductants is an important parameter to evaluate the performance of an indicator for NADH sensing. Glutathione (GSH) and ascorbic acid (AA) are known electron donors for the redox processes in biological systems. Potential interferences may also include nucleophiles, such as amino acids, due to electrophilic nature of **2ACy-2**.

The selectivity of **2ACy-2** for NADH was tested by screening its response to biologically relevant analytes (**Figure 3.10**). Indicator **2ACy-2** showed significantly higher absorbance and fluorescence response in the presence of NADH compared to other analytes. We did not observe signal increase above blank levels (ctrl) in the presence of reducing agents (AA) and amino acids (Asn and Lys). The addition of thiols (Cys and GSH) led to a new absorbance maximum at 528 nm, but the signals were by about 3- and 10-times weaker compared to NADH. The kinetic study showed that the reaction of thiols with **2ACy-2** (**2**) was completed instantly (**Figure 3.28S**). Kinetic data, in combination with the well-defined isobestic point at 442 nm, indicate the formation of a [**2**-SR] adduct. Importantly, the competitive assays revealed that these species can still undergo reduction with NADH (**Figure 3.11**). In all cases, the total colorimetric and fluorescent response to NADH was unaffected. This confirms that the [**2**-SR] adduct formation is easily reversible. Nucleophilic additions to C-3 substituted quinolinium cations has been well studied and their ability to adduct formation with nucleophiles typically reflects the electron density at C-2 and C-4 of the quinolinium ring.[32] The NMR study of **2ACy-2** shows that the quinolinium moiety has enhanced C2–C3 and C3–C4 bond polarities (**Table 3-3** above) and is structurally similar to Michael acceptors, which are known for reversible additions of thiols.[43] In summary, we found that **2ACy-2** reacts reversibly with amino acids and peptides having a free thiol group, but not with amino groups. Adduct formation with nucleophiles does not prevent the detection of large amounts of NADH. Moreover, the modular design of **2ACy-2** allows for the independent variation of each component (indolium group, side chain, π-conjugated bridge, electron deficient heterocycle) and facilitates the tailoring of **2A**-indicators for specific applications. An alternative strategy would be the use of thiol blocking reagents as an additional step in the sample preparation process.[44]

Even though, the selectivity of **2ACy-2** still has to be improved, the fast response and high sensitivity towards NADH encouraged us to study its potential applications in biological environment.

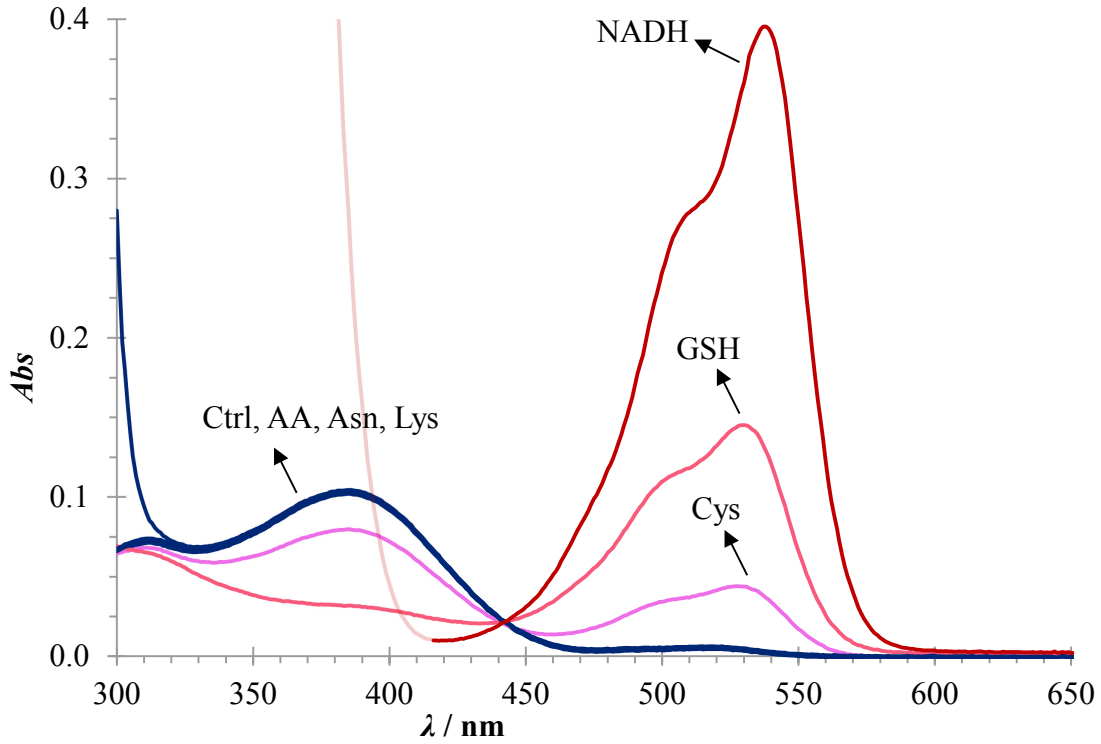

Figure 3.10 Absorbance response of **2ACy-2** (5 µM, ctrl) with analytes (400 µM): ascorbic acid (AA), amino acids (Asn, Lys), thiols (Cys, GSH) and NADH; in buffer (25 mM PIPES, 101 mM NaCl, pH 7.0). The spectra were obtained 5 min after addition of the analytes.

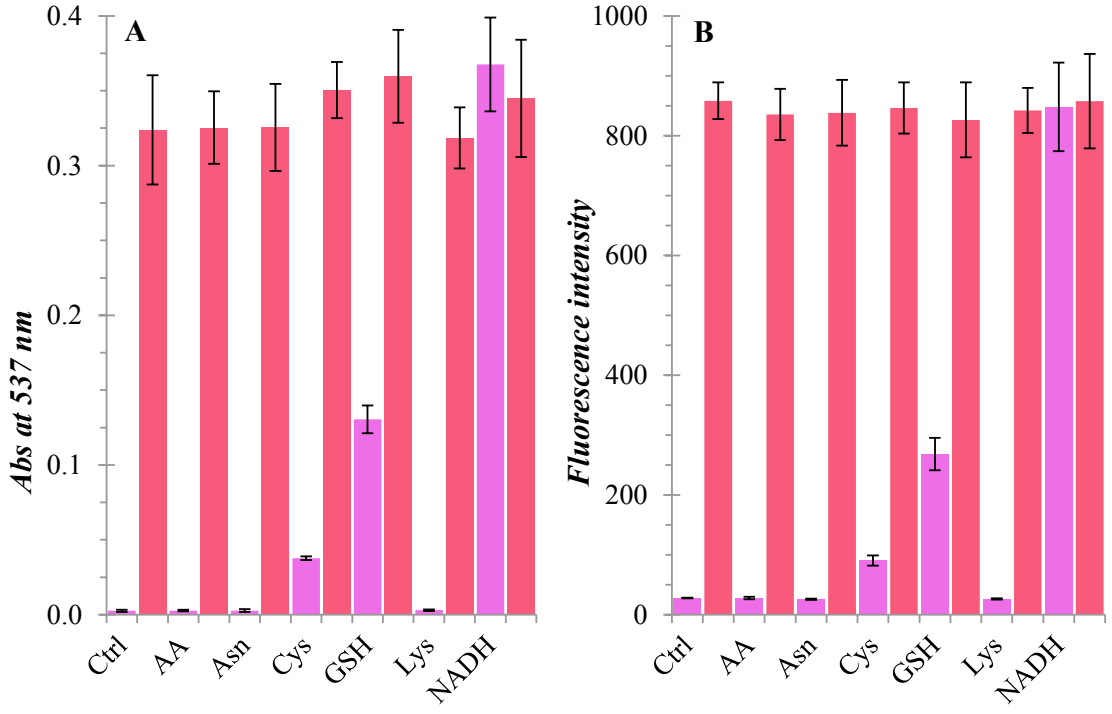

Figure 3.11 Competitive assays of NADH (400 µM) against **2ACy-2** (5 µM) with analytes (400 µM): AA, Asn, Cys, GSH, Lys and NADH; after 5 min of incubation in buffer (25 mM PIPES, 101 mM NaCl, pH 7.0). Purple columns for **2ACy-2** + analytes; red columns for **2ACy-2** + analytes + NADH. $\lambda_{ex}/_{em}$ = 537/561 nm, slit widths: 5/5 nm.

3.3 Applications

3.3.1 Sensing of glucose by **2ACy-2** via the NAD^+/GDH coupling reaction

The ability to detect NADH cofactor with **2ACy-2** allows monitoring the activity of NAD^+-dependent enzymes as well as their substrates. NADH indicator **2ACy-2** was applied to analyze glucose in the presence of the NAD^+-dependent glucose dehydrogenase (GDH). As shown in **Figure 3.12**, GDH catalyzes the oxidation of glucose to glucono-*δ*-lactone with concomitant reduction of NAD^+ to NADH. The resulting reduced cofactor reacts with **2ACy-2**, which leads to the formation of **DACy-2** and an increase in absorbance.

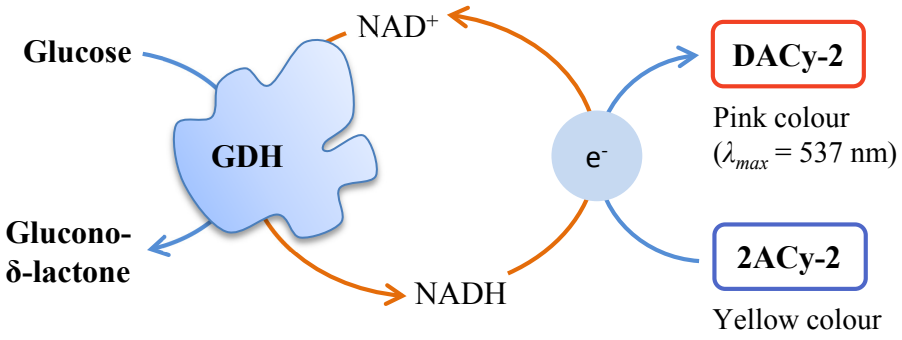

Figure 3.12 Sensing of glucose by **2ACy-2**.

The time-dependent spectral changes of **2ACy-2** (100 µM) upon treatment with glucose (10 µM) in the presence of NAD^+/GDH in phosphate buffer (100 mM, pH 7.0) are shown in **Figure 3.13**. Control experiments revealed that the absorbance of **2ACy-2** remained unchanged when NAD^+ or GDH were excluded from the system. Hence, the enzymatic reaction is essential to activate the formation of **DACy-2**. This experiment also suggests that **2ACy-2** is rather stable with all components of the assay. To verify that GDH-mediated formation of NADH enables the quantitative analysis of a substrate, the biocatalyzed reduction of **2ACy-2** was carried out with different concentrations of glucose (**Figure 3.13B**). As the concentration of glucose increases, the resulting NADH is higher, and consequently, the absorbance of **DACy-2** is intensified (**Figure 3.13C**). A good linearity was obtained in the range of 0.1–20.0 µM of glucose (R^2 = 0.999), with a slope of 71.7 OD_{537}/mM, which demonstrates a highly sensitive assay for dehydrogenase activity using indicator **2ACy-2**.

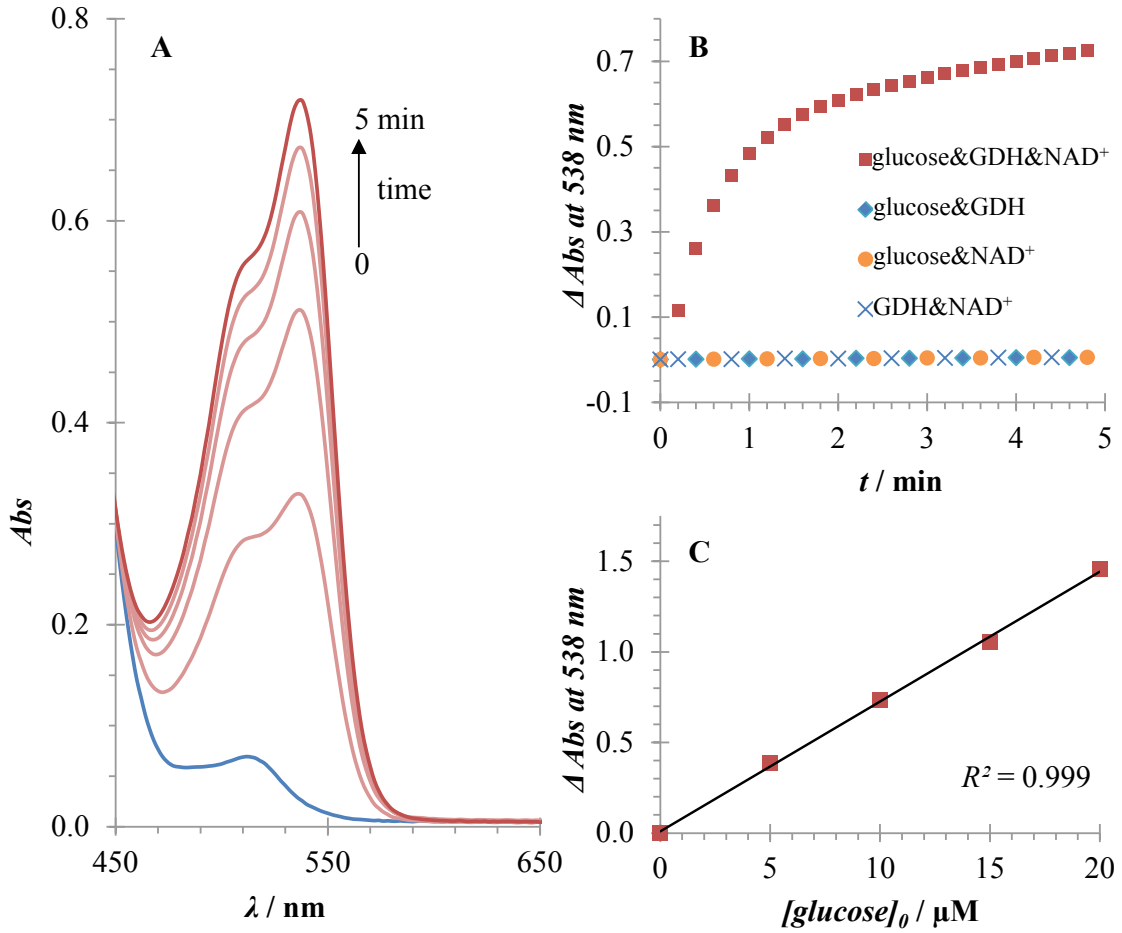

Figure 3.13 **A** — The spectral changes after addition of glucose (10 µM) to GDH-NAD^+ assay solution containing **2ACy-2** (100 µM) in phosphate buffer (100 mM, pH 7.0). The absorbance (400–700 nm) was recorded every 60 s for 5 min after addition of glucose. **B** — The plots of absorption intensity changes under different conditions. **C** — Calibration plot between concentration of glucose and absorption intensity changes of the assay solution.

3.3.2 Live cell imaging

Cell imaging was performed in collaboration with Oliver Tonn, Claudio Sustmann and Konrad Honold (Roche, Penzberg).

We then turned our attention to demonstrate the ability of **2ACy-2** to detect intracellular NADH levels. Live HEK-293 cells were incubated with a solution of indicator **2ACy-2** for thirty minutes. The confocal microscopy images showed cellular uptake of **2ACy-2** and strong fluorescence emission was observed (**Figure 3.14**). With increased time, the images did not show further fluorescence enhancement, and the resulting cells retained viability for at least 24 hours.

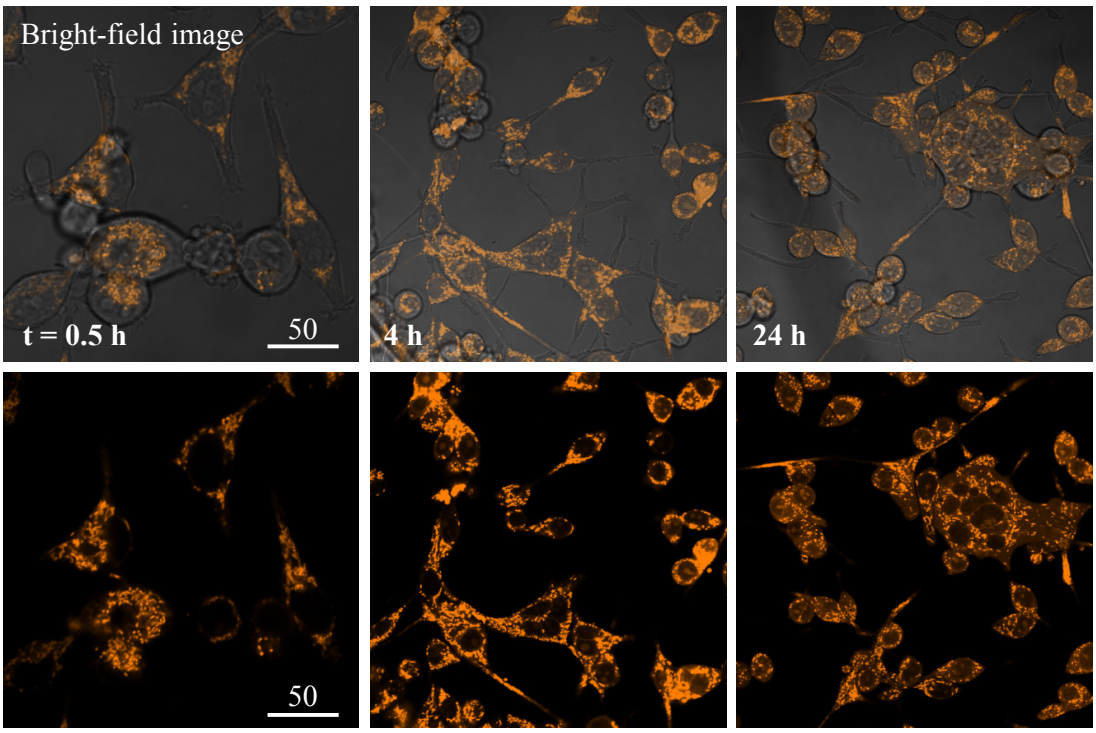

Figure 3.14 Bright field fluorescence overlay (top row) and fluorescence (bottom row) images of HEK-293F cells stained with **2ACy-2** (20 μM) at different times (0.5, 4, 24 h). Excitation: 561 nm; emission: 580–610 nm. Scale bar unit is μM.

In a control experiment, cells were pre-treated with 4% paraformaldehyde (PFA, cell fixation reagent), and then incubated with **2ACy-2** (20 μM) for an hour under the same conditions. Only negligible intracellular fluorescence was observed inside the fixed cells (**Figure 3.15**). This is consistent with the fact that NADH is generated by metabolism of living cells. In conclusion, these cell experiments revealed that **2ACy-2** can rapidly penetrate cell membranes and could be an effective NADH imaging agent. We have also demonstrated that **2ACy-2** has the potential to be a viability indicator in proliferation and cytotoxicity assays on a single-cell level, which may well be suited for high-throughput screening (HTS) in drug discovery.

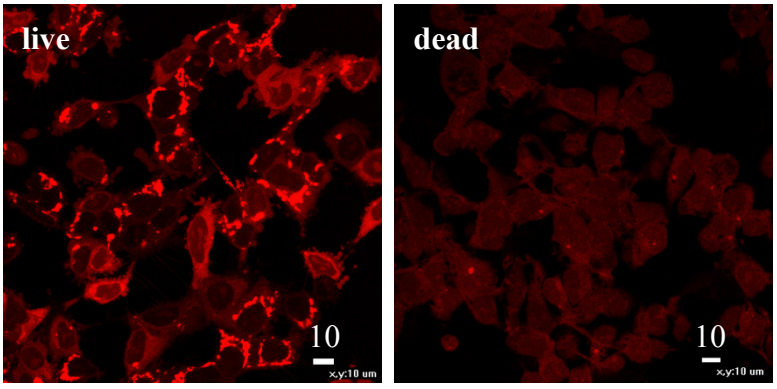

Figure 3.15 Fluorescence microscope images of living and PFA fixed HEK-293 cells stained with **2ACy-2** (20 μM) for 1 h. Excitation: 561 nm; emission: 611 ± 7 nm. Scale bar unit is μM.

3.3.3 Imaging of intracellular metabolic pathways by a "turn-on" fluorescent NADH indicator

Cell imaging was performed in collaboration with Ruslan Dmitriev and Dmitri Papkovsky (University College Cork).

For evaluation of cell staining, we chose HCT116 cells which display rapid growth in culture and active metabolism.[25] Best staining conditions with **2ACy-2** NADH-indicator were seen after six hours of incubation at 20-μM concentration (**Figure 3.16**, **Figure 3.17**). Indicator **2ACy-2** showed cytoplasmic localisation without accumulation in the nucleus.

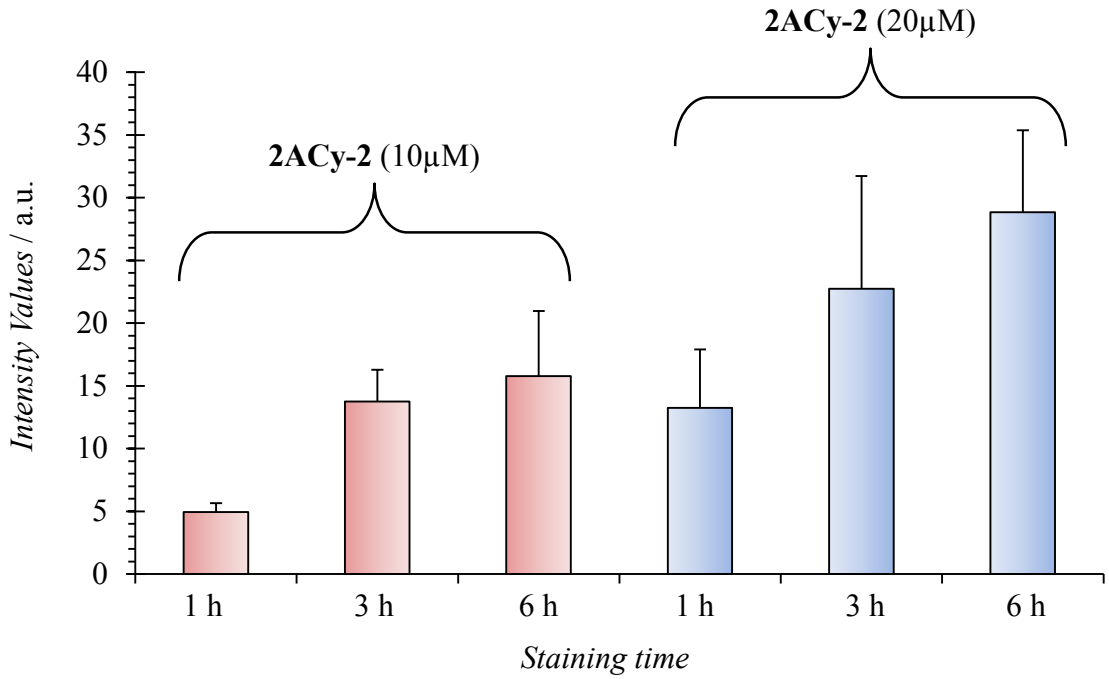

Figure 3.16 Optimisation of staining time and concentration of **2ACy-2**. Average fluorescence in HCT116 stained with **2ACy-2**.

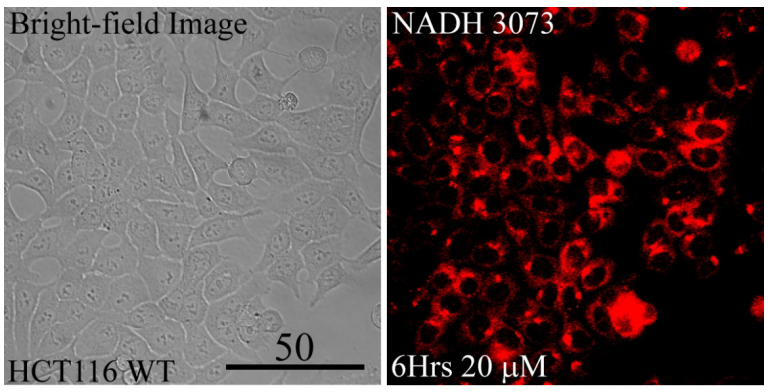

Figure 3.17 Transmission light (Bright-field) and fluorescence intensity images of HCT116 cells stained with **2ACy-2** (= 3073). Scale bar is in μm.

In order to investigate whether **2ACy-2** NADH-indicator intensity values changed depending on increased NADH levels in the cell, we stained two different cell types, HCT116 wild type (WT) and HCT116 SCO2 –/–. The latter ones have consistently higher NADH levels when compared to WT cells.[11, 25] When stained with the same concentration of **2ACy-2** (20 μM) for an equal time period, we consistently observed significantly higher intensity values for SCO2 –/– cells, indicating 1.5–2 times higher intracellular NADH concentration (**Figure 3.18**).

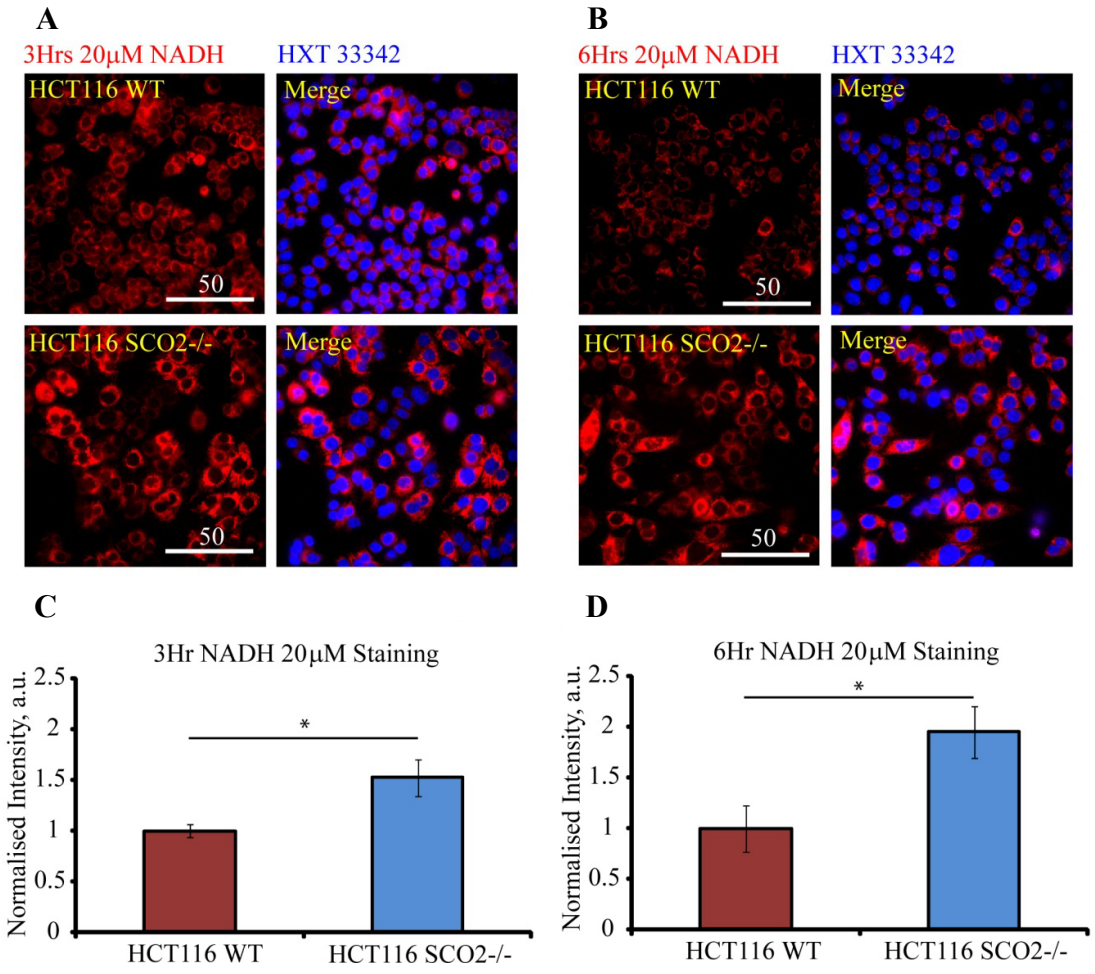

Figure 3.18 Comparison of NADH levels in two different cell lines. **A**, **B** — Both HCT116 WT and HCT SCO2 –/– cells stained with **2ACy-2** (20 μM) for 3 h and 6 h respectively. Fluorescence intensity images show staining compared to Hoechst 33342 (HXT 33342). **C**, **D** — Corresponding graphs showing the average intensity differences in NADH staining between HCT116 WT and SCO2 –/– cells for 3h and 6 h, respectively. Scale bar unit is μM. Asterisks indicate significance level of P = 0.05.

On the other hand, staining with **2ACy-2** (20 µM) did not show acute or significant effects on HCT116 cells viability. Using CellTox Green dye,[45] we analyzed membrane integrity of stained cells and compared it with a control (unstained) group. The cell morphology also did not change and there was no significant difference in the number of CellTox positive cells, when stained with **2ACy-2** (20 µM) for six hours (**Figure 3.19**). Indicator **2ACy-2** also displayed good photo-stability, which is comparable to mitochondria-specific probe TMRM[46-48] (**Figure 3.20**).

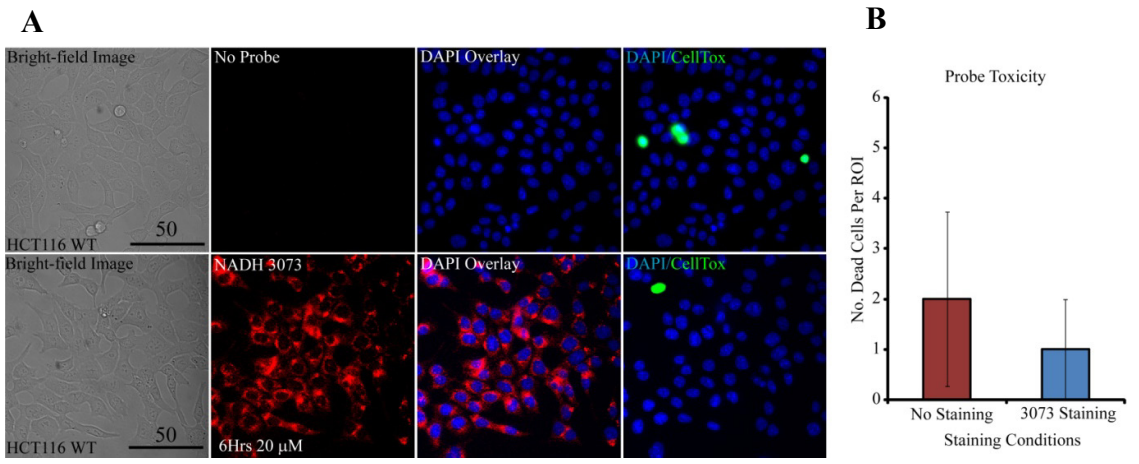

Figure 3.19 Investigation of probe toxicity and its effect on cell viability and morphology. **A** — Bright-field and fluorescence intensity images displaying cell morphology, NADH staining with **2ACy-2** (= 3073), DAPI and NADH merged as well as DAPI and CellTox Green merged respectively. **B** — graph displaying the number of dead cells in non-stained *vs* 6 h 20 µM staining with **2ACy-2** (= 3073). DAPI was used to visualise nuclei.[49] Scale bar unit is µM. ROI stands for region of interest.

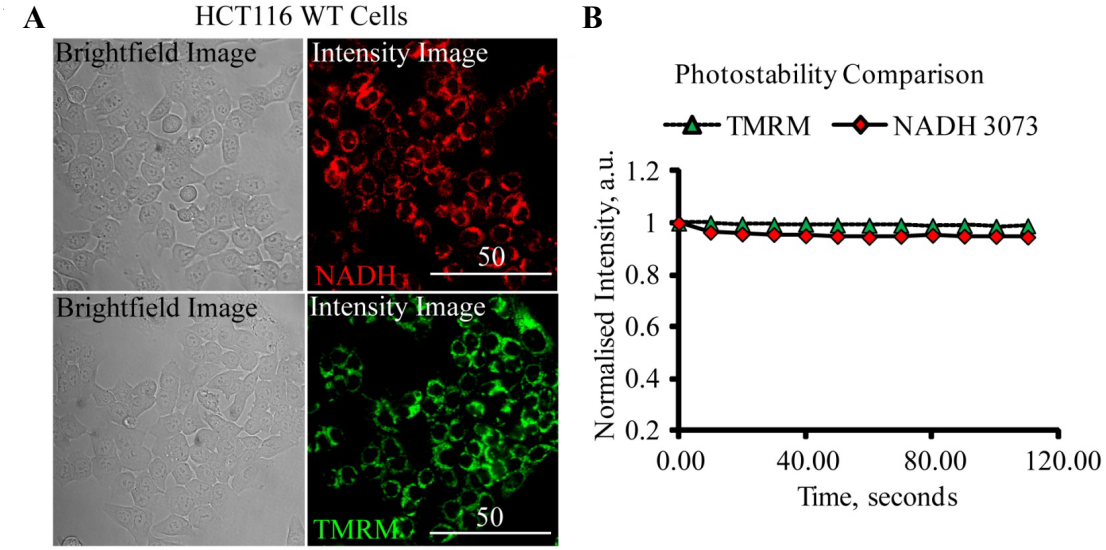

Figure 3.20 Evaluation of photostability of **2ACy-2**. **A** — Images showing bright-field cell images and corresponding NADH indicator **2ACy-2** (= NADH) staining and TMRM (20 µM) staining respectively. **B** — Corresponding graph showing the photo-stability of **2ACy-2** (= NADH 3073). Intensity values normalised over two minutes of constant stimulation at 300 ms.

Comparison of intracellular localisation between **2ACy-2** and TMRM showed a very similar pattern. Using co-staining with MitoTracker Green,[50] we found strong co-localisation of **2ACy-2** with this dye. In contrast, neither Hoechst 33342[51] nor Cholera Toxin (endocytosis) showed co-localisation with **2ACy-2** (**Figure 3.21**). However, in some SCO2 –/– cells we also saw diffuse cytoplasmic staining. This can be explained by increased levels of NADH in these cells and degradation of **2ACy-2**.

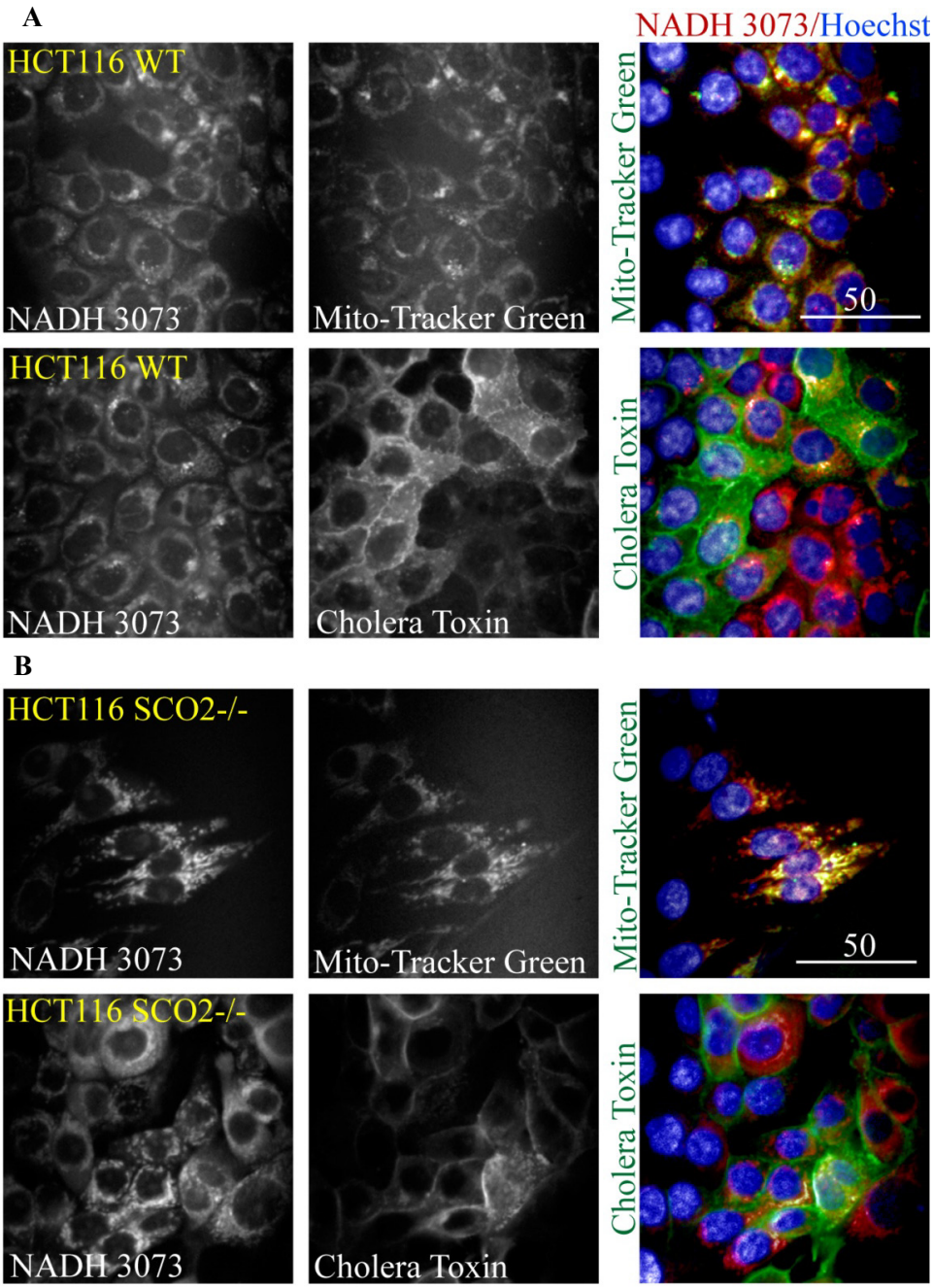

Figure 3.21 Intracellular localisation of **2ACy-2** (= NADH 3073) in HCT116 cells revealed by confocal fluorescence microscopy. HCT116 WT (**A**) and SCO2 –/– (**B**) cells stained with **2ACy-2** (= NADH 3073) and counter-stained with Mito-Tracker Green (20 µM) and Cholera Toxin-Alexa 488 conjugate[52-53] (0.5 µg/ml) respectively. Fluorescence intensity images show staining compared to Hoechst 33342 (HXT 33342). Scale bar unit is µM.

Cell Stimulation

We also looked at the ability of **2ACy-2** indicator to respond to dynamic changes of NADH in the cell. To do this, we stimulated stained cells with Antimycin A (inhibitor of complex III of mitochondrial electron transport chain), which is expected to increase NADH. However fluorescence intensity values showed varying effects with no consistent pattern. Instead, indicator **2ACy-2** was seen to change its localisation with intensities either increasing or decreasing depending on the region of interest (**Figure 3.22**). We also looked at the fluorescence lifetime of the converted (NADH-reacted) form of the **2ACy-2** indicator. In this case, we saw slight positive changes in the fluorescence lifetime (**Figure 3.22**). Overall, we found **2ACy-2** unsuitable for monitoring dynamic changes of NADH in the cell.

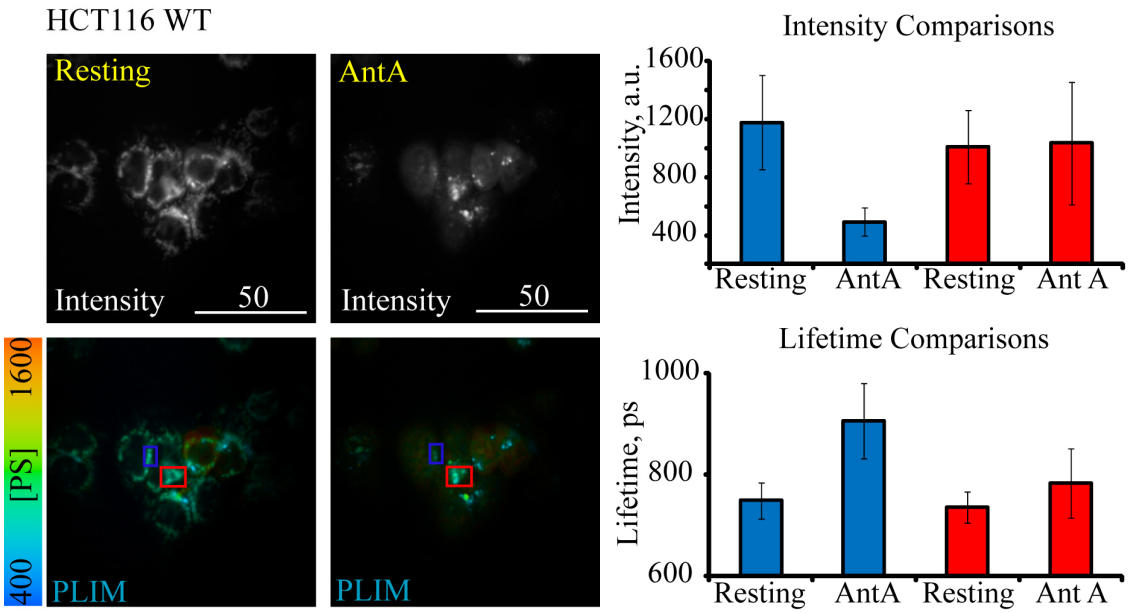

Figure 3.22 Response of **2ACy-2** in fluorescence intensity and lifetime to stimulation of mitochondrial NADH production with Antimycin A (10 μM). Graphs indicate the Intensity and Lifetime value changes of resting *vs* Antimycin A addition for the corresponding ROI (either blue region or red). Scale bar is in μm.

Evaluation of NADH levels in 3D spheroid culture model

We first optimised the spheroid staining method with HCT116 cells. Indicator **2ACy-2** provided the best staining conditions with formed spheroids at six-hour incubation at 20-μM concentration, similarly to monolayer cells. Longer incubation time surprisingly resulted in lower fluorescence intensity values. This can be explained by complete reduction of indicator **2ACy-2** by cellular NADH levels upon long-term incubation. Using these conditions, the staining showed higher intensity values as well as high in-depth penetration, virtually assessing all the cells within the spheroids (**Figure 3.23**).

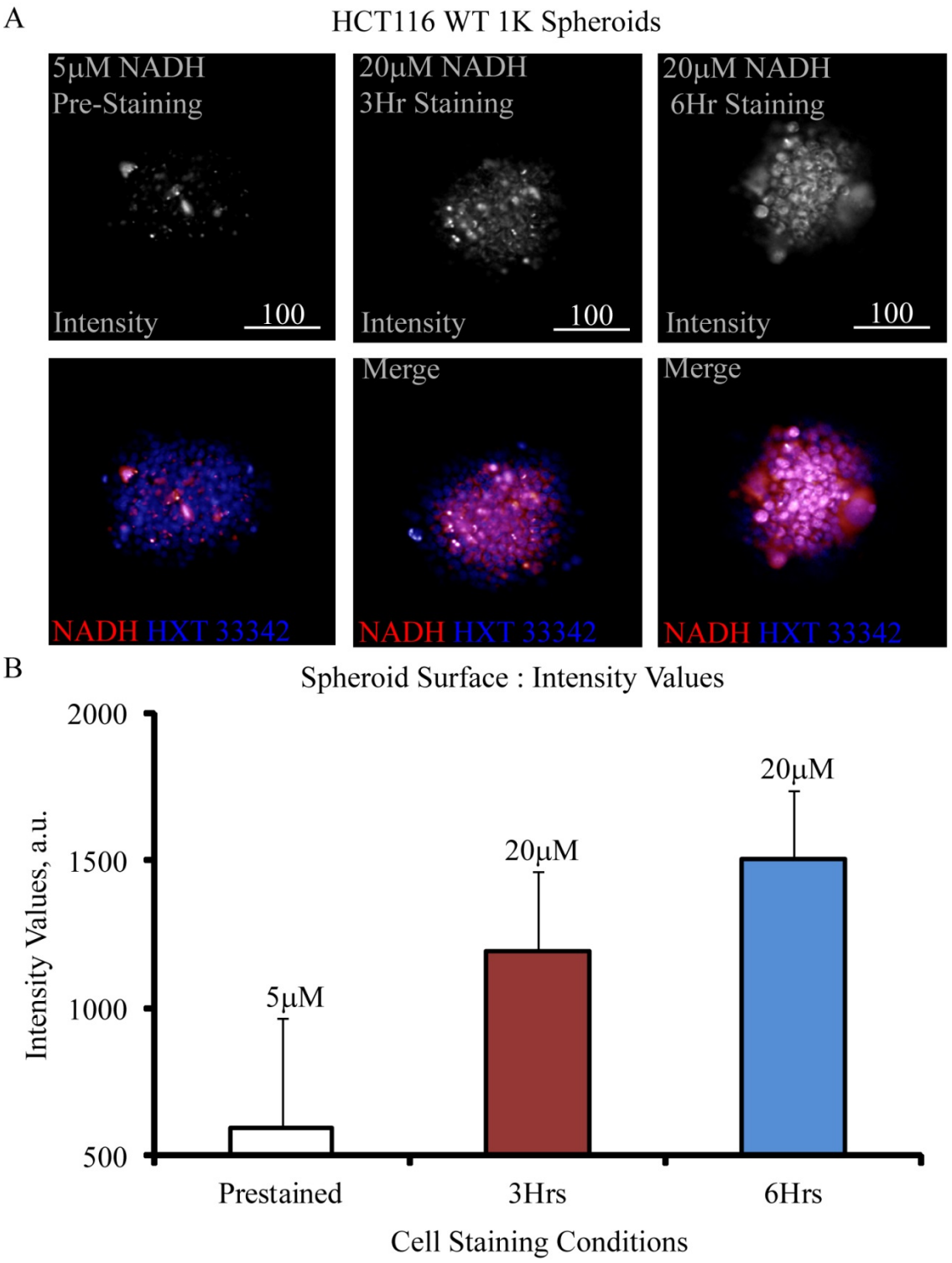

Figure 3.23 Staining of HCT116 spheroids with **2ACy-2** NADH indicator. **A —** Fluorescence intensity images showing staining compared to Hoechst 33342 (HXT 33342). **B —** average graph displaying intensity values measured for varying **2ACy-2** NADH indicator concentrations. Scale bar unit is μM.

Next, we formed spheroids from both HCT116 WT and SCO2 –/– cells, to compare their NADH levels occurring in 3D culture. While similar intensity values were seen on the periphery of both 3D models, intensity of **2ACy-2** NADH-indicator was much lower at the core of WT spheroids. In contrast, SCO2 –/– spheroids showed higher core intensities than those in the WT. We speculate that the lower intensity inside the core of WT spheroids indicates lower NADH concentrations, and not poor indicator penetration. WT spheroids also displayed local NADH gradients while in contrast SCO2 –/– spheroids displayed rather uniform staining throughout, indicating even amounts of NADH (**Figure 3.24**).

These results show that **2ACy-2** can not only be used for live-cell imaging, but also can be used as an indicator for quantitative determination of NADH levels in tumour cells.

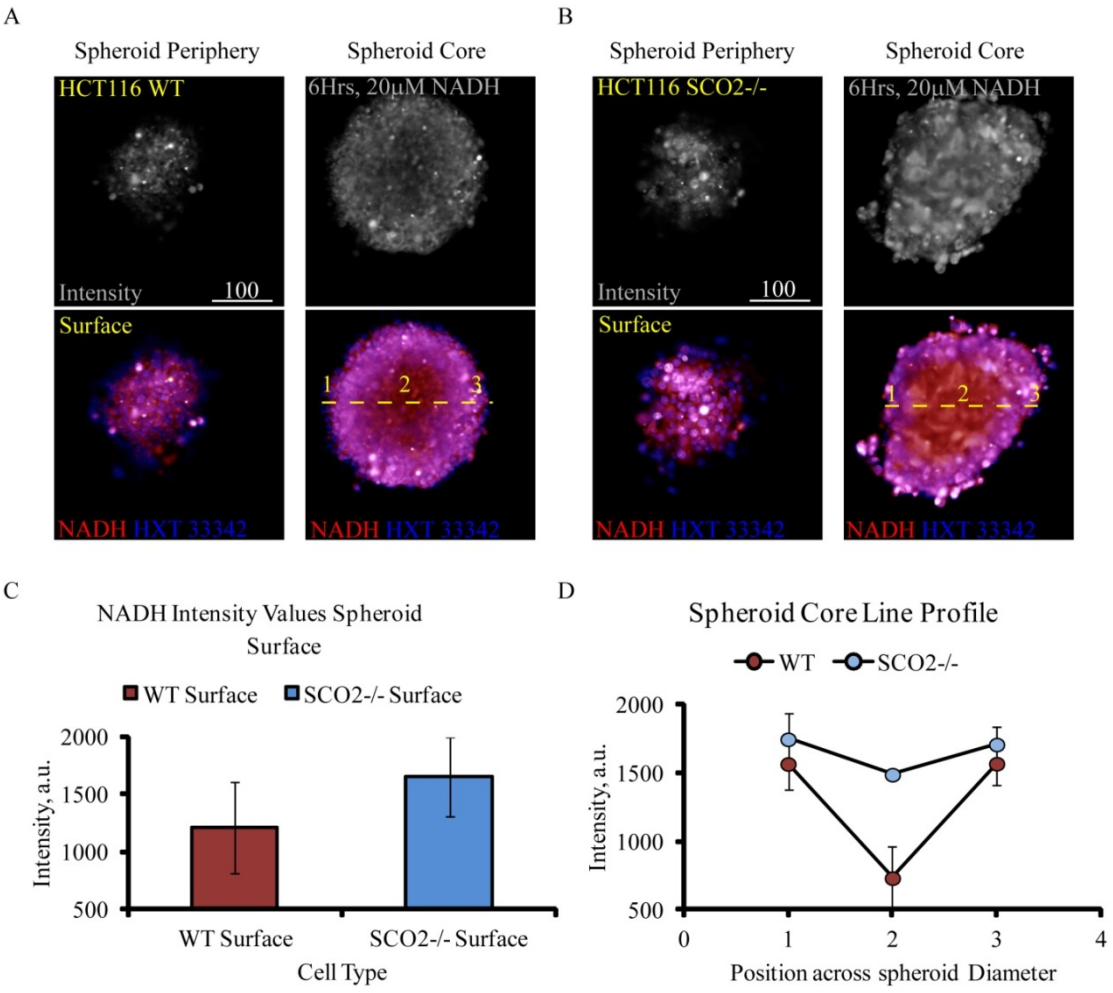

Figure 3.24 Analysis of NADH levels in 3D culture of HC116 cells with **2ACy-2** NADH indicator. Fluorescence intensity images of HCT116 WT (**A**) and SCO2 –/– (**B**) spheroids stained with **2ACy-2** NADH indicator and Hoechst 33342 (nuclei). **C** — Analysis of average intensities on the surface (indicated by 1 and 3 on **A**, **B** panels) of WT and SCO2 –/– spheroids. **D** — Intensity profiles for spheroids at the core (indicated by number 2 on **A**, **B** panels), that is 80 μM in depth from the surface (numbers 1 and 3). Scale bar unit is μM.

3.4 Conclusions

In summary, we designed a novel small molecule NADH indicator (**2ACy-2**) by introduction of an NADH reactive site to the backbone of a tuneable cyanine dye (two-acceptor design). Compound **2ACy-2** has been shown to be a highly sensitive and rapid NADH indicator with intense "turn-on" absorbance in the green range of the visible spectrum and strong on/off emission enhancement (up to 30-fold). We demonstrated its ability to detect NADH at low micromolar levels in aqueous solutions or to follow NAD^+-dependent biocatalyzed transformations. Our studies indicate the ability to use **2ACy-2** for the bio-imaging of NADH in living HEK-293 and HCT116 cells. In particular, **2ACy-2** showed good response to increased amounts of intracellular NADH in a tumour cell model (HCT116 SCO2 –/– compared to WT).

The modular nature of the indicator's design opens the possibility of tailored indicators for specific applications. We believe this approach could be extended to the screening of the specific activity of NAD(P)H-consuming enzymes at the single-cell level and may be suitable for FACS analysis, allowing the highest throughput assays currently possible.

3.5 Experimental part

3.5.1 Materials and methods

Synthesis

Reagents and solvents were purchased at the highest commercial quality from Acros Organics, Alpha-Aesar, Fluka, Sigma-Aldrich or VWR and used without further purification, unless otherwise stated. Solvents were dried according to literature procedures, if necessary.[54]

1,2,3,3-Tetramethyl-*3H*-indolium iodide (**7**), 3-pyridinecarboxaldehyde (**8**), 2,5−difluoroaniline (**21**) were from Sigma-Aldrich (Germany); 3-quinoline-carboxaldehyde (**9**), 5−quinolinecarboxaldehyde (**10**), 6-quinolinecarboxaldehyde (**11**), 4-isoquinolinecarboxaldehyde (**12**) were from ABCR GmbH (Germany); 1-phenazine−carboxaldehyde (**13**) was from Princeton Building Blocks (US); 2-bromo-3-nitrobenzoic acid (**22**) was from Activate Scientific GmbH (Germany).

All aqueous solutions were made up in deionized water with resistivity ≥ 18 MΩ cm^{-1}, obtained using a Millipore purification system (MQ-water).[31]

Yields refer to chromatographically (either HPLC or LC-MS) and spectroscopically (^{1}H NMR) homogeneous material, unless otherwise stated.

Counteranions are omitted for clarity.

Sealed vessel reactions

Sealed vessel reactions were performed in a 15-mL Ace pressure tube (bushing type, front seal, L × ø = 10.2 cm × 25.4 mm) or in microwave reaction vials (20 bar; Type I, Class A, VWR) equipped with 20-mm aluminum seals with installed blue PTFE-faced silicone septa. The heating was performed under conventional conditions in an oil bath.

TLC

Reactions were monitored by thin layer chromatography (TLC) carried out on Merck silica plates 60 F254 and 60 RP-18 F254s, using shortwave UV light as the visualizing agent and a solution of $KMnO_4$ and heat as developing agent. Some TLC plates were pretreated with MeOH solution of KBr (saturated) as described in literature.[55] In each case it is noted as SiO_2 KBr.

Analytical HPLC-MS (ESI-MS)

The purity of the compounds was determined with the help of an HPLC-MS apparatus from Waters (Milford, USA) containing the following components: 2695 Separation module, 2696 photodiode array and Waters Micromass ZQ (ESCI ionization mode) detectors. Data acquisition was carried out by MassLynx (V4.1) software.

Column: YMC-Triart C18 3 µM (4.6 x 150 mm)/Product Nr.TA12S03-1546WT
Flow: 0.7 mL/min.
Phase A: H_2O + 10 mM TEAAc, pH 7.0.
Phase B: MeCN.
Gradient 80: 5-80B (7 min); 80-80B (2 min); 80-5B (0.5 min); 5-5B (2.5 min).
Gradient 100: 5-100B (7 min); 100-100B (2 min); 100-5B (0.5 min); 5-5B (2.5 min).

Ultrapure water and HPLC-grade solvents were used as eluents.

NMR

NMR spectra were recorded on a Bruker AVIII-600, DRX-500 and an Agilent 400-MR instruments and were calibrated using residual nondeuterated solvent as an internal reference.[56] The following abbreviations were used to explain NMR peak multiplicities: s = singlet, d = doublet, t = triplet, q = quartet, m = multiplet, br = broad.

The following abbreviations were used for signal assignment: pyridines = Py, quinolines = Q, isoquinolines = IQ, phenazines = Pz, vinyl bridge = E, indolium = I; further numbering within molecular entities was according to IUPAC.

HRMS

For HRMS (high resolution mass spectra), samples were dissolved in HPLC-grade MeCN and analyzed by direct-flow injection (injection volume = 5 µL) electrospray ionization time-of-flight (ESI-TOF) mass spectrometry on a Waters Q-ToF Premier instrument in the positive ion mode.

Buffers

Piperazine-N,N'-bis(2-ethanesulfonic acid) (PIPES; Sigma-Aldrich) and sodium chloride (Sigma-Aldrich) were used to prepare PIPES buffer solutions (25 mM PIPES; 101 mM NaCl, pH 7.0) at rt.

Phosphate buffers (PB) were prepared by titration of 100 mM KH_2PO_4 (Sigma-Aldrich) with 100 mM K_2HPO_4 (Sigma-Aldrich) solutions and was adjusted to pH 7.0 at rt.

Phosphate-buffered saline (PBS) was prepared containing 138 mM NaCl, 8.1 mM Na_2HPO_4, 2.7 mM KCI, and 1.1 mM KH_2PO_4 (Sigma-Aldrich) and was adjusted to pH 7.4 by adding NaOH or HCI (Sigma-Aldrich) at rt.

pH

Values of pH were determined using a WTW pH 3310 meter with a SenTix81 electrode system. The electrode was calibrated by using standard buffers pH 4.0, 7.0 and 9.0.

Stock solutions

All probes were weighed out in quantities of ≥5 mg, which were then dissolved in MQ-water with the help of ultrasonic to prepare stock solutions. All solutions were freshly prepared directly before making absorption measurements.

Bioassays

β-Nicotinamide adenine dinucleotide, reduced disodium salt hydrate (NADH, Grade I), *β*-nicotinamide adenine dinucleotide hydrate (NAD^+ free acid, Grade I) and modified glucose dehydrogenase lyophilisate (GlucDH2 361 U/mg) were from Roche.

Anhydrous *β*-D-glucose was from Merck KGaA (Darmstadt, Germany).

UV-Vis and fluorescence

Fluorescence spectra were recorded on a Cary Eclipse fluorescence spectrophotometer and absorption spectra on a Cary 50 UV-Vis spectrometer from Varian. All measurements were performed in 1-cm UV-Vis disposable cuvettes (BRAND semi-micro) and air-equilibrated solutions at $25 \pm 0.1\,°C$. A total assay volume of 1000 µL was used for each measurement.

Emission spectra were recorded using following parameters: average time 0.1 s; data interval 1 nm; scan rate 600 nm/min.

UV-Vis scan spectra were recorded using following parameters: average time 0.1 s; data interval 1 nm; scan rate 600 nm/min; with base line correction.

3.5.2 General procedures

General procedure I. Synthesis of indolium salts

A mixture of the respective aldehyde (1 equiv.) and indolium iodide **7** (1 equiv.) in ethanol was refluxed for 2–16 h in the presence of piperidine (0.1–0.4 equiv.) under Ar. The reaction mixture was allowed to cool slowly to rt, and a deposited precipitate was filtered and washed with cold ethanol and ether, dried *in vacuo*.

General procedure II. General procedure for preparation of diquaternary salts

Alkylating agent TfOMe (4–20 equiv.) was added to the respective indolium salt (1 equiv.) in dry DCM at rt under Ar. After the mixture was stirred for 16 h, a deposited precipitate was filtered and washed with DCM and ether, dried *in vacuo*.

Extinction coefficients

An indicator was dissolved in MQ-water (5.0–10.0 mM) and then further diluted to prepare a stock solution of 1.0 mM. In a cuvette, 1000 µL of a buffer and 1–20 µL of the indicator were mixed. Absorbance spectra (240–1000 nm) were measured against a blank of the buffer. Linear regression analysis was used to generate extinction coefficients from the slope of indicator concentration *vs* absorbance plots using MS Excel software (Microsoft).

UV-Vis screening of an indicator with NADH

The following were mixed in a cuvette: 1000 µl of 0.2−2.0 mM solution of an indicator in phosphate buffer (50 mM, pH 7.0) and 2−50 µl of 10−50 mM NADH solution in MQ-water. To establish λ_{max}, absorbance spectra (400−1000 nm) were recorded every 12 s for 30 min after NADH addition. To monitor a kinetic response, an absorbance at λ_{max} was recorded every 0.1 s for 300 s. For the summary of obtained data, see **Table 3-4S**.

*UV-Vis and fluorescence response of **2ACy-2** to NADH excess*

All measurements were in PIPES buffer pH 7.0 (25 mM, 101 mM NaCl) at *25°C*. NADH stock solutions (50.0 mM) were prepared PIPES freshly before the measurements. Stock solution of **2ACy-2** (10.0 mM) was prepared in MQ-water and diluted to 1.0-mM (unused the solutions were stored at 4°*C*). In a 2-mL tube, 990 µL of PIPES and 1–6 µL of **2ACy-2** (1.0 mM) were mixed, followed by addition of NADH (final concentration, 500 µM). After incubation for 5 min in a thermostat, the reaction solution was transferred to a cuvette to measure absorbance (300–700 nm) or fluorescence (545–800 nm; λ_{ex} = 537 nm and both excitation and emission slit widths of 5 nm). In the meantime, a blank solution containing no NADH (control) was prepared and measured under the same conditions for comparison.

*UV-Vis assay procedure of **2ACy-2** for NADH*

All measurements were in PIPES buffer pH 7.0 (25 mM, 101 mM NaCl) at *25°C*. The **2ACy-2** stock solution (10.0 mM) was diluted to 5.0 mM. The NADH stock solutions (10.0, 50.0 mM) were diluted to 50–2000 μM aliquots. To a 1000-μL mixture containing **2ACy-2** (100 μM), 10 μL aliquots of NADH were added to yield final concentrations of 0.3–20.0 μM. The resulting solutions were mixed well with a disposable cuvette stirring rod. After the solution was incubated for 5 min, the absorbance (400–700 nm) was measured. The absorbance of **2ACy-2** (100 μM) without NADH was measured by 13 times and the standard deviation of blank was determined.

*Fluorescence assay procedure of **2ACy-2** for NADH*

All measurements were in PIPES buffer pH 7.0 (25 mM, 101 mM NaCl) at *25°C*. The **2ACy-2** stock solution (10.0 mM) was diluted to 1.0 mM. The NADH stock solutions (10.0 mM) were diluted to 50–500 μM aliquots. To a 1000-μL mixture containing **2ACy-2** (20.0 μM), 10 μL aliquots of NADH were added to yield final concentrations of 0.5–5.0 μM. The resulting solutions were mixed well with a disposable cuvette stirring rod. After the solution was incubated for 30 min, the fluorescence emission (545–800 nm) was measured, against a blank prepared in the same manner without NADH addition. λ_{ex} = 537 nm, slit widths: 5/5 nm.

*Kinetics studies of **2ACy-2** with NADH*

Reaction rates were studied in the presence of limiting concentrations of NADH (5 μM) and 10- to 50-fold excesses of **2ACy-2**. The following were mixed in a cuvette: 5–25 μL of 10.0 mM stock solution of **2ACy-2** in MQ-water, 1000 μL of PIPES buffer (25 mM, 101 mM NaCl, pH 7.0) and 5 μL of 1.0-mM NADH solution in buffer. Kinetic data were obtained by following the increase in absorbance at 536 nm as the reduced product was formed. The absorbance data were recorded every 0.1 s for 300 s after addition of NADH. A pseudo-first-order rate constant (k_{obs}) was calculated from the initial 30 s of the reaction, from slope of the plots of $ln(A_\infty - A_t)$ *vs.* time using MS Excel software. Under these conditions, all reactions proved to be kinetically first order in the reductant concentration within initial 30 s of the reaction. Pseudo-first-order rate constants were evaluated, and found to be proportional to **2ACy-2** concentration (**Figure 3.27S**). This allowed the evaluation of the second-order rate constant (k_2) for the oxidation of NADH in the presence of **2ACy 2**.

Selectivity studies

The experiments were performed analogously to *UV-Vis and fluorescence response of* ***2ACy-2*** *to NADH excess.* Stock solutions (20.0 mM) of analytes, including ascorbic acid (AA), amino acids (Asn, Lys), thiols (Cys, GSH) and NADH, were prepared in buffer (25 mM PIPES, 101 mM NaCl, pH 7.0).

Reaction of ***2ACy-2*** *with glucose/GlucDH2*

Glucose solution (1.1 M): 2 g of *β*-D-glucose was dissolved in 10 mL MQ water. The solution was ready-to-use after a standing time of 2 h at rt and adjustment of the mutarotation equilibrium. NAD^+ buffer solution (30.1 mM): 20.0 mg NAD^+ free acid was dissolved in 1.0 mL buffer solution. In order to prepare for the measurement, 10.0 mg of the GlucDH2 (361 U/mg) was dissolved in 1.0 mL of NAD^+ buffer solution and kept for 60 min at rt, in order to allow a reconstitution. Subsequently it was diluted with buffer to 491 U/mL.

The following were mixed in a cuvette: 500 µL of 0.2 mM solution of **2ACy-2** in 100 mM phosphate buffer pH 7.0, 500 µL of GlucDH2 solution (in 100 mM phosphate buffer pH 7.0 containing 4.0 mM NAD^+) at a concentration of 491 U/mL, 0.1–20.0 µL of 10.0 mM solution of glucose in MQ water. The assay was initiated by the addition of glucose and incubated for 5 min. A UV-Vis spectrum was recorded as mentioned in descriptions under the figures.

Fluorescence microscope experiment

These experiments were only possible with the help of Oliver Tonn, Claudio Sustmann and Konrad Honold (Roche, Penzberg).

HEK-293 cells were cultured in DMEM (Dulbecco Modified Eagle Medium) in an atmosphere of 5% CO_2 and 20% O_2 at 37°*C*. Staining with **2ACy-2** (20 µM) ranged between 0.5–24 h. As a control group, HEK-293 cells were pre-treated with 4% paraformaldehyde (Invitrogen GAS001 Fix & Perm Medium A). Before analysis, cells were washed with PBS buffer three times. Fluorescent images were acquired using a confocal laser scanning microscope Digital Eclipse TE 2000-E (Nikon GmbH Düsseldorf, Germany) with Nikon D-Eclipse C1si spectral detector and Nikon D-Eclipse C1 LSM, 4 laser system; and were analyzed using the confocal microscope Digital Eclipse C1 control software EZ-C1 (version 3.80). The excitation wavelength for imaging with NADH-indicator **2ACy-2** were 488 and 561 nm, and emission was selected and recorded using a 580 to 610 nm band-pass filter.

3.5.3 Imaging of intracellular metabolic pathways by a "turn-on" fluorescent NADH indicator

These experiments were only possible with the help of Ruslan Dmitriev and Dmitri Papkovsky (University College Cork)

Materials

NADH-indicator **2ACy-2** was dissolved in deionised water before use. Cholera toxin, subunit B-Alexa Fluor 488 conjugate, Mitotracker Green and Tetramethylrhodamine methyl ester (TMRM) were from Invitrogen. CellTox Green assay kit from Promega (MyBio Ireland). Lipidure 96-well plate (Lipidure-coat, Amsbio, UK). DAPI, Hoechst 33342, Antymycin A and all the other reagents from Sigma-Aldrich (Dublin, Ireland).

Optimisation of cell staining

Human colon carcinoma HCT116 cells (ATCC) were grown in McCoy 5A medium, supplemented with 10% fetal bovine serum, penicillin-streptomycin and HEPES buffer (10 mM, pH 7.0), as described before.[25] 8-well chambers (Ibidi, Germany) were pre-coated with Collagen IV/ poly-D-lysine as described before.[57] Cells were seeded at a density of 50.000 per well day before staining. Staining with NADH-indicator **2ACy-2** ranged from between 0.5–16 h at 10–20 μM concentrations. Before analysis, cells were washed in growth medium.

Generation of tumour spheroids

HCT116 spheroids were produced by addition of 1.000 HCT116 cells in 200 μl growth medium per well of Lipidure plate and incubation for 3 d, as described previously.[58] For pre-staining **2ACy-2** (5 μM) was mixed with the cells, prior to spheroid formation. For staining of formed spheroids cells were treated with **2ACy-2** (20 μM) for 3–6 h. To visualise nuclei, Hoechst 33342 (1 μM) was added 30 minutes prior to imaging. Before imaging, spheroids were allowed to attach on MatTek glass bottomed dishes pre-coated with Collagen IV-poly-D-lysine.

Assessment of toxicity

Cell viability was assessed by analyzing the membrane integrity (CellTox Green assay, Promega) and number of viable (stained with Hoechst) cells, in comparison with control samples (unstained cells). Cells were stained with Hoechst 33342 (1 μM, blue) and CellTox Green (0.1%, green) for 30 min, washed with fresh media and imaged on the wide-field fluorescence microscope.[59]

Fluorescence microscopy

NADH-indicator **2ACy-2** staining optimisation, toxicity testing and photo-bleaching experiments were performed on a wide-field inverted fluorescence microscope Axiovert 200 (Carl Zeiss) equipped with and oil-immersion objective 40×/1.3 EC Plan Neofluar, 590 nm LED excitation module, time-gated CCD camera and TXRED-4040 (Semrock, UK) emission filter 605-645 nm, ImSpector software (LaVision BioTec, Germany).[59] For the intensity imaging the following parameters were used: exposure time — 300 ms, devices — none, DC mode — ON, no binning. Photo-bleaching experiments were performed in DC mode with the following settings: exposure time — 300 ms, devices — time-time, numbers of steps — 12, wait time — 10 s.

Confocal fluorescence microscopy imaging, indicator localisation and PLIM were carried out on a system based on an upright fluorescent microscope Axio Examiner Z1 (Carl Zeiss) with 63×/1.0 W-Plan-Apochromat objective, heated stage (37°*C*) with motorized Z-axis control, DCS-120 confocal scanner (Becker & Hickl GmbH), R10467U-40 photon counting detector (Hamamatsu Photonics K.K.) and TCSPC hardware (Becker & Hickl GmbH).[60] NADH-indicator **2ACy-2** was excited with tunable picosecond supercontinuum laser SC400-4 (Fianium, UK). NADH-indicator **2ACy-2** was excited at 540 nm and collected with 565-605 nm bandpass filter, and fluorescence lifetimes were calculated by double-exponential fitting of decay curves in SPCImage software (Becker & Hickl GmbH) using the following settings: Shift: 0, Binning: 0, Threshold 10, T1: 120-140, T2: 230-250. Cholera Toxin and MitoTracker Green were excited at 488 nm with emission collected at 512–536 nm.

For consistency, the experiments were performed in triplicate.

3.5.4 Preparation of the indolium salts

*1,3,3-Trimethyl-2-((*E*)-2-pyridin-3-yl-vinyl)-*3H*-indolium iodide (**14**)*

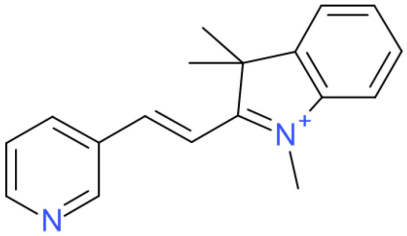

Compound **14** (637 mg, 1.63 mmol) was obtained following the general procedure I, from aldehyde **8** (200 µL, 2.13 mmol), indolium salt **7** (641 mg, 2.13 mmol) and piperidine (21 µL, 0.21 mmol) in ethanol (20 mL) refluxed for 8 h under Ar.

MF: $C_{18}H_{19}N_2$-I.

FW: 390.26.

Yield: 77%.

Physical State: orange needles.

R_f: 0.7 (RP-18 SiO_2; MeCN/H_2O/TFA – 80:20:0.1).

^{1}H NMR (DMSO-d_6, 400MHz): δ = 9.30 (d, J = 1.8 Hz, 1 H, Py-C^{2}H), 8.75 (dd, J = 4.8, 1.8 Hz, 1 H, Py-C^{6}H), 8.65 (dt, J = 8.1, 1.8 Hz, 1 H, Py-C^{4}H), 8.44 (d, J = 16.7 Hz, 1 H, E-CH), 7.92–7.98 (m, J = 6.1, 3.0 Hz, 1 H, I-CH), 7.87–7.93 (m, J = 5.8, 2.8 Hz, 1 H, I-CH), 7.82 (d, J = 16.7 Hz, 1 H, E-CH), 7.66 (dd, J = 5.8, 3.3 Hz, 2 H, I-CH), 7.63 (dd, J = 8.1, 4.8 Hz, 1 H, Py-C^{5}H), 4.19 (s, 3 H, I-N^1Me), 1.81 (s, 6 H, I-C^{3}Me$_2$) ppm.

^{13}C NMR (DMSO-d_6, 101MHz): δ = 181.8, 152.9, 151.6, 149.3, 143.8, 141.8, 136.1, 130.3, 129.8, 129.1, 124.2, 122.9, 115.6, 115.0, 52.5, 34.9, 25.0 (2C) ppm.

LC-MS (gradient 80) m/z 263.1 ([M − I]$^+$).

HRMS m/z 263.1561 ([M − I]$^+$) calculated for C18H19N2+: 263.1548 (Δ 4.9 ppm).

*1,3,3-Trimethyl-2-((*E*)-2-quinolin-3-yl-vinyl)-*3H*-indolium iodide (**15**)*

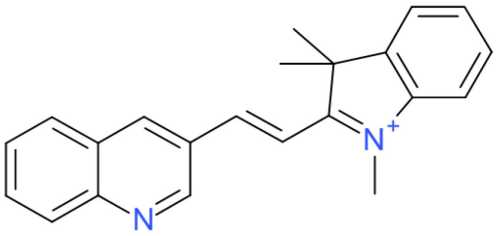

Compound **15** (400 mg, 0.91 mmol) was obtained following the general procedure I, from aldehyde **9** (200 mg, 1.25 mmol), indolium salt **7** (384 mg, 1.25 mmol) and piperidine (12 µL, 0.12 mmol) in ethanol (10 mL) refluxed for 2 h under Ar.

MF: $C_{22}H_{21}N_2$-I.

FW: 440.33.

Yield: 72%.

Physical State: red-orange powder.

^{1}H NMR (DMSO-d_6, 400MHz): δ = 9.66 (d, J = 1.8 Hz, 1 H, Q-CH), 9.23 (d, J = 1.8 Hz, 1 H, Q-CH), 8.62 (d, J = 16.7 Hz, 1 H, E-CH), 8.13 (dd, J = 8.3, 1.3 Hz, 1 H, Q-CH), 8.11 (dd, J = 8.1, 1.0 Hz, 1 H, Q-CH), 7.99 (d, J = 16.7 Hz, 1 H, E-CH), 7.86–7.99 (m, 1 H, I-CH), 7.86–7.99 (m, 1 H, I-CH), 7.93 (ddd, J = 8.3, 6.8, 1.3 Hz, 1 H, Q-CH), 7.76 (ddd, J = 8.1, 6.8, 1.0 Hz, 1 H, Q-CH), 7.63–7.70 (m, 2 H, I-CH), 4.25 (s, 3 H, I-N^1Me), 1.86 (s, 6 H, I-C^3Me_2) ppm.

^{13}C NMR (DMSO-d_6, 101MHz): δ = 181.7, 150.6, 149.5, 148.7, 143.8, 141.8, 138.5, 132.2, 129.8, 129.3, 129.1, 129.0, 127.9, 127.7, 127.1, 122.9, 115.5, 114.8, 52.4, 34.9, 25.1 (2C) ppm.

LC-MS (gradient 80) m/z 313.17 ($[M - I]^+$).

HRMS m/z 313.1720 ($[M - I]^+$) calculated for C22H21N2+: 313.1705 (Δ 4.8 ppm).

*1,3,3-Trimethyl-2-((*E*)-2-quinolin-5-yl-vinyl)-*3H*-indolium iodide (**16**)*

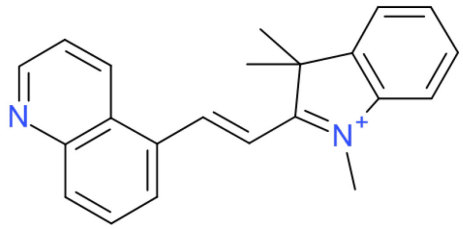

Compound **16** (450 mg, 1.02 mmol) was obtained following the general procedure I, from aldehyde **10** (200 mg, 1.27 mmol), indolium salt **7** (382 mg, 1.27 mmol) and piperidine (13 μL, 13 mmol) in ethanol (10 mL) refluxed for 3 h under Ar.

MF: $C_{22}H_{21}N_2$-I.

FW: 440.32.

Yield: 80%.

Physical State: orange powder.

R_f: 0.4 (NP SiO_2 KBr; $CHCl_3$/MeOH 9:1).

^{1}H NMR (DMSO-d_6, 400MHz): δ = 9.06 (dd, J = 4.0, 1.5 Hz, 1 H, Q-C^{2}H), 8.98 (d, J = 16.4 Hz, 1 H, E-CH), 8.89 (dd, J = 8.6, 1.5 Hz, 1 H, Q-C^{4}H), 8.56 (d, J = 7.3 Hz, 1 H, Q-C^{6}H), 8.30 (d, J = 8.3 Hz, 1 H, Q-C^{8}H), 7.96–8.03 (m, 1 H, I-CH), 8.00 (dd, J = 8.3, 7.3 Hz, 1 H, Q-C^{7}H), 7.92–7.96 (m, 1 H, I-CH), 7.84 (d, J = 16.4 Hz, 1 H, E-CH), 7.76 (dd, J = 8.6, 4.0 Hz, 1 H, Q-C^{3}H), 7.68 (dd, J = 5.8, 3.0 Hz, 2 H, I-CH), 4.24 (s, 3 H, I-N^1Me), 1.88 (s, 6 H, I-C^{3}Me$_2$) ppm.

^{13}C NMR (DMSO-d_6, 101MHz): δ = 182.0, 151.4, 147.7, 147.1, 143.7, 141.9, 133.9, 132.4, 132.0, 129.9, 129.4, 129.2, 127.7, 126.5, 123.1, 122.7, 116.6, 115.7, 52.6, 35.1, 25.2 (2C) ppm.

LC-MS (gradient 80) m/z 313.1 ([M − I]$^+$).

HRMS m/z 313.1710 ([M − I]$^+$) calculated for C22H21N2+: 313.1705 (Δ 1.6 ppm).

*1,3,3-Trimethyl-2-((*E*)-2-quinolin-6-yl-vinyl)-*3H*-indolium iodide (**17**)*

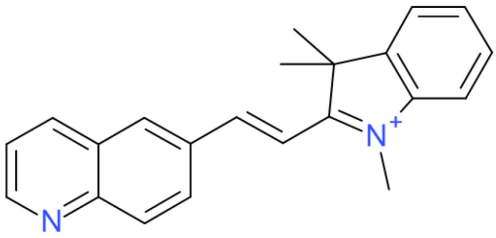

Compound **17** (436 mg, 0.99 mmol) was obtained following the general procedure I, from aldehyde **11** (200 mg, 1.23 mmol), indolium salt **7** (381 mg, 1.24 mmol) and piperidine (12 µL, 0.12 mmol) in ethanol (10 mL) refluxed for 16 h under Ar.

MF: $C_{22}H_{21}N_2$-I.

FW: 440.32.

Yield: 80%.

Physical State: orange powder.

R_f: 0.3 (NP SiO_2 KBr; DCM/MeOH 9:1).

^{1}H NMR (DMSO-d_6, 600MHz, HSQC): δ = 9.04 (dd, J = 4.1, 1.7 Hz, 1 H, Q-C^{2}H), 8.83 (d, J = 1.8 Hz, 1 H, Q-C^{5}H), 8.63 (dd, J = 8.9, 1.8 Hz, 1 H, Q-C^{7}H), 8.62 (d, J = 16.4 Hz, 1 H, E-C$^{\beta}$H), 8.48 (dd, J = 8.3, 1.7 Hz, 1 H, Q-C^{4}H), 8.17 (d, J = 8.9 Hz, 1 H, Q-C^{8}H), 7.94–7.97 (m, 1 H, I-CH), 7.90–7.93 (m, 1 H, I-CH), 7.87 (d, J = 16.4 Hz, 1 H, E-C$^{\alpha}$H), 7.68 (dd, J = 8.3, 4.1 Hz, 1 H, Q-C^{3}H), 7.64–7.70 (m, 2 H, I-CH), 4.23 (s, 3 H, I-N^1Me), 1.85 (s, 6 H, I-C^{3}Me$_2$) ppm.

^{13}C NMR (DMSO-d_6, 151MHz, HSQC): δ = 181.7 (C$_q$, I-C^2), 152.8 (Q-C^{2}H), 151.6 (E-C$^{\beta}$H), 149.3 (C$_q$), 143.6 (C$_q$), 141.7 (C$_q$), 137.1 (Q-C^{4}H), 133.6 (Q-C^{5}H), 132.5 (C$_q$), 129.8 (Q-C^{6}H), 129.5 (Q-C^{7}H), 128.9 (C$_q$), 127.9 (I-C^{6}H), 127.7 (I-C^{5}H), 122.8 (I-C^{4}H), 122.6 (Q-C^{3}H), 115.3 (I-C^{7}H), 114.3 (E-C$^{\alpha}$H), 52.3 (I-C^{3}H), 34.7 (I-N^1Me), 25.1 (2C, I-C^{3}Me$_2$) ppm.

HRMS *m*/*z* 313.1699 ([M − I]$^+$) calculated for C22H21N2+: 313.1705 (Δ 1.9 ppm).

*2-((*E*)-2-isoquinolin-4-yl-vinyl)-1,3,3-Trimethyl-*3H*-indolium iodide (**18**)*

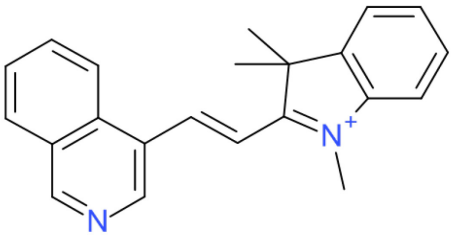

Compound **18** (438 mg, 1.00 mmol) was obtained following the general procedure I, from aldehyde **12** (200 mg, 1.27 mmol), indolium salt **7** (382 mg, 1.27 mmol) and piperidine (13 µL, 0.13 mmol) in ethanol (10 mL) refluxed for 3 h under Ar.

MF: $C_{22}H_{21}N_2$-I.

FW: 440.32.

Yield: 79%.

Physical State: orange powder.

R_f: 0.6 (RP18 SiO_2; MeCN/H_2O/TFA 80:20:0.1).

^{1}H NMR (DMSO-d_6, 400MHz): δ = 9.53 (s, 1 H, IQ-CH), 9.34 (s, 1 H, IQ-CH), 8.94 (d, J = 16.4 Hz, 1 H, E-CH), 8.44 (d, J = 8.3 Hz, 1 H, IQ-CH), 8.31 (d, J = 8.1 Hz, 1 H, IQ-CH), 8.03 (ddd, J = 8.3, 7.1, 1.3 Hz, 1 H, IQ-CH), 7.96–8.00 (m, 1 H, I-CH), 7.92–7.96 (m, 1 H, I-CH), 7.90 (d, J = 16.4 Hz, 1 H, E-CH), 7.86 (dd, J = 8.1, 7.1 Hz, 1 H, IQ-CH), 7.64–7.73 (m, 2 H, I-CH), 4.25 (s, 3 H, I-N^1Me), 1.88 (s, 6 H, I-C^3Me_2) ppm.

^{13}C NMR (DMSO-d_6, 101MHz): δ = 182.0, 156.0, 146.3, 143.7, 143.5, 141.9, 132.9, 132.4, 129.9, 129.1, 128.8, 128.5, 127.7, 125.5, 123.0, 122.9, 116.9, 115.7, 52.7, 35.1, 25.2 (2C) ppm.

LC-MS (gradient 80) *m*/*z* 313.2 ([M − I]$^+$).

HRMS *m*/*z* 313.1706 ([M − I]$^+$) calculated for C22H21N2+: 313.1705 (Δ 0.3 ppm).

*1,3,3-Trimethyl-2-((*E*)-2-phenazin-1-yl-vinyl)*-3H-*indolium iodide* (***19***)

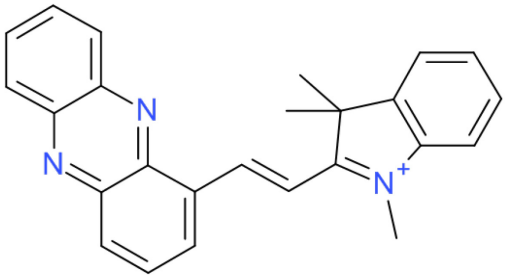

Compound **19** (810 mg, 1.65 mmol) was obtained following the general procedure I, from aldehyde **13** (400 mg, 1.92 mmol), indolium salt **7** (578 mg, 1.92 mmol) and piperidine (20 µL, 0.20 mmol) in ethanol (20 mL) refluxed for 8 h under Ar.

MF: $C_{25}H_{22}N_3$-I.

FW: 491.38.

Yield: 86%.

Physical State: red powder.

R_f: 0.3 (NP SiO_2 KBr; DCM/MeOH 9:1).

^{1}H NMR (DMSO-d_6, 600MHz, HSQC, HMBC): δ = 9.47 (d, J = 16.6 Hz, 1H, E-C$^{\beta}$H), 8.99 (dd, J = 7.1, 1.1 Hz, 1H, Pz-C^{2}H), 8.54 (dd, J = 8.7, 1.1 Hz, 1H, Pz-C^{4}H), 8.51 (d, J = 16.6 Hz, 1H, E-C$^{\alpha}$H), 8.39-8.44 (m, 1H, Pz-C^{9}H), 8.34-8.37 (m, 1H, Pz-C^{6}H), 8.22 (dd, J = 8.7, 7.1 Hz, 1H, Pz-C^{3}H), 8.07-8.14 (m, 2H, Pz-C^{7}/^{8}H), 8.00-8.05 (m, 1H, I-CH), 7.95-7.99 (m, 1H, I-CH), 7.68-7.73 (m, 2H, I-CH), 4.29 (s, 3H, I-N^1Me), 1.95 (s, 6H, I-C^{3}Me$_2$) ppm.

^{13}C NMR (DMSO-d_6, 151MHz, HSQC, HMBC): δ = 181.9 (C_q, I-C^2), 146.8 (E-C$^{\beta}$H), 143.5 (C_q), 143.1 (C_q), 142.7 (C_q), 142.1 (C_q), 141.8 (C_q), 140.8 (C_q), 134.1 (Pz-C^{4}H), 133.3 (Pz-C^{2}H), 132.2 (C_q), 131.9 (Pz-C^{7}/^{8}H), 130.7 (Pz-C^{3}H), 129.7 , 129.6, 129.3, 129.0 (Pz-C^{6}/^{9}H and I-C^{5}/^{6}H), 122.9 (I-C^{4}H), 116.2 (E-C$^{\alpha}$H), 115.5 (I-C^{7}H), 52.3 (C_q, I-C^3), 34.8 (I-N^1Me), 25.6 (I-C^{3}Me$_2$) ppm.

HRMS (pos. ESI) m/z 364.1807 ([M − I]$^+$) calculated for C25H22N3+: 364.1808 (Δ −0.3 ppm).

3.5.5 Preparation of the diquaternary salts

*1-Methyl-3-[(*E*)-2-(1,3,3-trimethyl-*3H*-indolium-2-yl)ethenyl]pyridinium iodide trifluoromethanesulfonate (**2ACy-1**)*

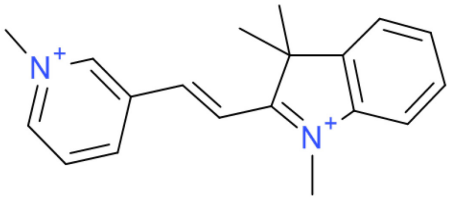

Compound **2ACy-1** (272 mg, 0.49 mmol) was obtained following the general procedure II, from a solution of indolium iodide **14** (200 mg, 0.51 mmol) in dry DCM (25 mL) and TfOMe (290 µL, 2.56 mmol) under Ar.

MF: $C_{19}H_{22}N_2(CF_3O_3S;I)$.

FW: 554.36.

Yield: 96%.

Physical State: yellow powder.

R_f: 0.5 (RP-18 SiO_2; MeCN/H_2O/TFA – 80:20:0.1).

UV-Vis (water) λ_{max} (ε $mM^{-1}cm^{-1}$) 363 (18.3), 290 (10.7), 257 (6.2) nm.

UV-Vis (50 mM PB pH 7.0) λ_{max} (ε $mM^{-1}cm^{-1}$) 363 (11.7), 291 (9.2), 251 (10.7) nm; after NADH addition, λ_{max} 546, 534sh. nm.

^{1}H NMR (DMSO-d_6, 400MHz): δ = 9.63 (s, 1 H, Py-C^{2}H), 9.26 (d, J = 8.3 Hz, 1 H, Py-C^{4}H), 9.09 (d, J = 6.1 Hz, 1 H, Py-C^{6}H), 8.41 (d, J = 16.7 Hz, 1 H, E-C$^{\beta}$H), 8.32 (dd, J = 8.3, 6.1 Hz, 1 H, Py-C^{5}H), 8.00–8.04 (m, 1 H, I-CH), 7.97 (d, J = 16.7 Hz, 1 H, E-C$^{\alpha}$H), 7.90–7.94 (m, 1 H, I-CH), 7.67–7.75 (m, 2 H, I-CH), 4.42 (s, 3 H, Py-N^1Me), 4.23 (s, 3 H, I-N^1Me), 1.81 (s, 6 H, I-C^{3}Me$_2$) ppm.

^{13}C NMR (DMSO-d_6, 101MHz): δ = 181.3, 146.9, 146.7, 144.1, 143.7, 143.4, 141.8, 133.9, 130.5, 129.3, 127.8, 123.0, 120.7 (q, J = 322 Hz, TfO), 118.6, 116.1, 52.8, 48.4, 35.4, 24.5 (2C) ppm.

LC-MS (gradient 80) m/z 277.1 ([M − H − TfO − I]$^+$), 295.2 ([M + OH – TfO – I]$^+$).

HRMS m/z 278.1795 ([M − TfO − I]$^+$) calculated for C19H22N2+: 278.1783 (Δ 4.3 ppm).

Solubility in water: ≥114 mM.

*1-Methyl-3-[(*E*)-2-(1,3,3-trimethyl-*3H*-indolium-2-yl)ethenyl]quinolinium iodide trifluoromethanesulfonate (**2ACy-2**)*

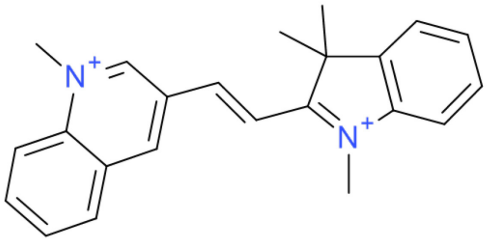

Compound **2ACy-2** (127 mg, 0.21 mmol) was obtained following the general procedure II, from a suspension of indolium iodide **15** (100 mg, 0.23 mmol) in dry DCM (10 mL) and TfOMe (103 µL, 0.91 mmol) under Ar.

MF: $C_{23}H_{24}N_2(CF_3O_3S;I)$.

FW: 604.43.

Yield: 91%.

Physical State: yellow powder.

R_f: 0.5 (RP-18 SiO_2; MeCN/H_2O/TFA – 80:20:0.1).

UV-Vis λ_{max} (ε $mM^{-1}cm^{-1}$) results:
(water) 385 (24.3), 312 (16.0) nm;
(50 mM PB pH 7.0) 512 (0.8), 384 (19.5), 312 (13.5) nm;
(25 mM PIPES, 101 mM NaCl, pH 7.0) 512 (0.4), 384 (19.2), 312 (14.5) nm;
after NADH addition, λ_{max} 537 nm.

^{1}H NMR (DMSO-d_6, 400MHz): δ = 10.16 (s, 1 H, Q-CH), 9.93 (s, 1 H, Q-CH), 8.61 (d, J = 8.6 Hz, 1 H, Q-CH), 8.59 (d, J = 16.7 Hz, 1 H, E-C$^{\beta}$H), 8.50 (d, J = 7.6 Hz, 1 H, Q-CH), 8.41 (ddd, J = 8.6, 7.6, 1.3 Hz, 1 H, Q-CH), 8.17 (dd, J = 7.6, 7.6 Hz, 1 H, Q-CH), 8.05 (d, J = 16.7 Hz, 1 H, E-C$^{\alpha}$H), 8.00–8.03 (m, 1 H, I-CH), 7.92–7.97 (m, 1 H, I-CH), 7.68–7.76 (m, 2 H, I-CH), 4.70 (s, 3 H, Q-N^1Me), 4.26 (s, 3 H, I-N^1Me), 1.85 (s, 6 H, I-C^{3}Me$_2$) ppm.

^{13}C NMR (DMSO-d_6, 101MHz): δ = 181.3, 150.9, 146.4, 144.8, 144.1, 141.9, 138.5, 137.2, 131.4, 131.1, 130.4, 129.3, 128.7, 128.3, 123.1, 120.7 (q, J = 322 Hz, TfO), 119.7, 117.4, 116.0, 52.7, 46.1, 35.3, 24.7 (2C) ppm.

^{1}H NMR (MeCN-d_3, 400MHz, COSY, HSQC, HMBC): δ = 9.73 (d, J = 1.2 Hz, 1H, Q-C^{2}H), 9.65 (d, J = 1.2 Hz, 1H, Q-C^{4}H), 8.49 (dd, J = 8.2, 1.5 Hz, 1H, Q-C^{8}H), 8.44 (dd, J = 9.0, 0.6 Hz, 1H, Q-C^{5}H), 8.38 (d, J = 16.5 Hz, 1H, Q-C$^{\beta}$H), 8.36 (ddd, J = 9.0, 7.0, 1.5 Hz, 1H, Q-C^{6}H), 8.13 (ddd, J = 8.2, 7.0, 0.6 Hz, 1H, Q-C^{7}H), 7.82-7.86 (m, 1H, I-C^{4}H), 7.78-7.82 (m, 1H, I-C^{7}H), 7.81 (d, J = 16.5 Hz, 1H, E-C$^{\alpha}$H), 7.73 (ddd, J = 7.4, 7.3, 1.4 Hz, 1H, I-C^{5}H), 7.70 (ddd, J = 7.6, 7.3, 1.6 Hz, 1H, I-C^{6}H), 4.69 (s, 3H, Q-N^{1}Me), 4.21 (s, 3H, I-N^{1}Me), 1.85 (s, 6H, I-C^{3}Me$_2$) ppm.

^{13}C NMR (MeCN-d_3, 101MHz, COSY, HSQC, HMBC): δ = 183.5 (C$_q$, I-C^{2}), 151.4 (Q-C^{2}H), 148.4 (Q-C^{4}H), 145.9 (E-C$^{\beta}$H), 145.4 (C$_q$, I-C^{3a}), 143.2 (C$_q$, I-C^{7a}), 140.5 (C$_q$, Q-C^{8a}), 139.1 (Q-C^{6}H), 133.1 (Q-C^{5}H), 132.7 (Q-C^{7}H), 132.4 (I-C^{5}H), 131.0 (I-C^{6}H), 130.8 (C$_q$, Q-C^{4a}), 129.6 (C$_q$, Q-C^{3}), 124.4 (I-C^{7}H), 120.9 (q, J = 322 Hz, TfO), 120.5 (Q-C^{8}H), 119.1 (E-C$^{\alpha}$H), 117.2 (I-C^{4}H), 54.7 (C$_q$, I-C^{3}), 47.5 (Q-N^{1}Me), 36.7 (I-N^{1}Me), 25.7 (2C, I-C^{3}Me$_2$) ppm.

LC-MS (gradient 80) m/z 327.2 ([M − H − TfO − I]$^{+}$), 345.1 ([M + OH – TfO – I]$^{+}$).

HRMS m/z 328.1935 ([M − TfO − I]$^{+}$) calculated for C23H24N2+: 328.1939 (Δ −1.2 ppm).

Solubility in water: ≥10 mM.

*1-Methyl-5-[(*E*)-2-(1,3,3-trimethyl-*3H*-indolium-2-yl)ethenyl]quinolinium iodide trifluoromethanesulfonate (**2ACy-3**)*

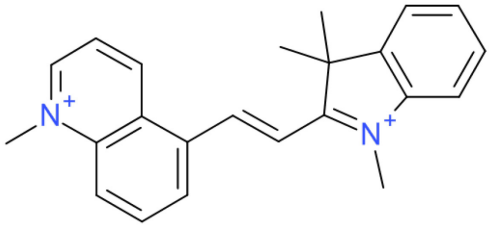

Compound **2ACy-3** (243 mg, 0.40 mmol) was obtained following the general procedure II, from a suspension of indolium iodide **16** (200 mg, 0.45 mmol) in dry DCM (15 mL) and TfOMe (206 µL, 1.82 mmol) under Ar.

MF: $C_{23}H_{24}N_2(CF_3O_3S;I)$.

FW: 604.43.

Yield: 89%.

Physical State: yellow powder.

R_f: 0.5 (RP-18 SiO_2; MeCN/H_2O/TFA – 80:20:0.1).

UV-Vis (water) λ_{max} (ε $mM^{-1}cm^{-1}$) 383 (22.5), 340sh. (13.6), 240 (23.6) nm.

UV-Vis (50 mM PB pH 7.0) λ_{max} (ε $mM^{-1}cm^{-1}$) 383 (22.8), 340 (14.1), 241 (28.0) nm.

^{1}H NMR (DMSO-d_6, 400MHz): δ = 9.63 (d, J = 8.8 Hz, 1 H, Q-C^{4}H), 9.60 (d, J = 5.6 Hz, 1 H, Q-C^{2}H), 9.02 (d, J = 16.2 Hz, 1 H, E-C$^\beta$H), 8.80 (d, J = 7.3 Hz, 1 H, Q-C^{6}H), 8.73 (d, J = 8.8 Hz, 1 H, Q-C^{8}H), 8.45 (dd, J = 8.8, 7.3 Hz, 1 H, Q-C^{7}H), 8.31 (dd, J = 8.8, 5.6 Hz, 1 H, Q-C^{3}H), 8.00–8.07 (m, 1 H, I-CH), 7.93–7.98 (m, 1 H, I-CH), 7.93 (d, J = 16.2 Hz, 1 H, E-C^{2}H), 7.67–7.75 (m, 2 H, I-CH), 4.71 (s, 3 H, Q-N^1Me), 4.27 (s, 3 H, I-N^1Me), 1.89 (s, 6 H, I-C^{3}Me$_2$) ppm.

^{13}C NMR (DMSO-d_6, 101MHz): δ = 182.3, 150.8, 145.0, 143.9, 143.8, 141.9, 138.9, 134.7, 134.1, 130.3, 130.0, 129.3, 127.3, 123.1, 122.6, 119.4, 116.0, 52.9, 46.2, 35.4, 24.8 (2C) ppm.

LC-MS (gradient 80) m/z 327.2 ([M – H – TfO – I]$^+$), 345.1 ([M + OH – TfO – I]$^+$).

HRMS m/z 328.1933 ([M − TfO − I]$^+$) calculated for C23H24N2+: 328.1939 (Δ −1.8 ppm).

Solubility in water: ≥29 mM.

*1-Methyl-6-[(*E*)-2-(1,3,3-trimethyl-*3H*-indolium-2-yl)ethenyl]quinolinium iodide trifluoromethanesulfonate (**2ACy-4**)*

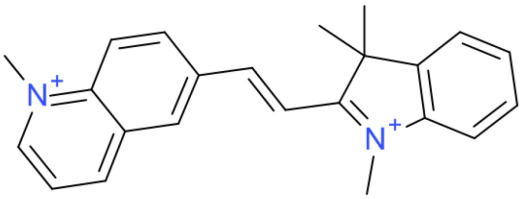

Compound **2ACy-4** (272 mg, 0.45 mmol) was obtained following the general procedure II, from a suspension of indolium iodide **17** (200 mg, 0.45 mmol) in dry DCM (20 mL) and TfOMe (206 µL, 1.82 mmol) under Ar.

MF: $C_{23}H_{24}N_2(CF_3O_3S;I)$.

FW: 604.43.

Yield: 99%.

Physical State: yellow powder.

UV-Vis (50 mM PB pH 7.0) λ_{max} (ε $mM^{-1}cm^{-1}$) 379 (23.2), 318 (15.9) nm; after NADH addition, λ_{max} 517 nm.

^{1}H NMR (DMSO-d_6, 600MHz, COSY, HMBC/HSQC): δ = 9.56 (d, J = 5.7 Hz, 1 H, Q-C^{2}H), 9.26 (d, J = 8.4 Hz, 1 H, Q-C^{4}H), 9.16 (d, J = 1.7 Hz, 1 H, Q-C^{5}H), 9.04 (dd, J = 9.4, 1.7 Hz, 1 H, Q-C^{7}H), 8.68 (d, J = 9.3 Hz, 1 H, Q-C^{8}H), 8.64 (d, J = 16.5 Hz, 1 H, E-C$^{\beta}$H), 8.26 (dd, J = 8.4, 5.7 Hz, 1 H, Q-C^{3}H), 8.01 (d, J = 16.5 Hz, 1 H, E-C$^{\alpha}$H), 7.96–8.01 (m, 1 H, I-CH), 7.92–7.96 (m, 1 H, I-CH), 7.67–7.73 (m, 2 H, I-CH), 4.69 (s, 3 H, Q-N^1Me), 4.27 (s, 3 H, I-N^1Me), 1.85 (s, 6 H, I-C^{3}Me$_2$) ppm.

^{13}C NMR (DMSO-d_6, 101MHz): δ = 182.2, 151.9, 149.3, 148.1, 144.4, 142.3, 140.2, 135.8, 134.3, 133.6, 130.6, 129.7, 129.6, 123.7, 123.4, 120.7, 117.4, 116.3, 53.1, 46.1, 35.6, 25.3 (2C) ppm.

LC-MS (gradient 80) m/z 327.1 ([M – H – TfO – I]$^+$), 345.2 ([M + OH – TfO – I]$^+$).

HRMS (pos. ESI): m/z 164.0946 ([M – TfO – I]$^{2+}$) calculated for C23H24N2++: 164.0969 (Δ −1.4 ppm).

Solubility in water: ≥ 14 mM.

*2-Methyl-4-[(*E*)-2-(1,3,3-trimethyl-*3H*-indolium-2-yl)ethenyl]isoquinolinium iodide trifluoromethanesulfonate (**2ACy-5**)*

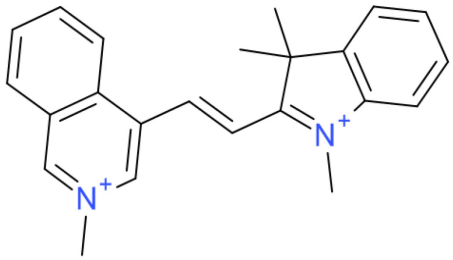

Compound **2ACy-5** (97 mg, 0.16 mmol) was obtained following the general procedure II, from a suspension of indolium iodide **18** (100 mg, 0.23 mmol) in dry DCM (10 mL) and TfOMe (129 µL, 1.14 mmol) under Ar.

MF: $C_{23}H_{24}N_2(CF_3O_3S;I)$.

FW: 604.43.

Yield: 70%.

Physical State: yellow powder.

UV-Vis (water) λ_{max} (ε $mM^{-1}cm^{-1}$) 371 (18.4) nm.

UV-Vis (50 mM PB pH 7.0) λ_{max} (ε $mM^{-1}cm^{-1}$) 514sh. (1.9), 487 (3.7), 372 (12.6), 345 (12.3) nm; after NADH addition, λ_{max} 524sh., 499 nm.

^{1}H NMR (DMSO-d_6, 400MHz, COSY, HMQC): δ = 10.10 (s, 1 H, IQ-H3), 9.35 (s, 1 H, IQ-H1), 8.86 (d, J = 16.4 Hz, 1 H, E-H1), 8.67 (d, J = 8.3 Hz, 1 H, IQ-H8), 8.60 (d, J = 8.3 Hz, 1 H, IQ-H5), 8.42 (dd, J = 8.3, 7.7 Hz, 1 H, IQ-H7), 8.19 (dd, J = 8.3, 7.7 Hz, 1 H, IQ-H6), 8.02–8.08 (m, 1 H, I-H4), 7.95–8.00 (m, 1 H, I-H7), 7.89 (d, J = 16.4 Hz, 1 H, E-H2), 7.69–7.77 (m, 2 H, I-H5,6), 4.56 (s, 3 H, IQ-Me), 4.28 (s, 3 H, I-Me), 1.88 (s, 6 H, I-Me_2) ppm.

^{13}C NMR (DMSO-d_6, 101MHz, HMQC): δ = 181.7 (C_q, I-C^2), 152.3 (IQ-C^3H), 143.9 (C_q), 141.9 (C_q), 141.7 (E-C^{β}H), 137.8 (IQ-C^7H), 135.5 (IQ-C^1H), 134.1 (C_q), 131.7 (IQ-C^6H), 131.3 (IQ-C^5H), 130.6 (I-$C^{5/6}$H), 130.3 (C_q), 129.3 (I-$C^{5/6}$H), 127.2 (C_q), 124.3 (IQ-C^8H), 123.2 (I-C^7H), 120.7 (q, J = 322 Hz, TfO), 120.5 (E-C^{α}H), 116.2 (I-C^4H), 53.1 (C_q, I-C^3), 48.3 (IQ-N^1Me), 35.6 (I-N^1Me), 24.5 (2C, I-C^3Me_2) ppm.

LC-MS (gradient 80) m/z 327.2 ($[M - H - TfO - I]^+$), 345.1 ($[M + OH - TfO - I]^+$).

HRMS m/z 164.0968 ($[M - TfO - I]^{2+}$) calculated for C23H24N2++: 164.0969 (Δ −0.6 ppm).

Solubility in water: ≥ 25 mM.

*5-Methyl-1-[(*E*)-2-(1,3,3-trimethyl-*3H*-indolium-2-yl)ethenyl]phenazinium iodide trifluoromethanesulfonate (**2ACy-6**)*

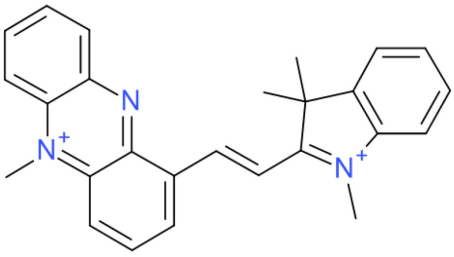

Compound **2ACy-6** (81 mg, 0.12 mmol) was obtained following the general procedure II, from a suspension of indolium iodide **19** (300 mg, 0.61 mmol) in dry DCM (50 mL) and TfOMe (345 µL, 3.05 mmol) under Ar.

MF: $C_{26}H_{25}N_3(CF_3O_3S;I)$. **FW:** 655.47. **Yield:** 20%. **Physical State:** orange powder.

R_f: 0.3 (RP-18 SiO_2; MeCN/H_2O/TFA – 80:20:0.1).

UV-Vis (50 mM PB pH 7.0) λ_{max} (ε $mM^{-1}cm^{-1}$) 481 (6.0), 394 (16.2), 377sh. (15.6), 261 (26.4) nm; after NADH addition, λ_{max} 740 nm.

^{1}H NMR (MeOD-d_3, 500MHz, HMBC, HSQC, TOCSY, NOESY): δ = 9.73 (d, J = 16.7 Hz, 1H, E-C$^{\beta}$H), 9.17 (d, J = 7.3 Hz, 1H, Pz-C^{2}H), 9.06 (d, J = 9.1 Hz, 1H, Pz-C^{4}H), 8.92 (d, J = 9.1 Hz, 1H, Pz-C^{6}H), 8.85 (d, J = 8.5 Hz, 1H, Pz-C^{9}H), 8.68 (dd, J = 9.1, 7.3 Hz, 1H, Pz-C^{3}H), 8.62 (dd, J = 9.1, 6.8 Hz, 1H, Pz-C^{7}H), 8.42 (dd, J = 8.5, 6.8 Hz, 1H, Pz-C^{8}H), 8.31 (d, J = 16.7 Hz, 1H, E-C$^{\alpha}$H), 7.98 (d, J = 7.3 Hz, 1H, I-C^{7}H), 7.90 (d, J = 7.3 Hz, 1H, I-C^{4}H), 7.69-7.79 (m, 2H, I-C^5/^{6}H), 5.14 (s, 3H, Pz-N^1Me), 4.37 (s, 3H, I-N^1Me), 2.03 (s, 6H, I-C^{3}Me$_2$) ppm.

^{13}C NMR (MeOD-d_3, 126MHz, HSQC): δ = 184.3 (C_q, I-C^2), 146.5 (E-C$^{\beta}$H), 145.5 (C_q), 144.7 (C_q), 143.5 (C_q), 142.1 (Pz-C^{7}H), 140.4 (Pz-C^{3}H), 136.5 (C_q), 135.3 (C_q), 135.1 (C_q), 134.6 (Pz-C^{8}H), 133.9 (Pz-C^{9}H), 133.0 (Pz-C^{2}H), 132.2 (I-C^{5}H), 131.0 (I-C^{6}H), 124.3 (I-C^{4}H), 123.6 (Pz-C^{4}H), 120.3 (Pz-C^{6}H), 119.4 (E-C$^{\alpha}$H), 117.0 (I-C^{7}H), 54.8 (C_q), 40.5 (Pz-N^5Me), 35.8 (I-N^1Me), 26.4 (I-C^{3}Me$_2$) ppm.

In case of a sample dissolved in DMSO-d_6, under the same concentration and settings, ^{1}H NMR signals were not observed.

HRMS (pos. ESI): m/z 189.6025 ($[M - TfO - I]^{2+}$) calculated for C26H25N3++: 189.6024 (Δ 0.5 ppm).

HRMS m/z 379.2048 ($[M - TfO - I]^{+}$) calculated for C26H25N3+: 379.2048 (Δ 0.0 ppm).

Solubility in water: ≥ 4 mM.

3.5.6 Preparation of 9-ethoxyphenazine-1-carbaldehyde (**25**)

*Synthesis of 9-ethoxyphenazine-1-carboxylic acid (**23**) as reported previously*[61]

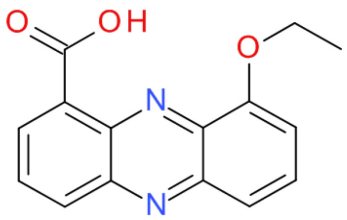

Step 1. A mixture of 2-bromo-3-nitrobenzoic acid **22** (10.00 g, 40.6 mmol), 2,5-difluoroaniline **21** (6.56 g, 50.8 mmol), cuprous chloride (0.35 g), copper powder (0.10 g) and *N*-ethylmorpholine (13.4 mL, 105.7 mmol) in butane-2,3-diol (20 mL) was vigorously stirred at 80°*C* for 8 h. The solution was diluted with 0.1M aqueous ammonia and filtered through celite. The resulting bright orange solution was poured slowly into 2-M HCl to give a precipitate containing *N*-(2,5-difluorophenyl)-3-nitroanthranilic acid, which was collected, washed well with water and dried *in vacuo*, yield: 5.3 g (44%);* **LC-MS** (gradient 80) *m*/*z* 293.0 ($[M-H]^-$), retention time 4.9 min; ^{1}H NMR (DMSO-d_6, 400MHz): δ = 10.11 (s, 1H), 8.22 (d, J = 7.3 Hz, 1H), 8.07 (d, J = 8.1 Hz, 1H), 7.14-7.23 (m, 1H), 7.11 (dd, J = 8.1, 7.3 Hz, 1H), 7.08 (d, J = 7.8 Hz, 1H), 7.06 (d, J = 7.8 Hz, 1H) ppm.

Step 2 To a solution of sodium metal (18.39 g, 800.0 mmol) in ethanol (400 mL) was added *N*-(2,5-difluorophenyl)-3-nitroanthranilic acid (5.00 g, 17.0 mmol) and $NaBH_4$ (6.36 g, 168.2 mmol). The reaction mixture was refluxed for 3 d. The sodium salt of the product precipitated during the reaction. The precipitate was dissolved on adding water (100 mL); and after boiling off the ethanol, the resulting aqueous solution was filtered and slowly acidified with HCl (conc.) to pH 4.5. The resulting precipitate was collected, washed with water and dried *in vacuo*, yield: 3.2 g (70%).*

* — The use of Cu powder (≥ 99%, 61141 Fluka) and $NaBH_4$ purum (≥ 96%, 71320 Sigma-Aldrich, Germany) was essential to achieve the reported yields. The characterization data for compound **23** are in accordance with Brooke *et al.*[62]

MF: 268.27. **FW:** $C_{15}H_{12}N_2O_3$. **Yield:** 31% (for 2 steps). **Physical State:** orange solid.

^{1}H NMR ($CDCl_3$, 400MHz): δ = 16.00 (s, 1H), 8.93 (dd, J = 7.1, 1.5 Hz, 1H), 8.49 (dd, J = 8.7, 1.5 Hz, 1H), 8.04 (dd, J = 8.7, 7.1 Hz, 1H), 7.86 (d, J = 4.1 Hz, 1H), 7.86 (d, J = 4.7 Hz, 1H), 7.17 (dd, J = 4.7, 4.1 Hz, 1H), 4.36 (q, J = 7.1 Hz, 2H), 1.68 (t, J = 7.1 Hz, 3H) ppm.

LC-MS (gradient 80) *m*/*z* 267.0 ($[M-H]^-$).

*(9-Ethoxyphenazin-1-yl)methanol (**24**)*

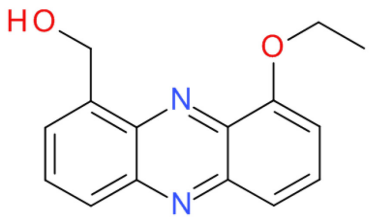

A suspension of carboxylic acid **23** (1.50 g, 5.59 mmol) in DMF (15 mL) was treated with 1,1'-carbonyldiimidazole (CDI) (1.85 g, 11.40 mmol), and the mixture was stirred at 50°*C* for 1 h. After cooling, the mixture was diluted with DCM/petroleum ether (1:1) to complete precipitation of the imidazolide, which was collected, washed with petroleum ether, dried, dissolved in THF (200 mL) then slowly added to a solution of $NaBH_4$ (1.3 g, 34.4 mmol) in H_2O (50 mL). After stirring for 1 h, the mixture was neutralized by dropwise addition of HCl (conc.), and then extracted with EtOAc. The organic layer was washed with aqueous Na_2CO_3 and water, dried (Na_2SO_4), and concentrated under reduced pressure, to give compound **24** (1.2 g, 4.71 mmol).

MF: 254.28.

FW: $C_{15}H_{14}N_2O_2$.

Yield: 84%.

Physical State: orange powder.

R_f: 0.4 (RP-18 SiO_2; MeCN/H_2O/TFA – 80:20:0.1).

^{1}H NMR ($CDCl_3$, 400MHz): δ = 8.16 (dd, J = 8.8, 1.3 Hz, 1H), 7.81 (dd, J = 8.8, 1.3 Hz, 1H), 7.79 (dd, J = 8.8, 6.8 Hz, 1H), 7.76 (dd, J = 8.8, 7.3 Hz, 1H), 7.68 (dd, J = 6.8, 1.3 Hz, 1H), 7.06 (dd, J = 7.3, 1.3 Hz, 1H), 5.36 (s, 2H), 5.26 (br s, 1H), 4.34 (q, J = 7.0 Hz, 2H), 1.66 (t, J = 7.0 Hz, 3H) ppm.

^{13}C NMR ($CDCl_3$, 101MHz): δ = 154.4, 144.2, 143.7, 141.1, 139.1, 135.1, 131.0, 130.6, 128.8, 127.7, 120.9, 107.6, 64.8, 64.6, 14.7 ppm.

LC-MS (gradient 100) *m/z* 255.2 ($[M + H]^+$), retention time 4.9 min.

HRMS *m/z* 255.1133 ($[M + H]^+$) calculated for C15H15N2O2+: 255.1134 (Δ −0.4 ppm).

*9-Ethoxyphenazine-1-carbaldehyde (**25**)*

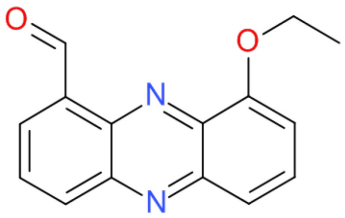

A mixture of alcohol **24** (750 mg, 2.95 mmol), activated manganese (IV) oxide (5.65 g, 58.5 mmol) and dry DCM (50 mL) was stirred at rt under Ar for 3 h. Then the reaction was filtered through a pad of silica gel and concentrated. The residue was dissolved in EtOAc and the solution was washed with aqueous Na_2CO_3, water, dried (Na_2SO_4), evaporated and dried *in vacuo* for 24 h to yield compound **25** (530 mg, 2.10 mmol).

MF: $C_{15}H_{12}N_2O_2$.

FW: 252.27.

Yield: 71%.

Physical State: yellow solid.

^{1}H NMR ($CDCl_3$, 400MHz): δ = 11.63 (s, 1H), 8.52 (dd, J = 8.7, 1.4 Hz, 1H), 8.48 (dd, J = 7.1, 1.4 Hz, 1H), 7.99 (dd, J = 8.7, 7.1 Hz, 1H), 7.84 (dd, J = 8.8, 1.8 Hz, 1H), 7.81 (dd, J = 8.8, 6.8 Hz, 1H), 7.14 (dd, J = 6.8, 1.8 Hz, 1H), 4.39 (q, J = 7.1 Hz, 2H), 1.70 (t, J = 7.1 Hz, 3H) ppm.

^{13}C NMR ($CDCl_3$, 101MHz): δ = 191.4, 154.7, 144.4, 142.6, 141.1, 137.2, 135.8, 132.1, 131.6, 130.2, 130.0, 121.2, 108.4, 65.1, 14.7 ppm.

LC-MS (gradient 100) *m/z* 253.1 ($[M + H]^+$), retention time 5.8 min.

HRMS *m/z* 253.0972 ($[M + H]^+$) calculated for C15H13N2O2+: 253.0977 (Δ −2.0 ppm).

*2-[(*E*)-2-(9-Ethoxyphenazin-1-yl)vinyl]-1,3,3-trimethyl-*3H*-indolium iodide (**26**)*

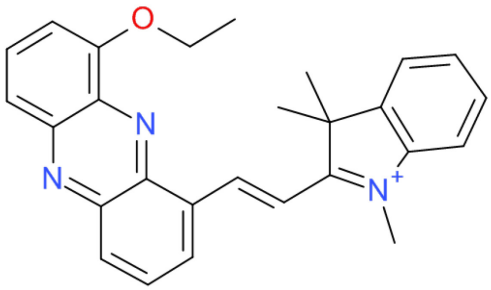

Compound **26** (120 mg, 0.22 mmol) was obtained following the general procedure I, from aldehyde **25** (120 mg, 0.40 mmol), indolium salt **7** (99 mg, 0.33 mmol) and piperidine (10 µL, 0.10 mmol) in ethanol (10 mL) refluxed for 3 h under Ar.

MF: $C_{27}H_{26}N_3O$-I.

FW: 535.42.

Yield: 68%.

Physical State: red powder.

UV-Vis (MeCN) λ_{max} 386, 264 nm.

^{1}H NMR (DMSO-d_6, 500MHz): δ = 9.58 (d, J = 16.7 Hz, 1H, E-C$^{\beta}$H), 8.94 (d, J = 6.9 Hz, 1H, Pz-CH), 8.49 (d, J = 8.5 Hz, 1H, Pz-CH), 8.48 (d, J = 16.7 Hz, 1H, E-C$^{\alpha}$H), 8.19 (dd, J = 8.5, 6.9 Hz, 1H, Pz-CH), 7.96-8.02 (m, 2H, I-CH), 7.96 (dd, J = 8.5, 7.6 Hz, 1H, Pz-CH), 7.85 (d, J = 8.5 Hz, 1H, Pz-CH), 7.64-7.76 (m, 2H, I-CH), 7.40 (d, J = 7.6 Hz, 1H, Pz-CH), 4.41 (q, J = 7.0 Hz, 2H, Pz-OEt), 4.28 (s, 3H, I-N^1Me), 1.96 (s, 6H, I-C^{3}Me$_2$), 1.62 (t, J = 7.0 Hz, 3H, Pz-OEt) ppm.

^{13}C NMR (DMSO-d_6, 101MHz): δ = 182.0, 154.1, 147.3, 144.0, 143.7, 142.6, 141.9, 139.5, 135.5, 134.0, 132.5, 132.4, 131.1, 129.8, 129.2, 123.1, 120.4, 116.1, 115.6, 109.0, 64.5, 52.4, 34.9, 25.9 (2C), 14.8 ppm.

LC-MS (gradient 80) m/z 408.0 ([M − I]$^+$).

HRMS m/z 408.2080 ([M − I]$^+$) calculated for C27H26N3O+: 408.2076 (Δ 1.0 ppm).

*9-Ethoxy-5-methyl-1-[(*E*)-2-(1,3,3-trimethyl-*3H*-indolium-2-yl)ethenyl]phenazinium chloride (**27**)*

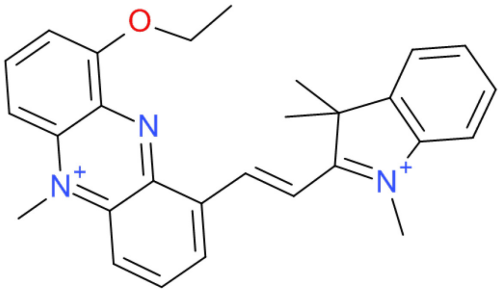

Indolium salt **26** (50 mg, 0.09 mmol) was suspended in DCE (5 mL) under Ar in a sealed vessel. The solution was heated at 60°*C* before TfOMe (1.0 mL, 8.8 mmol) was added *via* syringe. The reaction mixture was heated at 100°*C* for 30 min, allowed to cool to rt, slowly poured into 50 mL of ether, the precipitate was filtered off and then, dissolved in 200 mL of water, washed DCM (5 x 15 mL), and precipitated by addition of NH_4PF_6. The chloride salt was prepared by sonication of a solution of the PF_6-salt in MeOH (30 mL) with Amberlite ion exchange resin (chloride form) for 5 min. The solution was filtered and reduced in volume before being precipitated by slow addition of diethyl ether. The resulting precipitate was isolated by suction filtration and washed with diethyl ether (2 x 10 mL) to yield compound **27** (20 mg, 0.04 mmol).

MF: C28H29N3O.2Cl.

FW: 494.46.

Yield: 44%.

Physical State: brown solid.

UV-Vis (water) λ_{max} 442, 391, 278 nm.

^{1}H NMR although the NMR signals are broad for the solution of **27** (10 mg, 0.02 mmol) in D_2O (700 µL) preventing reliable integration, the presence of signals at δ = 4.0–5.5 ppm (see supplementary NMR spectra), characteristic of Q-N^5CH_3 protons of the phenazine fragment, confirms that **26** was successfully alkylated. ^{1}H NMR data obtained at the same concentration of **26** in DMSO-d_6 were poorly resolved (data not shown).

LC-MS (gradient 80) *m/z* 423.1 $([M - 2Cl]^+)$.

HRMS *m/z* 422.2237 $([M - H - 2Cl]^+)$ calculated for C26H25N3+: 422.2232 (Δ 1.2 ppm).

3.5.7 Synthesis and structure verification of a product formed upon reaction of **2ACy-2** with NADH

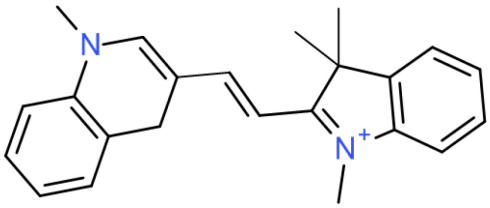

An MQ-water solution (7 mL) of **2ACy-2** (19.2 mg, 0.032 mmol) was mixed with a buffered aqueous solution (3 mL, pH = 7.0) of NADH (27.4 mg, 0.039 mmol) at rt. The reaction mixture was stirred for 2 h after which the organic product was extracted into DCM. After drying (Na_2SO_4), the solvent was removed on the rotary evaporator to give **DACy-2** (14.3 mg, 0.031 mmol).

MF: C23H25N2-I (TfO anion was not observed in ^{13}C NMR).

FW: 456.36.

Yield: 98%.

Physical State: dark pink solid.

UV-Vis (25 mM PIPES, 101 mM NaCl, pH 7.0) λ_{max} (ε $mM^{-1}cm^{-1}$) 537 (81.9±2.1), 515sh. (59.2±1.3) nm.*

* — UV-Vis absorbance at 535 nm gradually decreased during storage in air at rt (1 d — 100%; 4 d — 63%; 8 d — 24%).

^{1}H NMR (MeCN-d_3, 400MHz, COSY, HSQC, HMBC): δ = 7.98 (dt, J = 14.4, 1.5 Hz, 1H, E-C$^{\beta}$H), 7.70 (s, 1H, Q-C^{2}H), 7.50-7.55 (m, 1H, I-C^{4}H), 7.43-7.49 (m, 1H, I-C^{6}H), 7.34 (ddd, J = 7.9, 7.6, 1.0 Hz, 1H, I-C^{5}H), 7.27-7.35 (m, 3H, Q-C^{5}H, Q-C^{7}H, I-C^{7}H), 7.23-7.26 (m, 1H, Q-C^{8}H), 7.19-7.23 (m, 1H, Q-C^{6}H), 5.92 (d, J = 14.4 Hz, 1H, E-C$^{\alpha}$H), 3.96 (d, J = 1.5 Hz, 2H, Q-C^{4}H$_2$), 3.64 (s, 3H, I-N^1Me), 3.54 (s, 3H, Q-N^1Me), 1.69 (s, 6H, I-C^{3}Me$_2$) ppm.

^{13}C NMR (MeCN-d_3, 400MHz, COSY, HSQC, HMBC): δ = 176.6 (C$_q$, I-C^2), 154.5 (Q-C^{2}H), 153.1 (E-C$^{\beta}$H), 142.7 (C$_q$, I-C^{7a}), 141.4 (C$_q$, I-C^{3a}), 136.4 (C$_q$, Q-C^{8a}), 130.0 (Q-C^{5}H), 128.6 (I-C^{6}H), 127.8 (Q-C^{7}H), 126.5 (Q-C^{8}H), 125.9 (I-C^{5}H), 124.6 (C$_q$, C^{4a}), 122.3 (I-C^{4}H), 115.9 (Q-C^{6}H), 113.1 (C$_q$, Q-C^3), 111.6 (I-C^{7}H), 98.9 (E-C$^{\alpha}$H), 49.8 (C$_q$, I-C^3), 40.5 (Q-N^1Me), 31.5 (I-N^1Me), 26.5 (I-C^{3}Me$_2$), 25.6 (Q-C^{4}H$_2$) ppm.

LC-MS (gradient 80) m/z 329.19 ([M − I]$^+$); retention time 6.8 min.

3.6 References

[1] A. Zhu, R. Romero, H. R. Petty. An enzymatic fluorimetric assay for glucose-6-phosphate: application in an in vitro Warburg-like effect. *Anal. Biochem.* **2009**, *388*, 97-101.

[2] A. Zhu, R. Romero, H. R. Petty. An enzymatic colorimetric assay for glucose-6-phosphate. *Anal. Biochem.* **2011**, *419*, 266-270.

[3] G. W. Huisman, J. Liang, A. Krebber. Practical chiral alcohol manufacture using ketoreductases. *Curr. Opin. Chem. Biol.* **2010**, *14*, 122-129.

[4] P. Könst, H. Merkens, S. Kara, S. Kochius, A. Vogel, R. Zuhse, D. Holtmann, I. W. C. E. Arends, F. Hollmann. Enantioselective Oxidation of Aldehydes Catalyzed by Alcohol Dehydrogenase. *Angew. Chem. Int. Ed.* **2012**, *51*, 9914-9917.

[5] S. Siedler, G. Schendzielorz, S. Binder, L. Eggeling, S. Bringer, M. Bott. SoxR as a Single-Cell Biosensor for NADPH-Consuming Enzymes in Escherichia coli. *ACS Synth. Biol.* **2013**, *3*, 41-47.

[6] Y. Zhao, Q. Hu, F. Cheng, N. Su, A. Wang, Y. Zou, H. Hu, X. Chen, H.-M. Zhou, X. Huang, K. Yang, Q. Zhu, X. Wang, J. Yi, L. Zhu, X. Qian, L. Chen, Y. Tang, J. Loscalzo, Y. Yang. SoNar, a Highly Responsive NAD+/NADH Sensor, Allows High-Throughput Metabolic Screening of Anti-tumor Agents. *Cell Metab.* **2015**, *21*, 777-789.

[7] L. Zhang, Y. Li, D. W. Li, C. Jing, X. Chen, M. Lv, Q. Huang, Y. T. Long, I. Willner. Single gold nanoparticles as real-time optical probes for the detection of NADH-dependent intracellular metabolic enzymatic pathways. *Angew. Chem.* **2011**, *50*, 6789-6792.

[8] R. Freeman, R. Gill, I. Shweky, M. Kotler, U. Banin, I. Willner. Biosensing and Probing of Intracellular Metabolic Pathways by NADH-Sensitive Quantum Dots. *Angew. Chem.* **2009**, *121*, 315-319.

[9] R. A. Cairns, I. S. Harris, T. W. Mak. Regulation of cancer cell metabolism. *Nat. Rev. Cancer* **2011**, *11*, 85-95.

[10] B. Chance, G. R. Williams. A Method for the Localization of Sites for Oxidative Phosphorylation. *Nature* **1955**, *176*, 250-254.

[11] H. J. Sung, W. Ma, P.-y. Wang, J. Hynes, T. C. O'Riordan, C. A. Combs, J. P. McCoy, F. Bunz, J.-G. Kang, P. M. Hwang. Mitochondrial respiration protects against oxygen-associated DNA damage. *Nat. Commun.* **2010**, *1*, 5.

[12] M. Y. Berezin, S. Achilefu. Fluorescence Lifetime Measurements and Biological Imaging. *Chem. Rev.* **2010**, *110*, 2641-2684.

[13] T. S. Blacker, Z. F. Mann, J. E. Gale, M. Ziegler, A. J. Bain, G. Szabadkai, M. R. Duchen. Separating NADH and NADPH fluorescence in live cells and tissues using FLIM. *Nat. Commun.* **2014**, *5*.

[14] A. von Ketteler, D.-P. Herten, W. Petrich. Fluorescence Properties of Carba Nicotinamide Adenine Dinucleotide for Glucose Sensing. *ChemPhysChem* **2012**, *13*, 1302-1306.

[15] M.-P. Peng, W. Ma, Y.-T. Long. Alcohol Dehydrogenase-Catalyzed Gold Nanoparticle Seed-Mediated Growth Allows Reliable Detection of Disease Biomarkers with the Naked Eye. *Anal. Chem.* **2015**, *87*, 5891-5896.

[16] Y. Zhao, J. Jin, Q. Hu, H.-M. Zhou, J. Yi, Z. Yu, L. Xu, X. Wang, Y. Yang, J. Loscalzo. Genetically Encoded Fluorescent Sensors for Intracellular NADH Detection. *Cell Metab.* **2011**, *14*, 555-566.

[17] K. A. Lukyanov, V. V. Belousov. Genetically encoded fluorescent redox sensors. *BBA General Subjects* **2014**, *1840*, 745-756.

[18] M. V. Berridge, A. S. Tan, K. D. McCoy, R. Wang. The biochemical and cellular basis of cell proliferation assays that use tetrazolium salts. *Biochemica* **1996**, *4*, 14-19.

[19] M. V. Berridge, P. M. Herst, A. S. Tan, in Biotechnology Annual Review*, Vol. Volume 11* (Ed.: M. R. El-Gewely), Elsevier, **2005**, pp. 127-152.

[20] L. P. Candeias, D. P. S. MacFarlane, S. L. W. McWhinnie, N. L. Maidwell, C. A. Roeschlaub, P. G. Sammes, R. Whittlesey. The catalysed NADH reduction of resazurin to resorufin. *J. Chem. Soc., Perkin Trans. 2* **1998**, 2333-2334.

[21] S. N. Rampersad. Multiple Applications of Alamar Blue as an Indicator of Metabolic Function and Cellular Health in Cell Viability Bioassays. *Sensors* **2012**, *12*, 12347.

[22] N. L. Maidwell, M. R. Rezai, C. A. Roeschlaub, P. G. Sammes. On the development of NAD(P)H-sensitive fluorescent probes. *J. Chem. Soc., Perkin Trans. 1* **2000**, 1541-1546.

[23] D. W. Fink, W. R. Koehler. pH Effects on fluorescence of umbelliferone. *Anal. Chem.* **1970**, *42*, 990-993.

[24] M. Fomin, P. Gebauer, C. Horn, D. Heindl // EP patent application nr. EP14181964.9 (filed on Aug. 22, 2014; not published yet).

[25] A. V. Zhdanov, R. I. Dmitriev, D. B. Papkovsky. Bafilomycin A1 activates HIF-dependent signalling in human colon cancer cells via mitochondrial uncoupling. *Bioscience reports* **2012**, *32*, 587-595.

[26] J. W. Bunting, A. W. C. Ng. Rates of Oxidation of 1-Benzyl-1,4-dihydronicotinamide by Pyrazinium, Quinoxalinium, and Phenazinium Cations. *Bioorg. Chem.* **1993**, *21*, 156-169.

[27] J. W. Bunting, V. S. F. Chew, G. Chu. Kinetics of the reduction of isoquinolinium cations by 1,4-dihydronicotinamides. *J. Org. Chem.* **1982**, *47*, 2303-2307.

[28] C. Bernofsky, M. Swan. An improved cycling assay for nicotinamide adenine dinucleotide. *Anal. Biochem.* **1973**, *53*, 452-458.

[29] R. Hisada, W. Shinkai, T. Yagi. Photochemical stabilities and biochemical reactivities of some derivatives of 5-methylphenazinium methyl sulfate (phenazine methosulfate). *J. Appl. Biochem.* **1981**, *3*, 535-543.

[30] O. D. Mit'kin, M. A. Yurovskaya. Quaternization of electron-deficient pyridines containing two electron-withdrawing substituents. *Chem. Heterocycl. Compd.* **2000**, *36*, 47-48.

[31] E. Riché, A. Carrié, N. Andin, S. Mabic. High-purity water and pH. *Am. Lab.* **2006**, *38*, 22.

[32] J. W. Bunting, N. P. Fitzgerald. Kinetic and thermodynamic control of pseudobase formation from C-3 substituted 1-methylquinolinium cations. *Can. J. Chem.* **1984**, *62*, 1301-1307.

[33] J. Bunting. Equilibrium Constants for Heterocyclic Cation. Pseudobase Equilibration. *Heterocycles* **1980**, *14*, 2015-2044.

[34] J. W. Bunting, W. G. Meathrel. Quaternary Nitrogen Heterocycles. III. Kinetic and Thermodynamic Control of Pseudobase Formation from the 1-Methyl-3-nitroquinolinium Cation. *Can. J. Chem.* **1974**, *52*, 303-307.

[35] J. W. Bunting, W. G. Meathrel. Quaternary Nitrogen Heterocycles. I. Equilibrium and Spectral Data for Pseudobase Formation by the N-Methyl Cations of Diazanaphthalenes. *Can. J. Chem.* **1972**, *50*, 917-931.

[36] M. Ishiyama, Y. Miyazono, K. Sasamoto, Y. Ohkura, K. Ueno. A highly water-soluble disulfonated tetrazolium salt as a chromogenic indicator for NADH as well as cell viability. *Talanta* **1997**, *44*, 1299-1305.

[37] G. H. Czerlinski, B. Anderson, J. Tow, D. S. Reid. Coupling of redox indicator dyes into an enzymatic reaction cycle. *J. Biochem. Bioph. Methods* **1988**, *15*, 241-247.

[38] J. W. Bunting, M. A. Luscher. Kinetics of hydride transfer between nitrogen heteroaromatic cations. *Can. J. Chem.* **1988**, *66*, 2524-2531.

[39] J. W. Bunting, J. C. Brewer. Kinetics of the reduction of nicotinonitrile cations by 1,4-dihydronicotinamides. *Can. J. Chem.* **1985**, *63*, 1245-1249.

[40] R. M. G. Roberts, D. Ostovic, M. M. Kreevoy. Regioselectivity of hydride transfer to and between NAD+ analogs. *J. Org. Chem.* **1983**, *48*, 2053-2056.

[41] J. W. Bunting, N. P. Fitzgerald. Kinetics of the reduction of 1-methylquinolinium cations by 1-benzyl-1,4-dihydronicotinamide. *Can. J. Chem.* **1985**, *63*, 655-662.

[42] Q. Yu, A. A. Heikal. Two-photon autofluorescence dynamics imaging reveals sensitivity of intracellular NADH concentration and conformation to cell physiology at the single-cell level. *J. Photochem. Photobiol., B* **2009**, *95*, 46-57.

[43] M. H. Johansson. Reversible Michael Additions: Covalent Inhibitors and Prodrugs. *Mini. Rev. Med. Chem.* **2012**, *12*, 1330-1344.

[44] D. Zhang, N. O. Devarie-Baez, Q. Li, J. R. Lancaster, M. Xian. Methylsulfonyl Benzothiazole (MSBT): A Selective Protein Thiol Blocking Reagent. *Org. Lett.* **2012**, *14*, 3396-3399.

[45] M. McDougall, S. Dwight. Nucleic acid binding dyes and uses therefor. U.S. Patent 8,598,198 B2, Mar. 16, 2009.

[46] R. C. Scaduto Jr, L. W. Grotyohann. Measurement of Mitochondrial Membrane Potential Using Fluorescent Rhodamine Derivatives. *Biophys. J.* **1999**, *76*, 469-477.

[47] B. Ehrenberg, V. Montana, M. D. Wei, J. P. Wuskell, L. M. Loew. Membrane potential can be determined in individual cells from the nernstian distribution of cationic dyes. *Biophys. J.* **1988**, *53*, 785-794.

[48] C. Cottet-Rousselle, X. Ronot, X. Leverve, J.-F. Mayol. Cytometric assessment of mitochondria using fluorescent probes. *Cytometry Part A* **2011**, *79A*, 405-425.

[49] J. Kapuscinski. DAPI: a DNA-Specific Fluorescent Probe. *Biotech. Histochem.* **1995**, *70*, 220-233.

[50] A. D. Presley, K. M. Fuller, E. A. Arriaga. MitoTracker Green labeling of mitochondrial proteins and their subsequent analysis by capillary electrophoresis with laser-induced fluorescence detection. *J. Chromatogr. B* **2003**, *793*, 141-150.

[51] G. Cosa, K. S. Focsaneanu, J. R. N. McLean, J. P. McNamee, J. C. Scaiano. Photophysical Properties of Fluorescent DNA-dyes Bound to Single- and Double-stranded DNA in Aqueous Buffered Solution¶. *Photochem. Photobiol.* **2001**, *73*, 585-599.

[52] N. Panchuk-Voloshina, R. P. Haugland, J. Bishop-Stewart, M. K. Bhalgat, P. J. Millard, F. Mao, W.-Y. Leung, R. P. Haugland. Alexa Dyes, a Series of New Fluorescent Dyes that Yield Exceptionally Bright, Photostable Conjugates. *Journal of Histochemistry & Cytochemistry* **1999**, *47*, 1179-1188.

[53] W. L. Conte, H. Kamishina, R. L. Reep. Multiple neuroanatomical tract-tracing using fluorescent Alexa Fluor conjugates of cholera toxin subunit B in rats. *Nat. Protocols* **2009**, *4*, 1157-1166.

[54] W. L. Armarego, C. L. L. Chai. Purification of laboratory chemicals, Butterworth-Heinemann, **2013**.

[55] L. H. Bluhm, T. Li. Chromatographic purification of quaternary ammonium and pyridinium compounds on normal phase silica gel. *Tetrahedron Lett.* **1998**, *39*, 3623-3626.

[56] H. E. Gottlieb, V. Kotlyar, A. Nudelman. NMR Chemical Shifts of Common Laboratory Solvents as Trace Impurities. *J. Org. Chem.* **1997**, *62*, 7512-7515.

[57] Alexander V. Zhdanov, Ruslan I. Dmitriev, Dmitri B. Papkovsky, J. Hynes, in Conceptual Background and Bioenergetic/Mitochondrial Aspects of Oncometabolism (Ed.: G. K. Lorenzo G), Methods in Enzymology: Academic Press, **2014**, pp. 183-207.

[58] R. I. Dmitriev, S. M. Borisov, J. Jenkins, D. B. Papkovsky. Multi-parametric imaging of tumor spheroids with ultra-bright and tunable nanoparticle O2 probes. *Proc. SPIE* **2015**, *9328*, 932806-932808.

[59] R. I. Dmitriev, A. V. Zhdanov, Y. M. Nolan, D. B. Papkovsky. Imaging of neurosphere oxygenation with phosphorescent probes. *Biomaterials* **2013**, *34*, 9307-9317.

[60] R. I. Dmitriev, S. M. Borisov, H. Düssmann, S. Sun, B. J. Müller, J. Prehn, V. P. Baklaushev, I. Klimant, D. B. Papkovsky. Versatile Conjugated Polymer Nanoparticles for High-Resolution O2 Imaging in Cells and 3D Tissue Models. *ACS Nano* **2015**, *9*, 5275-5288.

[61] G. W. Rewcastle, W. A. Denny. Unequivocal synthesis of phenazine-1-carboxylic acids: selective displacement of fluorine during alkaline borohydride reduction of N-(2-fluorophenyl)-3-nitroanthranilic acids. *Synth. Commun.* **1987**, *17*, 1171-1179.

[62] P. K. Brooke, S. R. Challand, M. E. Flood, R. B. Herbert, F. G. Holliman, P. N. Ibberson. Synthesis of some methoxy- and hydroxy-phenazine-1-carboxylic acids. *J. Chem. Soc., Perkin Trans. 1* **1976**, 2248-2251.

3.7 Supplementary UV-Vis and fluorescence spectra

Table 3-4S Spectral characteristics and kinetic results from the reduction of compounds (**1–6**) with NADH.

Name	$[2A]_0$, mM	$[NADH]_0$, mM	λ_{max}, nm	ΔAbs_∞	$t_{½}$, min
2ACy-1	2.00	0.10	546, 535sh.	0.04	—
2ACy-1	1.90	0.48	546, 535sh.	0.26 ± 0.01	3.2 ± 0.3
2ACy-2	0.50	0.02	535, 515sh.	1.60 ± 0.04	0.12 ± 0.01
2ACy-3	1.90	0.5–1.9	—	—	—
2ACy-4	1.00	0.10	517	0.17	4.1 ± 0.2
2ACy-5	0.20	0.10	529sh., 503	1.5 ± 0.1	6.8 ± 0.7
2ACy-6	0.25	0.10	740	0.7 ± 0.07	$< (1.4 \pm 0.6) \cdot 10^{-3}$

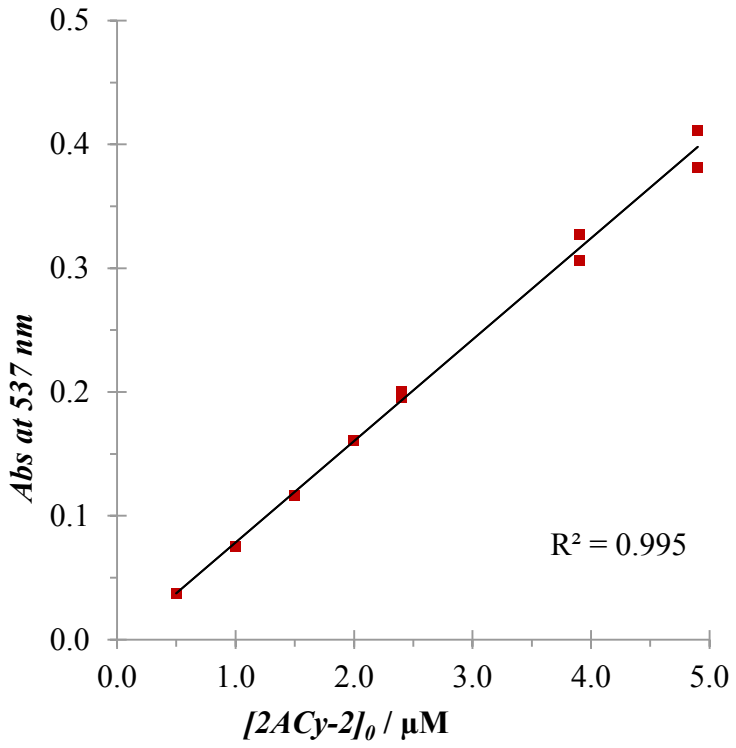

Figure 3.25S Absorbance responses at 537 nm of **2ACy-2** (0.5–5.0 µM) to the addition of excess NADH (500 µM) in buffer (25 mM PIPES, 101 mM NaCl, pH 7.0). The spectra were taken after incubation for 5 min at 25°*C*. The data are fitted by the following linear equation: $y = 0.0819x - 0.0036$ ($n = 10$).

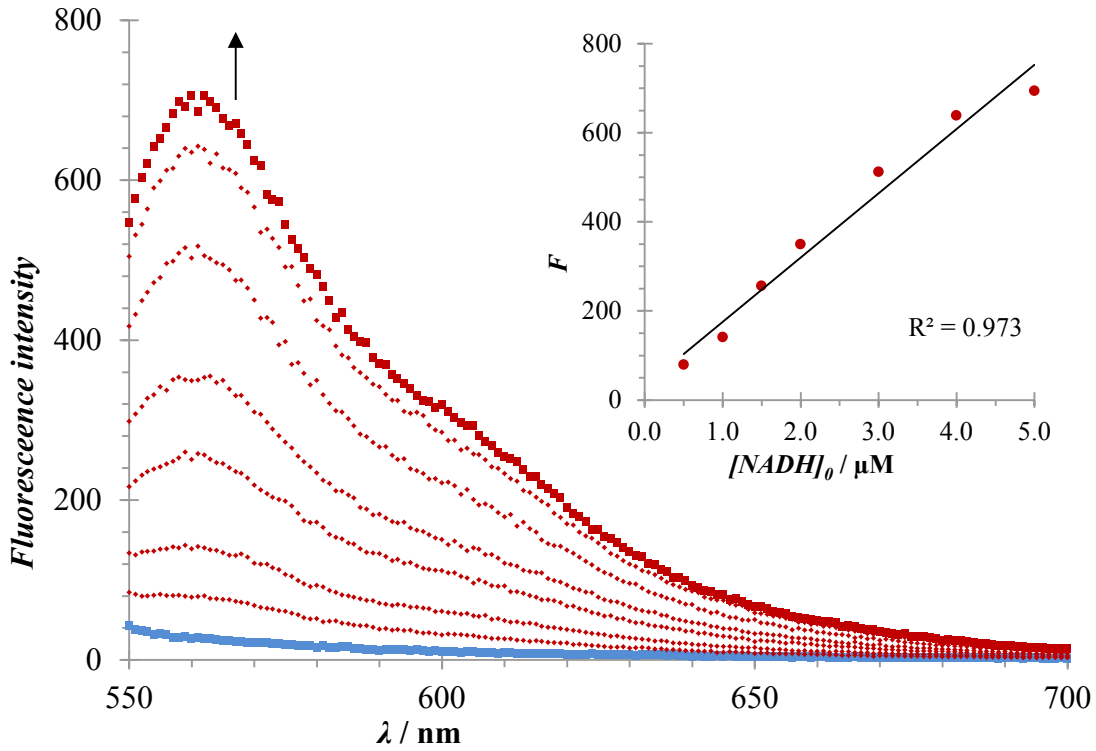

Figure 3.26S Fluorescence emission spectra of **2ACy-2** (20 μM, blue) to increasing concentrations of NADH (red): 0.5, 1.0, 1.5, 2.0, 3.0, 4.0, 5.0 μM, respectively. Inset: relationship between the concentration of NADH and fluorescence intensity (at 561 nm) of the reaction mixture. The spectra were taken after incubation for 30 min in buffer (25 mM PIPES, 101 mM NaCl, pH 7.0) at 25°*C*. λ_{ex} = 537 nm, slit widths: 5/5 nm. The data are fitted by the following linear equation: $y = 144.3x + 31.2$ ($n = 7$).

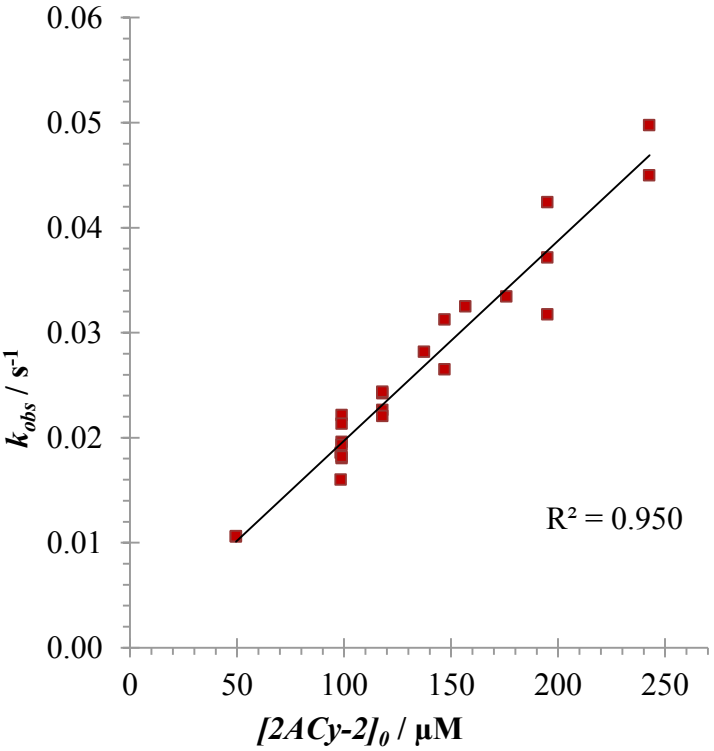

Figure 3.27S The kinetic study of the response of indicator **2ACy-2** to NADH at 25°*C* under pseudo-first-order conditions ($[2ACy\text{-}2]_0$ = 50-250 μM, *[NADH]* = 5 μM).

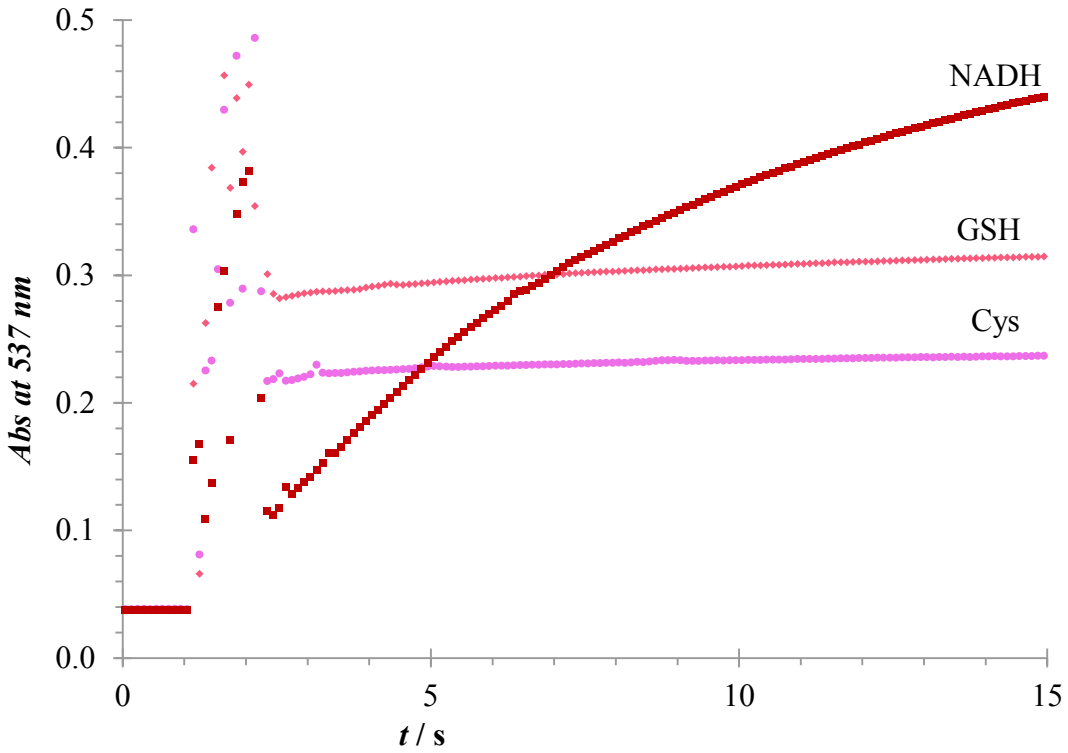

Figure 3.28S The kinetic response of indicator **2ACy-2** (10 μM) to analytes (400 μM): Cys, GSH and NADH; in buffer (25 mM PIPES, 101 mM NaCl, pH 7.0) at 25°*C*.

3.8 Supplementary NMR spectra

^{1}H NMR for **14** iodide salt in DMSO-d$_6$

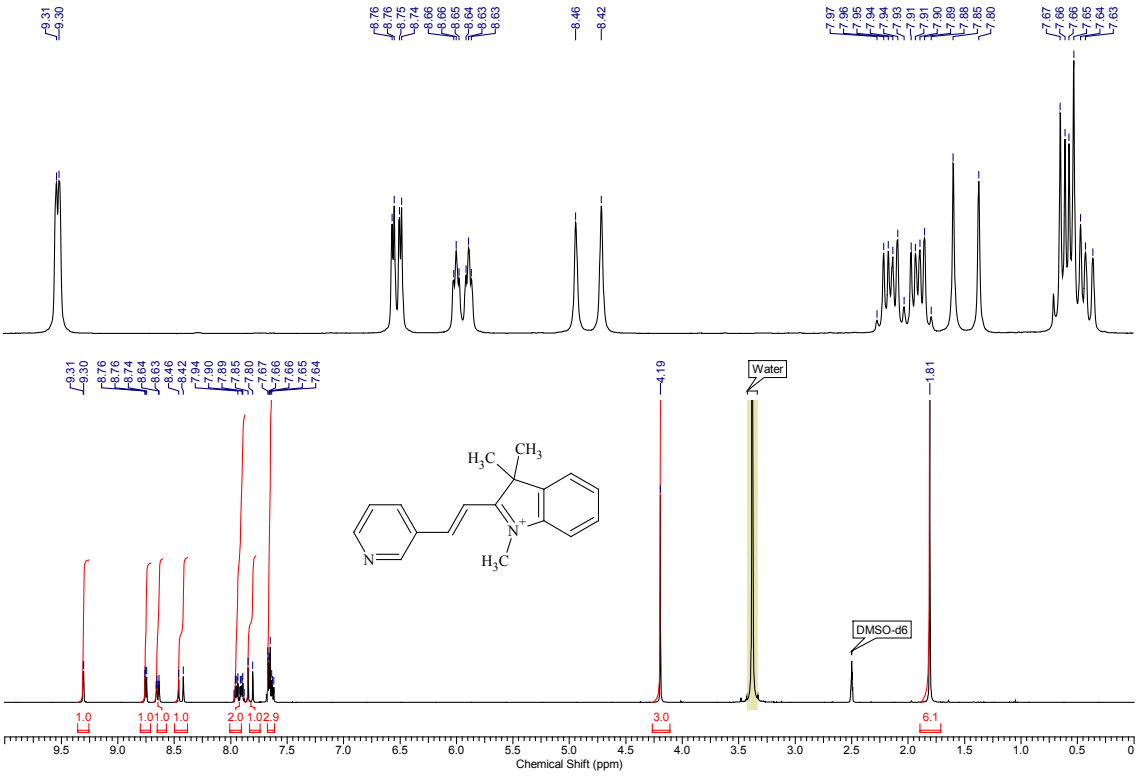

^{13}C NMR for **14** iodide salt in DMSO-d$_6$

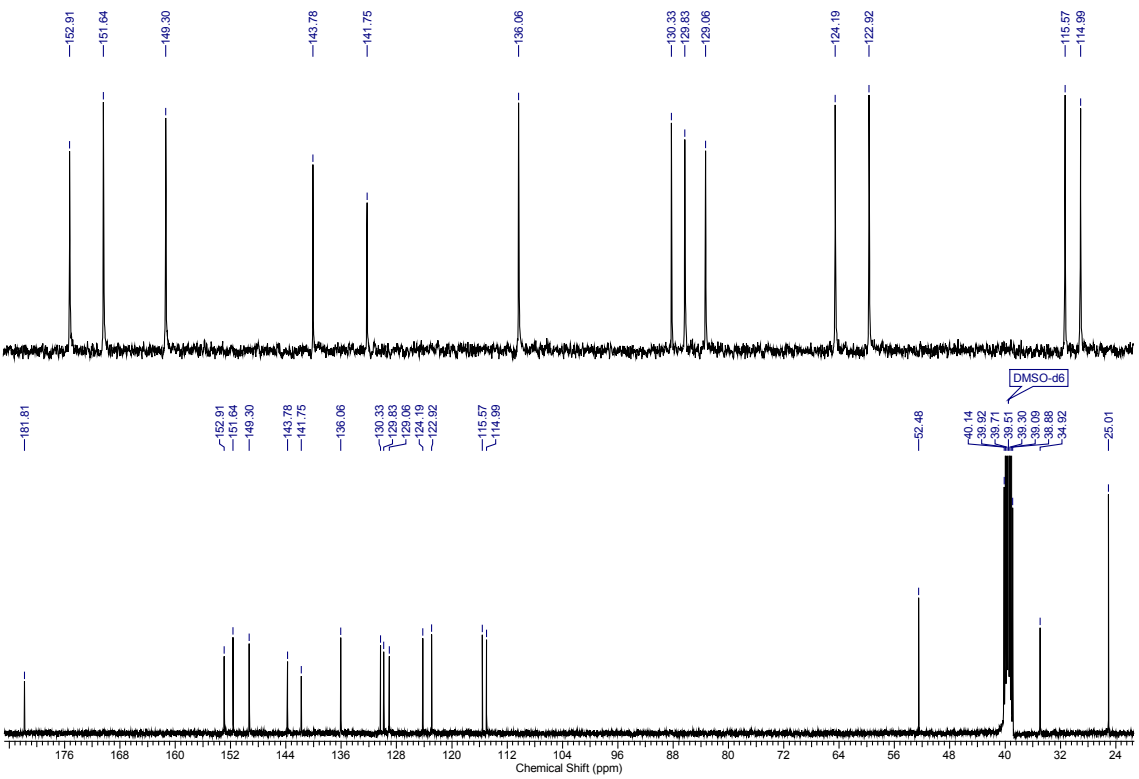

^{1}H NMR for **15** iodide salt in DMSO-d$_6$

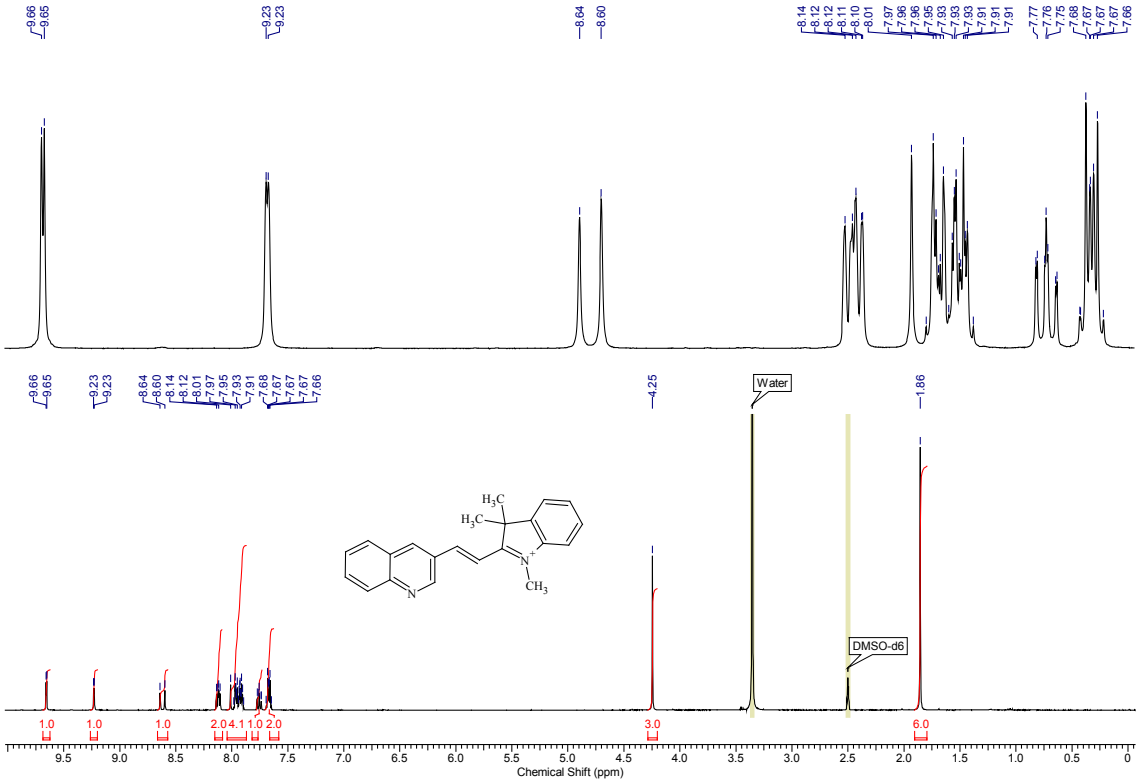

^{13}C NMR for **15** iodide salt in DMSO-d$_6$

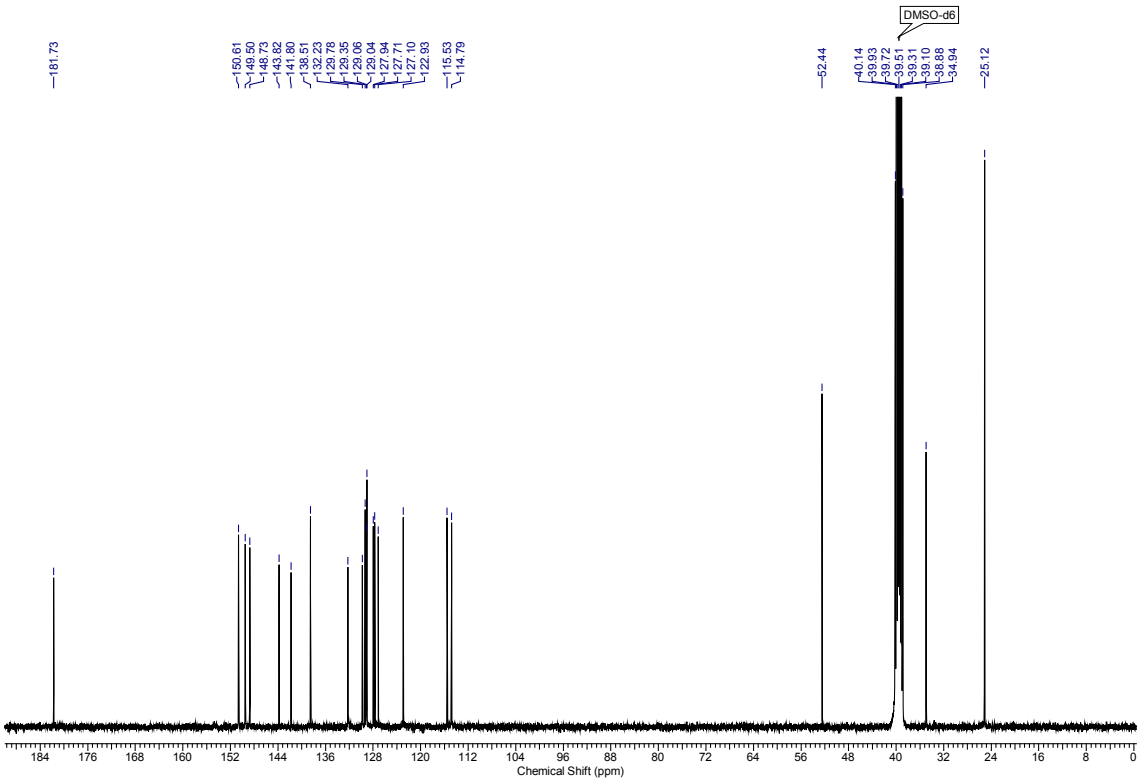

^{1}H NMR for **16** iodide salt in DMSO-d$_6$

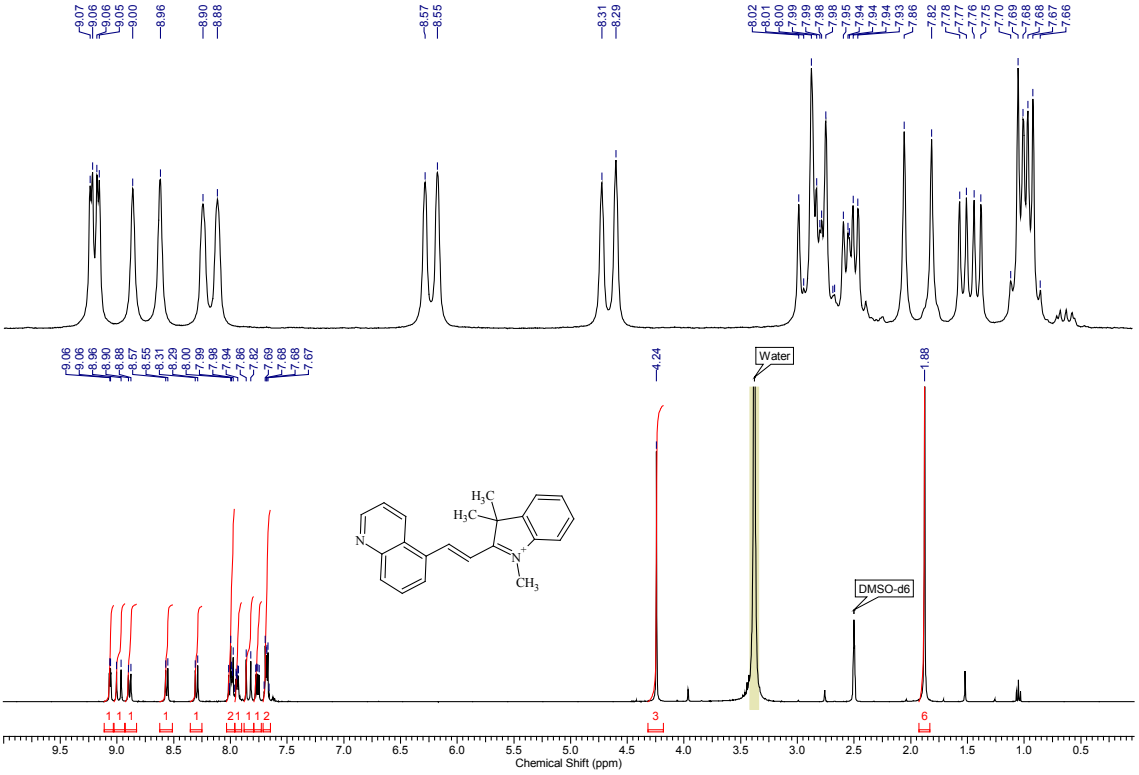

^{13}C NMR for **16** iodide salt in DMSO-d$_6$

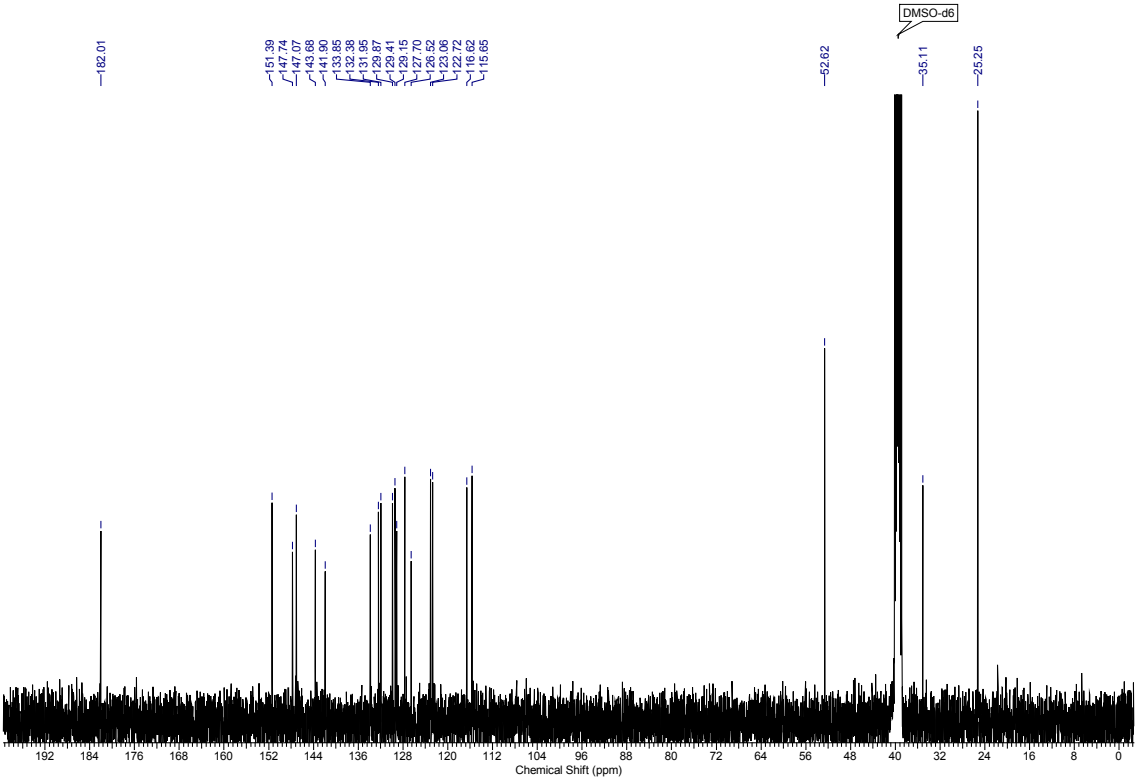

^{1}H NMR for **17** iodide salt in DMSO-d_6

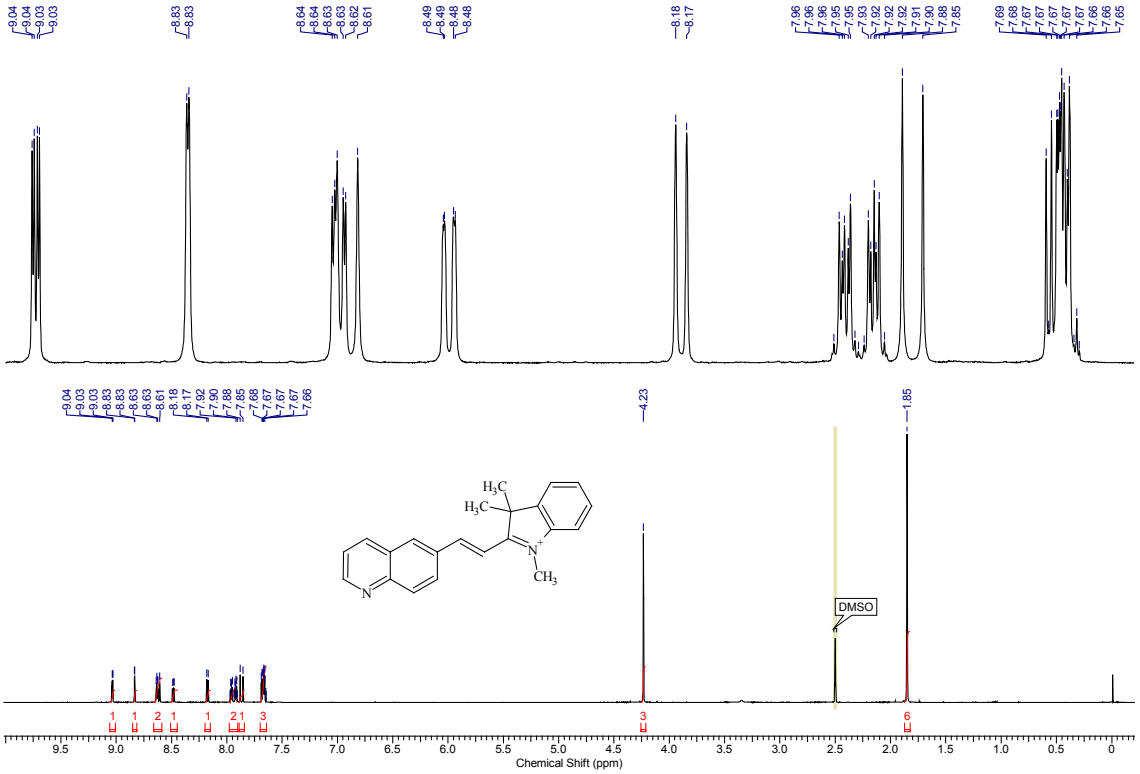

^{13}C NMR for **17** iodide salt in DMSO-d_6

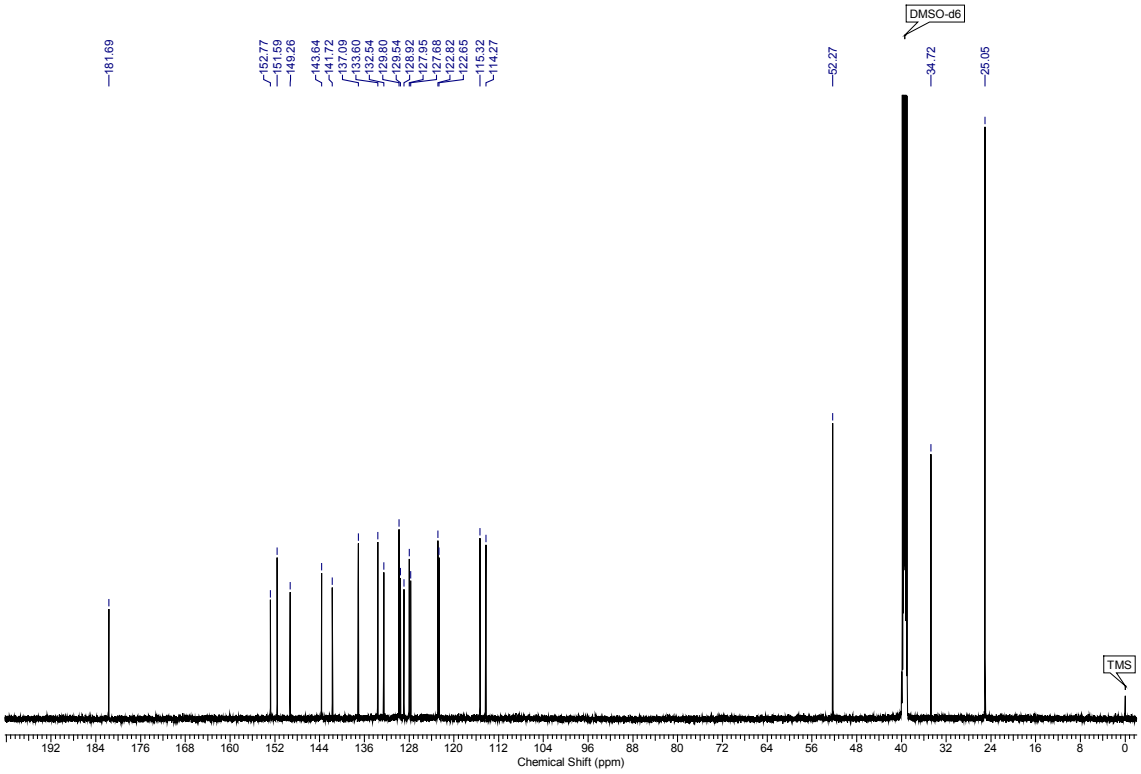

^{1}H NMR for **18** iodide salt in DMSO-d_6

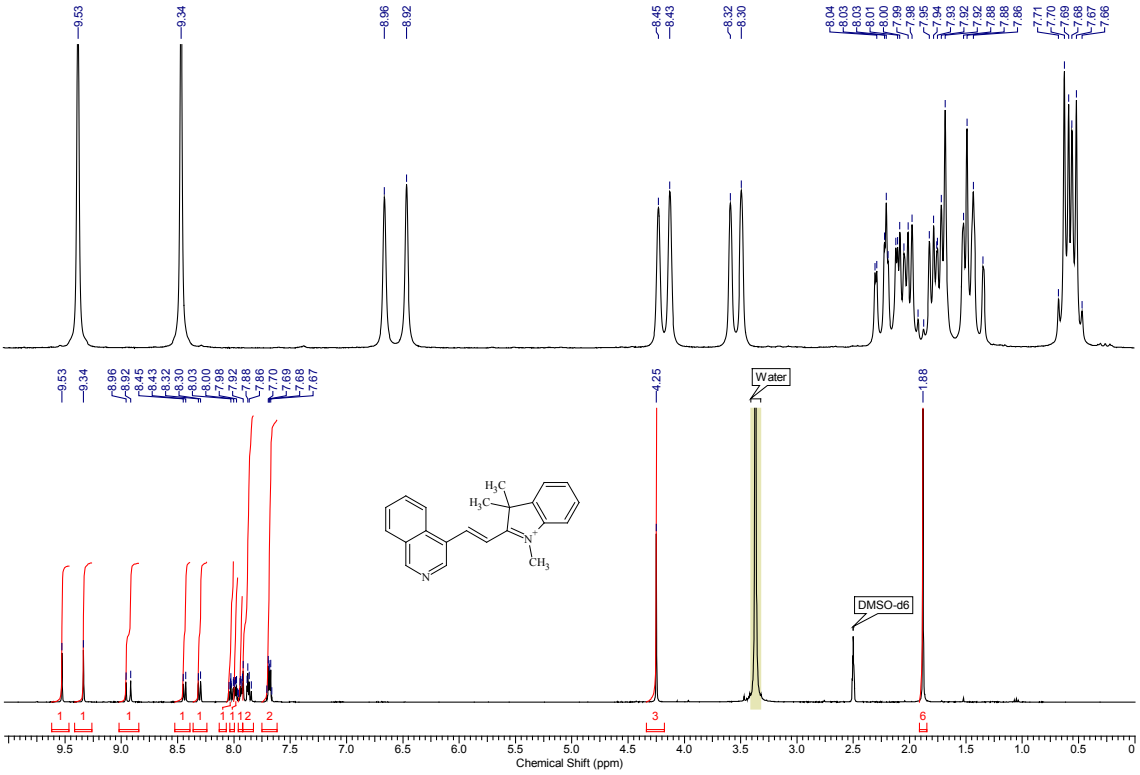

^{13}C NMR for **18** iodide salt in DMSO-d_6

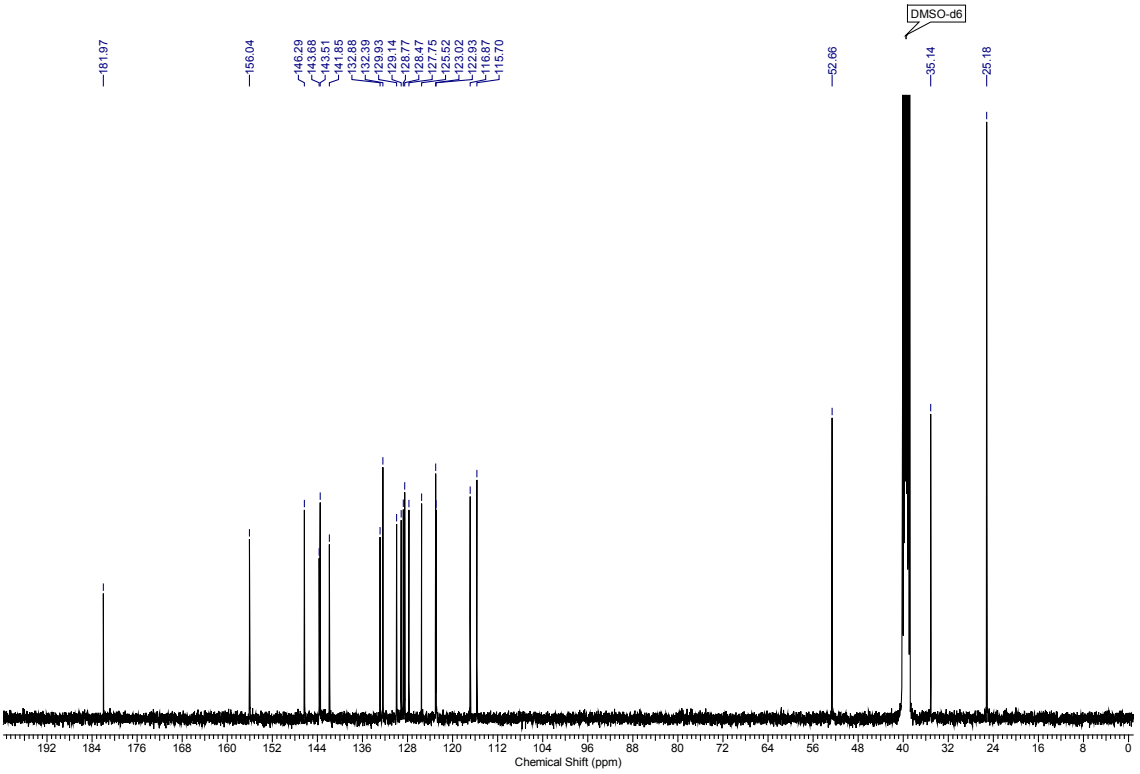

^{1}H NMR for **19** iodide salt in DMSO-d_6

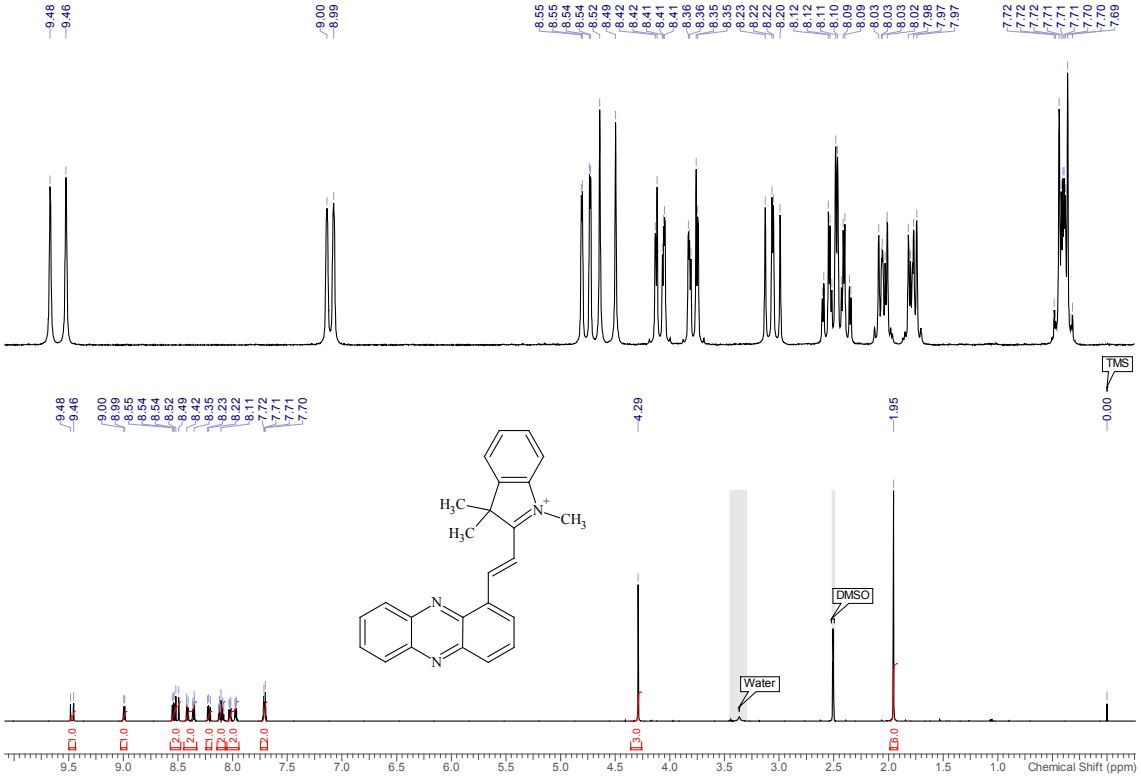

^{13}C NMR for **19** iodide salt in DMSO-d_6

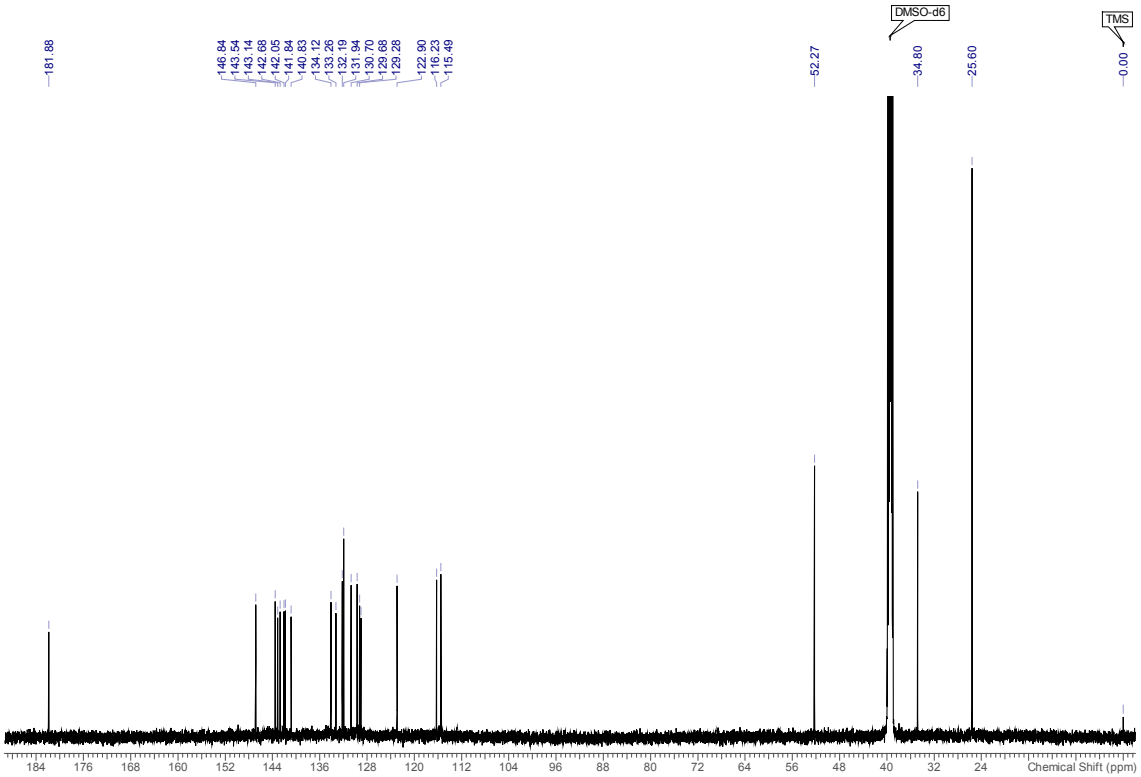

^{1}H NMR for **2ACy-1** iodide trifluoromethanesulfonate salt in DMSO-d_6

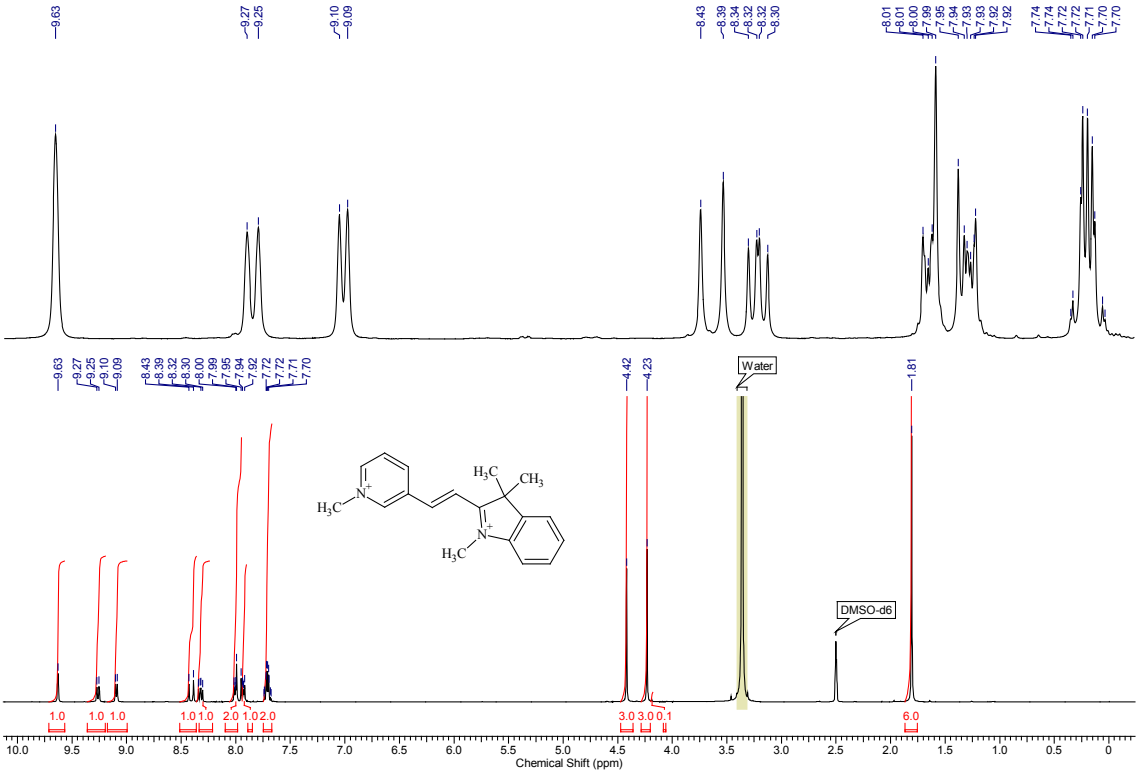

^{13}C NMR for **2ACy-1** iodide trifluoromethanesulfonate salt in DMSO-d_6

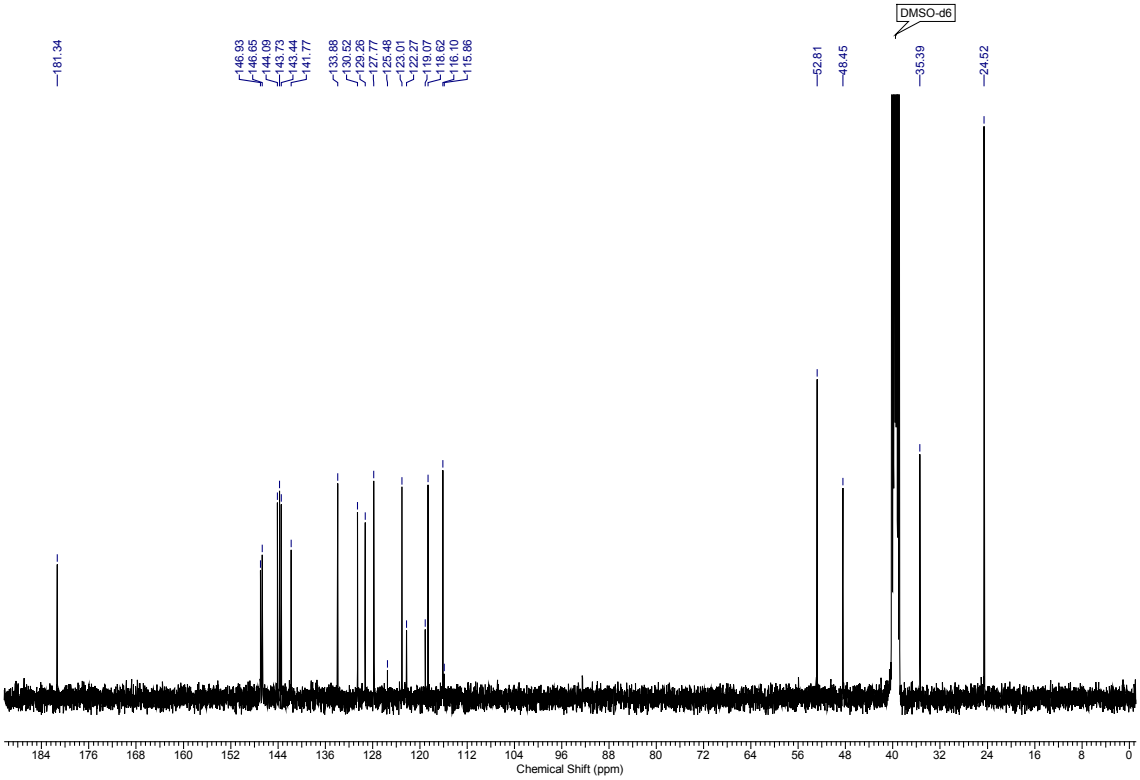

^{1}H NMR for **2ACy-2** iodide trifluoromethanesulfonate salt in DMSO-d_6

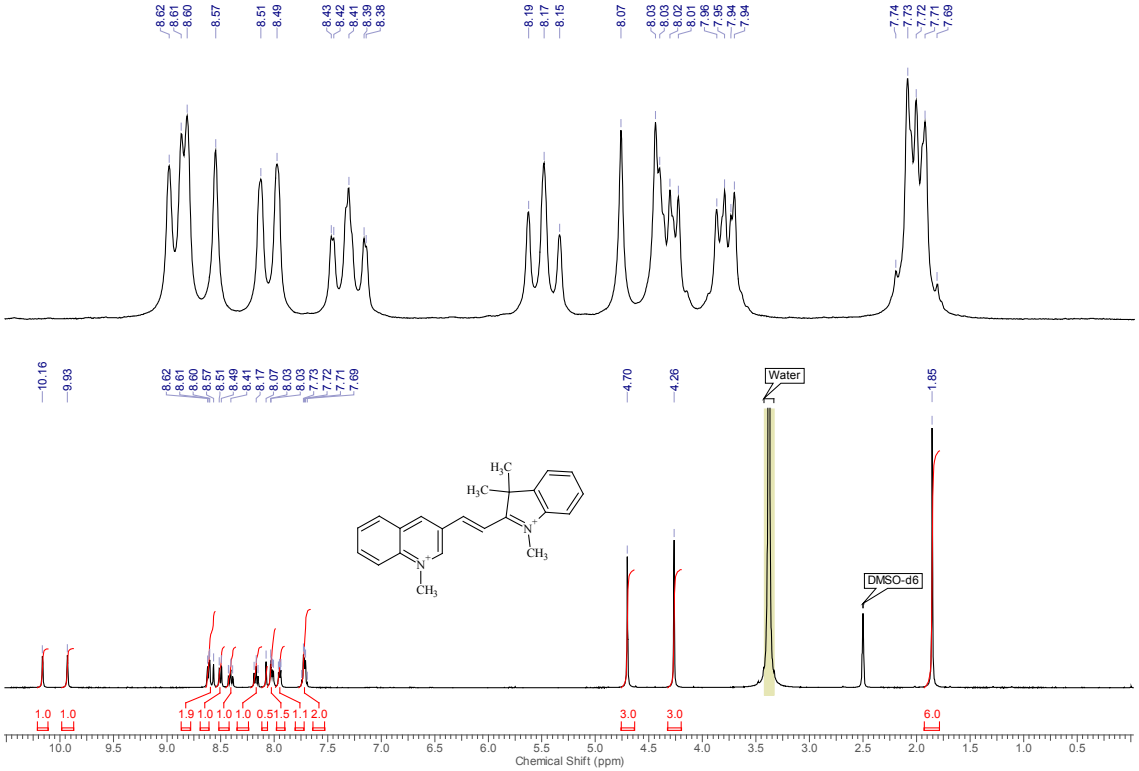

^{13}C NMR for **2ACy-2** iodide trifluoromethanesulfonate salt in DMSO-d_6

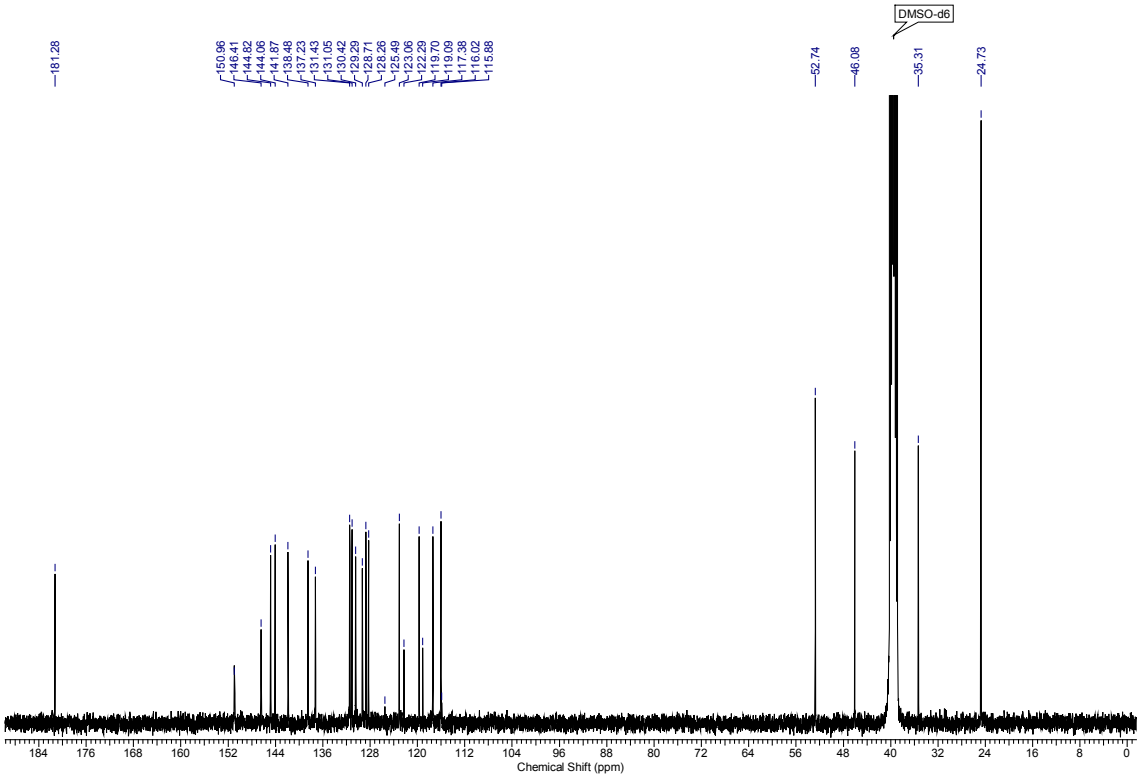

^{1}H NMR for **2ACy-2** iodide trifluoromethanesulfonate salt in MeCN-d_3

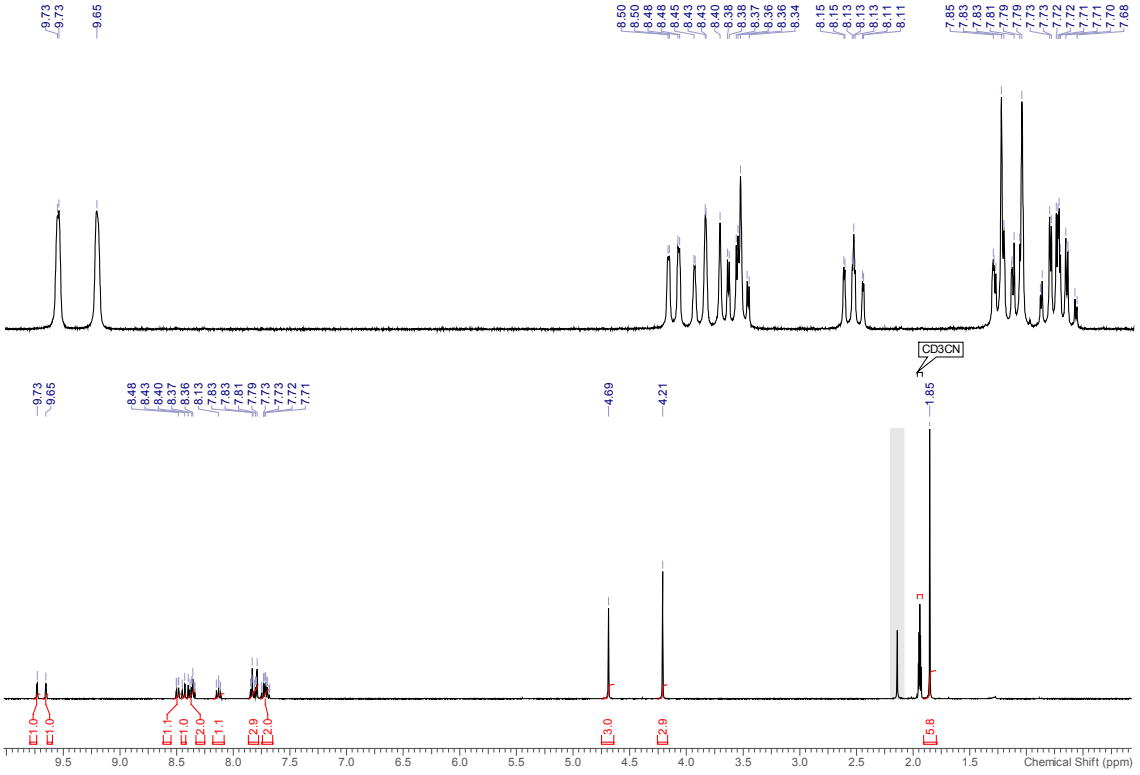

^{13}C NMR for **2ACy-2** iodide trifluoromethanesulfonate salt in MeCN-d_3

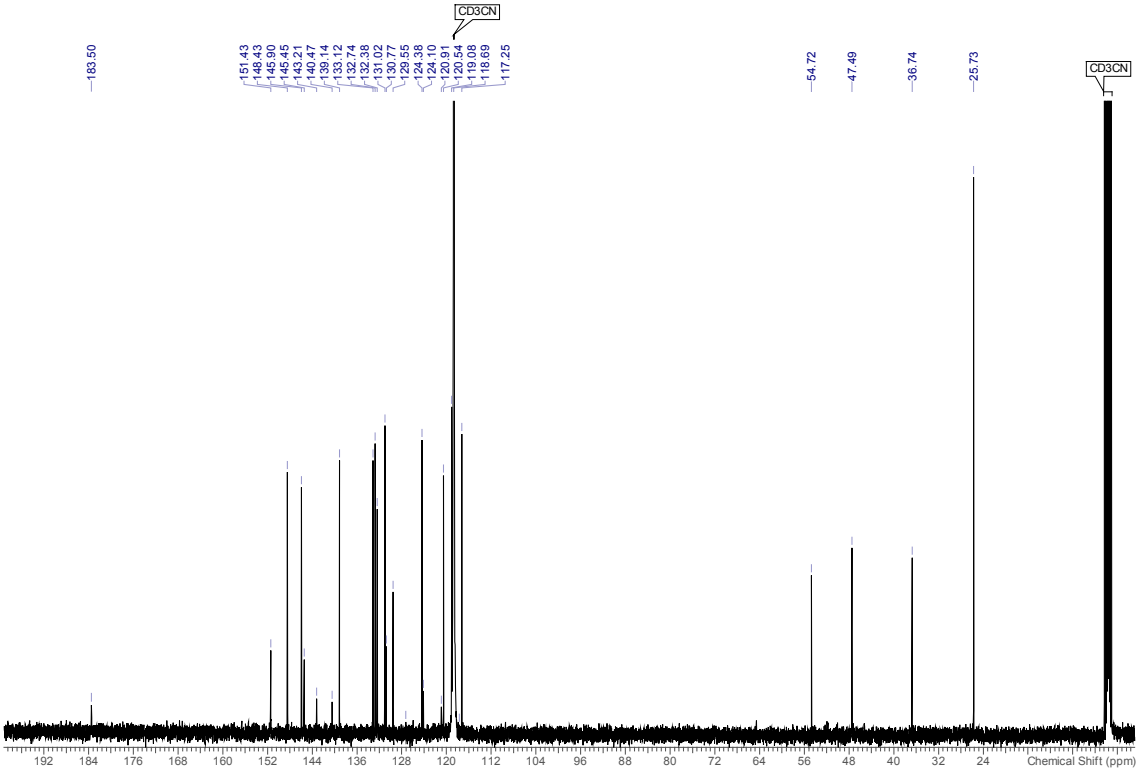

^{1}H NMR for **2ACy-3** iodide trifluoromethanesulfonate salt in DMSO-d_6

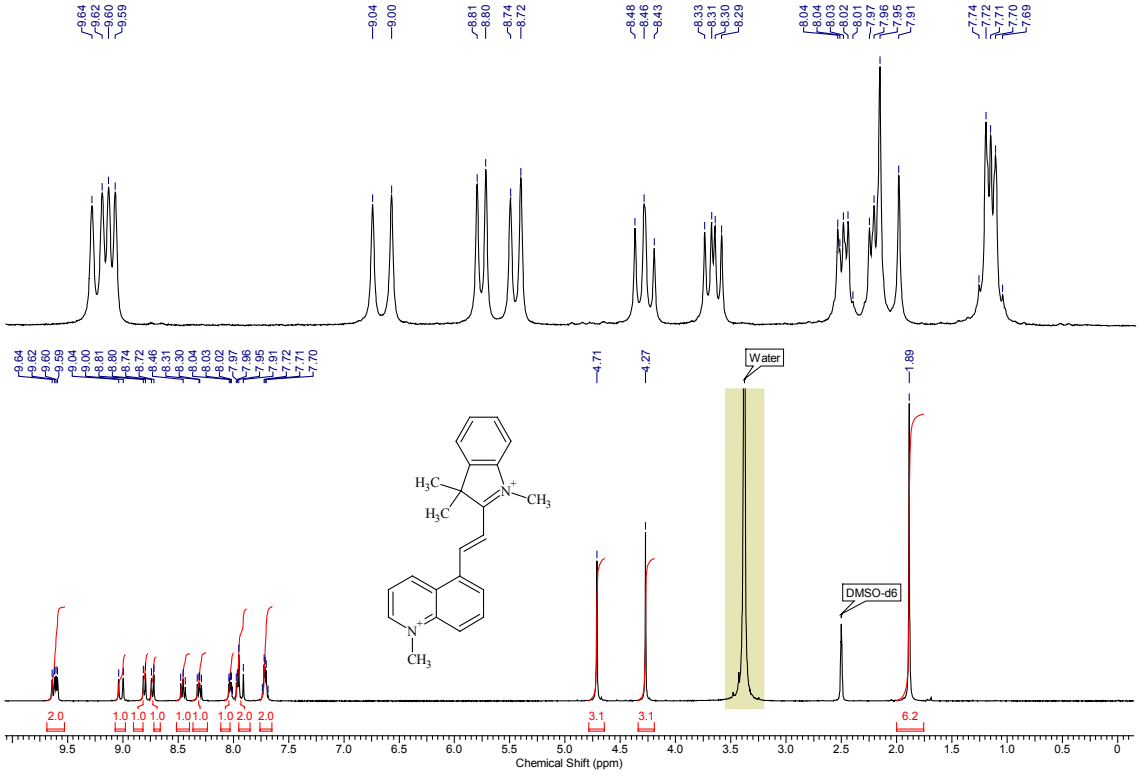

^{13}C NMR for **2ACy-3** iodide trifluoromethanesulfonate salt in DMSO-d_6

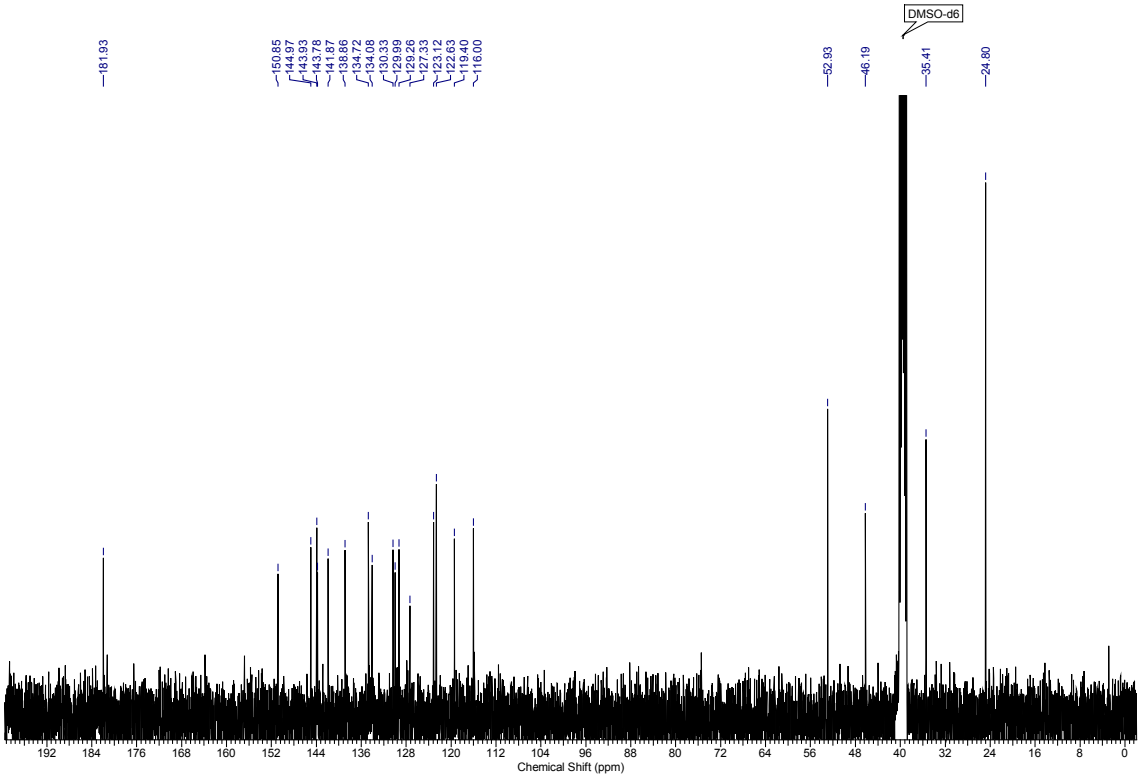

^{1}H NMR for **2ACy-4** iodide trifluoromethanesulfonate salt in DMSO-d_6

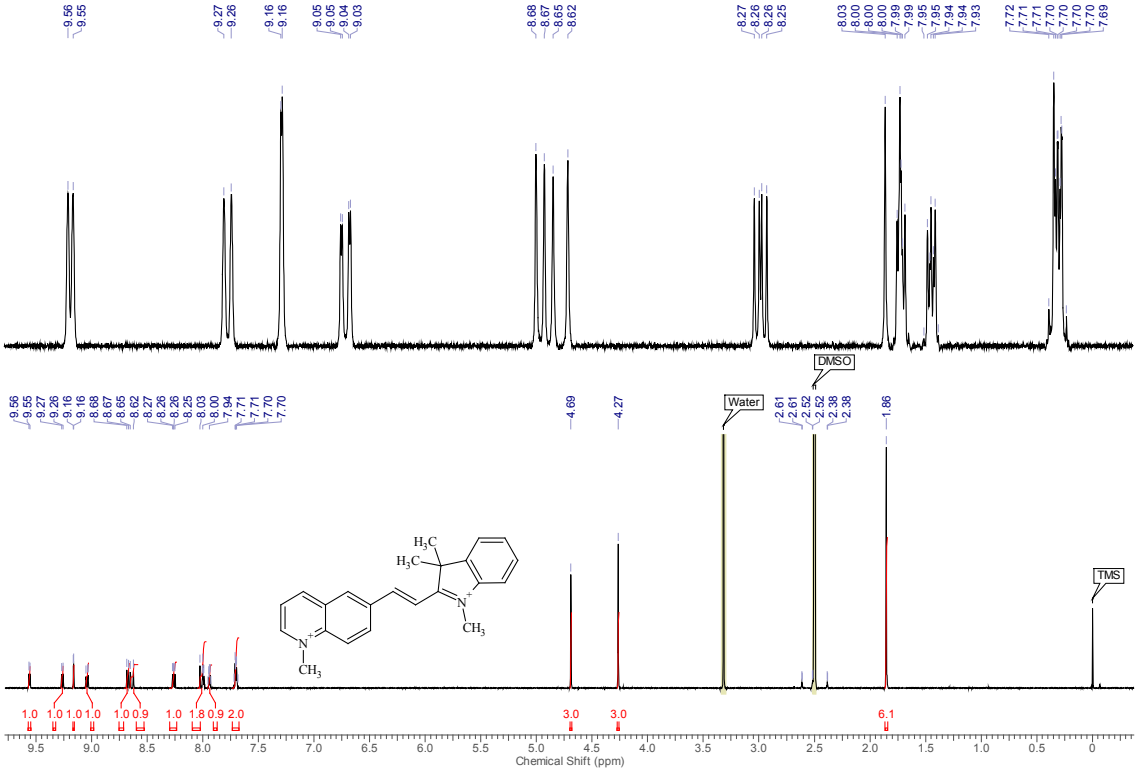

^{13}C NMR for **2ACy-4** iodide trifluoromethanesulfonate salt in DMSO-d_6

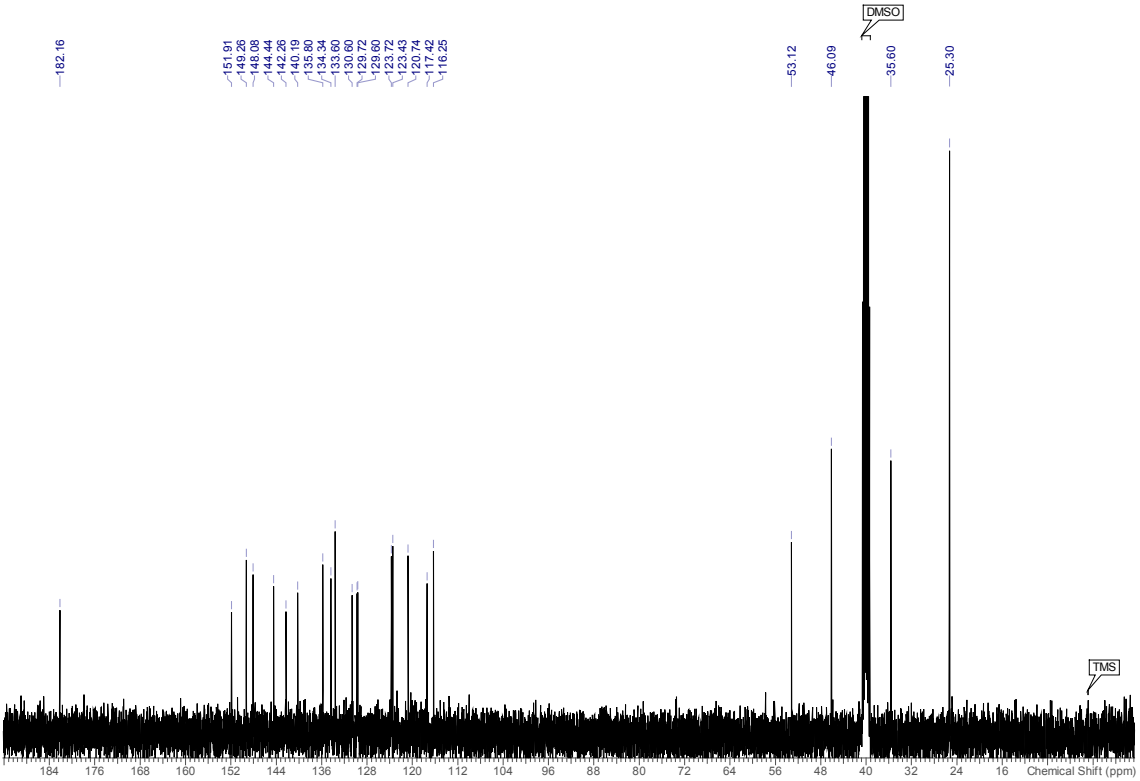

^{1}H NMR for **2ACy-5** iodide trifluoromethanesulfonate salt in DMSO-d_6

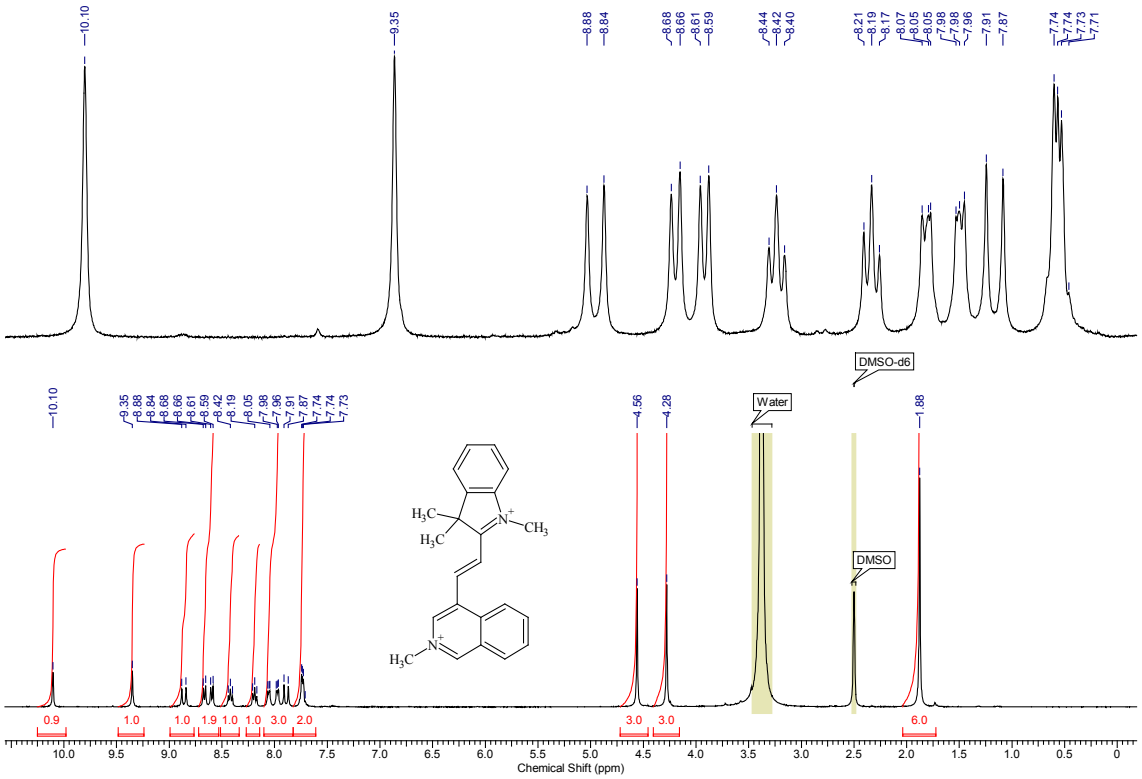

^{13}C NMR for **2ACy-5** iodide trifluoromethanesulfonate salt in DMSO-d_6

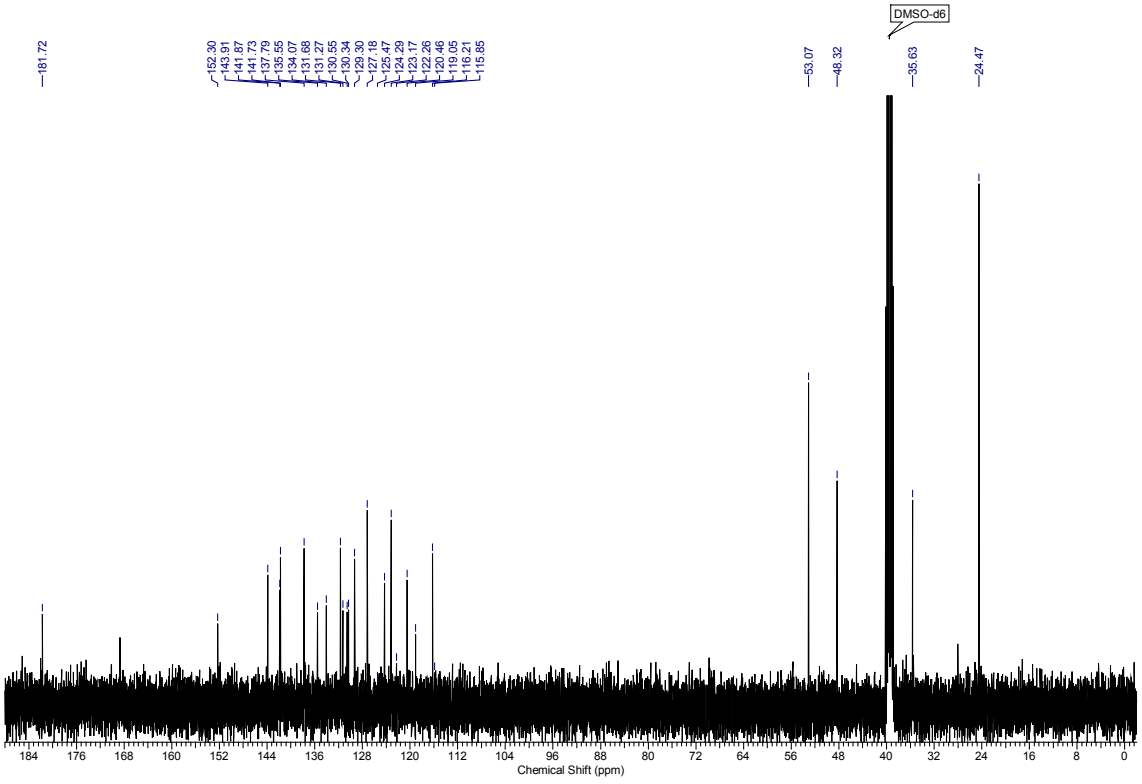

^{1}H NMR for **2ACy-6** iodide trifluoromethanesulfonate salt in MeOD-d_3

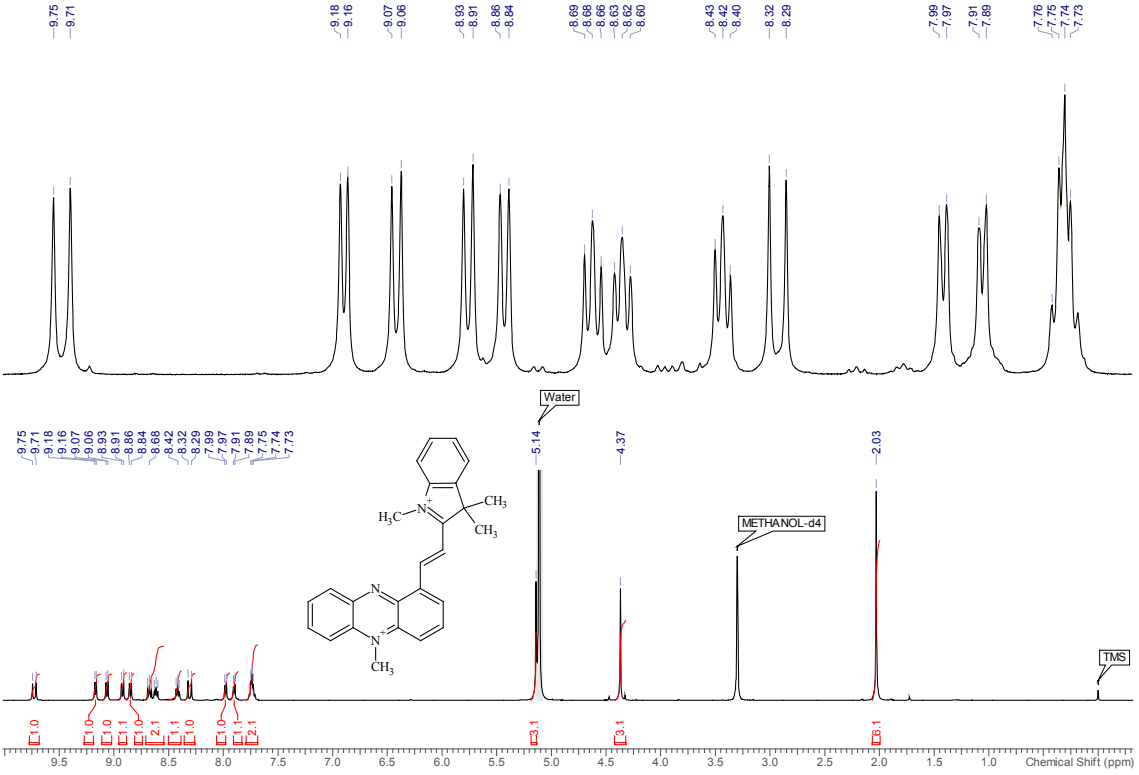

^{13}C NMR for **2ACy-6** iodide trifluoromethanesulfonate salt in MeOD-d_3

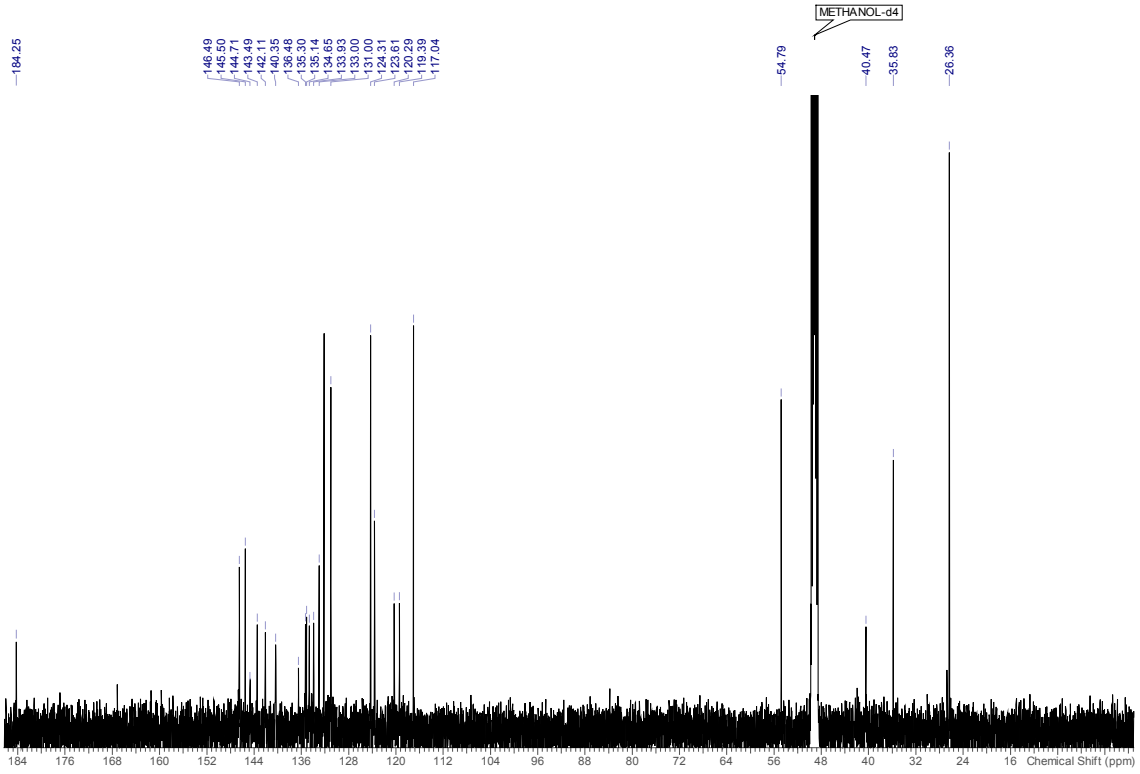

^{1}H NMR for 9-ethoxyphenazine-1-carboxylic acid (**23**) in $CDCl_3$

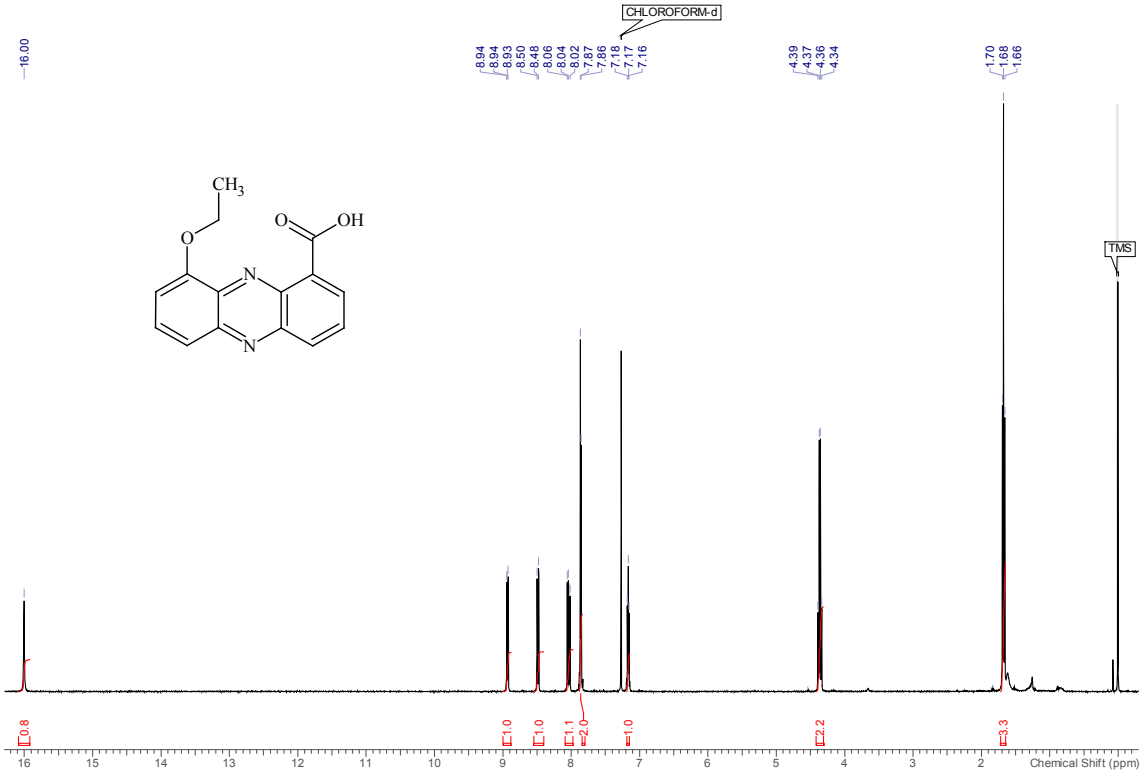

^{1}H NMR for (9-ethoxyphenazin-1-yl)methanol (**24**) in $CDCl_3$

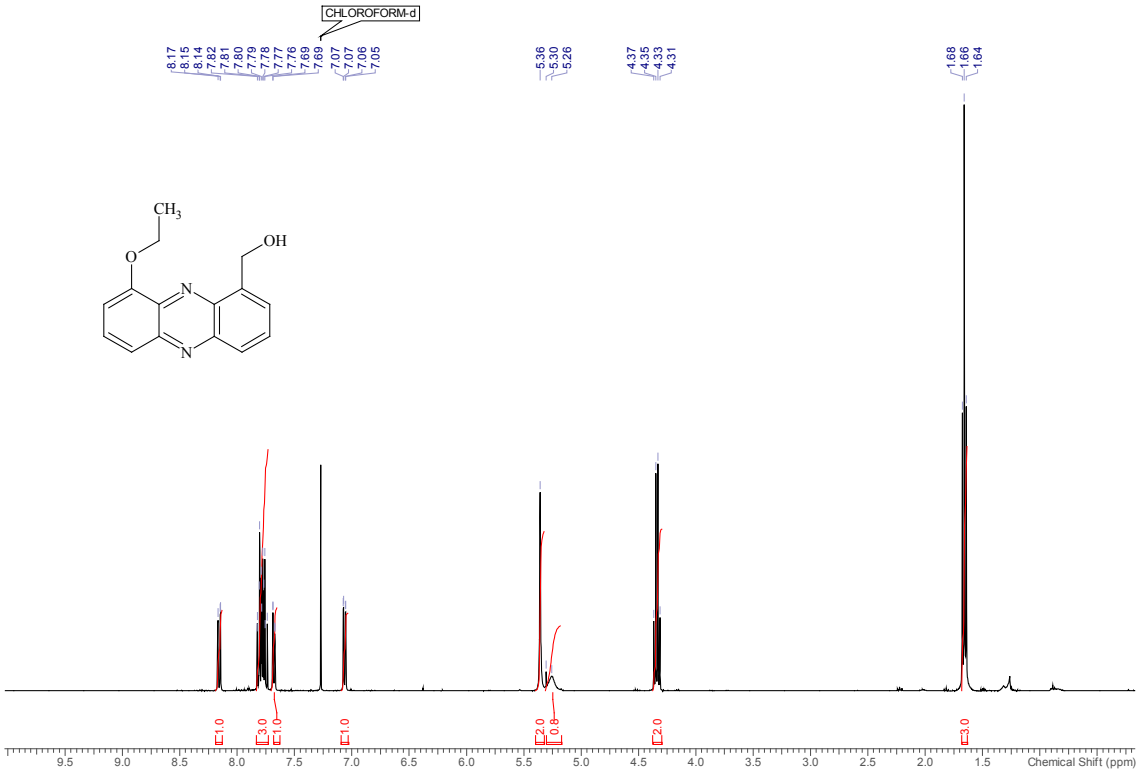

^{13}C NMR for (9-ethoxyphenazin-1-yl)methanol (**24**) in $CDCl_3$

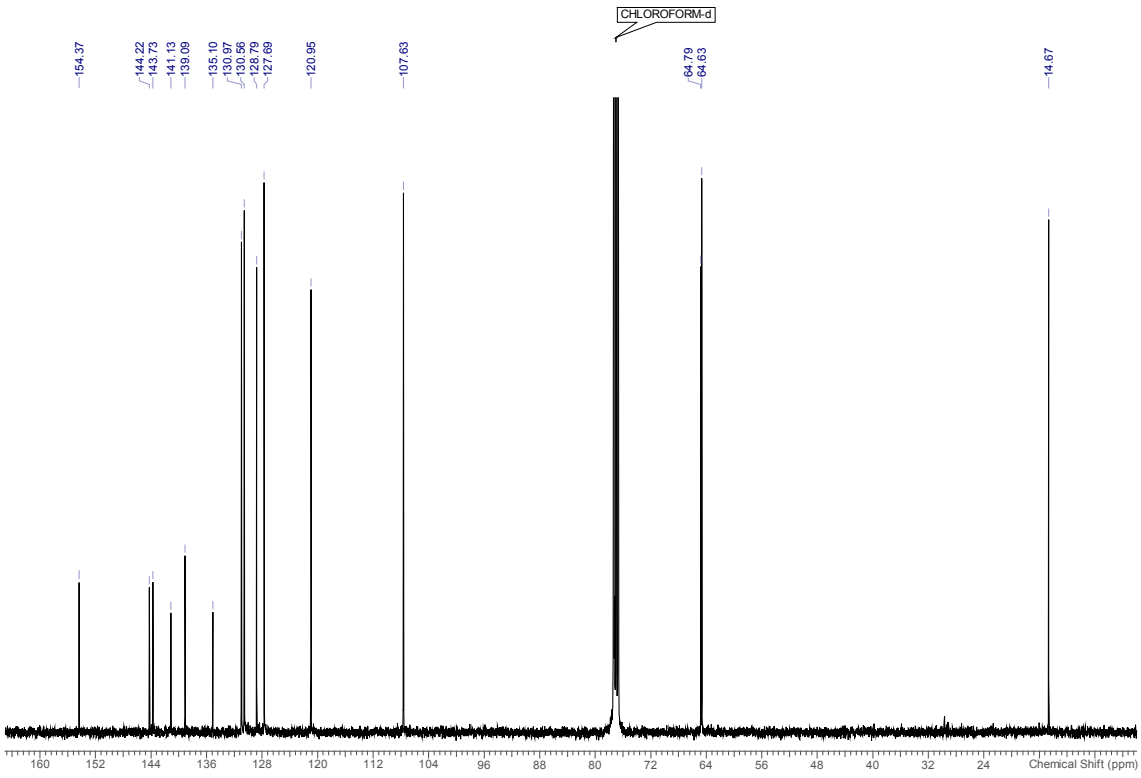

^{1}H NMR for 9-ethoxyphenazine-1-carbaldehyde (**25**) in $CDCl_3$

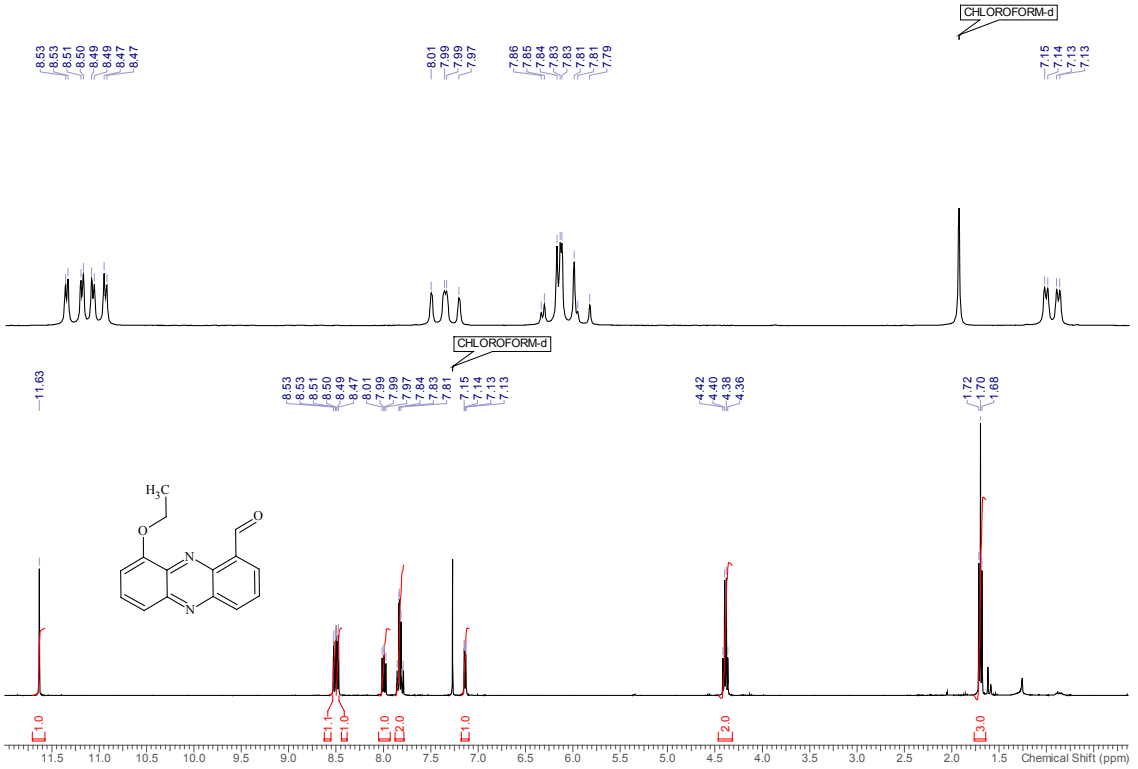

^{13}C NMR for 9-ethoxyphenazine-1-carbaldehyde (**25**) in $CDCl_3$

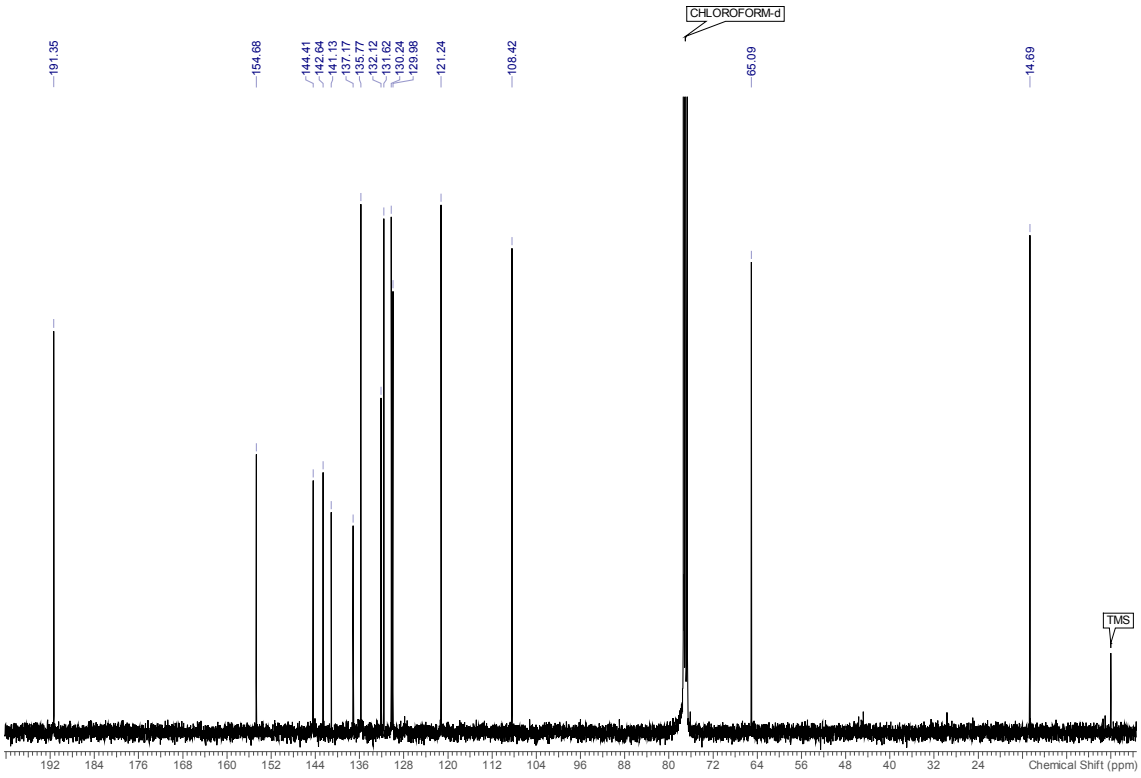

^{1}H NMR for **26** iodide salt in DMSO-d$_6$

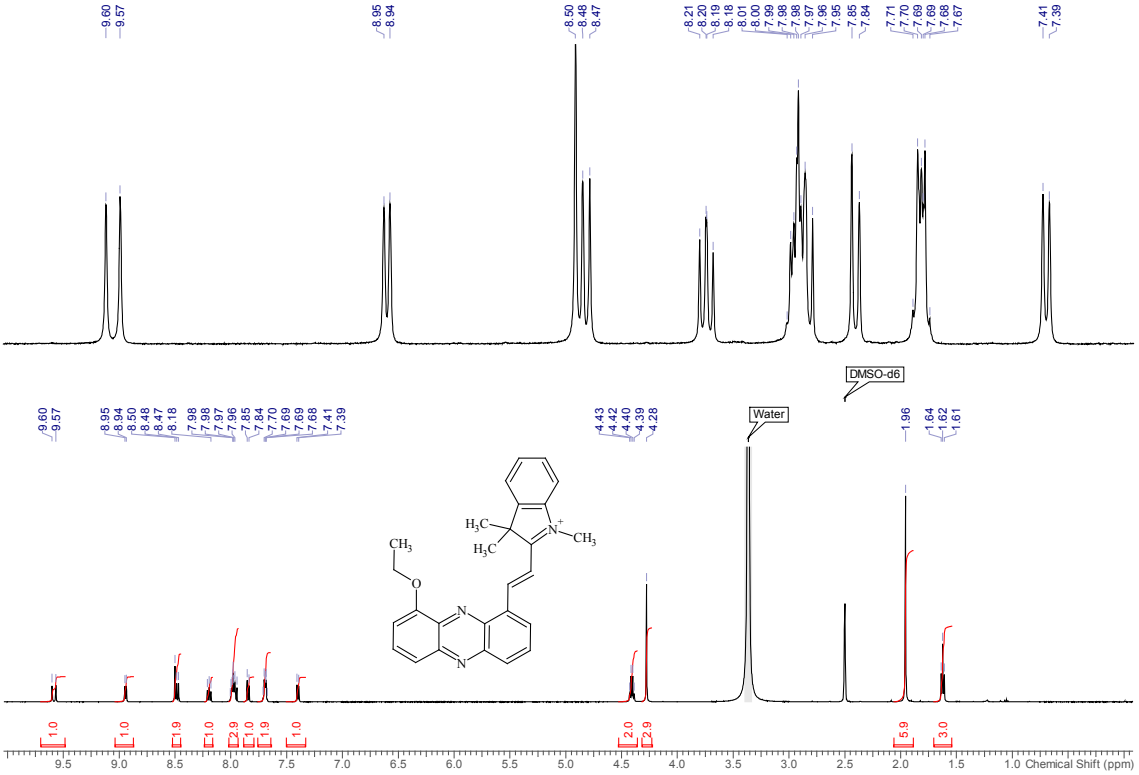

^{13}C NMR for **26** iodide salt in DMSO-d$_6$

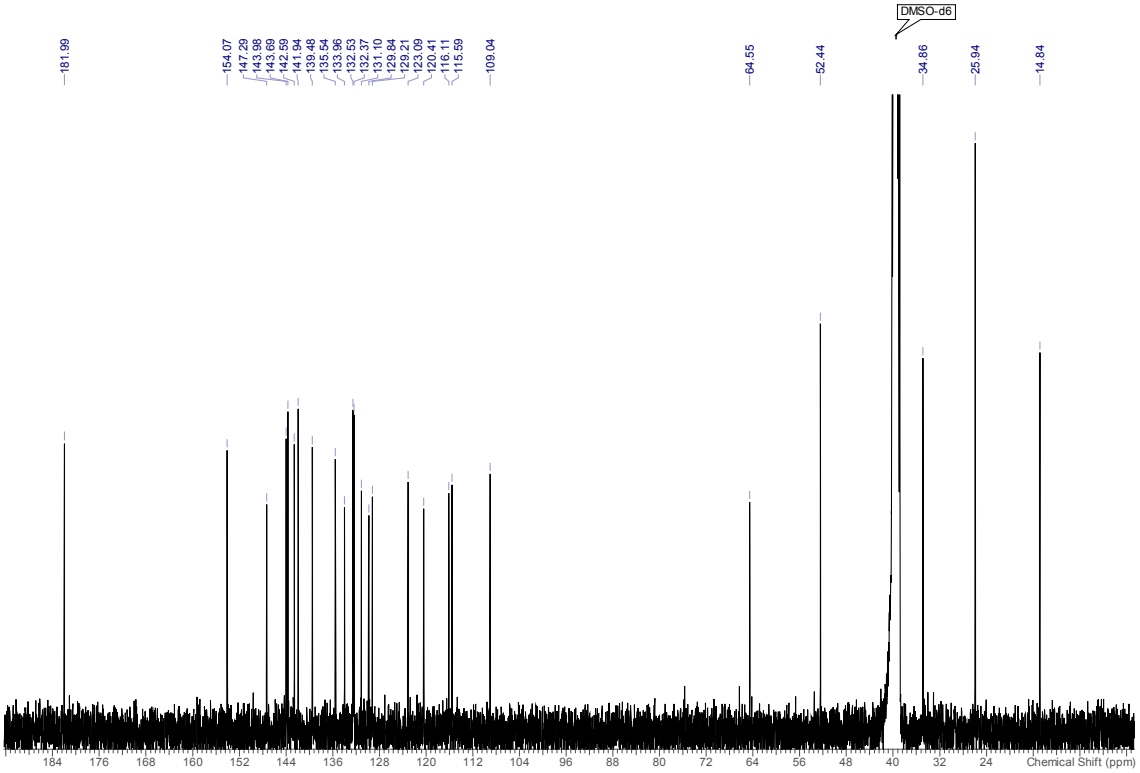

^{1}H NMR fragments for **27** chloride salt in D_2O

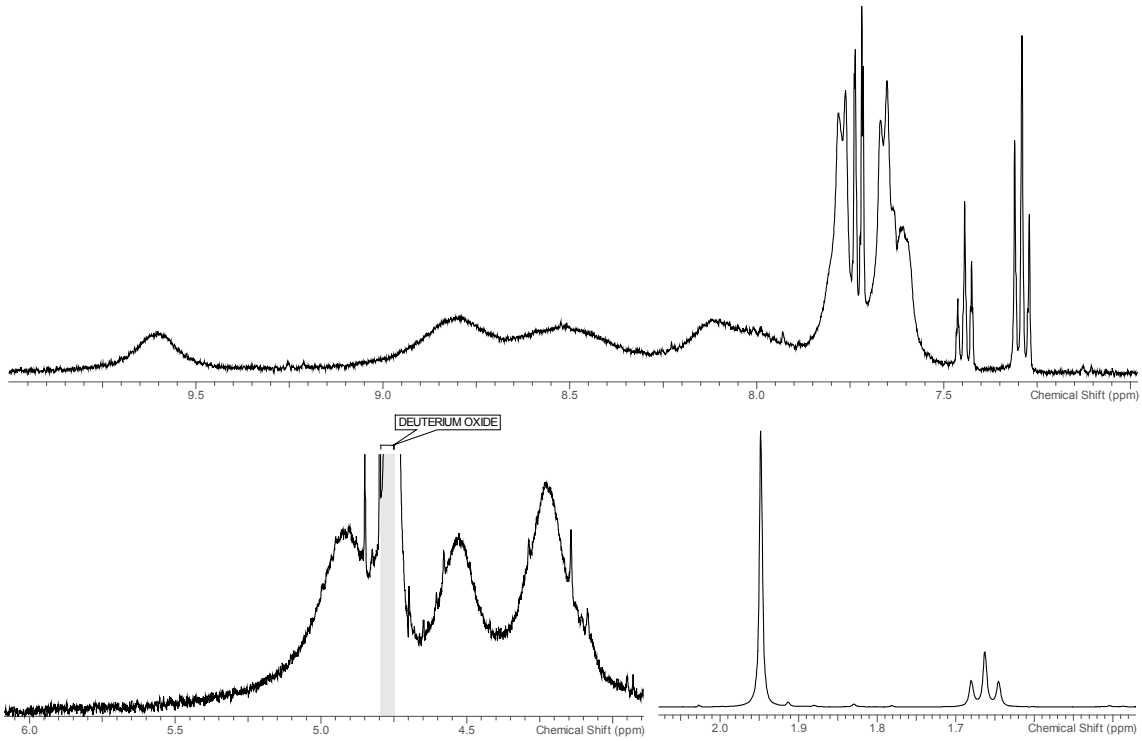

^{1}H NMR for **DACy-2** in MeCN-d_3 (**)

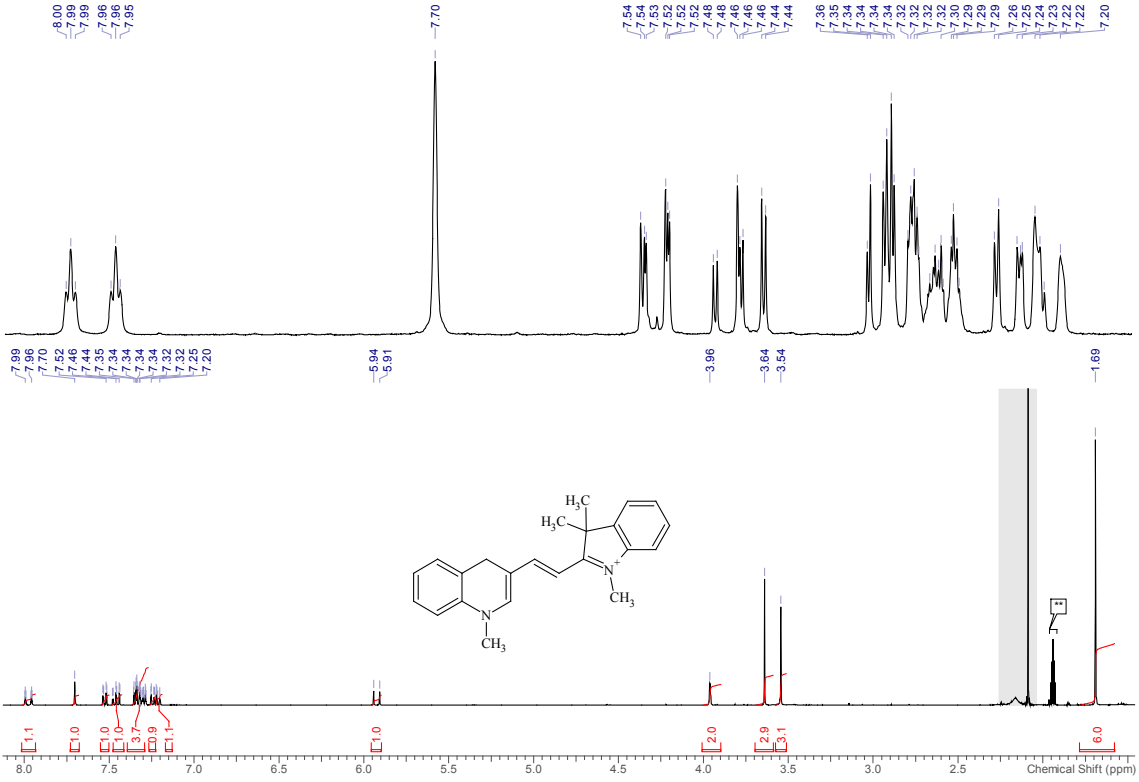

^{13}C NMR for **DACy-2** in MeCN-d_3 (**)

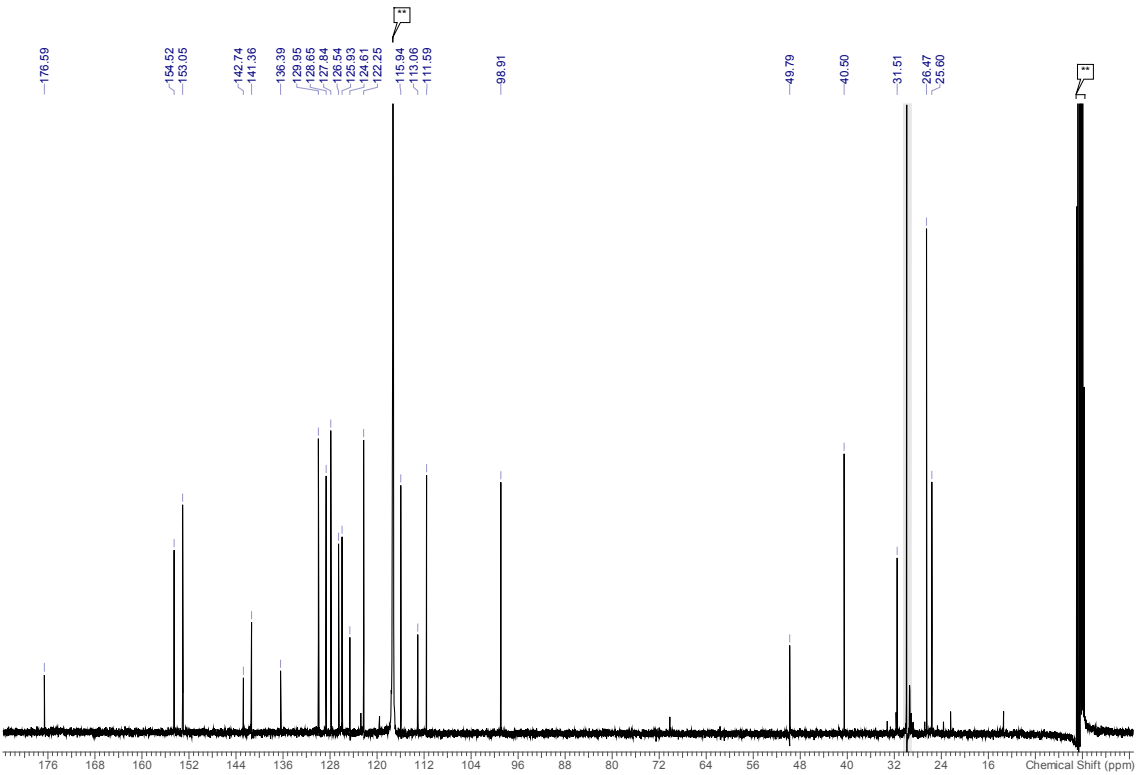

Proton-carbon network of **DACy-2**

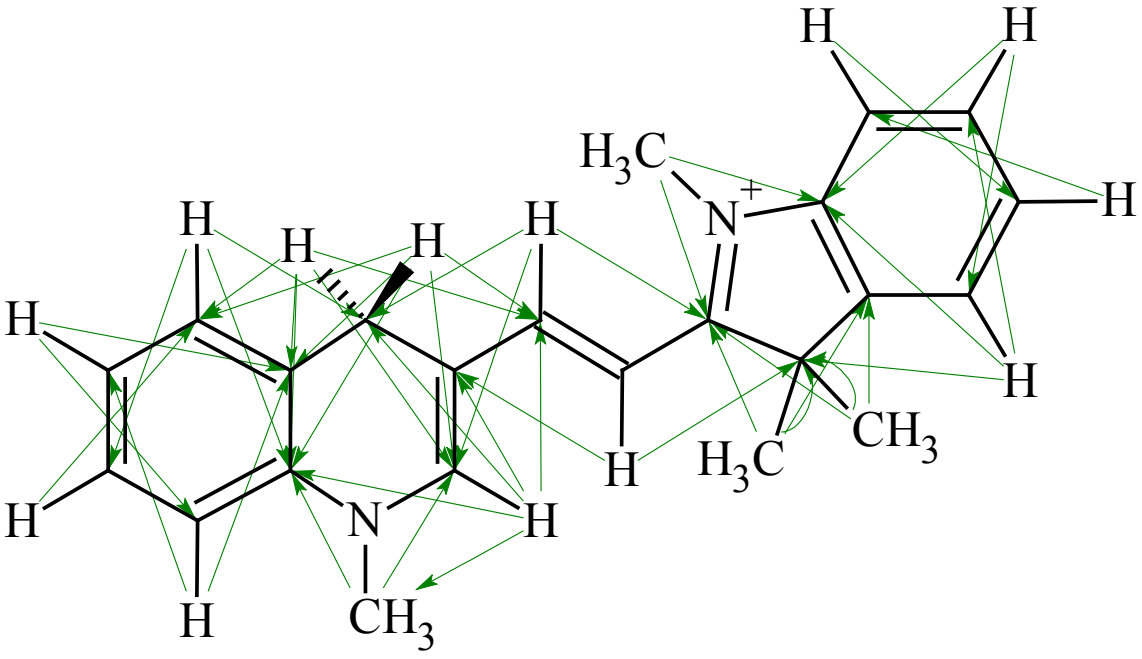

LIST OF ABBREVIATIONS

°	degree
^{13}C	carbon isotope 13
^{1}H	proton isotope 1
2A	two-acceptor
A	absorbance
AA	amino acid / ascorbic acid
abs	absorbance
AcOH	acetic acid
ADA	American Diabetes Association
aq.	aqueous
aqphen	10,11-[1,4-naphtalendione]-dipyrido[3,2-a;2',3'-c]-phenazine
Ar	argon
Asn	asparagine
BC	before Christ
bpy	bipyridyl
br.	broad
c	concentration
ca.	*circa* / about
cat.	catalytic
CCD	charge-coupled device
CDI	1,1'-carbonyldiimidazole
cNAD/cNADH	carba-NAD / carba-NADH
conc.	concentrated / concentration
COSY	correlation spectroscopy
Cq	quaternary carbon
Ctrl	control
CV	coefficient of variation
Cy	cyanine
Cys	cystein
d	day / deuterium / dublet
DAPI	4',6-diamidino-2-phenylindole
DCE	1,2-dichloroethane
DCM	dichloromethane
DMEM	Dulbecco Modified Eagle Medium
DMF	N,N-dimethylformamide
DMSO	dimethylsulfoxide
DNA	deoxyribonucleic acid
e.g.	*exempli gratia* / for example
EC number	The Enzyme Commission number
eq.	equation
equiv.	equivalents
ESI	electron spray ionization
Et	ethyl
et al	*et alii* / and others
etc	*et cetera* / and other things
EtOAc	ethyl acetate
EtOH	ethanol
FAD	flavin adenine dinucleotide
$FADH_2$	reduced flavin adenine dinucleotide

FLIM	fluorescence-lifetime imaging microscopy
FW	formula weight
GC	gas chromatography
GlucDH2	double mutant of GDH (E170K/Q252L)
GOx	glucose oxidase
GSH	reduced glutathione
h	hour
Hb	haemoglobin
HbO_2	oxygen–haemoglobin
HCT116	human colon cancer cells
HEK	human embryonic kidney cells
HEPES	4-(2-hydroxyethyl)-1-piperazineethanesulfonic acid
Het	heterocycle
HPLC	high-performance liquid chromatography
HR	high resolution
HRMS	high resolution mass spectrometry
HSQC	heteronuclear single quantum coherence
HTS	high throughput screening
Hz	hertz
i.e.	*id est* / that is
IL	intra-ligand
incl.	including
IQ	isoquinolyl / isoquinolinium
IR	infra-red
ISO	International Organization for Standardization
IUPAC	the International Union of Pure and Applied Chemistry
J	coupling constant
K_m	the Michaelis constant
kobs	pseudo-first-order rate constant
L	length / ligand / liter
LED	light emitting diode
Lys	lysine
m	milli / medium / mitte / multiplet / meter
m	mean
M	mega / mol
m/z	mass to charge
max	maximum
Me	methyl
MeCN	acetonitrile
MEG	ethylene glycol
MeOH	methanol
min	minute(s)
MLCT	metal-to-ligand charge-transfer
MQ-water	deionized water, obtained using a Millipore purification system
Mr	relative molecular weight
MS	mass spectrometry
MW	molecular weight
n	number
n.d.	not determined
$NAD(P)^+$	nicotinamide adenine dinucleotide (phosphate)
NAD(P)H	reduced nicotinamide adenine dinucleotide (phosphate)
NMR	nuclear magnetic resonance

NOESY	nuclear Overhauser effect spectroscopy
NP	nanoparticles / normal phase
nqphen	dipyrido[3,2-a:2′,3′-c]-benzo[3,4]-phenazine-11,16-quinone
ø	diameter
OD	optical density
PB	phosphate buffer
PBS	phosphate buffered saline
PMO	phosphomolybdic acids
PMS	5-methylphenazine methosulfate
POC	point-of-care
ppm	parts per million
PQQ	pyrroloquinoline quinone
$PQQH_2$	reduced pyrroloquinoline quinone
PTFE	polytetrafluoroethylene
Py	pyridyl / pyridinium
Pz	phenazyl / phenazinium
Q	quinolyl / quinolinium
q	quartet
QD	quantum dot
R^2	coefficient of determination
rcf	relative centrifugal force
R_f	retention factor
ROS	reactive oxygen species
RP	reversed phase
rpm	rotations per minute
RR	relative remittance
rt	room temperature
s	second / singlet / strong
S	supplementary material
SCO2	synthesis of cytochrome c oxidase 2
SD	standard deviation
SMBG	self-monitoring of blood glucose
t	time / triplet
T1D	type 1 diabetes
T2D	type 2 diabetes
TEAAc	tetraethylammonium acetate
TFA	trifluoroacetate anion / trifluoroacetic acid
TfO	trifluoromethanesulfonate
TfOMe	methyl trifluoromethanesulfonate
THF	tetrahydrofuran
TLC	thin layer chromatography
TMRM	tetramethylrhodamine, methyl ester
ToF	time-of-flight
UV	ultraviolet
Vis	visible
V_{max}	maximum velocity
vs	*versus*
WHO	World Health Organization
wt. / WT	weight / wild type
δ	chemical shift
λ	wavelength
σ	standard deviation

CURRICULUM VITAE

Personal data

Name: Maksim Fomin

Date of birth: 20.01.1989

Place of birth: Tomilino (Moscow Oblast, Russia)

Nationality: Russian

Email: maksim.a.fomin@gmail.com

LinkedIn: de.linkedin.com/in/mafomin

Education

PhD in Organic Chemistry

10/2011 – 12/2015 Roche Diagnostics GmbH, Mannheim&Penzberg, Germany
Universität Regensburg, Germany.

"*Novel redox indicators for optical detection of NADH,*" *magna cum laude*
supervised by Dr. Dieter Heindl and Prof. Dr. Burkhard König.

M.Sc. in Biotechnology

09/2009 – 06/2011 Lomonosov Moscow University of Fine Chemical Technology (MITHT), Russia.

GPA: 4.9/5.0

"*Synthesis of novel photochromic retinal analogs and study of their spectral properties,*" *summa cum laude*
supervised by Prof. Dr. Andrei Khodonov.

B.Sc. in Chemical Engineering and Biotechnology

09/2005 – 7/2009 Lomonosov Moscow University of Fine Chemical Technology (MITHT), Russia.

GPA: 4.1/5.0

"*Synthesis of 9Z-isomers of retinoids,*" *summa cum laude*
supervised by Prof. Dr. Andrei Khodonov.

High School leaving certificate with High Honours

09/1996 – 06/2006 Gymnasium 18 (Tomilino, Russia) specialized in natural sciences.

Research experience

PhD student

12/2013 – present Roche Professional Diagnostics, Penzberg, Germany.

- Introduced a new design for a colorimetric and fluorescent NADH indicator for application in bioassays. The design is based on a cyanine dye scaffold and two-acceptor molecular structure.
- Synthesized a series of novel NADH indicators.
- Identified the lead structure which has been used for optical NADH detection in enzyme and cell assays.
- Developed colorimetric glucose assays based on dehydrogenase enzymes.

Visiting graduate researcher

08/2013 – 11/2013 Universität Regensburg, Institut für Organische Chemie, Germany. Collaboration with the group of Prof. Dr. Burkhard König.

- Prepared nanosized DOPC vesicles incorporating recognition elements and fluorescent reporters.

PhD student

10/2011 – 07/2013 Roche Diabetes Care, Mannheim, Germany.

- Designed a novel optical glucose biosensor comprising an enzyme and a redox indicator.
- Prepared sensor coatings for blood glucose test strips.
- Measured glucose on test strips by remittance spectroscopy.

Visiting student

06/2011 – 10/2011 Lomonosov Moscow State University (MSU), Russia.

Four months research in the group of Dr. Alexander Voskoboynikov. Focus on advanced techniques used in synthetic organic chemistry, particularly on Schlenk and glove-box techniques for air- and moisture-sensitive reactions.

Visiting student

11/2010-02/2011	N.M. Emanuel Institute of Biochemical Physics of Russian Academy of Sciences, Russia. Four months of experimental training course in the laboratory of "Photochemistry and Photobiology" (Prof. Dr. S.D. Varfolomeev). Studied biophysical analytical techniques and purification methods, hands-on experience with LC-MS, HPLC and UV-Vis equipment. Investigated spectral-kinetic behavior of photochromic diarylethenes.

Skills

Research	Molecular design, organic synthesis and bioassays.
Analytics	NMR, HRMS, LC-MS, HPLC, UV-Vis, fluorescence, CD, DLS.
Literature	Scifinder, Reaxys, Google Scholar, scientific writing.
Patents	Thomson Innovation, Google Patent; writing of patent applications, researching state of the art and managing the reviewing process.
IT	MS Office (Word, Excel PowerPoint, OneNote), EndNote, ACDlabs, MDL ISIS/Base, Pymol, ChemBioOffice, Spartan, CoralDraw, Adobe Lightroom.

Spoken languages

English	Full professional proficiency.
German	Professional working proficiency.
Russian	Native language.

Honours and Awards

10/2011 – 10/2014	Marie Curie Actions fellowship, PhD project in ITN CHEBANA.
04/2011	The third place award of open scientific research student contest at The XVIII International student, postgraduate and young scientist conference "Lomonosov-2011", Section "Chemistry", subsection "Life science, Nanobiomaterials, and Nanobiotechnology."

12/2010 Golden Prize for innovation at Seoul International Invention Fair.

03/2010 Merit for innovation at The Moscow International Conference "Biotechnology: Ecology of Big Cities".

Patents

Fomin M, Gebauer P, Horn C, Heindl D // EP patent application nr. EP14181964.9 (filed on Aug. 22, 2014; not published yet).

Laptev AV, Lukin AYu, Belikov NE, Fomin MA, Demina OV, Shvets VI, Khodonov AA // Photochromic 5'-Vinyl-6-Nitro-Spirobenzopyran derivatives and production / Patent RF no. 2458927. Priority from 07.04.2011.

Fomin MA, Belikov NE, Lukin AYu., Laptev AV, Demina OV, Khodonov AA, Shvets VI // Method of retinal 11-cis-isomer preparation. / Patent RF no. 2417983. Priority from 30.10.2009.

Articles

Laptev AV, Lukin AYu, Belikov NE, Fomin MA, Zvezdin KV, Demina OV, Barachevsky VA, Varfolomeev SD, Shvets VI, Khodonov AA // Polyenic spirobenzopyrans: Synthesis and study of photochromic properties. / *J. Photochem. Photobiol. A: Chemistry*. **2011**. – V. 222. - №1. - Pp. 16-24.

Demina OV, Laptev AV, Lukin AYu, Khodonov AA, Belikov NE, Fomin MA, Gribkova IV, Shvets VI, Varfolomeev SD // Comparison of anti-aggregative activities of 5-phenyl-3-(3-pyridyl)isoxazole and 5-phenyl-3-(3-pyridyl)-1,2,4-oxadiazole. / *Biochemistry (Moscow) Supplemental Series A: Membrane and Cell Biology*. **2011**. – V. 5. – No 3. – Pp. 227-236.

Oral presentations

4th CHEBANA Summer School, The final CHEBANA Meeting, 1–3 September **2014**, Regensburg, Germany (oral+poster presentation): Development of a new colorimetric RedOx-indicator.

3rd CHEBANA Summer School held together with the ITN NANODRUG, 1–7 September **2013**, Biarritz, France (oral presentation): Development of a new colorimetric RedOx-indicator.

2nd CHEBANA Summer School with the Midterm Review Meeting, Mannheim, Germany, 18–20 September **2012**: (oral+poster presentation): Development of a new colorimetric RedOx-indicator.

1st CHEBANA Winter School, Barcelona, Spain, 14-17 February **2012**, (oral presentation): Development of a new colorimetric RedOx-indicator.

The XVIII International student, postgraduate and young scientist conference «Lomonosov», Moscow, Russia, 11–15 April, **2011**: Dithienylethene analogs of retinal: synthesis and study of their spectral properties.

Poster presentations

GDCh-Wissenschaftsforum Chemie 2015, Dresden, Germany, 30 August – 2 September **2015**: New redox indicators for optical detection of NADH.

The 4th EuCheMS Chemistry Congress, Prague, Czech Republic, 26–30 August **2012**: Development of new colorimetric redox indicators for NADH visualization.

The VI Moscow International Congress “Biotechnology: State of the Art and Prospects of Development”, Moscow, 21–25 March **2011**: Antiaggregatory agents of 3,5-substituted isoxazoles and their 4,5-dihydro derivatives.

ACKNOWLEDGEMENTS

I would like to express my gratitude to Dr. Dieter Heindl, whose outstanding scientific knowledge and intuition together with incredible optimism contributed a lot in the success of this project. I am thankful to Dr. Carina Horn for giving me the opportunity to work on this interesting and versatile topic. I am indebted to Prof. Dr. Burkhard König for being my supervisor on the academic side.

I am very thankful to Prof. Dr. Joachim Wegener and PD Dr. habil. Axel Dürkop for being the doctoral committee members of my thesis. I thank Prof. Dr. Frank-Michael Matysik for being Chairman in my PhD defense.

I acknowledge the Marie Skłodowska-Curie actions and Roche for financial support and ITN CHEBANA for numerous workshops and training events.

I appreciate help of Oliver Tonn, Dr. Claudio Sustman, Dr. Konrad Honold and Dr. Ruslan Dmitriev, Prof. Dr. Dmitri Papkovsky in the collaborative projects. I thank Dr. Heiko Mussauer for helping me to file the patent application and coordinating the reviewing process.

I thank all members of the analytical departments in Mannheim, Penzberg and Basel, especially Michael Klang, Gerhard Fink and Dr. Christian Geletneky for recording NMR spectra, Dr. Martin Rempt for recording mass spectra and Astrid Marks for helping me to run daily LC-MS experiments.

I am thankful to Dr. Nelli Steinke, Dr. Susanne Gawenda, Angelika Fürst and Gerhardt Lettau for guiding my first steps in Mannheim. I am indebted to Dr. Tobias Hausmann, Dr. Hannes Kuchelmeister and Dr. Christoph Seidel for organizing the workspace for me in Penzberg, and for the support and advices, which were vital to complete this project. I thank Dr. Mara Boenitz-Dulat for the frank discussions about enzymes and more. I thank Dr. Hans-Peter Josel and Isabell Barke for the kind gift when it was most needed. Big thanks to my lab fellows Peter Kratzsch, Herbert Schneider, Stefanie Wotschka, Corina Grobelny, Dirk Kessler, Heribert März and Sona Simonyiova. Not to forget the "secret sovereign" Ms. Christine Scholtyssek, Ms. Sabine Sporer, Ms. Franziska Hohenreiter and Ms. Viola Rappenegger, who helped me to manage all kinds of situations.

Many thanks to the international Postdoc group for the great time together, especially to Dr. Giuseppe Prencipe, Dr. Christian Wellner, Dr. Florian Huber,

Dr. Gaston Vondenhoff and Dr. Wojtek Steffen for having interest in reading my thesis and for the valuable scientific discussions. Thanks to another international scientific community, ITN CHEBANA, and also to Dr. Timo Valta and Dr. Thomas Zanni who became great friends of mine.

Thanks to all members of AK König for making me feel welcome in Regensburg and for being a wonderful community afterwards, the skiing trips, Chem-Cup, PhD parties.

A very big *spasibo* to Dr. Alex Lukin and Prof. Dr. Andrey Khodonov, who supervised my Master and Bachelor Thesis and contributed immensely to my scientific growth. I say *spasibo* to Dr. Alexander Voskoboynikov for the "survival" training in organic synthesis before starting this PhD project. Another *spasibo* goes to Prof. Dr. Vladimir Belov and Dr. Kirill Kolmakov for pointing out this PhD opportunity.

I would particularly like to mention my friends from the "school times" Artem Dmitrienko, Daria Ezerina, Anton Loginov and Timur Bagautdinov who inspired me to get out of the box and to try PhD abroad.

My biggest thanks go to Alexey and Svetlana, who are my parents, for never-ending support and encouragement.

Finally, thanks to all who came across the path and not mentioned in these acknowledgements. Thank you for reading this right now. Everything is connected and hence everything matters.

"When the spirits are low, when the day appears dark, when work becomes monotonous, when hope hardly seems worth having, just mount a bicycle and go out for a spin down the road, without thought on anything but the ride you are taking."

— Arthur Conan Doyle